

OCRWM	Scientific Analysis Cover Sheet	1. QA: N/A Page 1 of 172
-------	---------------------------------	-----------------------------

2. Scientific Analyses Title Characterize Eruptive Processes at Yucca Mountain, Nevada	
3. DI (including Revision Number) ANL-MGR-GS-000002, Rev 01	
4. Total Attachments - 1	5. Attachment Numbers - Number of pages in each - 1

	Printed Name	Signature	Date
6. Originator: D. Krier	Donathon Krier	SIGNATURE ON FILE	12-08-03
7. Checker: S.S. Levy	SCHÖN LEVY	SIGNATURE ON FILE	12/08/03
8. QER: K. McFall	KENNETH MCFALL	SIGNATURE ON FILE	12/15/03
9. Responsible Manager/Lead: M. Cline	K Michael Cline	SIGNATURE ON FILE	12/15/03
10. Responsible Manager: J. King	JERRY L. KING	SIGNATURE ON FILE	12/16/03

11. Remarks <i>This document addresses historical Technical Error Report TER-02-0009, now subsumed in Corrective Action # 136-001. JK 12/15/03</i>
---

Revision History	
12. Revision/ICN No.	13. Description of Revision/Change
00/00	Initial issue.
00/01	<p>00/00 Initial Issue</p> <p>00/01 REV 00 ICN 01 of this AMR incorporates changes to the text, which are indicated in the document with change bars.</p> <p><i>Major changes to the text occur in the following sections.</i></p> <p>Section 1: p. 11, sentence added in reference to AMR addressing Nuclear Regulatory Commission Igneous Activity Key Technical Issue. Paragraph added with purpose and scope of ICN.</p> <p>Section 2: p. 13, reference to the technical work plan for Disruptive Events added as update.</p> <p>Section 4: pp. 17-18, assumptions added to Table 1b. p. 19, sentence added describing how this ICN addresses Acceptance Criteria for the Igneous Activity Consequences Subissue.</p> <p>Section 7: pp. 47-49, conclusions updated to clarify technical output. pp. 50-53, Table 7 added as technical product output.</p> <p>Section 8.4: p. 60, added to document to list Output Data Tracking Number.</p> <p><i>Minor clarification of text and minor editorial changes have also been added.</i></p> <p><i>Changes to figures:</i> No changes.</p> <p><i>Changes to tables:</i> Addition of Table 7, which contains the technical product output of the document.</p>

<b>Revision History (Continued)</b>	
12. Revision/ICN No.	13. Description of Revision/Change
01/00	<p>01/00 REV 01 of this AMR is a complete revision of REV 00 ICN 01 with both major and minor changes; therefore, changes to text are not highlighted with change bars.</p> <p><i>The following sections have been added and/or expanded.</i></p> <p>Section 4.2, Criteria: Discussion added relating criteria described in the <i>Yucca Mountain Review Plan, Final Report (NUREG-1804)</i> (NRC 2003) to discussions in this revision.</p> <p>Section 6.3.1, Characteristics of Eruptive Conduits, Dike Widths, and Dike Swarms: Expansion of text on processes of conduit formation and growth. Conduits and their depths are the subject of Part 6.18.2 Geometry of Volcanic Feeder System Model (R.2) of the <i>Model Validation Status Report</i> (ANL-WIS-MD-000005 REV 00). No additional information related to potential conduit depths is added to this analysis due to absence of YMP focused investigations or other relevant studies in the open literature since REV 00 ICN 01. The inherent assumption that conduit depth extends to greater than repository depth is continued in the current revision. The consequences of conduit depth and diameter on waste packages are discussed in <i>Number of Waste Packages Hit by Igneous Intrusion</i> (ANL-MGR-GS-000003), and explored further in <i>Atmospheric Dispersal and Deposition of Tephra from a Potential Volcanic Eruption at Yucca Mountain, Nevada</i> (MDL-MGR-GS-000002 REV 00).</p> <p>Section 6.4, Physical Volcanology of the Lathrop Wells Cone: Includes results of field studies on physical attributes of the Lathrop Wells Cone, tephra fall, xenolith incorporation, and volumes of volcanic products (cone, lava, and tephra).</p> <p>Section 6.5, Redistribution Processes of Basaltic Ash and Waste Particles: Discussion of sedimentary processes resulting in erosion, secondary transport, and deposition of volcanic ash and waste particles affecting the Reasonably Maximally Exposed Individual. Ash redistribution is the subject of Part 6.21.2 Soil Removal Model for Volcanic Disruption (U.1-2) of ANL-WIS-MD-000005 REV 00 (<i>Model Validation Status Report</i>). Information is included, which addresses soil removal in the context of redistribution and mixing/dilution of volcanic tephra near Lathrop Wells Cone, and which reports results of an investigation, using cesium-137 (<sup>137</sup>Cs), of erosion and deposition on various landforms on the Fortymile Wash alluvial fan.</p> <p>Section 6.6: Potential eruption scenario at Yucca Mountain: Discussion based on volcanological characteristics of Lathrop Wells Cone deposits.</p> <p>Section 7.2, Output Parameters and Uncertainties: Addition of several volcanological parameters including number of dikes associated with formation of a new volcano, dike spacing, and duration of a single explosive phase constituting a violent Strombolian phase.</p>

## CONTENTS

	<b>Page</b>
1. PURPOSE .....	11
2. QUALITY ASSURANCE .....	12
3. USE OF SOFTWARE.....	13
4. INPUTS.....	13
4.1 DATA, PARAMETERS, AND OTHER INPUTS.....	13
4.1.1 Data .....	14
4.1.2 Other Inputs.....	14
4.2 CRITERIA .....	16
4.2.1 Description of Site Characterization Work Criteria.....	17
4.2.2 Description of Volcanic Disruption of Waste Packages Criteria.....	18
4.2.3 Description of Airborne Transport of Radionuclides Criteria.....	22
4.2.4 Description of Redistribution of Radionuclides in Soil Criteria.....	26
4.3 CODES AND STANDARDS.....	37
5. ASSUMPTIONS .....	37
6. SCIENTIFIC ANALYSIS.....	39
6.1 INTRODUCTION .....	39
6.1.1 Scientific Approach and Technical Methods .....	39
6.1.2 Units of Measurement .....	39
6.1.3 Definition of Terms .....	39
6.2 FEATURES, EVENTS, AND PROCESSES .....	46
6.3 ERUPTIVE PROCESSES ANALYSIS .....	48
6.3.1 Characteristics of Eruptive Conduits, Dike Widths, and Dike Swarms.....	48
6.3.2 Characteristics of Igneous Material.....	52
6.3.3 Eruptive Processes.....	58
6.3.4 Entrainment of Radioactive Waste in Ascending Magma .....	73
6.3.5 Ash Plumes and Their Deposits .....	74
6.4 PHYSICAL VOLCANOLOGY OF THE LATHROP WELLS CONE.....	81
6.4.1 Scoria Cone .....	81
6.4.2 Tephra Distribution and Description.....	88
6.4.3 Lathrop Wells Volcano—Volume Estimations.....	115
6.4.4 Eruption Mechanisms and History for the Lathrop Wells Cone and Tephra Fall .....	118
6.5 REDISTRIBUTION PROCESSES OF BASALTIC ASH AND WASTE PARTICLES .....	126
6.5.1 Characteristics of Ash Redistribution Processes.....	126
6.5.2 Cesium-137 Studies.....	139
6.5.3 Discussion .....	143
6.6 POTENTIAL ERUPTION SCENARIO AT THE YUCCA MOUNTAIN REPOSITORY .....	145

**CONTENTS (Continued)**

	<b>Page</b>
6.7 UNCERTAINTIES (INPUT).....	147
6.7.1 Input Parameters and Uncertainty .....	147
7. CONCLUSIONS .....	150
7.1 SUMMARY OF SCIENTIFIC ANALYSIS .....	150
7.2 OUTPUT PARAMETERS AND UNCERTAINTY .....	154
8. INPUTS AND REFERENCES .....	158
8.1 DOCUMENTS CITED.....	158
8.2 CODES, STANDARDS, REGULATIONS, AND PROCEDURES .....	171
8.3 SOURCE DATA, LISTED BY DATA TRACKING NUMBER .....	171
8.4 OUTPUT DATA, LISTED BY DATA TRACKING NUMBER .....	171
ATTACHMENT I - ACRONYMS.....	172

## FIGURES

	Page
1. Basaltic Bomb from the Lathrop Wells Scoria Cone.....	40
2. Scanning Electron Micrograph of a Sideromelane (Basaltic Glass) Pyroclast.....	41
3. Scanning Electron Micrograph of a Tachylite Pyroclast .....	42
4. Scanning Electron Micrograph of a Glassy Tachylite .....	42
5. Scanning Electron Micrograph of a Lithic Clast in Strombolian Tephra .....	43
6. Plot of the Depth at Which Volatile ( $H_2O$ ) Exsolution Begins in a Lathrop Wells Basalt ( $d_{exs}$ ) for Initial Dissolved Water Content ( $n_i$ ) up to 0.05 .....	61
7. Plot of the Variation of Gas Volume Fraction ( $\phi$ ) with Depth ( $d$ ) for a Lathrop Wells Basalt, Assuming Pressure in the Magma is Lithostatic, for Initial Dissolved Water Content $n_i = 0.01, 0.02, 0.03, 0.04,$ and $0.05$ .....	63
8. Plot of the Variation of Eruption Velocity ( $u_{erupt}$ ) with Initial Dissolved Water Content ( $n_i$ ) for Various Mass Discharge Rates Along a Fissure .....	64
9. Plot of the Variation of Eruption Velocity ( $u_{erupt}$ ) with Initial Dissolved Water Content ( $n_i$ ) for Various Mass Discharge Rates from a Circular Conduit.....	65
10. Changes in Cone Height During an Eruption Based on Observed Strombolian Activity .....	66
11. Scoria Cone Volumes .....	67
12. Basal Cone Diameters of 629 Scoria Cones .....	69
13. Scoria Cone Volume Versus Cone Basal Diameter.....	70
14. Relating Column Height and Areal Extent of Ash Fall.....	75
15. Eruption Cloud Height Versus Volume Eruption Rate.....	76
16. Lathrop Wells Scoria Cone and Adjacent Lava Flows (Capped by Beige, Eolian Sand) Viewed from the North.....	81
17. Topographic Map and Tephra Sample Locations for Lathrop Wells Cone Area .....	82
18. Cone Interior Showing Scoria and Close-up of Ejecta .....	83
19. Angular Unconformity Between Outward-Sloping Lapilli-Ash Avalanche Deposits and Deposits Sloping Toward the Vent .....	84
20. Hydrovolcanic Beds Near the Top of Lathrop Wells Volcano.....	85
21. Grain Size Variations of Hydrovolcanic Beds and Overlying Lapilli Fall Near the Top of Lathrop Wells Volcano .....	86
22. Volume Fractions of Lithic Clasts .....	89
23. Isopach Map (Estimated) of Tephra Fall from the Lathrop Wells Volcano .....	91
24. Grain Size Variations in Scoria Fall Section Close to the Southern Cone Base ("boneyard") .....	92
25. Tephra Fall Stratigraphy for Section D.....	95
26. Schematic Diagram of Hydrovolcanic Tephra Sequence .....	96
27. Hydrovolcanic Deposits West and near the Base of the Lathrop Wells Cone.....	96
28. Grain Size Variations in Ash-Rich Hydrovolcanic Sequence .....	98
29. Scanning Electron Micrograph of the 0.125- to 0.250-mm Fraction of Sample DK-LW-048.....	99
30. Scanning Electron Micrograph of the 0.125- to 0.250-mm Fraction of Sample DK-LW-049.....	99
31. Scanning Electron Micrograph of the 0.125- to 0.250-mm Fraction of Sample DK-LW-050.....	100

**FIGURES (Continued)**

	<b>Page</b>
32. Scanning Electron Micrograph of the 0.125- to 0.250-mm Fraction of Sample DK-LW-051 .....	100
33. Scanning Electron Micrograph of the 0.125- to 0.250-mm Fraction of Sample DK-LW-052 .....	101
34. Scanning Electron Micrograph of the 0.125- to 0.250-mm Fraction of Sample DK-LW-053 .....	101
35. Grain Size Variations in Colluvium and Tephra Fall Section .....	102
36. Grain Size Variations in Tephra Section Overlying Ridge of Miocene Welded Tuff.....	104
37. Tephra Fall Stratigraphy for Section F .....	105
38. Grain Size Variations in Tephra Fall for Section F .....	106
39. Scanning Electron Micrograph of the 0.125- to 0.250-mm Fraction of Sample DK-LW-021 .....	107
40. Scanning Electron Micrograph of the 0.125- to 0.250-mm Fraction of Sample DK-LW-020 .....	107
41. Scanning Electron Micrograph of the 0.125- to 0.250-mm Fraction of Sample DK-LW-022 .....	108
42. Scanning Electron Micrograph of the 0.125- to 0.250-mm Fraction of Sample DK-LW-023 .....	108
43. Scanning Electron Micrograph of the 0.125- to 0.250-mm Fraction of Sample DK-LW-024 .....	109
44. Tephra Fall Stratigraphy for Section E .....	110
45. Grain Size Variations in Tephra Fall for Section E .....	111
46. Scanning Electron Micrograph of the 0.125- to 0.250-mm Fraction of Sample DK-LW-014 .....	112
47. Scanning Electron Micrograph of the 0.125- to 0.250-mm Fraction of Sample DK-LW-018 .....	112
48. Scanning Electron Micrograph of the 0.125- to 0.250-mm Fraction of Sample DK-LW-019 .....	113
49. Tephra Fall Stratigraphy for Section B .....	113
50. Grain Size Variations in Tephra Fall for Section B .....	114
51. Potential Volume of Erupted Ash for a Yucca Mountain Region Basaltic Volcano .....	118
52. Stages of Scoria Cone Formation .....	120
53. Pyroclasts from Fallout Sequence in the 0.125- to 0.250-mm Fraction of Sample DK-LW-021 .....	121
54. Scanning Electron Micrographs Showing Differences in Fall Deposits (left) Versus Surge Deposits (right) of Hydrovolcanic Tephra.....	122
55. Scanning Electron Micrographs of Individual Grains Showing Differences in Fall Deposits (left) Versus Surge Deposits (right) of Individual Grains of Tephra.....	123
56. Median Diameter Versus Sorting of Tephra Deposits Around the Lathrop Wells Cone .....	124
57. Pyroclasts from Fallout Sequence in the 0.125- to 0.250-mm Fraction of Sample DK-LW-023 .....	125
58. Detailed View of Tachylite Grain Surface.....	126

**FIGURES (Continued)**

	<b>Page</b>
59. Ortho-Photograph of the Lathrop Wells Volcanic Cone .....	129
60. Sample Locations for Ash Dilution and Cesium Studies.....	130
61. Ash Dilution Percentages in Drainage Along the West Side of Lathrop Wells Cone.....	132
62. Ash Dilution Percentages in Drainage Along the East Side of Lathrop Wells Cone .....	133
63. Ashfall Thicknesses from the ASHPLUME v. 1.4LV Model .....	135
64. Sediment Yields Using ARC Map™ .....	138
65. Cesium-137 Profile with Depth in Sediment for Composite of 15 Reference Samples.....	141

INTENTIONALLY LEFT BLANK

## TABLES

		<b>Page</b>
1.	Summary of Data Used as Inputs for Calculations in This Scientific Analysis Report .....	14
2.	Summary of Sources of Information to Support Methodologies, Assumptions, and Calculations in This Scientific Analysis Report .....	15
3.	Project Requirements and YMRP Acceptance Criteria Applicable to This Analysis Report.....	17
4.	Disruptive Events Included FEPs for This Scientific Analysis Report and Their Disposition in TSPA-LA.....	29
5.	Grain-Size Limits and Terms for Pyroclastic Rocks .....	46
6.	Mean Lathrop Wells Lava Chemistry with Associated Statistics (all values except count are in weight percent).....	52
7.	Mole Percent Concentration of Volcanic Gases and Associated Uncertainty Estimates .....	55
8.	Calculated Saturation Pressures, Liquidus Temperatures, Viscosities, and Densities as a Function of Water Content for Lathrop Wells Magmas .....	56
9.	Comparison of Lathrop Wells Cone with Scoria Cone Data Sets .....	67
10.	Basal Diameters of Scoria Cones - Platform Cone Fields .....	69
11.	Trans-Mexican Volcanic Belt Cone Field Basal Diameters and Cone Volumes .....	71
12.	Other Volcano Basal Diameters and Cone Volumes.....	71
13.	Explosive Eruptive Events, Duration, Power, and Estimated Mass Discharge Rates Used to Develop Probability Distributions for Eruptive Plume Dispersal Calculations .....	73
14.	Range of Observed Column Heights of Strombolian and Violent Strombolian Eruptions.....	77
15.	Estimated Bulk Clast Size Distribution Parameters for Three Violent Strombolian Eruptions (Tolbachik and Cerro Negro 1971 and 1968) and One Strombolian Eruption (Etna 1971).....	78
16.	Median Grain Sizes for the 80,000-year-Old Lathrop Wells Cone Tephra.....	79
17.	Grain Size Data for Crater Deposits in the Lathrop Wells Cone.....	86
18.	Lithic Clast Measurements in the Lathrop Wells Scoria Cone.....	87
19.	Samples Used to Characterize the Proximal Scoria Fall Section .....	92
20.	Grain Size Variations in Scoria Fall Section Close to the Southern Base of Lathrop Wells Cone.....	92
21.	Percent Pyroclasts in Samples in Scoria Fall Section Close to the Southern Cone Base.....	93

**TABLES (Continued)**

	<b>Page</b>
22. Composite of Samples Used to Characterize the Hydrovolcanic Sequence and Underlying Tephra Fall Sequence ( <i>tephra fall samples are in italics</i> ).....	97
23. Grain Size Variations in Hydrovolcanic Sequence and Underlying Tephra Fall Sequence ( <i>tephra fall samples are in italics</i> ).....	97
24. Percent Pyroclasts in Samples in Hydrovolcanic Sequence .....	98
25. Grain Size Variations in the Colluvium and Tephra Fall Section .....	102
26. Percent Pyroclasts in Samples in the Colluvium and Tephra Fall Section.....	103
27. Grain Size Variations in Tephra Section Overlying Ridge of Miocene Welded Tuff.....	103
28. Grain Size Variations in Tephra Fall for Section F .....	104
29. Percent Pyroclasts in Samples in Tephra Fall for Section F.....	106
30. Grain Size Variations in Tephra Fall for Section E .....	109
31. Percent Pyroclasts in Samples in Tephra Fall for Section E.....	111
32. Grain Size Variations in Tephra Fall for Section B.....	114
33. Percent Pyroclasts in Samples in Tephra Section B .....	115
34. Volumes of Lathrop Wells Cone, Lava, and Tephra .....	116
35. Ash Weight Percentages in Samples of Drainage Channels near Lathrop Wells Cone .....	132
36. Interpretation of 137-Cesium Profile Values for Samples from the Fortymile Wash Alluvial Fan .....	142
37. List of Input Parameters and Uncertainty Type.....	148
38. Technical Product Output for This Scientific Analysis Report .....	155

## 1. PURPOSE

The purpose of this scientific analysis report, *Characterize Eruptive Processes at Yucca Mountain, Nevada*, is to present information about natural volcanic systems and the parameters that can be used to model their behavior. This information is used to develop parameter-value distributions appropriate for analysis of the consequences of volcanic eruptions through a repository at Yucca Mountain.

The current revision to this report accomplishes the following four objectives:

1. Updates values from scientific literature sources for the volcanic or magmatic parameters listed in REV 00 ICN 01 (BSC 2001 [DIRS 160130]) of this report. (Note: The six-digit numerical identifier in brackets next to each reference callout throughout this report is the Yucca Mountain Project's (YMP) Document Input Reference System [DIRS] number, the purpose of which is to assist the reader in locating a specific reference in the DIRS database.)
2. Includes results of investigation of the physical volcanology, including calculation of eruptive volumes, of the Lathrop Wells Cone cinder cone, lava flows, and tephra sheet, and interprets the eruption sequence at the cone.
3. Reports on the findings of a study of volcanic ash redistribution that could occur after a hypothetical eruption of basaltic magma at Yucca Mountain.
4. Includes the eruption volumes of relevant (analog) volcanoes that were previously reported in the scientific analysis report *Characterize Framework for Igneous Activity at Yucca Mountain, Nevada*, (CRWMS M&O 2000 [DIRS 151551]).

Many aspects of this work apply to the resolution of several Igneous Activity Key Technical Issues identified by the U.S. Nuclear Regulatory Commission (NRC) (NRC 1999 [DIRS 151592], p. 3; NRC 2002 [DIRS 159538], p. 3.2.2-3). Sub-issues 1 and 2 address the probability and consequence of igneous activity at the repository site, respectively.

This scientific analysis report provides information for the calculations in three other reports that are currently under revision or development: *Number of Waste Packages Hit by Igneous Intrusion*, (BSC 2003 [DIRS 164650]); model report *Atmospheric Dispersal and Deposition of Tephra from a Potential Volcanic Eruption at Yucca Mountain, Nevada* [DIRS 161840]; and *Dike/Drift Interactions*, (BSC 2003 [DIRS 165923]).

Section 6 of this document lists the parameters and values that can be used to model processes of shallow subsurface and surface volcanic activity relevant to a repository at Yucca Mountain. Section 6.1 discusses the scientific approach, background, and data sources. Features, events, and processes (FEPs) supported by the analysis within this report are listed in Section 6.2. The eruptive processes analysis is documented in Section 6.3 and includes considerations of the geometry of volcanic feeder systems, which are of primary importance in modeling how much area and volume of the repository might be affected by an intrusion of a feeder system. The analysis of the intersection of ascending magma with repository drifts is the subject of the model

report *Dike/Drift Interactions*, (BSC 2003 [DIRS 165923]). This discussion in Section 6.3 is followed by a description of the physical and chemical properties of the basaltic magma, which influence both eruptive styles and mechanisms for interaction with radioactive waste packages. Eruptive processes, including the ascent velocity of magma at depth, onset of bubble nucleation and growth in the rising magmas, magma fragmentation, and velocity of the resulting gas-particle mixture, are then discussed. The duration of eruptions, their power output, and mass discharge rates are also described.

Section 6.4 provides results of both the field work and laboratory analyses and the interpretation of eruptive scenarios for the Lathrop Wells Cone, which is a young cinder cone/tephra sheet/lava flow complex 18 kilometers (km) south of the repository site. Emphasis on the Lathrop Wells Cone is engendered by its young age and the cone's excellent state of preservation, combined with active quarrying operations that expose some of the cone interiors. Additionally, the *Final Report of the Igneous Activity Peer Review Panel* (Detournay et al. 2003 [DIRS 162914], pp. 12-13) concurs with the earlier conclusion in Perry et al. (1998 [DIRS 144335], p. vi) that the younger post-Timber Mountain caldera basalts (less than ~5 million years [Ma] old) provide the critical basis for forecasting future possible magmatic activity in the Yucca Mountain region (YMR). The Lathrop Wells Cone retains many volcanic products and features of a young vent and, therefore, provides the best analog of a potential eruptive center.

Section 6.5 discusses results from field and laboratory studies on the natural processes of redistribution of ash after deposition of a basaltic tephra sheet from a hypothetical volcanic eruption near the site of the Yucca Mountain repository. Ash redistribution, if incorporating radioactive waste particles brought up during eruption directly through a repository, might be a contributor to dose to a potential receptor in areas removed from the initial ash deposition area.

The revision to this scientific analysis report is conducted in accordance with the *Technical Work Plan for Igneous Activity Analysis*, (BSC 2003 [DIRS 164143]), and *Test Plan for Ash Redistribution, Lava Morphology, and Igneous Processes Studies*, (BSC 2002 [DIRS 158185]). There were no deviations from the work scope and procedures as described in the *Technical Work Plan* (BSC 2003 [DIRS 164143]).

## 2. QUALITY ASSURANCE

This analysis reports on igneous and sedimentary processes that are important to the demonstration of compliance with the post-closure performance objectives prescribed in 10 CFR 63.113. Therefore, it is classified as a "Safety Category - 1" with regard to importance to waste isolation, as defined in AP-2.22Q, *Classification Criteria and Maintenance of the Monitored Geologic Repository Q-List*.

This report was prepared under procedure AP-SIII.9Q, *Scientific Analyses*. The report contributes to the analysis and modeling data used to support performance assessment. The conclusions do not directly impact engineered features important to preclosure safety, as defined in AP 2.22Q. There were no deviations from the work scope and procedures as described in the *Technical Work Plan* (BSC 2003 [DIRS 164143]). In addition, the electronic management of

data was accomplished in accordance with the controls specified in the aforementioned *Technical Work Plan* (BSC 2003 [DIRS 164143]).

### **3. USE OF SOFTWARE**

Standard, built-in functions of Microsoft Excel X, Service Release 1, for the Macintosh and personal computers were used to calculate parameters. This software is exempt from the requirements of AP-SI.1Q, *Software Management*. All other calculations were done using a hand-held calculator. The output was visually checked for correctness, and results were spot-checked for accuracy and reasonableness using an electronic calculator.

Standard functions of Microsoft Excel X for Macintosh running Mac OS X (V 10.2) were used to obtain averages, medians, modes, and standard deviations as listed in this report.

Input for these standard functions consisted of subsets of sieve-fraction weight percent (wt%), microscopic grain counts for pyroclast types in samples, and counts of lithic clasts quantities and sizes as measured in outcrops at Lathrop Wells volcano. Outputs consisted of averages and medians along with the associated standard deviations and modes, depending on the type of statistical function required for sufficient description of the data distribution.

A scoping study presented in Section 6.5.1.5 provides information on ash and sediment redistribution due to slope and fluvial processes after a hypothetical volcanic eruptive event at Yucca Mountain. The scoping study uses results of ASHPLUME v. 1.4LV (BSC 2002 [DIRS 161296]) (Section 4.2) and an analysis from ARC Map Geographic Information System (GIS) based on a digital elevation model (DEM) of the Fortymile Wash watershed near Yucca Mountain. The conclusions of this scoping study are not technical product output of this analysis report, but suggest a direction for future landscape modeling for an eruptive event scenario.

### **4. INPUTS**

#### **4.1 DATA, PARAMETERS, AND OTHER INPUTS**

In this scientific analysis report, pertinent scientific literature is reviewed and some simple theoretical concepts are developed. This information is used to recommend parameter distributions for use in the YMP total system performance assessment (TSPA) calculations. Where possible, parameter distributions are based on data available in published sources. In cases where there are insufficient published data, parameter distributions are recommended that conservatively capture the expected range based on the judgment of the authors. Data derived from field observations, sampling, and laboratory measurements are used to infer the volcanic history of Lathrop Wells Cone volcano, including volume calculations for effusive and explosive products. These data refine the distribution of volumes of eruptions used in the TSPA for sampling eruptive volumes for analysis of volcanic disruption of the repository.

### 4.1.1 Data

The location and a brief description of data and assumed values that were used as input for this report are listed in Table 1. Qualification status of the inputs is indicated in the DIRS database.

Table 1. Summary of Data Used as Inputs for Calculations in This Scientific Analysis Report

<b>Data Used</b>	<b>Application of Data</b>	<b>Data Sources (Data Tracking Number [DTN])</b>	<b>Location in This Report</b>
45 chemical analyses of products from Lathrop Wells volcano	Calculation of mean chemical composition of Lathrop Wells products	LA00000000099.002	Section 6.3.2.1
18 1-m <sup>2</sup> areas in quarry or road-cut exposures and manual counts of xenolithic material in Lathrop Wells volcano	Calculation of percent xenoliths in support of volcanic history of Lathrop Wells volcano	LA0302GH831811.003	Section 6.4.1.2
53 grain size data for Lathrop Wells volcano tephra	Description of volcanic history of Lathrop Wells volcano, including grain size distribution and sorting characteristics	LA0302GH831811.002	Sections 6.3.5.2, 6.4.1.1, 6.4.2.2, and 6.4.2.3
Grain counts from tephra deposits around Lathrop Wells volcano	Description of volcanic history of Lathrop Wells volcano, including particle morphology and composition	LA0302GH831811.004	Sections 6.1.3.1, 6.4.2.2 and 6.4.2.3
Tephra thicknesses at specific locations at Lathrop Wells volcano	Description of volcanic history of Lathrop Wells volcano, including tephra volume	LA0305DK831811.001	Section 6.5.1.4
66 cesium-137 analyses for Fortymile Wash alluvial fan in Amargosa Valley (Attachment, this report)	Ash redistribution analyses in a YMR drainage alluvial fan	LA0302CH831811.002	Section 6.5.2.3
9 basaltic ash contents of surficial material samples in drainages around Lathrop Wells Cone	To evaluate ash distribution along drainages below the Lathrop Wells Cone	LA0302CH831811.001	Section 6.5.1.4

### 4.1.2 Other Inputs

Locations and descriptions of information inputs to support methodologies, assumptions, and calculations in this report are listed in Table 2 and discussed as assumptions in Section 5.

Table 2. Summary of Sources of Information to Support Methodologies, Assumptions, and Calculations in This Scientific Analysis Report

Information Used	Application of Information	Sources	Location in This Report
Discussion of Lathrop Wells volcano conduit diameter. Xenolith (lithic) content at Lathrop Wells volcano.	Development of distribution of conduit diameters for potential volcano in the YMR. Discussion of entrainment of waste during a potential eruption.	Doubik and Hill (1999 [DIRS 115338], pp. 60-61); this report, Section 6.4.1.2	Sections 6.3.1, 6.3.4, 6.4.1.2
Diameter of Grants Ridge plug.	Development of distribution of conduit diameters for potential volcano in the YMR.	Keating and Valentine (1998 [DIRS 111236], p. 41); WoldeGabriel et al. (1999 [DIRS 110071], p. 392)	Section 6.3.1
Dike width measurements in the YMR. Ratios of fallout-sheet volume to cone volume for violent Strombolian eruptions.	Comparison with dike width distribution suggested in this report. Discussion of characteristics of fallout and cone deposits from violent Strombolian eruptions.	Crowe et al. (1983 [DIRS 100972], pp. 266, 272)	Sections 6.3.1, 6.3.3.4.2, 6.3.3.4.3, 6.3.5.2, 6.4.1.2, 6.4.3.1, and 6.4.4
Experimental constraints on water content of basaltic magmas.	Constraints in developing distribution for water content of potential volcano in the YMR.	Knutson and Green (1975 [DIRS 106299], Fig. 1, p. 126)	Sections 6.3.2.2, 6.3.2.4
Relationship between temperature and composition for basaltic magmas.	Calculation of temperatures of magmas forming potential YMR volcanoes.	Sisson and Grove (1993 [DIRS 122564], pp. 167, 178)	Sections 6.3.2.2, 6.3.2.4
Composition of gases from eight historically active volcanoes.	Calculation of mean gas composition and associated uncertainty.	Symonds et al. (1994 [DIRS 101029], Tables 3-5)	Section 6.3.2.3
Equation relating water saturation to pressure in basaltic magmas.	Calculation of saturation pressures, exsolution depths, and volume fraction of gas in magma as a function of pressure.	Jaupart and Tait (1990 [DIRS 118292], p. 219)	Sections 6.3.2.4, 6.3.3, and 6.3.3.2
Method for calculating magma viscosity as a function of composition.	Calculation of viscosities of magmas forming potential YMR volcanoes.	Shaw (1972 [DIRS 126270], pp. 873, 878)	Section 6.3.2.4
Equation for density of basaltic magmas.	Calculation of magma density for potential YMR volcanoes.	Ochs and Lange (1999 [DIRS 144330], pp. 1314-1315, Eq. 2)	Section 6.3.2.4
Estimate of magma flow rate necessary to form aa lavas.	Discussion of constraints on magma discharge rates at YMR volcanoes.	Rowland and Walker (1990 [DIRS 115463], p. 626)	Section 6.3.3
Theoretical equations and results describing the ascent of basaltic magmas.	Equation for velocity of magma below exsolution depths, relationship between magma-gas mixture density and water mass fraction, plots of eruption velocity as a function of initial water content of magmas.	Wilson and Head (1981 [DIRS 101034], pp. 2974, 2983, Eqs. 16-18)	Sections 6.3.3.1, 6.3.3.3, Figs. 8, 9

Table 2. Summary of Sources of Information to Support Methodologies, Assumptions, and Calculations in this Scientific Analysis Report (Continued)

Information Used	Application of Information	Sources	Location in This Report
Review of studies on the volume fraction of gas in a magma at which the magma fragments.	Discussion of magma fragmentation criteria.	Mader (1998 [DIRS 144419], pp. 55-56)	Section 6.3.3.2
Data on volumes and durations of scoria (cinder) cone-forming eruptions.	Constraints on duration of potential volcanic eruptions in the YMR.	Wood (1980 [DIRS 116536], p. 402)	Section 6.3.3.4.1, and 6.3.3.4.3
Duration and power output of explosive eruptive phases at Cerro Negro, Hekla, Tolbachik, Parícutin, and Heimaey volcanoes.	Calculation of mass discharge rates of explosive eruptive phases.	Jarzemba (1997 [DIRS 100460], p. 136)	Sections 6.3.3.4.3, 6.3.5.2, and 6.3.5.3
Bulk grain size for eruptions at Cerro Negro, Tolbachik, and Mount Etna.	Estimation of statistics of grain size distributions for explosive basaltic eruptions.	Maleyev and Vande-Kirkov (1983 [DIRS 144325], pp. 61-62); Rose et al. (1973 [DIRS116087], p. 342); McGetchin et al. (1974 [DIRS 115469], p. 3264)	Section 6.3.5.2
Estimated bulk density of pyroclastic fallout deposits.	Recommendations for treatment of bulk deposit density in consequence analyses.	Blong (1984 [DIRS 144263], p. 208); Sparks et al. (1997 [DIRS 144352], p. 366)	Section 6.3.5.4

## 4.2 CRITERIA

This scientific analysis report provides technical bases for parameters that will be used by the License Application (LA) related to the effects of a volcanic eruption through the YMR. The report provides discussion and summaries of uncertainties associated with inputs to the analysis and outputs from the analysis. The information and data in this report, which is direct input to the TSPA, are based largely on literature values and simple calculations as described in Section 6 and discussed in *Data Qualification Report: Data Related to Characterization of Eruptive Processes for Use on the Yucca Mountain Project* (CRWMS M&O 2000 [DIRS 156980], p. 17). Other information that indirectly relates to assessment of a potential igneous disruption of the repository and post-eruption processes, such as descriptions of the Lathrop Wells Cone and redistribution of ash, is based on field studies and supporting laboratory analyses. The following text identifies information in this report that addresses the *Yucca Mountain Review Plan* (YMRP) (NRC 2003 [DIRS 163274]) acceptance criteria and/or review methods related to descriptions of site characterization work, volcanic disruption of waste packages, airborne transport of radionuclides, and redistribution of radionuclides in soil.

The general requirements to be satisfied by TSPA are stated in 10 CFR 63.114. Technical requirements to be satisfied by TSPA are identified in the *Yucca Mountain Projects Requirements Document* (Canori and Leitner 2003 [DIRS 161770]). The acceptance criteria that will be used by the NRC to determine whether the technical requirements have been met are

identified in the YMRP (NRC 2003 [DIRS 163274]). The pertinent requirements and criteria for this scientific analysis report are summarized in Table 3.

Table 3. Project Requirements and YMRP Acceptance Criteria Applicable to This Analysis Report

Requirement Number <sup>a</sup>	Requirement Title <sup>a</sup>	10 CFR 63 Link	YMRP Acceptance Criteria <sup>b</sup>
PRD-002/T-004	Content of Application	10 CFR 63.21(b)(5)	Criteria 2 for <i>Description of Site Characterization Work</i>
PRD-002/T-015	Requirements for Performance Assessment	10 CFR 63.114 (a-c, e-g)	Criteria 1-5 for <i>Volcanic Disruption of Waste Packages</i>
PRD-002/T-004	Content of Application	10 CFR 63.21(c)(1), (9), (15), and (19)	Criteria 1-5 for <i>Airborne Transport of Radionuclides</i>
PRD-002/T-004	Content of Application	10 CRF 63.21(c)(1), (9), (15), and (19)	Criteria 1-5 for <i>Redistribution of Radionuclides in Soil</i>

NOTES: <sup>a</sup>From Canori and Leitner (2003 [DIRS 161770]).

<sup>b</sup>From NRC (2003 [DIRS 163274], Sections 1.5.3; 2.2.1.3.10.3; 2.2.1.3.11.3; 2.2.1.3.13.3).

#### 4.2.1 Description of Site Characterization Work Criteria

The acceptance criteria identified in Section 1.5, Description of Site Characterization Work, of the YMRP (NRC 2003 [DIRS 163274]) are given below, followed by a description (indented) of how elements in this report satisfy the criteria.

YMRP Section 1.5.3, Acceptance Criteria:

Acceptance Criterion 2: The “General Information” section of the license application contains an adequate description of site characterization results.

1. A sufficient understanding is provided of current features and processes present in the Yucca Mountain region.

Section 6 of this report provides basic descriptive information about the volcanic eruptive products and processes that resulted in the surface deposition of the scoria cone, lava flows, and tephra fall associated with the Lathrop Wells Cone. The Lathrop Wells Cone is the youngest volcanic expression known in the YMR and is considered to exemplify the type of eruptive phenomena that would occur during a future eruption of basaltic magma in the region. The Lathrop Wells Cone is the southernmost surface expression of the Crater Flat Volcanic Zone, which, in large part, defines the probabilistic volcanic hazard for the repository (*Characterize Framework for Igneous Activity at Yucca Mountain, Nevada*, BSC 2003 [DIRS 163769]). The eruptive volumes of scoria (cone), lava, and tephra help define the eruption volume for future use in the model report *Atmospheric Dispersal and Deposition of Tephra from a Potential Volcanic Eruption at Yucca Mountain, Nevada*. The eruptive processes at Lathrop Wells Cone, as inferred from analysis of lithologies preserved in the cone and tephra sheet, help define the processes of mass ejection from the volcanic vent for both proximal (ballistic) and distal (ash

cloud) distances. Further, this report defines properties of magma that directly influence the interaction of a magma-filled dike(s) with a subsurface repository that are direct inputs to TSPA. Finally, the report discusses the processes of ash and sediment redistribution from the Yucca Mountain site to depositional sites along Fortymile Wash and the Fortymile Wash alluvial fan located in the Amargosa Valley.

2. An adequate understanding is provided for future events and processes likely to be present in the Yucca Mountain region that could affect repository safety.

This report provides basic descriptive information about the volcanic eruptive processes that are characteristic of the YMR, as exemplified by features observed at Lathrop Wells Cone. The information also recommends parameter values that are needed to model igneous processes or as inputs to TSPA-LA models that support the analysis of the direct-release and indirect-release volcanic scenarios. The report identifies information that has been collected from the YMR, as well as information developed from studies at analog sites or developed from the review of published literature. The report also provides the technical basis for the use of the Lathrop Wells volcanic center as the most appropriate analog for a future volcanic eruption through the repository at Yucca Mountain.

#### **4.2.2 Description of Volcanic Disruption of Waste Packages Criteria**

The acceptance criteria identified in Section 2.2.1.3.10, Volcanic Disruption of Waste Packages, of the YMRP (NRC 2003 [DIRS 163274]) are given below, followed by a short description (indented) of how elements in this report satisfy the criteria.

YMRP Section 2.2.1.3.10.3, Acceptance Criteria:

Acceptance Criterion 1: System description and model integration are adequate.

1. TSPA adequately incorporates important design features, physical phenomena, and couplings, and uses consistent and appropriate assumptions throughout the volcanic disruption of the waste package abstraction process.

This report provides basic descriptive information about the volcanic eruptive processes that are characteristic of the YMR, as exemplified by features observed at Lathrop Wells Cone. The report also recommends parameter values that are needed to model igneous processes or as inputs to TSPA-LA models that support the analysis of the direct-release and indirect-release volcanic scenarios. This report describes the basis for the parameters used in the models and traces the use of inputs forward into analyses and models that use these parameters (e.g., *Interactions* (BSC 2003 [DIRS 165923]) and *Igneous Intrusion Impacts on Waste Packages and Waste Forms* (BSC 2003 [DIRS 165002])).

2. Models used to assess volcanic disruption of waste packages are consistent with physical processes generally interpreted from igneous features in the Yucca Mountain region and/or observed at active igneous systems.

This report provides basic descriptive information about the volcanic eruptive processes that are characteristic of the YMR, as exemplified by features observed at Lathrop Wells Cone. The report also recommends parameter values that are needed to model igneous processes or as inputs to TSPA-LA models that support the analysis of the direct-release and indirect-release volcanic scenarios. Characteristics of eruptive conduits, dike widths, and dike swarms are described in Section 6.3.1. Chemical characteristics of igneous material are described in Section 6.3.2. The processes associated with volcanic eruptions are described in Section 6.3.3, and processes that might entrain radioactive waste in eruption products are described in Section 6.3.4. Finally, ash plumes and associated deposits are described in Section 6.3.5. The report describes the basis for the parameters used in the volcanic scenarios and traces the outputs forward into analyses that use these parameters. The report identifies information that has been collected from the YMR, as well as information developed from studies at analog sites or developed from the review of published literature. The report also provides the technical basis for the use of the Lathrop Wells volcanic center as the most appropriate analog for a future volcanic eruption through the repository at Yucca Mountain. A potential eruption scenario at the Yucca Mountain repository is described in Section 6.6.

3. Models account for changes in igneous processes that may occur from interactions with engineered repository systems.

This report does not address changes in igneous processes that might occur as a result of interactions with engineered repository systems. Possible changes have been analyzed and documented in *Dike/Drift Interactions* (BSC 2003 [DIRS 165923]). Interactions between magma and engineered repository materials is addressed in *Igneous Intrusion Impacts on Waste Packages and Waste Forms* (BSC 2003 [DIRS 165002]). The technical basis for the waste particle size distribution used in the TSPA volcanic eruption model is provided in *Miscellaneous Waste-Form FEPs* (CRWMS M&O 2001 [DIRS 153938]).

4. Guidance in NUREG-1297 and NUREG-1298 (Altman et al. 1988 [DIRS 103597]; 1988 [DIRS 103750]) or other acceptable approaches is followed.

Peer review methods and qualification of existing data were not used in the development of this report.

Acceptance Criterion 2: Data are sufficient for model justification.

1. Parameter values used in the license application to evaluate volcanic disruption of waste packages are sufficient and adequately justified. Adequate description of how the data were used, interpreted, and appropriately synthesized into the parameters are provided.

This report provides basic descriptive information about the volcanic eruptive processes that are characteristic of the Yucca Mountain region. The report describes the synthesis of the information into parameter values that are needed to model igneous processes and provides the technical basis for inputs to TSPA-LA models that support the analysis of the direct-release and indirect-release volcanic scenarios. The report also traces the parameter outputs forward into analyses and models that use these parameters. A potential eruption scenario at the Yucca Mountain repository is described in Section 6.6.

2. Data used to model processes affecting volcanic disruption of waste packages are derived from appropriate techniques. These techniques may include site-specific field measurements, natural analog investigations, and laboratory experiments.

The report identifies information that has been collected from site-specific field measurements in the Yucca Mountain region as well as information that has been developed from studies at analog sites or developed from the review of published literature. Data have also been obtained from samples collected and analyzed by procedures governed by a strict quality assurance program. Data, parameters, and other inputs are described in Section 4.1. A potential eruption scenario at the Yucca Mountain repository is described in Section 6.6. Data uncertainties for inputs to, and outputs from, this analysis and limitations on use of outputs are described in detail in Sections 6.7.1 and 7.2. The report also provides the technical basis for the Lathrop Wells volcanic center being the most appropriate analog for a future volcanic eruption through the repository at Yucca Mountain.

3. Sufficient data are available to integrate features, events, and processes relevant to the volcanic disruption of waste packages into process-level models, including determination of appropriate interrelationships and parameter correlations.

The report identifies information that has been collected from the Yucca Mountain region as well as information that has been developed from studies at analog sites or developed from the review of published literature. FEPs relevant to this analysis are discussed in Section 6.2. These FEPs have guided the approach to field observation and collection/analysis of appropriate samples and sample parameters. Sufficient data are collected to help integrate the relevant FEPs into process-level models (Section 4.1). The report describes the relevant

eruptive processes and describes the development of parameters based on the integration of those FEPs. Characteristics of igneous material are described in Section 6.3.2. Relationships between various magma characteristics and their effects on an eruption are described in Section 6.3.3. Processes related to entrainment of waste in an ascending magma are described in Section 6.3.4, and ash plumes and their deposits are discussed in Section 6.3.5. The physical volcanology of the Lathrop Wells Cone and its suitability as an analog for a future eruption through the repository are discussed in Section 6.3.5. A potential eruption scenario at the Yucca Mountain repository is described in Section 6.6. Process-level models that use the parameters developed from these processes are described in other reports (e.g., *Dike/Drift Interactions* (BSC 2003 [DIRS 165923]); *Igneous Intrusion Impacts on Waste Packages and Waste Forms* (BSC 2003 [DIRS 165002])). Output parameters from this analysis and associated uncertainties are described in Section 7.2. Interrelationships and correlations between parameters are described in Section 6.

4. Where sufficient data do not exist, the definition of parameter values and associated conceptual models is based on the appropriate use of expert elicitation, conducted in accordance with NUREG-1563 (Kotra et al. 1996 [DIRS 100909]). If other approaches are used, the U.S. Department of Energy adequately justifies their use.

Expert elicitation was not used to develop parameter values and associated conceptual models described in this report.

Acceptance Criterion 3: Data uncertainty is characterized and propagated through the model abstraction.

1. Models use parameter values, assumed ranges, probability distributions, and bounding assumptions that are technically defensible, and reasonably account for uncertainties and variabilities, and do not result in an under-representation of the risk estimate.

The report identifies information that has been collected from the Yucca Mountain region as well as information that has been developed from studies at analog sites or developed from the review of published literature. Data uncertainties for inputs to, and outputs from, this analysis and limitations on use of outputs are described in detail in Sections 6.7.1 and 7.2. The report also traces the parameter outputs forward into analyses that use these parameters. However, the report does not discuss the specific uses of the parameters in the downstream models, nor does the report discuss potential effects of parameter variations on the representation of risk.

2. Parameter uncertainty accounts quantitatively for the uncertainty in parameter values observed in site data and available literature (i.e., data precision) and the uncertainty in abstracting parameter values to process-level models (i.e., data accuracy).

Data uncertainties for inputs to, and outputs from, this analysis and limitations on use of outputs are described in detail in Sections 6.7.1 and 7.2, and are discussed individually with each derived parameter. The report also traces the parameter outputs forward into analyses that use these parameters. However, the report does not discuss how the parameters are used in the downstream models, nor does this report describe methods used to abstract parameter values into the downstream, process-level models.

3. Where sufficient data do not exist, the definition of parameter values and associated conceptual models is based on the appropriate use of expert elicitation, conducted in accordance with NUREG-1563 (Kotra et al. 1996 [DIRS 100909]). If other approaches are used, the U.S. Department of Energy adequately justifies their use.

Expert elicitation was not used to develop parameter values and associated conceptual models described in this report.

Acceptance Criterion 4: Model uncertainty is characterized and propagated through the model abstraction.

Data uncertainties for inputs to, and outputs from, this analysis and limitations on use of outputs are described in detail in Sections 6.7.1 and 7.2. The report also traces the parameter outputs forward into analyses that use these parameters. However, the analysis documented in this report does not produce process-level models of the volcanic disruption of waste packages, nor does it describe how uncertainties are propagated through downstream model abstractions.

Acceptance Criterion 5: Model abstraction output is supported by objective comparisons.

The analysis documented in this report does not produce abstractions of the volcanic disruption of waste packages.

#### **4.2.3 Description of Airborne Transport of Radionuclides Criteria**

The acceptance criteria identified in Section 2.2.1.3.11, Airborne Transport of Radionuclides, of the YMRP (NRC 2003 [DIRS 163274]) are given below, followed by a short description (indented) of how elements in this report satisfy the criteria.

YMRP Section 2.2.1.3.11.3, Acceptance Criteria

Acceptance Criterion 1: System description and model integration are adequate.

1. Total system performance assessment adequately incorporates important design features, physical phenomena, and couplings and uses consistent and appropriate assumptions throughout the airborne transport of radionuclides abstraction process.

This analysis report describes parameters that directly or indirectly influence the airborne transport of radionuclide particles via surface

volcanic eruption of basaltic magma after intersection with the waste-packages-filled drifts. This report provides the technical basis for the parameters, assumptions, and conceptual models used in modeling the airborne transport of radionuclides in *Atmospheric Dispersal and Deposition of Tephra from a Potential Volcanic Eruption at Yucca Mountain, Nevada* (BSC 2003 [DIRS 161840]).

2. Models used to assess airborne transport of radionuclides are consistent with physical processes generally interpreted from igneous features in the Yucca Mountain region and/or observed at active igneous systems.

Physical processes of eruption and emplacement of basaltic particulate matter are described in this report. Parameters that define many aspects of the processes and resulting deposits are provided for use in downstream models used to assess the airborne transport of radionuclides. The report provides basic descriptive information about the volcanic eruptive processes that are characteristic of the Yucca Mountain region, as exemplified by features observed at Lathrop Wells Cone. Characteristics of eruptive conduits, dike widths, and dike swarms are described in Section 6.3.1. Chemical characteristics of igneous material are described in Section 6.3.2. The processes associated with volcanic eruptions are described in Section 6.3.3, and processes that could entrain radioactive waste in eruption products are described in Section 6.3.4. Finally, ash plumes and associated deposits are described in Section 6.3.5. The report carefully identifies information that has been collected from the Yucca Mountain region as well as information developed from studies at analog sites or developed from the review of published literature. A potential eruption scenario at the Yucca Mountain repository is described in Section 6.6. The report also provides the technical basis for the use of the Lathrop Wells volcanic center as the most appropriate analog for a future volcanic eruption through the repository at Yucca Mountain (Section 6.4).

3. Models account for changes in igneous processes that may occur from interactions with engineered repository systems.

This report does not address changes in igneous processes that might occur as results of interactions with engineered repository systems. Such possible changes have been analyzed and documented in *Dike/Drift Interactions* (BSC 2003 [DIRS 165923]). Interactions between magma and engineered repository materials are addressed in *Igneous Intrusion Impacts on Waste Packages and Waste Forms* (BSC 2003 [DIRS 165002]).

4. Guidance in NUREG-1297 and NUREG-1298 (Altman et al. 1988 [DIRS 103597]; 1988 [DIRS 103750]) or other acceptable approaches is followed.

As noted previously, peer review methods and qualification of existing data were not used in the development of this report.

Acceptance Criterion 2: Data are sufficient for model justification.

1. Parameter values used in the license application to evaluate airborne transport of radionuclides are sufficient and adequately justified. Adequate description of how the data were used, interpreted, and appropriately synthesized into the parameters is provided.

This report provides basic descriptive information about the volcanic eruptive processes that are characteristic of the Yucca Mountain region. This report provides the technical basis for the parameters used in modeling the airborne transport of radionuclides in *Atmospheric Dispersal and Deposition of Tephra from a Potential Volcanic Eruption at Yucca Mountain* (BSC 2003 [DIRS 161840]). A potential eruption scenario at the Yucca Mountain repository that might result in airborne transport of radionuclides is described in Section 6.6. The report also traces the parameter outputs forward into analyses that use these parameters.

2. Data used to model processes affecting airborne transport of radionuclides are derived from appropriate techniques. These techniques may include site-specific field measurements, natural analog investigations, and laboratory experiments.

The report identifies information that has been collected from site-specific field measurements in the Yucca Mountain region as well as information that has been developed from the studies at analog sites or developed from the review of published literature (Section 6). A potential eruption scenario at the Yucca Mountain repository is described in Section 6.6. Data uncertainties for inputs to, and outputs from, this analysis and limitations on use of outputs are described in detail in Sections 6.7.1 and 7.2. The report also provides the technical basis for the Lathrop Wells volcanic center being the most appropriate analog for a future volcanic eruption through the repository at Yucca Mountain.

3. Sufficient data are available to integrate features, events, and processes relevant to the airborne transport of radionuclides into process-level models, including determination of appropriate interrelationships and parameter correlations.

The report identifies information that has been collected from site-specific field measurements in the Yucca Mountain region as well as information that has been developed from studies at analog sites or developed from the review of published literature (Sections 4.1 and 6). FEPs relevant to this analysis are discussed in Section 6.2. The report describes the relevant eruptive processes and describes the development of parameters based on

the integration of those processes. Characteristics of igneous material are described in Section 6.3.2. Relationships between various magma characteristics and their effects on an eruption are described in Section 6.3.3. Processes related to entrainment of waste in an ascending magma are described in Section 6.3.4, and ash plumes and their deposits are discussed in Section 6.3.5. The physical volcanology of the Lathrop Wells Cone and its suitability as an analog for a future eruption through the repository are discussed in Section 6.3.5. A potential eruption scenario at the Yucca Mountain repository is described in Section 6.6. Process-level models that use the parameters developed from these processes are described in other reports (e.g., *Dike/Drift Interactions* (BSC 2003 [DIRS 165923]); *Igneous Intrusion Impacts on Waste Packages and Waste Forms* (BSC 2003 [DIRS 165002])). Interrelationships and correlations between parameters are described in Section 6.

4. Where sufficient data do not exist, the definition of parameter values and associated conceptual models is based on appropriate use of expert elicitation, conducted in accordance with NUREG-1563 (Kotra et al. 1996 [DIRS 100909]). If other approaches are used, the U.S. Department of Energy adequately justifies their use.

Expert elicitation was not used to develop parameter values and associated conceptual models described in this report.

Acceptance Criterion 3: Data uncertainty is characterized and propagated through the model abstraction.

1. Models use parameter values, assumed ranges, probability distributions, and bounding assumptions that are technically defensible, and reasonably account for uncertainties and variabilities, and do not result in an under-representation of the risk estimate.

The report identifies information that has been collected from the Yucca Mountain region as well as information that has been developed from studies at analog sites or developed from the review of published literature. Data uncertainties for inputs to, and outputs from, this analysis and limitations on use of outputs are described in detail in Sections 6.7.1 and 7.2. The report also traces the parameter outputs forward into analyses that use these parameters. However, the report does not discuss the specific uses of the parameters in the downstream models, nor does the report discuss potential effects of parameter variations on the representation of risk.

2. Parameter uncertainty accounts quantitatively for the uncertainty in parameter values observed in site data and the available literature (i.e., data precision) and the uncertainty in abstracting parameter values to process-level models (i.e., data accuracy).

Data uncertainties for inputs to, and outputs from, this analysis and limitations on use of outputs are described in detail in Sections 6.7.1 and 7.2. The report also traces the parameter outputs forward into analyses that use these parameters. However, the report does not discuss how the parameters are used in the downstream models, nor does this report discuss methods used to abstract parameter values into the downstream, process-level models.

3. Where sufficient data do not exist, the definition of parameter values and associated conceptual models is based on appropriate use of expert elicitation, conducted in accordance with NUREG-1563 (Kotra et al. 1996 [DIRS 100909]). If other approaches are used, the U.S. Department of Energy adequately justifies their use.

Expert elicitation was not used to develop parameter values and associated conceptual models described in this report.

Acceptance Criterion 4: Model uncertainty is characterized and propagated through the model abstraction.

Data uncertainties for inputs to, and outputs from, this analysis and limitations on use of outputs are described in detail in Sections 6.7.1 and 7.2. The report also traces the parameter outputs forward into analyses that use these parameters. However, the analysis documented in this report does not produce process-level models of the airborne transport of radionuclides.

Acceptance Criterion 5: Model abstraction output is supported by objective comparisons.

The analysis documented in this report does not produce abstractions of the airborne transport of radionuclides.

#### **4.2.4 Description of Redistribution of Radionuclides in Soil Criteria**

The acceptance criteria identified in Section 2.2.1.3.13, Redistribution of Radionuclides in Soil, of the YMRP (NRC 2003 [DIRS 163274]) are given below, followed by a short description (indented) of how elements in this report satisfy the criteria.

YMRP Section 2.2.1.3.13.3, Acceptance Criteria

Acceptance Criterion 1: System description and model integration are adequate.

1. Total system performance assessment adequately incorporates important design features, physical phenomena, and couplings and uses consistent and appropriate assumptions throughout the redistribution of radionuclides in the soil abstraction process.

Section 6.5 of the report describes the processes that could redistribute ash and waste particles from an eruption through a repository at Yucca Mountain. The conceptual model for ash redistribution is described in

Section 6.5.1.1. A study of ash dilution at the Lathrop Wells Cone is described in Section 6.5.1.2, and the results and interpretation are presented in Section 6.5.1.4. An ash-redistribution scoping study is described in Section 6.5.1.5, and the results of a study of cesium-137 concentrations in surficial material are presented in Section 6.5.2. Tephra thicknesses for the Lathrop Wells volcano are described in Section 6.7.1.5. Cesium-137 analysis results for the Fortymile Wash alluvial fan are described in Section 6.7.1.6, and the basaltic ash content of surficial materials around the Lathrop Wells Cone is described in Section 6.7.1.7. However, the analyses described in the report do not address the redistribution of radionuclides in the soil abstraction process. Model implementation is described in *Atmospheric Dispersal and Deposition of Tephra from a Potential Volcanic Eruption at Yucca Mountain, Nevada* (BSC 2003 [DIRS 161840]).

2. The total system performance assessment model abstraction identifies and describes aspects of redistribution of radionuclides in soil that are important to repository performance, including the technical bases for these descriptions. For example, the abstraction should include modeling of the deposition of contaminated material in the soil and determination of the depth distribution of deposited radionuclides.

Section 6.5 of the report describes the processes that could redistribute ash and waste particles from an eruption through a repository at Yucca Mountain. The conceptual model for ash redistribution is described in Section 6.5.1.1. A study of ash dilution at the Lathrop Wells Cone is described in Section 6.4.2, and the results and interpretation are presented in Section 6.5.1.4. An ash-redistribution scoping study is described in Section 6.5.1.5, and the results of a study of cesium-137 concentrations in surficial material are presented in Section 6.5.2. Tephra thicknesses for the Lathrop Wells volcano are described in Section 6.4.2. Cesium-137 analysis results for the Fortymile Wash alluvial fan are described in Section 6.5.2, and the basaltic ash content of surficial materials around the Lathrop Wells Cone is described in Section 6.5.1.2. The model abstraction used to assess the redistribution of radionuclides from secondary transport processes is discussed in *Atmospheric Dispersal and Deposition of Tephra from a Potential Volcanic Eruption at Yucca Mountain, Nevada* (BSC 2003 [DIRS 161840]).

3. Relevant site features, events, and processes have been appropriately modeled in the abstraction of redistribution of radionuclides from surface processes, and sufficient technical bases are provided.

A summary of the TSPA-LA disposition of FEP 1.2.04.07.0C, Ash Redistribution via Soil and Sediment Transport, is provided in Table 4 of this report. Information in this report constrains the consideration of the FEP and provides the basis to include the FEP in the TSPA-LA. The

previous item describes specific technical items that are addressed by information in this report.

4. Guidance in NUREG-1297 and NUREG-1298 (Altman et al. 1988 [DIRS 103597]; 1988 [DIRS 103750]) or other acceptable approaches is followed.

As noted previously, peer review methods and qualification of existing data were not used in the development of this report.

Acceptance Criterion 2: Data are sufficient for model justification.

1. Behavioral, hydrological, and geochemical values used in the license application are adequately justified (e.g., irrigation and precipitation rates, erosion rates, radionuclide solubility values, etc.). Adequate descriptions of how the data were used, interpreted, and appropriately synthesized into the parameters are provided.

Section 6.5 of the report describes the processes that could redistribute ash and waste particles from an eruption through a repository at Yucca Mountain. The conceptual model for ash redistribution is described in Section 6.5.1.1. A study of ash dilution at the Lathrop Wells Cone is described in Section 6.5.1.2, and the results and interpretation are presented in Section 6.5.1.4. An ash-redistribution scoping study is described in Section 6.5.1.5, and the results of a study of cesium-137 concentrations in surficial material are presented in Section 6.5.2. Tephra thicknesses for the Lathrop Wells volcano are described in Section 6.7.1.5. Cesium-137 analysis results for the Fortymile Wash alluvial fan are described in Section 6.7.1.6, and the basaltic ash content of surficial materials around the Lathrop Wells Cone is described in Section 6.7.1.7. Consideration of behavioral, hydrological, and geochemical processes referred to in the criteria (e.g., irrigation rates, plow depth, etc.) are discussed in biosphere analysis or model reports.

Table 4. Disruptive Events Included FEPs for This Scientific Analysis Report and Their Disposition in TSPA-LA

TSPA-SR FEP Number, Name, and Description	TSPA-LA FEP Number, Name, and Description	Section Where Disposition is Described	Summary of TSPA-LA Disposition
<p>1.2.04.03.00 Igneous Intrusion into Repository Magma from an igneous intrusion flows into the drifts and extends over a large portion of the repository site, forming a sill. The sill could be limited to the drifts or a continuous sill could form along the plane of the repository, bridging between adjacent drifts.</p>	<p>1.2.04.03.0A Igneous Intrusion into Repository Magma from an igneous intrusion flows into the drifts and extends over a large portion of the repository site, forming a sill, dike, or dike swarm depending on the stress conditions. This could involve multiple drifts. The sill could be limited to the drifts or a continuous sill could form along the plane of the repository, bridging between adjacent drifts.</p>	<p>Sec. 6.3.1</p>	<p>This report describes and constrains consideration of the FEP 1.2.04.03.0A, Igneous Intrusion Into Repository, and provides a technical basis for inclusion of the FEP in the TSPA-LA. This analysis report presents information about volcanic systems and parameters that can be used to model their behavior. This information is used to develop parameter value distributions appropriate for evaluation of the related FEPs and analysis of the consequences of volcanic eruptions through a repository at Yucca Mountain, Nevada. In particular, this report addresses the following aspects of the related FEP:</p> <ul style="list-style-type: none"> <li>• The geometry of volcanic feeder systems, which is of primary importance in predicting how much of a repository would be affected by an eruption</li> <li>• The physical and chemical properties of the magmas, which influence both eruptive styles and mechanisms for interaction with radioactive waste packages.</li> </ul> <p>The specific parameters developed in this document related to this FEP, include the following:</p> <ul style="list-style-type: none"> <li>• Magma chemistry (12 compounds) and magma water-content distribution</li> <li>• Gas composition (10 gases)</li> <li>• Magmatic temperature, viscosity, density, and ascent rate below vesiculation depth</li> <li>• Volatile exsolution depths and fragmentation depths.</li> </ul> <p>The use of the outputs from this report in other reports is summarized as follows:</p> <p><i>Number of Waste Packages Hit by Igneous Intrusion</i> (BSC 2003 [DIRS 164650])</p> <ul style="list-style-type: none"> <li>• Conduit diameter distribution</li> <li>• Dike-width distribution</li> <li>• Distribution of number of dikes in a swarm.</li> </ul> <p><i>Dike/Drift Interactions</i> (BSC 2003 [DIRS 165923])</p> <ul style="list-style-type: none"> <li>• Magmatic temperatures, viscosities, and densities used to determine the bulk density and bulk viscosity of magma, magma vesicle-free density, and intrusion temperature</li> <li>• Magma ascent rate below vesiculation depth (magma velocities)</li> <li>• Volatile exsolution depths and fragmentation depths</li> <li>• Dike width used to determine the dike far-field width.</li> </ul> <p>The results of this analysis report do not directly feed to the TSPA-LA model. Rather, the results provide input for the listed reports. Because the outputs of the listed reports are used either implicitly or explicitly in the TSPA-LA model, and the outputs of the listed reports are dependent on the underlying inputs documented in this analysis report, the underlying inputs and related FEPs are considered to be implicitly included in the TSPA-LA model.</p>

Table 4. Disruptive Events Included FEPs for This Scientific Analysis Report and Their Disposition in TSPA-LA (Continued)

TSPA-SR FEP Number, Name, and Description	TSPA-LA FEP Number, Name, and Description	Section Where Disposition is Described	Summary of TSPA-LA Disposition
<p>1.2.04.04.0A Magma Interacts with Waste</p> <p>An igneous intrusion in the form [of a dike] occurs through the repository, intersecting waste. This leads to accelerated waste container failure (e.g., attack by magmatic volatiles, damage by fragmented magma, thermal effects) and dissolution of waste (CNSF, DSNF, DHLW).</p>	<p>1.2.04.04.0A Igneous intrusion Interacts with EBS Components</p> <p>An igneous intrusion in the form of a dike occurs through the repository, intersecting the repository drifts. Magma, pyroclastics, and volcanic gases enter the drift and interact with the EBS components including the drip shields, the waste packages, pallet, and invert. This leads to accelerated drip shield and waste package failure (e.g., attack by magmatic volatiles, damage by flowing or fragmented magma, thermal effects) and dissolution or volatilization of waste.</p>	<p>Sec. 6.3.2</p>	<p>The report describes and constrains the consideration of the FEP 1.2.04.04.0A, Igneous Intrusion Interacts with EBS (Engineered Barrier System) Components, and provides a technical basis for inclusion of the FEP in the TSPA-LA. This analysis report includes the results of literature surveys of Peer-reviewed research and reporting of laboratory analysis of basaltic magmas and associated volatile-gases geochemistry. This information is used to develop parameter value distributions appropriate for evaluation of the related FEPs and analysis of the consequences of magma interusion and volcanic eruptions through a repository at Yucca Mountain, Nevada. In particular, this report addresses the following aspects of the related FEP:</p> <ul style="list-style-type: none"> <li>• The physical and chemical properties of the magmas, which influence both the mechanisms for interaction with radioactive waste packages and waste forms, and eruptive styles</li> <li>• Subsurface magma properties and eruptive processes, including the ascent velocity of magma at depth, the onset of bubble nucleation and growth in the rising magma, magma fragmentation, and velocity of the resulting gas-particle mixture</li> <li>• Geologic constraints (thermal, mechanical, and chemical) regarding the interaction between magma and waste packages.</li> </ul> <p>The use of the outputs from this analysis in the related report is summarized as follows: <i>Igneous Intrusion Impacts on Waste Packages and Waste Forms</i> (BSC 2003 [165002])</p> <ul style="list-style-type: none"> <li>• Magma chemistry</li> <li>• Water content of magmas</li> <li>• Volcanic gas composition</li> <li>• Magmatic temperatures, viscosities, and densities.</li> </ul> <p>The results of this analysis report do not directly feed to the TSPA-LA model. Rather, the results provide input for the listed reports. Because the outputs of the listed reports are used either implicitly or explicitly in the TSPA-LA model, and the outputs of the listed reports are dependent on the underlying inputs documented in this analysis report, the underlying inputs and related FEPs are considered to be implicitly included in the TSPA-LA model.</p>

Table 4. Disruptive Events Included FEPs for This Scientific Analysis Report and Their Disposition in TSPA-LA (Continued)

TSPA-SR FEP Number, Name, and Description	TSPA-LA FEP Number, Name, and Description	Section Where Disposition is Described	Summary of TSPA-LA Disposition
<p>1.2.04.06.00 Basaltic Cinder Cone Erupts through the Repository</p> <p>As a result of an igneous intrusion, a cinder cone forms at land surface. The conduit(s) supplying the vent(s) of the cone pass(es) through the repository, interacting with and entraining waste.</p>	<p>1.2.04.06.0A Eruptive Conduit to Surface Intersects Repository</p> <p>As a result of an igneous intrusion, a scoria cone forms at land surface. The conduit(s) supplying the vent(s) of the cone pass(es) through the repository, interacting with and entraining waste</p>	<p>Secs. 6.3.3, 6.3.4</p>	<p>This report describes and constrains the consideration of the FEP 1.2.04.06.0A, Eruptive Conduit to Surface Intersects Repository, and provides a technical basis for inclusion of the FEP in the TSPA-LA. This analysis report includes the results of field investigations dealing with physical volcanology and describes the conceptual models for eruptive processes including conduit formation. This information is used to develop parameter value distributions appropriate for evaluation of the related FEPs and analysis of the consequences of volcanic eruptions through a repository at Yucca Mountain, Nevada. In particular, this report addresses the following aspects of the related FEP:</p> <ul style="list-style-type: none"> <li>• The geometry of volcanic feeder systems, which is of primary importance in predicting how much of a repository would be affected by an eruption</li> <li>• The physical and chemical properties of the magmas, which influence both eruptive styles and mechanisms for interaction with radioactive waste packages</li> <li>• Eruptive processes, including the ascent velocity of magma at depth, the onset of bubble nucleation and growth in the rising magmas, magma fragmentation, and velocity of the resulting gas-particle mixture</li> <li>• Geologic constraints (thermal, mechanical, and chemical) regarding the interaction between magma and waste packages.</li> </ul> <p>The parameters related to this FEP developed in this document include the following:</p> <ul style="list-style-type: none"> <li>• Conduit diameter distribution</li> <li>• Eruptive power</li> <li>• Eruption duration for formation of an entire volcano</li> <li>• Eruption volume</li> <li>• Velocity as a function of depth.</li> </ul> <p>The use of the outputs from this report in other reports is summarized as follows:</p> <p><i>Number of Waste Packages Hit by Igneous Intrusion</i> (BSC 2003 [DIRS 164650])</p> <ul style="list-style-type: none"> <li>• Conduit diameter distribution</li> <li>• Dike width distribution</li> <li>• Distribution of number of dikes in a swarm.</li> </ul> <p><i>Igneous Intrusion Impacts On Waste Packages and Waste Forms</i> (BSC 2003 [DIRS 165002])</p> <ul style="list-style-type: none"> <li>• Magma chemistry</li> <li>• Water content of magmas</li> <li>• Volcanic gas composition</li> <li>• Magmatic temperatures, viscosities, and densities.</li> </ul> <p>The results of this analysis report do not directly feed to the TSPA-LA model. Rather, the results provide input for the listed reports. Because the outputs of the listed reports are used either implicitly or explicitly in the TSPA-LA model, and the outputs of the listed reports are dependent on the underlying inputs documented in this analysis report, the underlying inputs and related FEPs are considered to be implicitly included in the TSPA-LA model.</p>

Table 4. Disruptive Events Included FEPs for This Scientific Analysis Report and Their Disposition in TSPA-LA (Continued)

TSPA-SR FEP Number, Name, and Description	TSPA-LA FEP Number, Name, and Description	Section Where Disposition is Described	Summary of TSPA-LA Disposition
<p>1.2.04.07.00 Ashfall Finely-divided waste particles are carried up a volcanic vent and deposited at land surface from an ash cloud or pyroclastic flow.</p>	<p>1.2.04.07.0A Ashfall Finely-divided waste particles are carried up a volcanic vent and deposited at land surface from an ash cloud.</p>	<p>Sec. 6.3.5</p>	<p>This report describes and constrains the consideration of the FEP 1.2.04.07.0A, Ashfall, and provides a technical basis for inclusion of the FEP in the TSPA-LA. This analysis report includes the results of field investigations dealing with physical volcanology and with ash and tephra redistribution and includes the conceptual model for eruptive processes and for ash and tephra redistribution. This information is used to develop parameter value distributions appropriate for analysis of the consequences of volcanic eruptions through a repository at Yucca Mountain, Nevada. In particular, this report addresses the following aspects of the related FEP:</p> <ul style="list-style-type: none"> <li>• The duration of eruptions, their power output, and mass discharge rates</li> <li>• The bulk grain size produced by relevant explosive eruptions and grain shapes.</li> </ul> <p>The parameters developed in this document related to this FEP include the following:</p> <ul style="list-style-type: none"> <li>• Eruptive power</li> <li>• Eruption duration for formation of an entire volcano</li> <li>• Duration of a single explosive phase constituting a violent Strombolian eruptive phase</li> <li>• Eruption volume</li> <li>• Mean particle size erupted during violent Strombolian phases</li> <li>• Standard deviation of particle size distribution for a given mean</li> <li>• Clast characteristics/shape factor</li> <li>• Density of erupted particles</li> <li>• Tephra deposit density.</li> </ul> <p>The use of the outputs from this report in the relevant report is summarized as follows: <i>Atmospheric Dispersal and Deposition of Tephra from a Potential Volcanic Eruption at Yucca Mountain, Nevada</i> (BSC 2003 [DIRS 161840])</p> <ul style="list-style-type: none"> <li>• Mean ash particle diameter</li> <li>• Mean ash particle diameter standard deviation for particle size distribution</li> <li>• Ash particle shape factor</li> <li>• Density of erupted particles</li> <li>• Eruptive power, eruption duration, and eruption velocity at vent.</li> </ul> <p>The results of this analysis report do not directly feed to the TSPA-LA model. Rather, the results provide input for the listed report: Because the outputs of the listed report are used either implicitly or explicitly in the TSPA-LA model, and the outputs of the listed report are dependent on the underlying inputs documented in this analysis report, the underlying inputs and related FEPs are considered to be implicitly included in the TSPA-LA model.</p>

Table 4. Disruptive Events Included FEPs for This Scientific Analysis Report and Their Disposition in TSPA-LA (Continued)

TSPA-SR FEP Number, Name, and Description	TSPA-LA FEP Number, Name, and Description	Section Where Disposition is Described	Summary of TSPA-LA Disposition
	<p>1.2.04.07.0C Ash Redistribution Via Soil and Sediment Transport</p> <p>Following deposition of contaminated ash on the surface (see FEP 1.2.04.07.0A Ashfall) contaminated ash may be redistributed along the surface to the compliance point via eolian and fluvial processes.</p> <p>(NOTE: Preliminary screening decision is to include screening decision subject to change, although field studies may result in sufficient argument for exclusion based on low consequence.</p>	<p>Sec. 6.5.1</p>	<p>This report describes and constrains the consideration of the FEP 1.2.04.07.0C, Ash Redistribution via Soil and Sediment Transport, and provides a technical basis for inclusion of the FEP in the TSPA-LA. This analysis report includes both the results of field investigations of ash redistribution processes and products and the conceptual model for ash redistribution. This information from field investigations is used to develop values that constrain amounts of erosion, deposition, and dilution of ash and which are appropriate for analysis of the consequences of volcanic eruptions through a repository at Yucca Mountain, Nevada. In particular, this report addresses the following aspects of the related FEP:</p> <ul style="list-style-type: none"> <li>• The erosion/deposition of sediments on the Fortymile Wash alluvial fan.</li> </ul> <p>The parameters developed in this document related to this FEP include the following:</p> <ul style="list-style-type: none"> <li>• Ash dilution rate</li> <li>• Site erosion/aggradation estimate.</li> </ul> <p>The parameters for the FEP 1.2.04.07.0C, Ash Redistribution Via Soil and Sediment Redistribution, developed in this analysis report directly feed to the TSPA-LA model and the FEP is, therefore, explicitly included.</p>

2. Sufficient data (e.g., field, laboratory, and natural analog data) are available to adequately define relevant parameters and conceptual models necessary for developing the abstraction of redistribution of radionuclides in soil in the total system performance assessment.

The previous item describes the information provided in this report that is relevant to the analysis of ash deposition and redistribution from an eruption at a Yucca Mountain repository. The report does not address the abstraction of redistribution of radionuclides in soil for the TSPA.

Acceptance Criterion 3: Data uncertainty is characterized and propagated through the model abstraction.

1. Models use parameter values, assumed ranges, probability distributions, and bounding assumptions that are technically defensible, reasonably account for uncertainties and variabilities, do not result in an under-representation of the risk estimate, and are consistent with the characteristics of the reasonably maximally exposed individual.

Item 1, for Acceptance Criterion 1, describes the information provided in this report that is relevant to the analysis of ash deposition and redistribution from an eruption at a Yucca Mountain repository. The report does not address the representation of the risk estimate, nor does it address the characteristics of the reasonably maximally exposed individual.

2. The technical bases for the parameter values and ranges in the total system performance assessment abstraction are consistent with data from the Yucca Mountain region [e.g., Amargosa Valley survey (Cannon Center for Survey Research 1997)], studies of surface processes in the Fortymile Wash drainage basin, applicable laboratory testing, natural analogs, or other valid sources of data. For example, soil types, crop types, plow depths, and irrigation rates should be consistent with current farming practices, and data on the airborne particulate concentration should be based on the resuspension of appropriate material in a climate and level of disturbance similar to that which is expected to be found at the location of the reasonably maximally exposed individual during the compliance time period.

Item 1, for Acceptance Criterion 1, describes the information provided in this report that is relevant to the analysis of ash deposition and redistribution from an eruption at a Yucca Mountain repository. Studies specific to the Fortymile Wash drainage are described in Sections 6.5.1.3, 6.5.2.1, and 6.5.2.4. Effects of storms and climate changes on natural soil redistribution processes are described in Section 6.5.3.2. The report does not address biosphere topics of crop types, plow depths, irrigation rates, current farming practices, or airborne particulate concentrations.

3. Uncertainty is adequately represented in parameters for conceptual models, process models, and alternative conceptual models considered in developing the total system

performance assessment abstraction of redistribution of radionuclides in soil, either through sensitivity analyses, conservative limits, or bounding values supported by data, as necessary. Correlations between input values are appropriately established in the total system performance assessment.

Item 1, for Acceptance Criterion 1, describes the information provided in this report that is relevant to the analysis of ash deposition and redistribution from an eruption at a Yucca Mountain repository. Uncertainties associated with tephra thicknesses for the Lathrop Wells Volcano are described in Section 6.7.1.5. Uncertainties associated with cesium-137 analyses for the Fortymile Wash alluvial fan are described in Section 6.7.1.6, and uncertainties associated with the basaltic ash content of surficial material around the Lathrop Wells Cone are described in Section 6.7.1.7. Alternative conceptual models and parameters correlations are discussed in *Atmospheric Dispersal and Deposition of Tephra from a Potential Volcanic Eruption at Yucca Mountain, Nevada* (BSC 2003 [DIRS 161840]).

4. Parameters or models that most influence repository performance based on the performance measure and time period of compliance, specified in 10 CFR Part 63, are identified.

Discussion of the sensitivity of repository performance to specific TSPA-LA models or parameters is beyond the scope of this report and is not discussed.

5. Where sufficient data do not exist, the definition of parameter values and conceptual models on appropriate uses of other sources, such as expert elicitation, are conducted in accordance with appropriate guidance, such as NUREG-1563 (Kotra et al. 1996 [DIRS 100909]).

Expert elicitation was not used to develop parameter values and associated conceptual models described in this report.

Acceptance Criterion 4: Model uncertainty is characterized and propagated through the model abstraction.

1. Alternative modeling approaches of FEPs are considered and are consistent with available data and current scientific understanding, and the results and limitations are appropriately considered in the abstraction.

The characteristics of ash-redistribution processes, including a conceptual model for ash-dilution processes, are described in Section 6.5.1. A summary of the TSPA-LA disposition of FEP 1.2.04.07.0C, Ash Redistribution via Soil and Sediment Transport, is provided in Table 4 of this report. Information in this report constrains the consideration of the FEP and provides the basis to include the FEP in the TSPA-LA. This report does not address model abstraction.

2. Sufficient evidence is provided that appropriate alternative conceptual models of FEPs have been considered; that the preferred models (if any) are consistent with available data (e.g., field, laboratory, and natural analog) and current scientific understanding; and that the effect on total system performance assessment of uncertainties from these alternative conceptual models has been evaluated.

The characteristics of ash-redistribution processes, including a conceptual model for ash-dilution processes, are described in Section 6.5.1. A summary of the TSPA-LA disposition of FEP 1.2.04.07.0C, Ash Redistribution via Soil and Sediment Transport, is provided in Table 4 of this report. Information in this report constrains the consideration of the FEP and provides the basis to include the FEP in the TSPA-LA. This report does not address the effect on TSPA of uncertainties associated with consideration of alternative conceptual models.

3. Consideration of conceptual model uncertainty is consistent with available site characterization data, laboratory experiments, field measurements, natural analog information and process-level modeling studies; and the treatment of conceptual model uncertainty does not result in an under-representation of the risk estimate.

The characteristics of ash-redistribution processes, including a conceptual model for ash-dilution processes, are described in Section 6.5.1, and the TSPA-LA parameters related to ash deposition and redistribution that have been developed by this analysis are identified in Table 4. Principal uncertainties associated with the conceptual model are identified in Section 6.5.1.5.3. A discussion of specific uncertainties associated with tephra thicknesses for the Lathrop Wells Cone is presented in Section 6.7.1.5. Uncertainties associated with cesium-137 analyses for the Fortymile Wash alluvial fan are summarized in Section 6.7.1.6. Uncertainties associated with basaltic ash content of surficial material around the Lathrop Wells Cone are briefly discussed in Section 6.7.1.7. Treatments of conceptual model uncertainty in terms of effects on the representation of the risk estimate are beyond the scope of this report and are not discussed.

Acceptance Criterion 5: Model abstraction output is supported by objective comparisons.

1. Models implemented in the abstraction provide results consistent with output from detailed process-level models and/or empirical observations (e.g., laboratory testing, field measurements, and/or natural analogs).

The report provides the technical basis for the redistribution model discussed in *Atmospheric Dispersal and Deposition of Tephra from a Potential Volcanic Eruption at Yucca Mountain, Nevada* (BSC 2003 [DIRS 161840]). The TSPA-LA parameters related to ash deposition and redistribution that have been developed by this analysis are identified in Table 4. Section 6.5 of the report describes the processes that could

redistribute ash and waste particles from an eruption through a repository at Yucca Mountain. The conceptual model for ash redistribution is described in Section 6.5.1.1. A study of ash dilution at the Lathrop Wells Cone is described in Section 6.5.1.2, and the results and interpretation are presented in Section 6.5.1.4. An ash redistribution scoping study is described in Section 6.5.1.5, and the results of a study of cesium-137 concentrations in surficial material are presented in Section 6.5.2. Tephra thicknesses for the Lathrop Wells volcano are described in Section 6.7.1.5. Cesium-137 analysis results for the Fortymile Wash alluvial fan are described in Section 6.7.1.6, and the basaltic ash content of surficial materials around the Lathrop Wells Cone is described in Section 6.7.1.7. Discussion of models implemented in the abstraction of the ash redistribution process is beyond the scope of this report.

### 4.3 CODES AND STANDARDS

No specific formally established codes or standards have been identified as applying to this analysis and modeling activity.

## 5. ASSUMPTIONS

Analyses of eruptive processes are primarily based on the assumption that a plausible future volcanic eruption would be of the same character as Quaternary basaltic eruptions in the YMR. Another overall assumption is that the event probabilities established in the scientific analysis report under current revision *Characterize Framework for Igneous Activity at Yucca Mountain, Nevada*, (BSC 2003 [DIRS 163769]), pertain to the potential formation of a new volcano that would be accompanied by one or more dikes in the subsurface and some combination of scoria cone, spatter cones, ash and lapilli fall, and lava flows on the surface. Eruptive styles and magmatic composition recorded at the Lathrop Wells volcano, the most recent in the YMR, are emphasized. The following assumptions fall into two types: (1) assumptions that establish general equivalency of data (such as gas compositions), and (2) assumptions that support a reasonable technical approach to issue resolution. Assumptions specific to each component of this report are described in the main text of Section 6 and summarized below with corresponding section numbers.

1. *Assumption:* The most likely future eruptive event will have a magmatic chemical composition that is adequately represented by the mean composition of products of the Lathrop Wells volcano. This assumption is discussed in Section 6.3.2.1.

*Rationale:* The Lathrop Wells volcano is the youngest volcano in the YMR. It is chemically well-characterized and represents relatively violent eruptions for cone-building Strombolian eruptions. Also, its chemical composition does not substantially differ from other Quaternary volcanoes in the Crater Flat volcanic field, which is adjacent to Yucca Mountain. Therefore, this assumption is reasonable from the two perspectives of potential magmas that might intrude near the repository depth and of atmospheric dispersal of ash and waste by a subsequent eruption.

*Need for confirmation:* Confirmation is not required because additional data should negligibly alter the mean composition values and, therefore, would not affect the conservatism inherent in the assumption.

2. *Assumption:* The most likely eruptive event will exhibit eruptive styles that are adequately represented by nearby Quaternary basaltic volcanic cones and, specifically, by the Lathrop Wells Cone. This assumption is discussed in Section 1 and forms the technical basis for the study of physical volcanology of Lathrop Wells Cone presented in Section 6.4.

*Rationale:* Nearby Quaternary-age volcanoes are the best analog for future eruptive styles in the YMR because they are representative of the same persistent eruption style, tectonic setting, magma type, and erupted volume. Also, the Lathrop Wells volcano, at ~80,000 years old, is the youngest eruptive Cone in the YMR.

*Need for confirmation:* Confirmation is not needed because this assumption is based on the best available approach.

3. *Assumption:* Pressure in dikes and conduits during eruption is equal to lithostatic pressure. This assumption is discussed in Section 6.3.3.2.

*Rationale:* Actual pressure is a complex function of the velocity, density, and composition of the magma as it rises, and of the strength of wall rocks. Because a general model for these effects does not exist, lithostatic pressure is used as a first-order approximation.

*Need for confirmation:* Confirmation is not needed because this assumption is based on the best available approach.

4. *Assumption:* Rising magma, composed of melt liquid and volatile gases, can be considered homogeneous and characterized by equilibrium between melt and exsolved volatiles. This assumption is discussed in Section 6.3.3.2.

*Rationale:* Actual ascent velocities of melt and bubbles (exsolved volatiles) are different (Wilson and Head 1981 [DIRS 101034]). Kinetic effects between volatiles and melt may be influential factors, but a general theory for basaltic magmas is not yet available to account for these effects.

*Need for confirmation:* Confirmation is not needed because this assumption is based on the best available approach, as discussed in Section 6.3.3.2.

5. *Assumption:* Fluvial transport and the mixing of basaltic ash with other sediment through the Fortymile Wash drainage system can be adequately described by scaling analog data from nearby sites, such as drainages around the Lathrop Wells Cone.

*Rationale:* The Fortymile Wash drainage system is the major southerly drainage for the YMR, eventually delivering sediment to its alluvial fan and beyond in the

Amargosa Valley. However, there are no relevant data from the Fortymile Wash drainage because there is no basaltic volcanic ash identified in the deposits in this area.

*Need for Confirmation:* Confirmation is not needed because this assumption is based on the best available approach, as described in Section 6.5.1.

## **6. SCIENTIFIC ANALYSIS**

### **6.1 INTRODUCTION**

#### **6.1.1 Scientific Approach and Technical Methods**

This analysis report is a compilation of values from refereed literature sources and from field and laboratory studies of properties of magmatic/volcanic materials and processes. Magma properties (e.g., water content, viscosity) and characteristics of buoyant rise (e.g., velocity, volatile exsolution) that best reflect the basaltic magma characteristics of the YMR are taken from the literature, whereas the basaltic composition that might define the potential future volcanic event is derived from multiple chemical analyses from the nearby Lathrop Wells volcano. Because of its relative youth, exposure, composition, and position in the sequence of basaltic eruptive events in the YMR, the Quaternary Lathrop Wells Cone volcano is an appropriate example of the type of eruptive event that could disrupt the proposed repository at Yucca Mountain. Eruptive processes are derived from observations and literature on eruptions of similar compositional type and from the eruptive sequences deduced from investigation of tephra deposited at the Lathrop Wells volcano. The character of redistribution of ash from a potential volcanic eruption at Yucca Mountain is derived from geomorphological principles applied to the YMR and laboratory analyses of sediment and ash samples from drainage systems surrounding and leading away from the Lathrop Wells volcano.

#### **6.1.2 Units of Measurement**

Measurement units employed in this analysis follow System Internationale (SI) standards except where English units are also used to help convey the scales of distance or volume.

#### **6.1.3 Definition of Terms**

This section defines and discusses terms commonly used in the description of the characteristics of pyroclasts from Strombolian and hydrovolcanic eruptions.

##### **6.1.3.1 Strombolian Pyroclast Characteristics**

In the evaluation of explosive eruption phenomena that produced a particular volcano, the pyroclasts (ejecta) provide evidence through analysis of particle shapes, textures, grain size, and compositions on probable magma properties and eruption type. Changes in particle types observed in stratigraphic sections of tephra provide an interpretation of the eruption history.

### *Coarse Materials (Bombs and Blocks)*

A volcanic “bomb” is a pyroclast “larger than 64 millimeters (mm) in diameter” that was “ejected while viscous [partly or completely fluid] and shaped while in flight” (Jackson 1997 [DIRS 109119], p. 75). Bombs are ballistically ejected from the crater and typically land around the vent, eventually accumulating to form a scoria cone. Depending upon the gas content, magma composition, and viscosity, basaltic bombs form a variety of shapes from spindles to “cowpies” that were deformed on impact with the ground surface (Figure 1). Bombs range in size from 64 mm to as much as several meters. Most are finely crystalline, with the quench-crystal, diktytaxitic textures (finely crystalline phases separated by open space and/or glass) found in most scoria of all clast sizes. Similarly, a volcanic block is a pyroclast larger than 64 mm in diameter and angular, having been ejected in a solid state.

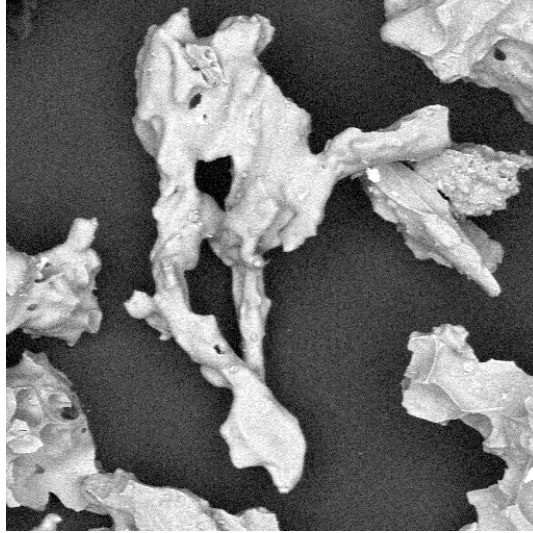


Figure 1. Basaltic Bomb from the Lathrop Wells Scoria Cone

### *Lapilli (grain sizes of 2 to 64 mm) and Ash (grain size < 2 mm)*

Ash and lapilli are separated for the purpose of grain size analysis and characterization, but have the same variety of particle types.

1. *Sideromelane droplets*. Clear brown basaltic glass is usually found as a product of energetic lava fountains where exsolving gases are released to form a “spray” of droplets and bombs ranging in size from only a few micrometers ( $\mu\text{m}$ ) to decimeters. Many sideromelane pyroclasts are highly vesicular with low bulk densities. These are common in Hawaiian eruptions, but are also components in Strombolian eruptions, the main difference being that the Strombolian sideromelane clasts may have been more viscous when ejected as reflected in the pyroclast shapes (Figure 2). Pyroclasts are smooth-skinned, light brown, and have vesicularities ranging from 20 to 70 percent (Heiken and Wohletz 1985 [DIRS 106122], pp. 6, 34-41). Variations in pyroclast colors depend upon the absence or presence of phenocrysts and/or finely crystalline phases. There are gradations between sideromelane and tachylite (finely crystalline) pyroclasts and some grains can exhibit both textures.



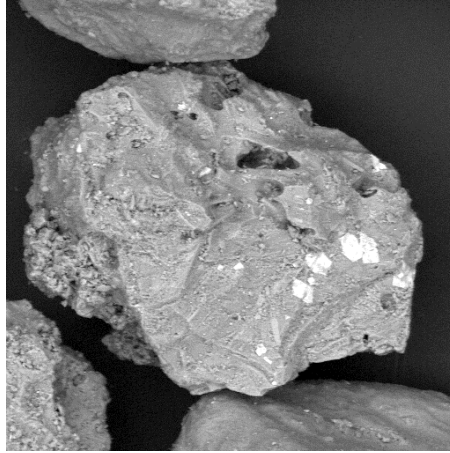
DTN: N/A

NOTE: The smooth glass surfaces and fluidal shape of sideromelane pyroclasts are characteristic of fountaining basaltic magmas. Scale: width of image is ~580  $\mu\text{m}$ . Lathrop Wells volcano, Sample DK-LW-021.

Figure 2. Scanning Electron Micrograph of a Sideromelane (Basaltic Glass) Pyroclast

2. *Tachylite pyroclasts*. Finely crystalline, diktytaxitic textures are characteristic of most scoria bombs and ash from Strombolian eruptions. The “quench crystal” textures correlate with a slight increase in cooling times, perhaps caused by the clogging of the vent during slumping of talus into the crater or by decreased eruption rates (Heiken 1978 [DIRS 162817], Table 5) (Figure 3).

In the field, tachylite bombs, scoria, and ash simply look black (or red if oxidized). In transmitted light, a thin section of scoria also looks more or less opaque. In polished thin sections and when viewed with a scanning electron microscope (SEM) at high enough magnification, tachylite pyroclasts have well-developed pyroxene and plagioclase laths on the order of a few  $\mu\text{m}$  to a few tens of  $\mu\text{m}$  wide, which are surrounded by dendritic growths of 0.2- to 2- $\mu\text{m}$ -wide pyroxene and Fe-Ti oxides. There are traces of glass between the dendritic phases.

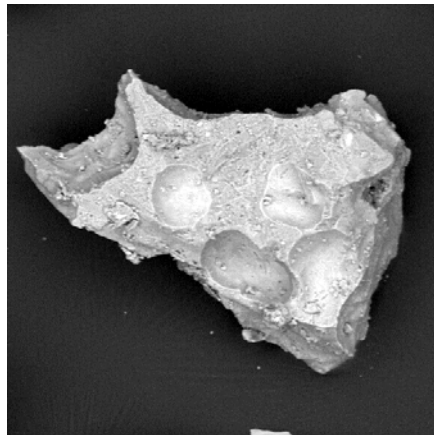


DTN: LA0302GH831811.004

NOTE: These are the most common pyroclast types in Strombolian eruptions, consisting of poorly-vesicular, blocky particles with hyalocrystalline, diktytaxitic textures. The textures are products of quench crystallization. Scale: width of image is ~330  $\mu\text{m}$ . Lathrop Wells volcano, Sample DK-LW-014.

Figure 3. Scanning Electron Micrograph of a Tachylite Pyroclast

3. “Glassy tachylite” pyroclasts. Tephra from the Lathrop Wells volcano contain an unusual pyroclast type in which the vesicles are lined with glass, but the bulk of the grain has a diktytaxitic texture. These glass linings show deformation by growth of quench crystals beneath the linings (Figure 4).

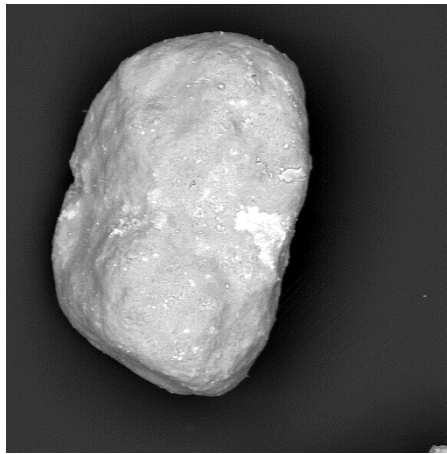


DTN: For illustration purposes only

NOTE: Angular, blocky vesicular tachylite. Hyalocrystalline, diktytaxitic textures characterize the pyroclasts, but the vesicle cavities are lined with basaltic glass. Scale: width of image is ~450  $\mu\text{m}$ . Lathrop Wells volcano, Sample DK-LW-020.

Figure 4. Scanning Electron Micrograph of a Glassy Tachylite

4. *Phenocrysts*. Most tephra from Strombolian eruptions contain phenocrysts that were separated during the fragmentation processes in the vent; some have thin glass coatings.
5. *Lithic clasts*. Of special importance to interpreting subsurface processes during explosive eruptions are lithic clasts derived from magma flow in the dike or conduit formation due to the interaction between rising magma and wall rocks. Information can be derived concerning energies related to fragmentation and magma/ground water interactions if the stratigraphy of the rock sequence underlying the volcano is known. Lithic clasts vary widely in size and shape, ranging from large angular blocks to individual sand grains (Figure 5).



DTN: LA0302GH831811.004

NOTE: This example is a rounded, fine-grained tuff grain. Scale: width of image is ~470  $\mu\text{m}$ . Lathrop Wells volcano, Sample DK-LW-021.

Figure 5. Scanning Electron Micrograph of a Lithic Clast in Strombolian Tephra

### 6.1.3.2 Hydrovolcanic Pyroclast Characteristics

Very energetic explosive eruptions are triggered by the rapid mixing of ground or surface water with rising magma (hydrovolcanic) eruptions. Magma that would have reached the surface to erupt as lava fountains or Strombolian bursts is instead highly fragmented in the water/magma mixing process; the excess energy widens conduits. Rather than formation of scoria cones by ballistic deposition, tephra and lithic clasts are deposited as fallout and pyroclastic density currents (leaving surge deposits) (Heiken and Wohletz 1985 [DIRS 106122], pp. 85-91), typically forming wide, shallow tuff rings. Eruptions can alternate between magmatic and hydrovolcanic activity.

Hydrovolcanic tephra are usually finer grained and better sorted than magmatic counterparts with the same composition. In most cases there is a larger component of blocky sideromelane pyroclasts than in an equivalent Strombolian ash. Pyroclasts deposited in pyroclastic density currents can be rounded by grain-to-grain interactions.

### 6.1.3.3 Violent Strombolian

In studies of the Lathrop Wells volcano, the term “violent Strombolian” is frequently used to describe the inferred eruption history. The origin of the term dates to 1972.

Macdonald (1972 [DIRS 162821], p. 212) states:

The Strombolian type, for example, ranges from rhythmic mild explosions that throw out sparse showers of scoria to heights of only a few tens of feet to violent blasts that project voluminous showers of scoria and bombs to heights of hundreds or thousands of feet, accompanied by a dense black ash cloud. The unifying feature in these widely differing Strombolian eruptions is that in each case the ejecta are new magmatic material, liquid when they are thrown out but solid by the time they strike the ground. Mercalli (1907) called the mild activity “normal Strombolian,” because it is the commonest type of activity at Stromboli, and the violent explosions “Strombolian paroxysms.” However, since the latter are sometimes of quite long duration, instead of being truly paroxysmal, it seems best to call them *violent Strombolian*\* eruptions and to classify Strombolian activity as mild or gentle, moderate or violent, long-continued or brief, continuous or rhythmic.

Walker (1973 [DIRS 125609], pp. 438, 441) developed the following terminology:

In normal strombolian/hawaiian activity the mildly explosive disruption and ejection of relatively fluid basaltic or near-basaltic lava typically produces a scoria (cinder) or spatter cone, usually with an ash bed of limited areal extent around or down-wind of it. The writer has visited more than 150 such cones, and they constitute a very distinctive type. Some, like Stromboli and the Northeast Crater of Etna, are the sites of activity persisting over decades or longer. Others, like Teneguia 1971 or Kilauea Iki 1959, are monogenic cones generally between 20 and 200 meters (m) high produced by eruptions lasting typically a few weeks to a few years.

The eruptive column in normal strombolian/hawaiian eruptions is generally not more than about 300 m high, although higher columns also occur at times... (Walker [1973 (DIRS 125609), p. 438])\*

Like many basaltic provinces, the Azores and Canary Islands contain large numbers—many hundreds—of scattered basaltic cones. The majority are composed of relatively coarse scoria with an  $F$  value of 10% or less [ $F$  value is the fraction of a sample less than 1 mm]\*. Some, however, perhaps 10% of the total, are ash cones built of finer-grained material and reflect an increased explosive violence. The 1677 cone of San Antonio at the southern end of the island of La Palma is an example. No numerical data are yet available for such cones, but Parícutin (Mexico), for which an isopach map and grain-size data are available (Segerstrom 1950 [in Luhr and Simkin 1993 (DIRS 144310),

---

\* Italics added; comments by compiler are in brackets.

pp. 283-311]), seems to be of the same type. Parícutin is about 400 m high. Of the 24 sieved samples collected inside or on the 0.01  $T_{\max}$  isopach [the area enclosed by the 0.01  $T_{\max}$  isopach], 18 contained more than 50% material finer than 1 mm, and two channel samples from the upper part of the deposit within this isopach contain more than 90% of such material.

It is desirable to separate such cones from the normal Strombolian ones, and this can be done by designating them “*violent Strombolian*” as, for example, by MacDonald (1972). (Walker [1973 (DIRS 125609)], p. 441])

The problem of where to draw the divisions between “Strombolian,” “violent Strombolian,” and “subplinian” has come up recently in a paper by Arrighi et al. (2001 [DIRS 162795], pp. 146-148), in which they describe the many eruptions of Vesuvius since 1631 AD.

In the classification terminology of Walker (1973), they [the post-1631 eruptions of Vesuvius]\* fall between the “violent Strombolian” and the “sub-plinian” eruptions, with a  $D$  parameter between 5 and 500. However, *the distinction between these two categories is not stated clearly in the literature.*\* (Arrighi et al. [2001 (DIRS 162795), p. 146])

Amos et al. (1981) studied the 1065 eruption of Sunset Crater in Arizona, which produced a total  $V_{\text{DRE}} = 0.30 \text{ km}^3$  of scoria fall composed of several individual fall units with  $V_{\text{DRE}}$  up to  $4 \times 10^6 \text{ m}^3$ . Volume and dispersal data indicate that the magnitude of this eruption was much larger than a normal Strombolian event. In addition, inferences from the study of those deposits suggest that the eruption was characterized by a sustained convective column much higher than a typical Strombolian one. According to Francis (199[3]), the presence of a sustained eruptive column is a parameter that categorizes that Sunset Crater eruption as subplinian. (Arrighi et al. [2001 (DIRS 162795), p. 146])

A general classification of plinian and Strombolian eruptions has been made by Newhall and Self (1982), using the volcanic explosivity index ( $VEI$ ) to define the magnitude of an eruption on the basis of gross variation intervals of volume and column height. (Arrighi et al. [2001 (DIRS 162795), p. 147])

...it seems that one of the most relevant parameters in discriminating between “subplinian,” “plinian,” and “violent Strombolian” eruptions is the intensity value (MDR [mass discharge rate]). The MDR is lower for subplinian events than for plinian, and this is the main factor controlling eruption column heights and dispersal areas. Bower and Woods (1996) give intensity values for subplinian eruptions between  $10^6$  and  $10^7 \text{ kg/s}$ . These values are applicable only to those [eruptions of Vesuvius] of 1822 and 1906, which for this reason are the only two post-1631 eruptions that can be classified as subplinian. All other post-1631 eruptions with an explosive component can be classified as violent Strombolian, due to the presence of lapilli fall generated by eruptive columns just

---

\* Italics added; comments by compiler are in brackets.

a few kilometers high, a volume of the lapilli fall deposits not exceeding  $10^6 \text{ m}^3$ ,  $\text{MDR} < 10^6 \text{ kg/s}$ , and  $b_t < 1.5$ . (The parameter  $b_t$  = the distance over which the thickness of the deposit halves [Pyle 1995 (DIRS 162829), p. 379]. (Arrighi et al. [2001 (DIRS 162795), pp. 147-148]).

### 6.1.3.4 Grain Size Limits and Terms for Pyroclastic Rocks

Grain size terminology for pyroclastic rocks follows the scheme of Fisher (1961 [DIRS 162805], Table 2) and is accepted by the *Subcommission on the Systematics of Igneous Rocks of the International Union of Geological Sciences* (Schmid 1981 [DIRS 107243], Table 1) (Table 5).

Table 5. Grain-Size Limits and Terms for Pyroclastic Rocks

Clast Size (mm)	Pyroclastic Deposit		
	Pyroclast	Mainly Unconsolidated: Tephra	Mainly Consolidated: Pyroclastic Rock
>64	bomb, block	agglomerate	agglomerate, pyroclastic breccia
>2	lapillus	layer, bed of lapilli (lapilli tephra)	lapilli tuff
<2	coarse ash grain	coarse ash	coarse (ash) tuff
1/16	fine ash grain	fine ash	fine (ash) tuff

Source: Schmid (1981 [DIRS 107243], Table 1)

Median (Md) grain size refers to the size (in mm or  $\phi$ ) at 50 percent on a cumulative weight percent curve.

Sorting characteristics of pyroclastic rocks, based on the graphic standard deviation  $\sigma_\phi$  (Heiken and Wohletz 1985 [DIRS 106122], p. 18) are:

well sorted:  $\sigma_\phi < 1\phi$

moderately sorted:  $\sigma_\phi = 1\phi$  to  $2\phi$

poorly sorted:  $\sigma_\phi > 2\phi$

where:  $\sigma_\phi = (\phi_{84} - \phi_{16})/2$ .  $\phi_{84}$  is the 84th percentile grain size and  $\phi_{16}$  is the 16th percentile grain size expressed in  $\phi$  units. Phi ( $\phi$ ) scale is a logarithmic transformation of the ratio of a grain diameter (in mm) to a standard grain diameter of 1 mm:  $\phi = -\log_2 d$ , where  $d$  is the particle diameter in mm.

## 6.2 FEATURES, EVENTS, AND PROCESSES

The development of a comprehensive list of FEPs potentially relevant to post-closure performance of the Yucca Mountain repository is an ongoing, iterative process based on site-specific information, design, and regulations. The approach for developing an initial list of FEPs in support of the *Total System Performance Assessment for the Site Recommendation* (TSPA-SR) (CRWMS M&O 2000 [DIRS 153246]) was documented in Freeze et al.

(2001 [DIRS 154365]). The initial FEPs list contained 328 FEPs, of which 176 were included in TSPA-SR models (CRWMS M&O 2000 [DIRS 153246], Tables B-9 through B-17). To support the TSPA-LA, the FEPs list was re-evaluated in accordance with the Enhanced FEP Plan (BSC 2002 [DIRS 158966], Section 3.2). Table 4 provides a list of FEPs that are included in the TSPA-LA through the use of the results of the analysis described in this document. Details of the implementation of these FEPs are summarized in Section 6.

Tables 2 and 3 of the TWP for igneous activity analysis (BSC 2003 [DIRS 164143]) provide a listing of both included and excluded FEPs for each of the disruptive events analysis and model reports. One FEP that was listed as *included* in the TWP 1.2.04.01.00, Igneous Activity, was deleted during the FEPs review for TSPA-LA and conducted as part of the Enhanced FEPs Plan. The description of the FEP was found to be entirely redundant with more specific igneous related FEPs. The FEPs 1.2.04.02.0A, Igneous Activity Causes Changes to Rock Properties, and 1.2.10.02.00, Hydrologic Response to Igneous Activity, were previously, and continue to be, excluded. The technical basis for exclusion of these FEPs was previously provided in CRMWS M&O (2000 [DIRS 151553]). Although the current analysis report may provide information cited in the technical basis for exclusion, the following discussions address only implementation (either implicit or explicit) within the TSPA-LA model, consistent with guidance provided in Appendix C of the *Scientific Processes and Guidelines Manual* (BSC 2002 [DIRS 160313]). An additional FEP 1.2.04.07.0C, Ash Redistribution via Soil and Sediment Transport, was also added to the FEP list as a result of the FEPs review.

For each of the included FEPs in Table 4, the implementation in TSPA-LA is described in this analysis report. Details of the implementation are summarized in the table, including specific reference to sections within this document. The parameters that address the included FEPs are also listed. The sources of input for these parameters are described in Section 4 for input parameters and elsewhere in Section 6, if they were specifically developed within this document.

For the igneous eruptive scenario, the TSPA-LA presumes that a hypothetical dike propagates upward, intersects the repository, provides a source for magma to enter the repository drifts, and magma and ash, potentially with entrained waste, are released to the surface via an eruptive conduit. The FEPs listed in Table 4 are part of the conceptual basis for such a scenario. However, this report does not provide a direct basis for the inclusion in TSPA-LA of the FEPs listed in Table 4, with the exception of parameters developed to address ash redistribution. Rather, the results of this analysis are used by the reports cited in the table to develop a basis for implementing the FEP in TSPA-LA. This report, therefore, provides supporting analysis to help constrain the potential consequences of the listed FEPs. As such, a partial treatment of the included FEPs is provided herein, and the results of this analysis report and listed FEPs are considered to be implicitly included in the TSPA-LA.

Although some YMP-derived information was used as input to this analysis report, most of the input was taken from a review of the published literature. As a result, the report relies heavily on values and concepts that were developed for volcanoes that are analogous in some way to those in the YMR. Inputs that originated with the YMP included the major-element composition of products of the Lathrop Wells volcano and quantities of xenoliths erupted from volcanoes that shared some eruptive characteristics with YMR volcanoes. The xenolith data were originally collected to constrain the amount of waste that could be ejected if a volcano penetrated the

repository. Inputs from the published literature included values, or inferences, on volcanic conduit size; dike system geometry; volatile contents, material properties, and water saturation pressures of basaltic magmas; relationships describing the dynamics of ascending magmas; volumes, durations, and power outputs of historical scoria cone-forming eruptions; bulk grain sizes of explosive basaltic eruptions; and estimates of the in-situ bulk density of pyroclastic fallout deposits. Because this information forms the basis of the eruptive concepts, this information and related FEPs listed above are considered to be implicitly included in the TSPA-LA.

## **6.3 ERUPTIVE PROCESSES ANALYSIS**

### **6.3.1 Characteristics of Eruptive Conduits, Dike Widths, and Dike Swarms**

Most observed basaltic eruptions begin as fissure eruptions, discharging magma where a dike intersects the Earth's surface, and they rapidly become focused into roughly cylindrical conduit eruptions. Some eruptions, such as Parícutin in Mexico (Luhr and Simkin 1993 [DIRS 144310], p. 62), originated from single-point sources, although the vent was located on a long fissure that opened just before eruption began. The fissure is likely the surface expression of the tip of an ascending dike that fed the eruptions. Because of the effect of (1) the conduit diameter and (2) the depth (to which a conduit extends before merging into a simple feeder dike) on the number of waste packages disrupted by a potential eruption at Yucca Mountain, it is important to constrain both these variables.

The best potential data for these parameters would come from a study of basaltic volcanic necks exposed by erosion where direct measurements could be made of conduit diameter and variation with depth. However, such data are lacking. Although many volcanic necks have been mapped as part of regional studies, they were not measured in detail, at least for the range of compositions of interest to the YMP. Without access to direct measurements of conduit diameter, estimates of this parameter are based on analog studies (see Section 5, Assumption 2). However, first we consider some of the processes of conduit formation and enlargement.

The transition from magma flow in a subplanar dike to flow in a cylindrical plug has been inferred at many field locations (e.g., Delaney and Pollard 1978 [DIRS 162800], p. 1212; Hallett 1992 [DIRS 124671], p. 140). From a continuum mechanics view, a planar dike is the preferred form for propagation of magma through brittle and elastic host rock, whereas a cylindrical conduit is the preferred form for magma flow and delivery to the surface (Delaney and Pollard 1981 [DIRS 162801], p. 1). Several processes have been put forward to facilitate this transition, including:

- Magma viscosity variations induced by solidification of magma at dike margins (Wylie et al. 1999 [DIRS 162861], p. 438)
- Brecciation and erosion of dike wall rocks, local enlargement, e.g., the Shiprock NE dike (Delaney and Pollard 1978 [DIRS 162800], p. 1212; Delaney and Pollard 1981 [DIRS 162801], pp. 17-18), and the San Rafael dikes (Delaney and Gartner 1997 [DIRS 145370], p. 1178)

- Progressive melting of the host rocks, enhancing localized flow (Quarenì et al. 2001 [DIRS 162830], p. 218) [a slightly different permutation of the brecciation mechanism of Delaney and Pollard (1978 [DIRS 162800]), p. 1212]; but as pointed out by Delaney and Pollard (1981 [DIRS 162801], p. 58), the emplacement process must be driven by more than heat flow, since this process is diffusional in nature and tends to produce semispherical intrusive forms (cf., Hardee and Larson 1977 [DIRS 162815], p. 128).

Once a “bud” or zone of widening and flow focusing has initiated, the evolving conduit may continue to widen. Several hypothetical processes, similar to those for the initial dike enlargement, have been described to explain this process:

- Erosion from shear stress of flowing magma (below fragmentation level) (Dobran 2001 [DIRS 162802], p. 481)
- Thermoelastic stressing of wall rock (McBirney 1959 [DIRS 162826], p. 443; Valentine and Groves 1996 [DIRS 107052], p. 85)
- Erosion from particle collision (above fragmentation level) (Valentine and Groves 1996 [DIRS 107052], p. 85; Dobran 2001 [DIRS 162802], p. 481)
- Conduit wall collapse due to variations in magmatic pressure as a result of conduit processes (variations in magma pressure, shock/rarefaction waves) (Dobran 2001 [DIRS 162802], pp. 480-484)
- Hydromagmatic processes: interaction of magma with groundwater or saturated sediments (McBirney 1959 [DIRS 162826], pp. 443-445; Valentine and Groves 1996 [DIRS 107052], p. 85)
- Conduit wall collapse due to offshoot dikes (Valentine and Groves 1996 [DIRS 107052], p. 85)
- Pore pressure buildup (Delaney 1982 [DIRS 162799], p. 7753; Valentine and Groves 1996 [DIRS 107052], p. 85; McBirney 1959 [DIRS 162826], p. 443).

As a result of these processes, the final width of a conduit could be larger near the end of the eruption. Also, the entire cross-sectional area of a conduit may be actively transferring magma to the vent (e.g., WoldeGabriel et al. 1999 [DIRS 110071], p. 403) or only a small fraction of its cross-sectional area may be active (e.g., due to variations in flow velocity or viscosity as a function of composition and temperature) to produce localized flow (subsection or annulus) (Hallett 1992 [DIRS 162813], pp. 21-22; Detournay et al. 2003 [DIRS 162914], p. 65).

Doubik and Hill (1999 [DIRS 115338], pp. 60-61) proposed that the Lathrop Wells conduit may have been as wide as 50 m at depths equivalent to repository depth during the last stages of eruption. Their estimate was derived from an inferred analogy with modern eruptions at Tolbachik (Kamchatka, Russia). The conceptual model is that conduit diameter increases during successive stages of an eruption and that the maximum diameter achieved near the end of an

eruption is the value of this parameter to be considered in evaluating volcanic disruption of a nuclear waste repository. The method for calculating conduit diameter of the Tolbachik volcanic vents is based on estimates of eruption volume, xenolith content of the pyroclastic deposits, and source depths of the xenoliths. By assuming an initial conduit diameter and calculating the volume of country rock removed along part of the length of the conduit, one can calculate the progressive enlargement of the conduit as the eruption proceeds.

The 50-m estimate of conduit diameter for Lathrop Wells Cone is large, considering that Doubik and Hill (1999 [DIRS 115338], p. 59) calculated a 48-m diameter for the Tolbachik conduit developed during a much larger eruption. This result is forced by their estimation of xenolith volume and their assumption that xenoliths at Lathrop Wells Cone were derived only from a 550-m thick Tertiary ignimbrite section (compared to a 1.7-km source section at Tolbachik; Doubik and Hill 1999 [DIRS 115338], pp. 57, 59), so that the erupted volume of xenoliths was derived from a shallower (but wider) conduit.

Entrainment rates for subvolcanic sedimentary lithics in the tephra deposits at Alkali Buttes, Lucero Volcanic Field, New Mexico, provide data for evaluating the variations in conduit size beneath a monogenetic, alkali basalt center (Valentine and Groves 1996 [DIRS 107052]). The well-established Colorado Plateau stratigraphy beneath these volcanoes provides good constraint on the depth of origin of xenoliths and insights into the effect of variable rock properties on conduit diameter. Measured xenoliths ranged in size from ash-sized particles (measured in thin section) to 3-m blocks of competent sandstone (Valentine and Groves 1996 [DIRS 107052]), pp. 79-80). Based on the xenolith data in Valentine and Groves (1996 [DIRS 107052], pp. 86-87) and assuming an initial 1.5-m-thick feeder dike, the conduit that formed in the sedimentary country rock at > 500 m depth can be calculated to range in diameter from 3.5 to 10 m (Krier and Harrington 2003 [DIRS 165893], pp. 26-28). The subvolcanic rock units used to calculate this conduit size range include the sandstone and limestone formations (San Andres Glorieta, Abo, and Madera) that are most analogous to the tuffaceous country rock in the YMR.

The upper 500 m of the country rock at Alkali Buttes consists of Triassic Chinle Formation, which is composed predominantly of mudstones and shales. This material evidently provided a wet host rock and it was finely comminuted by explosive interaction of the ascending (and fragmenting) magma with water. The Chinle Formation forms an average of 50 volume percent (vol%) of the matrix of some volcanic deposits. Conduit-size calculations, based on estimated proportion of xenoliths within these hydrovolcanic deposits, indicate that a cylindrical conduit up to 78 m wide might have formed in the uppermost strata (Krier and Harrington 2003 [DIRS 165893], pp. 26-28.) However, a flared conduit shape could vary in size from 6 m at depth to 300 m at the surface, which is equivalent to the mapped extent of the hydrovolcanic deposits (lapilli and block-rich tuff of Valentine and Groves 1996 [DIRS 107052], Figure 2, p. 74).

In a similar study, Mastin (1991 [DIRS 124749]) calculated the size of a conduit beneath South Inyo Crater, California, using both the proportion of lithics in the eruption deposits and results from a cored drillhole through the conduit beneath the crater (Eichelberger et al. 1988 [DIRS 162803], p. 13,208). Mastin (1991 [DIRS 124749], p. 590) estimated that the conduit at 300 to 600 m beneath the vent was on the order of 22 to 31 m in diameter. The dominant eruption mechanism in this case was phreatic or hydromagmatic, with < 10 percent juvenile

(rhyolite) material (Mastin 1991 [DIRS 124749], p. 593). The estimated eruption volume from measured tephra thicknesses is  $0.8$  to  $1.2 \times 10^9 \text{ m}^3$  ( $\sim 1 \text{ km}^3$ ) (Mastin 1991 [DIRS 124749], p. 585).

Thick Miocene volcanic units beneath the Lathrop Wells Cone are very similar, making it difficult to assign relative proportions of those units represented by xenoliths there. Given the limitations on specific data to test the assumptions made by Doubik and Hill (1999 [DIRS 115338], p. 59), their estimate of a 50-m conduit diameter for the Lathrop Wells Cone is suggested as a mode or most likely value for conduit diameter at depth for potential eruptions at Yucca Mountain. The maximum value for the conduit diameter in the distribution to be used for performance assessment is 150 m, which corresponds to the diameter of the Grants Ridge conduit/plug in New Mexico (Keating and Valentine 1998 [DIRS 111236], p. 41; WoldeGabriel et al. 1999 [DIRS 110071], p. 392). The large size of the Grants Ridge plug reflects that it erupted a volume on the order of a few  $\text{km}^3$  of alkali basalt and, therefore, is expected to be a conservative upper bound for conduit diameter at Yucca Mountain (compared, for example, to the Lathrop Wells volcano with its approximate total volume of  $0.086 \text{ km}^3$ ; this report, Section 6.4.3). The minimum conduit diameter value for a performance assessment realization should be the same as the dike width selected for that realization. The distribution should be triangular. This simple triangular distribution reflects the few data that exist for conduit diameter measurement, but will capture the range of conduit diameters for a potential volcanic event at Yucca Mountain. Dike widths should be described with a log-normal distribution with a minimum of 0.5 m, a mean of 1.5 m, and a 95<sup>th</sup> percentile width of 4.5 m. This distribution is consistent with data reported by Crowe et al. (1983 [DIRS 100972], p. 266), who measured dikes in the YMR.

Volcanoes in the YMR are fed by one main dike along which a central cone and other vents may form, but subsidiary dikes are also present. For example, the Lathrop Wells volcano is likely underlain by three dikes (inferred from Perry et al. 1998 [DIRS 144335], Figure 2.10): 1) the dike that fed the main cone and small spatter vents in a chain to the north and south of the cone, 2) a dike that fed spatter and scoria mounds in a parallel chain just to the east of the main dike, and 3) possibly a dike that fed scoria vents near the northern edge of the volcano, although it could be an extension of 2) above. In addition, there are likely to be small dikes that radiate outward from the main cone's feeder conduit that are not exposed, even in the growing quarry excavation. The Paiute Ridge intrusive complex,  $\sim 55 \text{ km}$  NE of Yucca Mountain, which appears to have fed at least one volcanic vent (evidenced by the presence of lava-flow remnants and a plug-like body), may have as many as 10 dikes, in addition to sill-like bodies (as inferred from examination of Perry et al. 1998 [DIRS 144335], Figures 5.15 and 5.16). To account for the likelihood of dike swarms, rather than single dikes, during formation of a new volcano, a log-normal distribution is recommended for the number of dikes that has a minimum value of 1, a mode of 3 (reflecting our assumption that the most likely new volcano will be similar to the Lathrop Wells volcano), and a 95<sup>th</sup> percentile of 6. This distribution ensures that a number of dikes greater than or equal to 10 dikes (treating Paiute Ridge as a large event) will be represented in a number of realizations. The simple triangular distribution reflects the few data that exist for number of dikes in dike swarms.

In addition to the number of possible dikes, the spacing between dikes is another important variable. Based upon field observation and map measurement (Krier and Harrington 2003

[DIRS 165893] pp. 20-21), estimated dike spacing at Lathrop Wells Cone is ~320 m between the two inferred NW-trending dikes that fed the cone and linear set of scoria mounds (vents) immediately east of the cone. Spacing is ~700 m between the mounds and an inferred third dike related to scoria mounds on the eastern lava flows. For the Paiute Ridge intrusion, mean dike spacing for dikes greater than 1 km long is ~995 m (maximum 1,440 m; minimum 250 m) (Byers and Barnes 1967 [DIRS 101859]; Perry et al. 1998 [DIRS 144335], Figure 5-15; Krier and Harrington 2003 [DIRS 165893], pp. 16-18). For the 3.7-Ma-old Crater Flat basalts, dike spacing is ~385 m (Perry et al. 1998 [DIRS 144335], Appendix 2-M1; Krier and Harrington 2003 [DIRS 165893] pp. 22-23). A fourth set of map measurements from the Rim Rock, Texas, dike swarm (18-23 Ma) (Dasch et al. 1969 [DIRS 162798], Figure 2), for a subset of ~100 dikes, gives an average of 410 m (standard deviation = 430 m) for an N-trending dike set and 690 m (standard deviation = 482 m) for a NW-trending dike set (Krier and Harrington 2003 [DIRS 165893], pp. 24-25). Based on this limited, diverse data set, the recommended dike spacing for the Yucca Mountain region can be described by a random uniform distribution ranging from 100 m to 690 m.

### 6.3.2 Characteristics of Igneous Material

#### 6.3.2.1 Magma Chemistry

Magma-chemistry data are used to determine parameters for important variables such as magma viscosity, temperature, and density. Two approaches are possible for predicting the chemistry of future magmas. The first is to calculate a volume-weighted mean composition based on analysis of basaltic rocks from the YMR, which is a method that would capture the existing magma chemistry record. A second approach is to use the most recent eruption at Lathrop Wells volcano as the one that most likely represents the composition of future eruptions. The second approach was selected because it emphasizes the composition that produced more violent explosive eruptions compared to other YMR volcanoes (as inferred from Perry et al. 1998 [DIRS 144335], Chapter 2); therefore, it is the more conservative of the two approaches because it represents a greater potential dispersal of radionuclides (see Section 5, Assumption 1).

The major element variation for Lathrop Wells is based upon 45 chemical analyses (DTN: LA000000000099.002). Table 6 lists statistical parameters associated with the 12 most abundant oxides from these analyses.

Table 6. Mean Lathrop Wells Lava Chemistry with Associated Statistics (all values except count are in weight percent)

SiO <sub>2</sub>		TiO <sub>2</sub>		Al <sub>2</sub> O <sub>3</sub>	
Mean	48.50	Mean	1.93	Mean	16.74
Standard Error	0.09	Standard Error	0.01	Standard Error	0.03
Median	48.57	Median	1.93	Median	16.75
Mode	48.55	Mode	1.97	Mode	16.87
Standard Deviation	0.58	Standard Deviation	0.06	Standard Deviation	0.22
Sample Variance	0.34	Sample Variance	0.00	Sample Variance	0.05
Count	45.00	Count	45.00	Count	45.00

Table 6. Mean Lathrop Wells Lava Chemistry with Associated Statistics (all values except count are in weight percent) (Continued)

<b>Fe<sub>2</sub>O<sub>3</sub>T<sup>a</sup></b>		<b>Fe<sub>2</sub>O<sub>3</sub><sup>b</sup></b>		<b>FeO<sup>b</sup></b>	
Mean	11.63	Mean	1.74	Mean	8.90
Standard Error	0.03	Standard Error	0.00	Standard Error	0.02
Median	11.58	Median	1.74	Median	8.86
Mode	11.56	Mode	1.73	Mode	8.84
Standard Deviation	0.22	Standard Deviation	0.03	Standard Deviation	0.17
Sample Variance	0.05	Sample Variance	0.00	Sample Variance	0.03
Count	45.00	Count	45.00	Count	45.00
<b>MnO</b>		<b>MgO</b>		<b>CaO</b>	
Mean	0.17	Mean	5.83	Mean	8.60
Standard Error	0.00	Standard Error	0.02	Standard Error	0.03
Median	0.17	Median	5.83	Median	8.55
Mode	0.17	Mode	5.88	Mode	8.41
Standard Deviation	0.00	Standard Deviation	0.11	Standard Deviation	0.22
Sample Variance	0.00	Sample Variance	0.01	Sample Variance	0.05
Count	45.00	Count	45.00	Count	45.00
<b>Na<sub>2</sub>O</b>		<b>K<sub>2</sub>O</b>		<b>P<sub>2</sub>O<sub>5</sub></b>	
Mean	3.53	Mean	1.84	Mean	1.22
Standard Error	0.01	Standard Error	0.01	Standard Error	0.00
Median	3.55	Median	1.84	Median	1.22
Mode	3.59	Mode	1.84	Mode	1.21
Standard Deviation	0.09	Standard Deviation	0.04	Standard Deviation	0.03
Sample Variance	0.01	Sample Variance	0.00	Sample Variance	0.00
Count	45.00	Count	45.00	Count	45.00

DTN: LA00000000099.002

NOTES: <sup>a</sup> Total iron is reported as Fe<sub>2</sub>O<sub>3</sub>T.

<sup>b</sup> Fe<sub>2</sub>O<sub>3</sub> and FeO were recalculated assuming a 0.15 mole fraction of ferric iron (Fe<sub>2</sub>O<sub>3</sub>) (Perry and Straub 1996 [DIRS 106490]).

The following sample analyses is from Perry and Straub (1996 [DIRS 106490], Appendix A; DTN: LA00000000099.002) were used to develop the statistics in this table: LW11FVP, LW12FVP, LW74FVP, LW45FVP, LW72FVP, LW73FVP, LW100FVP, LW120FVP, LW121FVP, LW30FVP, LW31FVP, LW32FVP, LW63FVP, LW64FVP, LW65FVP, LW66FVP, LW67FVP, LW110FVP, LW115FVP, LW20FVP, LW21FVP, LW22FVP, LW23FVP, LW06FVP, LW07FVP, LW40FVP, LW41FVP, LW44FVP, LW55FVP, LW56FVP, LW19FVP, LW25FVP, LW26FVP, LW27FVP, LW28FVP, LW29FVP, LW04FVPA, LW54FVP, LW57FVP, LW58FVP, LW05FVPA, LW59FVP, LW60FVP, LW61FVP, LW62FVP.

### 6.3.2.2 Water Content of Primary Basaltic Magma

Eruptive styles in the YMR ranged from violent Strombolian on one end of the spectrum to quiescent aa lava on the other (Perry et al. 1998 [DIRS 144335], Chapter 2). Eruption style was primarily controlled by volatile content (which is dominated by water) and the rate at which volatiles were exsolved from the magma. The observed eruptive styles indicate a large range in volatile contents and, hence, water content of YMR magmas. In addition, variations in energy are suggested at individual volcanic centers such as those of the Quaternary Crater Flat field and Lathrop Wells volcanoes.

Amphibole, possibly of magmatic origin, is found as a rare and sparse phase in some Quaternary Crater Flat basalts. Knutson and Green (1975 [DIRS 106299], Figure 1, p. 126), performing experiments on material similar in composition to YMR basalts, observed that magmatic amphibole was stabilized at water contents of between 2 and 5 wt%. Baker and Eggler (1983 [DIRS 122601], p. 387) showed that at 2 Kbar pressure, water content in excess of 4.5 wt% is required to stabilize amphibole in high-alumina basalt similar to YMR basalts. However, water content substantially greater than 5 wt% is not considered likely because this high water content is most commonly associated with more chemically evolved magmatic compositions (e.g., rhyolite) than those observed in young volcanoes near the YMR. Also, Sisson and Grove (1993 [DIRS 122564], p. 167) note that low-Mg basalts with high alumina content cannot erupt as liquids with water content in excess of 4 wt% (by mass) because they will exsolve liquid and rapidly crystallize to form phenocryst-rich magmas as they approach the surface. Based on this, it is argued that 4 wt% is an upper bound on initial dissolved water content. At the lower end of the range, aa lava may form from relatively low-volatile-content eruptions.

Even if one could tie a particular concentration of volatiles to a particular eruptive style, the YMR post-Miocene (i.e., 5 Ma) record is sparse; therefore, it is difficult to rigorously define a probability distribution function for primary magma water content for use in performance assessment. The following distribution is recommended:

No magmatic water has a zero probability of occurrence. This statement reflects our knowledge that very low volatile contents are very rare. With 1 to 3 percent magmatic water, the probability should be uniform, reflecting that this is the most likely range of water contents. The probability should decrease linearly between 3 and 4 wt%, so that it is zero at 4 wt%, representing the expectation that at about 4 wt%, basaltic magmas will crystallize before reaching the surface to erupt.

Direct measurements of water in mafic (low silica) magmas or magmatic products from a range of tectonic settings indirectly support the recommended parameter values and cover the range of values that can be reasonably expected for future basaltic igneous activity. Garcia et al. (1989 [DIRS 122542], Table 1, p. 10527), Byers et al. (1985 [DIRS 122532], Figure 4, p. 1891), and Muenow et al. (1979 [DIRS 125093], Table 1, p. 74) found total water contents in Hawaiian tholeiites and transitional alkalic basalts that range from near 0 to nearly 1 percent. These melts probably represent higher degrees of partial melting than YMR basalts, so their low water contents are expected. On the other hand, Gaetani et al. (1993 [DIRS 144274], pp. 332-334) and Sisson and Grove (1993 [DIRS 144351], p. 163) present experimental evidence that high-alumina basalt and basaltic andesite magmas commonly contain up to several wt% water. Sisson and Layne (1993 [DIRS 122549], Table 1, p. 622) measured water contents in glass inclusions from arc basalts and basaltic andesites that range from 1 to 6 percent. True magmatic values could be somewhat lower because of concentration of water in the inclusions, which is caused by partial crystallization of the melt after entrapment. Water contents of 0.2 to 2 percent have been reported for back arc basin lavas and 1.2 to 3 percent for island arc tholeiites and boninites (Danyushevsky et al. 1993 [DIRS 149303], Tables 1 and 4, pp. 349 and 358).

### 6.3.2.3 Mole Percent of Constituents in Volcanic Gas

A survey of data compilations from the literature, including volcanoes from convergent, divergent, and hot-spot tectonic settings, must suffice to constrain the relative proportions of major gas constituents in YMR basalts owing to the absence of current activity in the YMR from which gases could be directly sampled. Three types of data exist in the literature: 1) measurements of emitted volcanic gases, and 2) measurements of gases trapped in volcanic glass or melt inclusions, and 3) experiments on gas solubilities in silicate melts. The first type of data is more directly relevant to eruptive scenarios at Yucca Mountain because the gases released from an igneous event will include corrosive species. Also, gases will fractionate between the magma and the gas phase during exsolution. Consequently, gas composition data for glasses may not directly represent their relative abundances in the gas phase after exsolution.

Measured concentrations of volcanic-gas constituents were taken from a compilation by Symonds et al. (1994 [DIRS 101029], Tables 3-5), and only the data for mafic centers were included in the present analysis. Data include hawaiite from Mt Etna; tholeiitic basalt from Momotombo, Poas, Kilauea, Ardoukoba, and Erta Ale; nephelinite from Nyiragongo; and alkali basalt from Surtsey (Table 7). The Table 7 statistics were calculated by first computing the mean for each of the above mentioned volcanic centers from the data in Symonds et al. (1994 [DIRS 101029], Tables 3-5) and then using these individual means to generate the overall statistics.

Table 7. Mole Percent Concentration of Volcanic Gases and Associated Uncertainty Estimates

	H <sub>2</sub> O	H <sub>2</sub>	CO <sub>2</sub>	CO	SO <sub>2</sub>
Mean	73.16	1.17	14.28	0.57	9.45
Square Root of the Sum of the Squares	17.97	0.89	16.03	0.59	8.90
Standard Deviation	19.81	0.67	15.32	0.75	8.95
	S <sub>2</sub>	HCl	HF	H <sub>2</sub> S	<i>f</i> <sub>O<sub>2</sub></sub> *
Mean	0.41	0.87	0.17	0.74	-10.63
Square Root of the Sum of the Squares	0.63	0.21	0.04	1.04	1.92
Standard Deviation	0.40	1.12	0.08	0.69	1.80

Source: Eighty-eight analyses in Symonds et al. (1994 [DIRS 101029], Tables 3-5)

NOTE: \* *f*<sub>O<sub>2</sub></sub> is listed as log bars.

This is a closed data set, indicating that each parameter (other than *f*<sub>O<sub>2</sub></sub>) must vary between 0 and 100 percent. Clearly, a species such as H<sub>2</sub>O will rarely be present at levels less than 50 percent and probably has some mean or median value of geologic significance. If data from sufficient eruptions and individual volcanoes were gathered, a normal distribution of values seems likely. As for the minor species, which are also corrosive, the cited uncertainties are quite large relative to mean values. Thus, it seems likely that adequate conservatism will be accommodated by a normal, or even a uniform, distribution.

### 6.3.2.4 Magmatic Temperatures, Viscosities, and Densities

Many direct measurements of magmatic temperatures have been made for erupting lavas. However, this is only possible when water contents are low enough, or rates of magmatic

outgassing are slow enough, to permit direct measurement. Thus, although direct measurements are available for the low end of the spectrum of water content, experiments must be relied on to constrain magmatic temperatures for magmas with elevated water content (see Section 5, Assumption 3).

YMR basaltic lavas are generally aphyric to sparsely porphyritic (Perry and Straub 1996 [DIRS 106490], p. 6), which indicates that they erupted at near-liquidus or superliquidus temperatures. The liquidus for dry basaltic magmas has a positive slope and varies as a function of pressure. Wet liquids, however, have negative slopes, so that water-bearing magmas may exist at a temperature less than that of the dry liquidus. Jaupart and Tait (1990 [DIRS 118292], p. 219) present a simple expression for the solubility of water in basaltic magma

$$n = 6.8 \times 10^{-8} P^{0.7} \quad (\text{Eq. 1})$$

where  $n$  is the mass fraction of water and  $P$  is the pressure in Pascals. Because of the negative slope of the basalt solidus, corresponding temperatures on the solidus represent minimum liquidus temperatures. As magmas decompress, not only will they tend to exsolve more fluid, they will also tend to crystallize. A magma is saturated with respect to water when the pressure is such that  $n$  equals the initial water content. Table 8 shows saturation pressures, calculated from Equation 1, for initial water contents of 0.5, 1.0, 2.0, 3.0, and 4.0 wt% (wt% = 100 times the mass fraction). At lower pressures, water vapor would begin to exsolve and form bubbles (see also Section 6.3.3.2 below).

Table 8. Calculated Saturation Pressures, Liquidus Temperatures, Viscosities, and Densities as a Function of Water Content for Lathrop Wells Magmas

Water Content (wt%)	Saturation Pressure (Pa)	Liquidus Temperature (°C)	Viscosity (log poise)	Density (kg/m <sup>3</sup> )
0	$1 \times 10^5$	1169	2.678	2663
0.5	$9.0 \times 10^6$	1153	2.572	2633
1	$2.4 \times 10^7$	1137	2.472	2605
2	$6.5 \times 10^7$	1106	2.284	2556
3	$1.2 \times 10^8$	1076	2.112	2512
4	$1.7 \times 10^8$	1046	1.957	2474

NOTE: Derived using mean Lathrop Wells compositions from Table 6.

Using saturation pressures derived from Table 8, the following expression of Sisson and Grove (1993 [DIRS 122564], p. 178) can be used to estimate multiple phase-saturation (liquidus) temperatures in the magmas:

$$T(^{\circ}\text{C}) = 969 - (33.1 \times H_2O) + 0.0052 (P_b - 1) + 742.7 \times Al^{\#} - 138 \times NaK^{\#} + 125.3 \times Mg^{\#} \quad (\text{Eq. 2})$$

where

$H_2O$  is the wt% of water,

$P_b$  is pressure in bars (note that elsewhere in this document pressure is in Pascals)

$Al^\#$  is the ratio of mass fractions of  $Al_2O_3/(Al_2O_3 + SiO_2)$

$NaK^\#$  is the ratio of mass fractions of  $(Na_2O + K_2O)/(Na_2O + K_2O + CaO)$

$Mg^\#$  is molar  $Mg/(Mg + 2Fe_2O_3T)$ .

It should be noted that  $Al^\#$ ,  $NaK^\#$ , and  $Mg^\#$  do not vary as a function of water content in Lathrop Wells magmas as these parameters simply express relative proportions.

Liquidus temperatures for Lathrop Wells magmas with different hypothetical water contents were calculated as follows: First, the mean Lathrop Wells composition (from Table 6) was normalized to 100 percent (anhydrous). Then, major element oxides were renormalized to sum to 99.5, 99.0, 98.0, 97.0, and 96.0 wt%. To these values, 0.5, 1.0, 2.0, 3.0, and 4.0 wt%  $H_2O$  were added, respectively, so that the sum of the renormalized major element oxide content and water content sum to 100 wt% in each case. With these new hypothetical compositions, and the saturation pressure calculated as described above, Equation 2 was used to compute the liquidus temperatures shown in Table 8. The same hypothetical compositions and calculated temperatures were used to calculate bubble- and crystal-free viscosity using the method of Shaw (1972 [DIRS 126270], pp. 873, 878).

Density can also be calculated as a function of composition (including water content), pressure, and temperature using the formulation and data of Lange and Carmichael (1990 [DIRS 147767], Table 3) with additional data for  $H_2O$  (Ochs and Lange 1999 [DIRS 144330], pp. 1314-1315). Equation 2 from Ochs and Lange (1999 [DIRS 144330], p. 1315) produces the molar volume of the silicate liquid, which only requires a simple conversion to density. The density conversion can be done as follows: Assume that 100 g of magma are present. In doing the calculation, one converts the weight of each oxide (equivalent to the wt%) to the number of moles of each constituent. These terms can be summed to give a total number of moles. The density is then equal to the inverse of the product of molar volume ( $cm^3/mole$ ) and number of moles per 100 g of liquid. This result, in  $g/cm^3$ , can then be converted to  $kg/m^3$  as shown in Table 8.

A review of relevant experimental data reveals that these values are reasonable. The liquidus temperature for a mildly alkalic basalt similar in composition to the mean Lathrop Wells lava composition is between 1,174 and 1,188°C (Mahood and Baker 1986 [DIRS 104663]). The Mahood and Baker (1986 [DIRS 104663]) temperature calculations are close to temperatures reported by Knutson and Green (1975 [DIRS 106299], Figure 1) for a hawaiite that is also similar in composition to Lathrop Wells basalt. Yoder and Tilley (1962 [DIRS 122589], Figure 28) published results on the water-saturated liquidus for a high-alumina basalt. At  $1.75 \times 10^8$  Pa water pressure, the liquidus was more than 100°C cooler than the  $10^5$  Pa liquidus temperature. Thus, our calculated parameter values are consistent with a well-established body of experimental data.

### 6.3.3 Eruptive Processes

Quaternary basalts of the YMR display textural and depositional facies that indicate a range of eruptive processes. Explosive processes, in which fragments (clasts), or clots, of melt were erupted in a stream of gas, are evidenced by the presence of scoria cones and remnants of ash fallout blankets. Effusive processes, in which magma fragmentation did not occur in the feeding system, are recorded by the presence of lava flows, although it is also common in basaltic eruptions to produce lava flows by the coalescence and remobilization of explosively erupted clasts. Within these two broad categories of eruptive facies (regarding explosive and effusive, *facies* refers to the general appearance and characteristics of a rock unit), there are further distinctions. Explosively erupted deposits, for example, may display a range of facies depending on the local rate of accumulation and on the temperature of clasts when they are deposited. Very high accumulation rates of hot (still molten) clasts result in coalescence and formation of lava flows. Somewhat lower accumulation rates and temperatures may result in welded spatter, in which relicts of individual clast shapes may still be observed to varying degrees. Still lower accumulation rates and temperatures (such that the clasts are still plastic upon deposition) result in partly welded spatter, in which clast shapes are quite obvious but the deposit is resistant to erosion. Low accumulation rates of very hot clasts result in individual spatter clasts that flatten upon deposition but solidify before subsequent clasts are deposited on top and, therefore, do not weld. Nonindurated deposits of brittle cinders (or scoria) result from deposition of already cooled clasts. All of these explosive facies are present to some degree in the Yucca Mountain basalts. Effusive lava flows in the YMR are mainly of the aa type, indicating relatively high effusion rates (greater than ca  $1.5\text{-}3 \times 10^4$  kg/s; Rowland and Walker 1990 [DIRS 115463], p. 626), although the limited extent of the flows suggests relatively short eruption duration.

The Lathrop Wells volcano is a good example of a range of eruptive processes recorded by a single volcano (Perry et al. 1998 [DIRS 144335], Chapter 2). The surface of the main cone is composed mainly of loose scoria with a relatively high vesicularity. The cone is surrounded, particularly to the south, west, and north, by a fallout blanket up to ca 3 m thick (within 1 km of the cone) composed of the same loose scoria. Remnants of this fallout deposit are exposed northward up to 2 km from the crater; ~20 km north of the crater, its reworked equivalent is exposed in trenches excavated across the Solitario Canyon fault (Perry et al. 1998 [DIRS 144335], pp. 4.24-4.30). These features all suggest a relatively high-energy eruption with an ash column that rose kilometers into the air so that clasts were cool when they fell to the ground and finer ash was dispersed widely by winds (termed a “violent Strombolian eruption” by many volcanologists). Other parts of the Lathrop Wells volcano were emplaced by quite different mechanisms. For example, mounds of coarse, partially welded spatter indicate a local, relatively low-energy Strombolian eruption. Recent quarry exposures reveal welded scoria, typical of a Strombolian eruption, in the main cone, raising the possibility that only the late stages of the cone-forming eruptions were violent Strombolian. Thick, stubby aa flows suggest short-duration, high-mass-flux effusive eruption. The Lathrop Wells volcano and its deposits are discussed in detail in Section 6.4. Other volcanoes of the YMR (e.g., Sleeping Butte, Red Cone, and Black Cone) are less well preserved, but they seem to exhibit a similar range in eruptive styles at individual centers. This observation means that it is reasonable to assume a range of eruption mechanisms and, therefore, multiple exposure pathways for volcanic disruption of a repository.

The solubilities of volatiles such as H<sub>2</sub>O and CO<sub>2</sub> in basaltic magmas are proportional to pressure (Jaupart and Tait 1990 [DIRS 118292], p. 219). At depth (for example, in a magma chamber), magmas will have relatively high volatile contents. As they ascend through progressively lower lithostatic pressure, they will become oversaturated and bubbles will nucleate. Continued rise results in increasing numbers and sizes of bubbles (caused by combined exsolution of volatiles and decompression and coalescence growth of the bubbles), these two processes increase the specific volume of the magma, and as a consequence, its velocity also increases gradually (according to conservation of mass). Explosive eruption occurs when, at shallow depths, the magma reaches a foamy state, and with further decompression, it fragments, switching from being a melt with dispersed bubbles to a gas with dispersed fragments or clots of melt. At and above this fragmentation depth, the gas-melt mixture accelerates rapidly until it leaves the volcanic vent at speeds of tens to a few hundreds of meters per second. A further complication in this sequence of events is the possibility of loss of volatiles through the walls of the conduit or dike as magma ascends. This action can reduce the effective volatile content for the eruption.

The dynamics of magma ascent, and particularly the fragmentation process, are currently a topic of intense research in the volcanological community. Most recent advances in this area focus on silicic rather than basaltic magmas. The reasons for this are twofold. First, silicic magmas are responsible for the most explosive eruptions and present the most severe hazard to populations; understanding their dynamics is key in mitigating these hazards. Second, silicic magmas have viscosities several orders of magnitude higher than basaltic magmas. This condition greatly reduces the effects of bubbles rising more rapidly than their host melts and coalescing with each other. Thus, theoretical modeling is made more tractable by having to consider only nucleation, decompression growth, and growth by diffusion of exsolving volatiles into bubbles. In other words, the dynamics are closely approximated by a “homogeneous flow” approach, in which the gas and melt move at about the same velocity everywhere and are in thermal equilibrium. However, the rise of basaltic magmas with their lower viscosities is complicated by the potential for rapid rise and coalescence of bubbles (Vergnolle and Jaupart 1986 [DIRS 115585], pp. 12,842-12,846). Extreme results of this process are represented by classic Strombolian bursts, which are basically large bubbles rising through and bursting at the top of a magma column, producing eruptions of mostly gas with small amounts of melt (fragments of bubble walls) thrown out ballistically. Another example is the Hawaiian fire fountain eruptions, which have been observed to erupt molten pyroclasts with H<sub>2</sub>O vapor content much higher than the H<sub>2</sub>O solubility at depth. A general theory for the rise of basaltic magmas, accounting fully for the important two-phase flow effects, does not exist. Instead, the treatment below simplifies the problem by assuming homogeneous flow.

### 6.3.3.1 Magma Ascent Rate below Volatile Exsolution

Wilson and Head (1981 [DIRS 101034]) developed a theory for the ascent of basaltic magmas along dikes and cylindrical conduits using the homogeneous flow simplification. At depth, where magma is under sufficient pressure that all volatiles are dissolved, the buoyancy-driven ascent velocity,  $u_f$ , is (Wilson and Head 1981 [DIRS 101034], p. 2,974):

$$u_f = \frac{A\eta}{4K\rho_m r} \left[ \left( 1 + \frac{64gr^3(\rho_c - \rho_m)K\rho_m}{A^2\eta^2} \right)^{1/2} - 1 \right] \quad (\text{Eq. 3})$$

where

$A = 64$  (circular conduit) or  $24$  (dike)  
 $\eta$  is magma viscosity  
 $K = 0.01$   
 $\rho_m$  is the melt density (no bubbles)  
 $\rho_c$  is the wall rock density  
 $r$  is the conduit radius or dike half width  
 $g$  is gravitational acceleration.

Note that flow described in Equation 3 can occur only when  $\rho_c > \rho_m$ .

### 6.3.3.2 Volatile Exsolution and Fragmentation

As magmas rise, volatiles may begin to exsolve. The solubility of water ( $n$ ), the major volatile species in basalt, is approximated by Equation 1 (Jaupart and Tait 1990 [DIRS 118292], p. 219). The depth at which exsolution of water vapor begins to occur is the depth at which the magma becomes saturated with respect to its original water content, which, assuming lithostatic pressure ( $P = \rho_c g d$ , where  $d$  is depth; see Section 5, Assumption 3), can be derived as:

$$d_{\text{exs}} = \frac{(n_i / 6.8 \times 10^{-8})^{10/7}}{\rho_c g} \quad (\text{Eq. 4})$$

where

$d_{\text{exs}}$  is exsolution depth in meters (m)  
 $n_i$  is the initial dissolved mass fraction of water at the magma's depth of origin,  
 $\rho_c$  is the average density of the crust above  $d_{\text{exs}}$  in  $\text{kg/m}^3$   
 $g$  is gravitational acceleration ( $\text{m/s}^2$ ).

This relation is plotted in Figure 6. The mass fraction of water exsolved from a basaltic magma,  $n_{\text{exs}}$ , at a given depth is

$$n_{\text{exs}} = n_i - n \quad \text{when } d < d_{\text{exs}} \quad (\text{Eq. 5a})$$

$$n_{\text{exs}} = 0 \quad \text{when } d > d_{\text{exs}}. \quad (\text{Eq. 5b})$$

The density of the mixture of silicate melt and water vapor bubbles ( $\rho_{\text{mix}}$ ) can be calculated from (Wilson and Head 1981 [DIRS 101034], p. 2973)

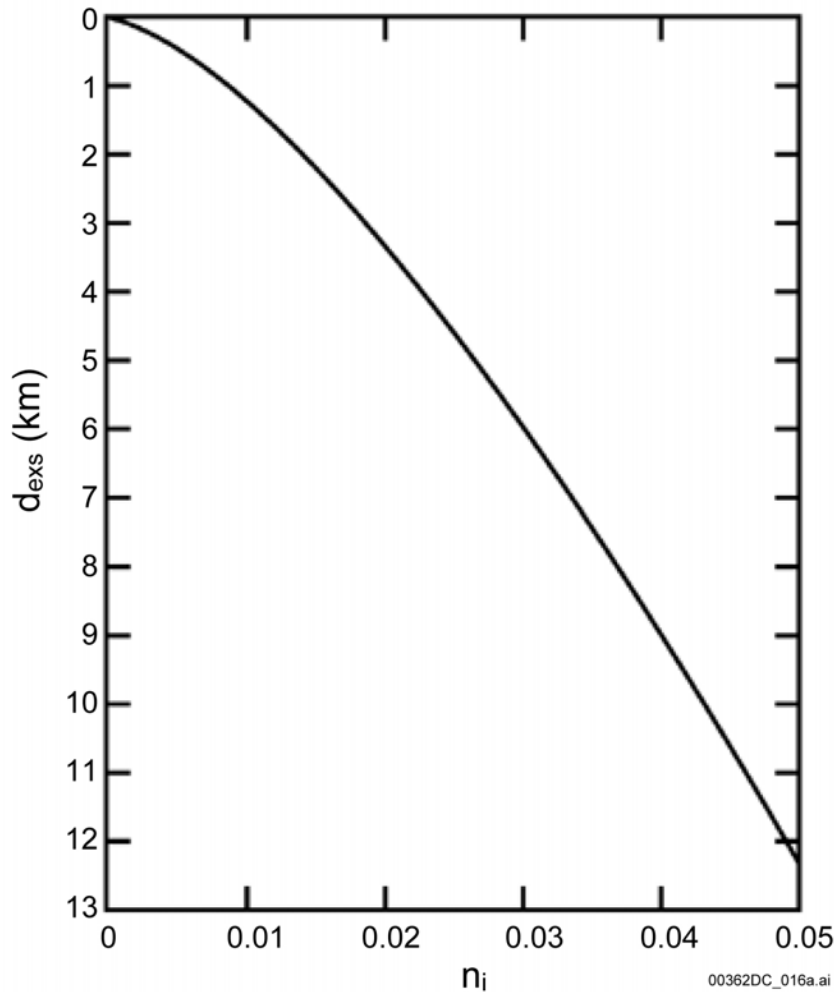
$$\frac{1}{\rho_{\text{mix}}} = \frac{n_{\text{exs}}}{\rho_g} + \frac{(1 - n_{\text{exs}})}{\rho_m} \quad (\text{Eq. 6})$$

The density of the gas phase ( $\rho_g$ ) can be calculated using the ideal gas law:

$$\rho_g = \frac{P}{RT} \quad (\text{Eq. 7})$$

where  $R$  is the gas constant for water (in this report, a value of 461 J/kg-K is used) and  $T$  is temperature. If it is assumed that the pressure in a conduit or dike is determined by the lithostatic pressure,  $\rho_g$  can be computed as a function of depth  $d$ :

$$\rho_g = \frac{\rho_c g d}{RT} \quad (\text{Eq. 8})$$



DTN: N/A (plot of equation 4)

NOTE: The calculations assume that pressure in the magma column is lithostatic and that bubble nucleation kinetics can be ignored. The average (shallow) crustal density ( $\rho_c$ ) is taken to be 2,000 kg/m<sup>3</sup>, as an example.

Figure 6. Plot of the Depth at Which Volatile (H<sub>2</sub>O) Exsolution Begins in a Lathrop Wells Basalt ( $d_{exs}$ ) for Initial Dissolved Water Content ( $n_i$ ) up to 0.05

Equations 1 and 4 to 8 can be used to calculate the mixture density for any initial volatile content at any depth, which may be useful for estimating the interactions between the mixture and the repository. The mixture density can also be expressed in terms of gas volume fraction,  $\phi$ , as

$$\rho_{mix} = \phi\rho_g + (1-\phi)\rho_m \quad (\text{Eq. 9})$$

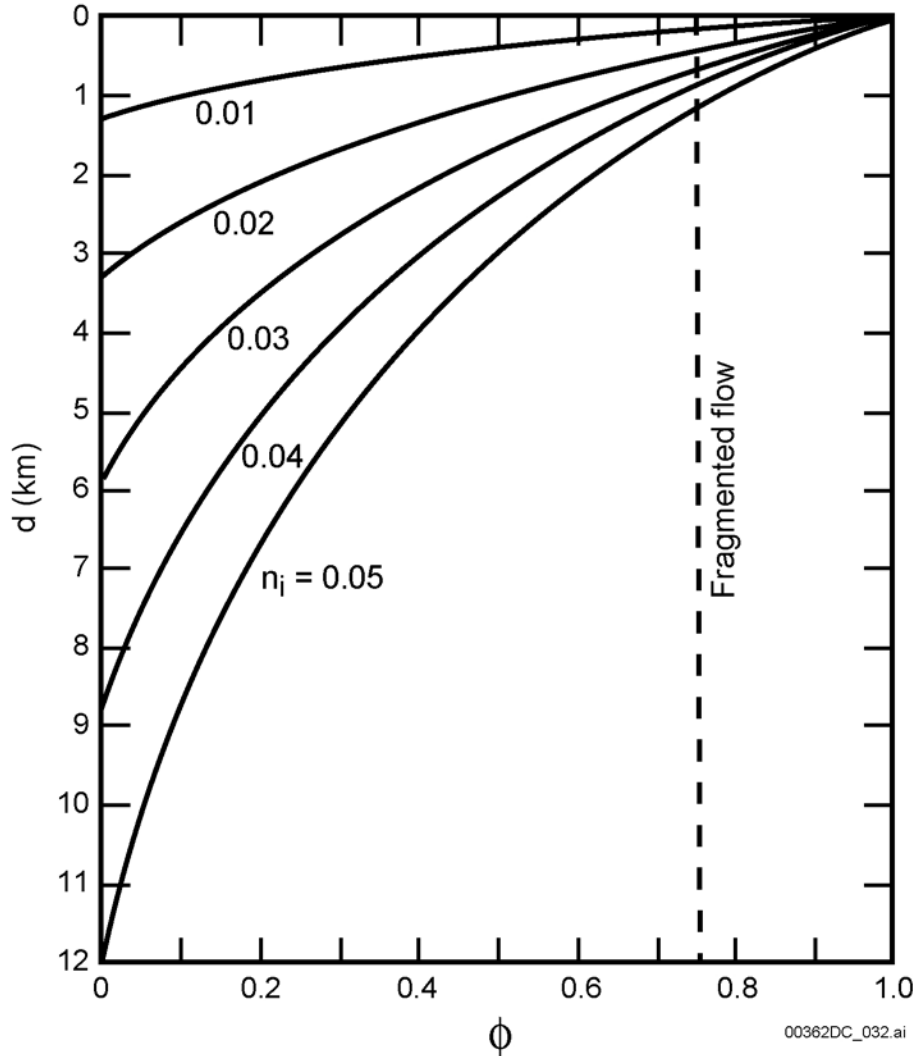
Re-arranging, the gas volume fraction is here derived as:

$$\phi = \frac{\rho_{mix} - \rho_m}{\rho_g - \rho_m} \quad (\text{Eq. 10})$$

Figure 7 shows the depth at which fragmentation occurs in rising basaltic magma, assuming that:

1. The flow is steady and homogeneous, the system is closed (no gas loss into country rock), and bubble nucleation and growth kinetics can be ignored (see Section 5, Assumption 4).
2. The vertical pressure profile in the dike/conduit below the fragmentation depth is very close to the lithostatic pressure profile (see Section 5, Assumption 3).
3. A gas volume fraction at which fragmentation commences can be established.

The limitations of the first assumption have already been discussed. The second assumption is very good at depths where  $\phi$  is small, but it becomes less accurate toward the fragmentation depth, and it is probably very inaccurate above the fragmentation depth. However, the second assumption is a good estimate of the “average” fragmentation depth for a variety of different scenarios. The third assumption is currently a subject of intense research. A critical value of  $\phi$  at which fragmentation occurs has commonly been assumed to be close to 0.75 (Mader 1998 [DIRS 144419], p. 55), and this is adopted in Figure 7. Recent studies have demonstrated, however, that fragmentation can take place in a range from  $0.60 < \phi < 0.95$  (for example, Mader 1998 [DIRS 144419], p. 56). The commonly assumed critical fragmentation value of  $\phi_{crit} = 0.75$  is adopted as a reasonable estimate given how little is understood about this process, particularly with regard to basaltic magmas. With all these assumptions, Figure 7 illustrates that estimated fragmentation depths for initial volatile contents between 0 and 4 wt% range from about 0 to 900 m.



00362DC\_032.ai

DTN: N/A (plot of equation 10)

NOTE: Calculations assume  $p_c = 2,000 \text{ kg/m}^3$ ,  $p_m = 3,000 \text{ kg/m}^3$ ,  $T = 1,300 \text{ K}$ , and  $R = 461 \text{ J/kg/K}$ . The dashed line defines a critical gas volume fraction of 0.75, which, in this report, is assumed to be the threshold for fragmentation of the magma. Plot is derived by solving Equations 1 and 5 as functions of depth for a given value of  $n_i$ , Equations 8 and 6, and finally Equation 10 for each value of  $n_i$ .

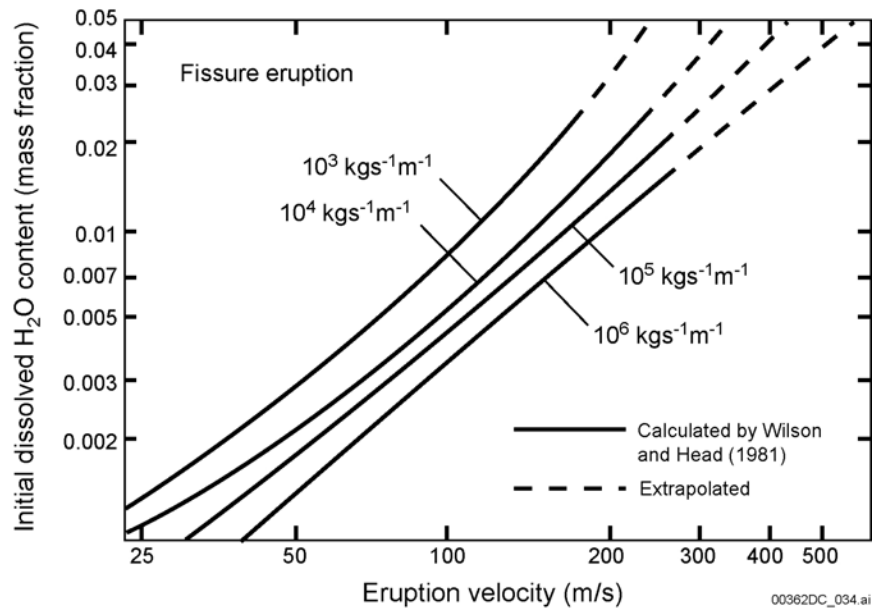
Figure 7. Plot of the Variation of Gas Volume Fraction ( $\phi$ ) with Depth ( $d$ ) for a Lathrop Wells Basalt, Assuming Pressure in the Magma is Lithostatic, for Initial Dissolved Water Content  $n_i = 0.01, 0.02, 0.03, 0.04,$  and  $0.05$

### 6.3.3.3 Velocity as a Function of Depth above Exsolution Depth

Descriptions of the magma velocity, conduit/dike dimensions, and magma pressure as functions of depth ( $d$ ) require, even with the homogeneous-flow approximation and a steady-state assumption, solution of three coupled equations (Wilson and Head 1981 [DIRS 101034], Eqs. 16-18, p. 2974). Two of these equations are ordinary differential equations. The detailed solution of these equations for a range of parameters appropriate to volcanism in the YMR is beyond the scope of this report. However, Wilson and Head (1981 [DIRS 101034], p. 2983) do provide some plots that relate eruption velocity,  $u_{erupt}$ , (where the magma-gas mixture exits the

vent) to initial dissolved water content ( $n_i$ ) of the magma, assuming that the pressure in the conduit/dike is equal to lithostatic pressure. Their solutions, shown with the solid curves in Figures 8 and 9, are for values of  $n_i$  up to approximately 0.02 for both dike (fissure) and circular conduit geometries. As discussed in Section 6.3.2.2, it is possible that  $n_i$  values for basalts of the YMR have been as high as 0.03 to 0.04, and the possibility of values as high as 0.05 is allowed in these plots. It is expected that YMR basaltic magmas with such high water contents would not erupt (Section 6.3.2.2). Thus, Figures 8 and 9 show the extrapolated values (dashed parts of the curves) for velocity at these higher initial water contents. Note that these are only graphical extrapolations, not actual solutions to the governing equations. However, given the various simplifications that are made in arriving at the Wilson and Head (1981 [DIRS 101034], p. 2983) results, these extrapolations are reasonable approximations.

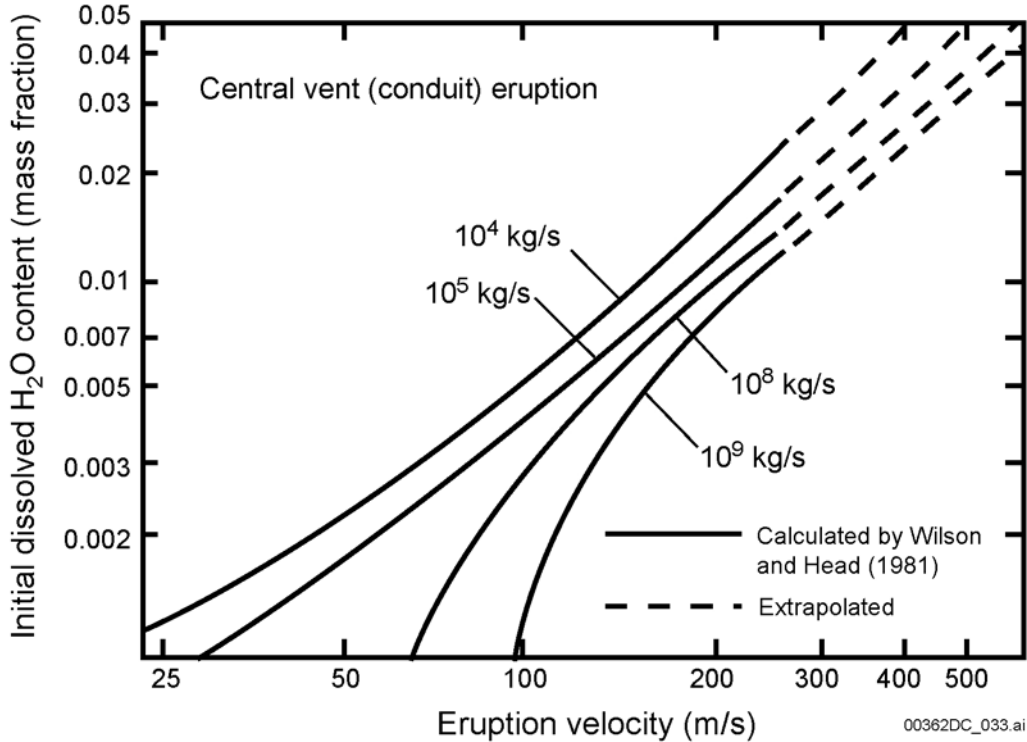
The velocity of magma ascending from some depth to the vent probably can be estimated with sufficient accuracy for modeling by simplifying such that velocity increases linearly from  $0.01u_{erupt}$  at  $d_{exs}$  to  $0.1u_{erupt}$  at the fragmentation depth, thence increasing linearly to  $u_{erupt}$  at the vent ( $u_{erupt}$  obtained from Figures 8 and 9). Using such an approach will account for the greater accelerations that are thought to occur above the fragmentation depth and the more gradual acceleration below it. In addition, this approach guarantees consistency in the calculations of velocity at various depths (as opposed to random sampling from distributions at different depths).



Source: Wilson and Head (1981 [DIRS 101034]); plot of equations from reference and extrapolations

NOTE: Solid curves show values calculated by Wilson and Head (1981 [DIRS 101034], p. 2983), whereas dashed lines are graphical extrapolations to include the range of initial volatile contents of concern for Yucca Mountain. The Wilson and Head calculations assume homogeneous flow and lithostatic pressure in the rising magma column.

Figure 8. Plot of the Variation of Eruption Velocity ( $u_{erupt}$ ) with Initial Dissolved Water Content ( $n_i$ ) for Various Mass Discharge Rates Along a Fissure



Source: Wilson and Head (1981 [DIRS 101034]); plot of equations 17 to 18 from reference and extrapolations

NOTE: Solid curves show values calculated by Wilson and Head (1981 [DIRS 101034], p. 2983), whereas dashed lines are graphical extrapolations to include the range of initial volatile contents of concern for Yucca Mountain. The Wilson and Head calculations are based on the assumption of homogeneous flow and lithostatic pressure in the rising magma column.

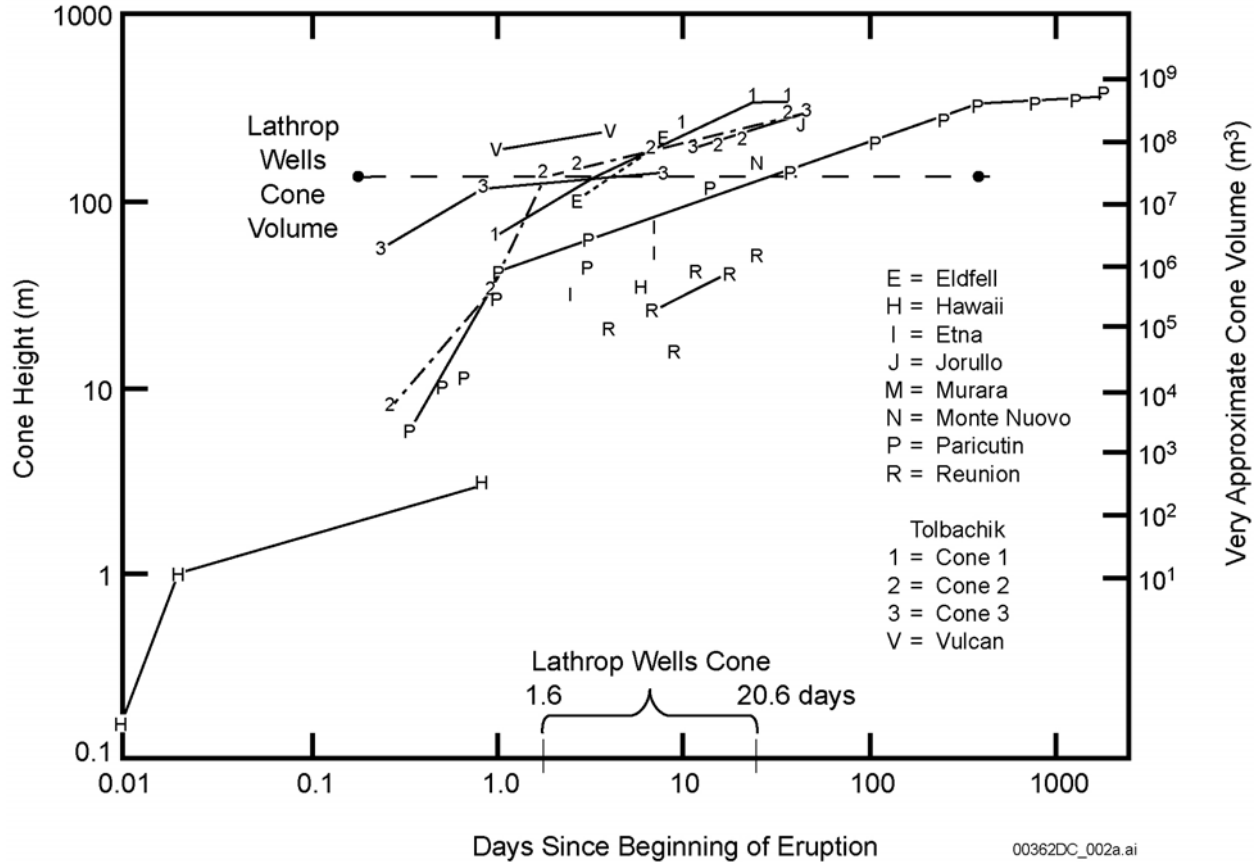
Figure 9. Plot of the Variation of Eruption Velocity ( $u_{erupt}$ ) with Initial Dissolved Water Content ( $n_i$ ) for Various Mass Discharge Rates from a Circular Conduit

### 6.3.3.4 Eruption Duration and Volumes

Lathrop Wells Cone and the other Crater Flat volcano remnants are examples of the most likely eruptive phenomena to affect the YMR. The characteristics associated with the surface manifestations are discussed in context in the next sections.

#### 6.3.3.4.1 Duration of Strombolian or Scoria-Cone-Forming Eruptions

The duration of Strombolian eruptions ranges from days to more than a decade. Figure 10 plots data on cone height and volume as related to eruption duration (Wood 1980 [DIRS 162860], p. 402). Lathrop Wells Cone height is plotted for comparison with other cone-forming eruptions. Using historical eruptions plotted on Figure 10 for comparison, a scoria cone of the height and volume of Lathrop Wells Cone could have been formed in approximately 1 to 21 days.



Source: Wood (1980 [DIRS 162860], p. 402)

NOTE: The Lathrop Wells Cone height is ~140 m.

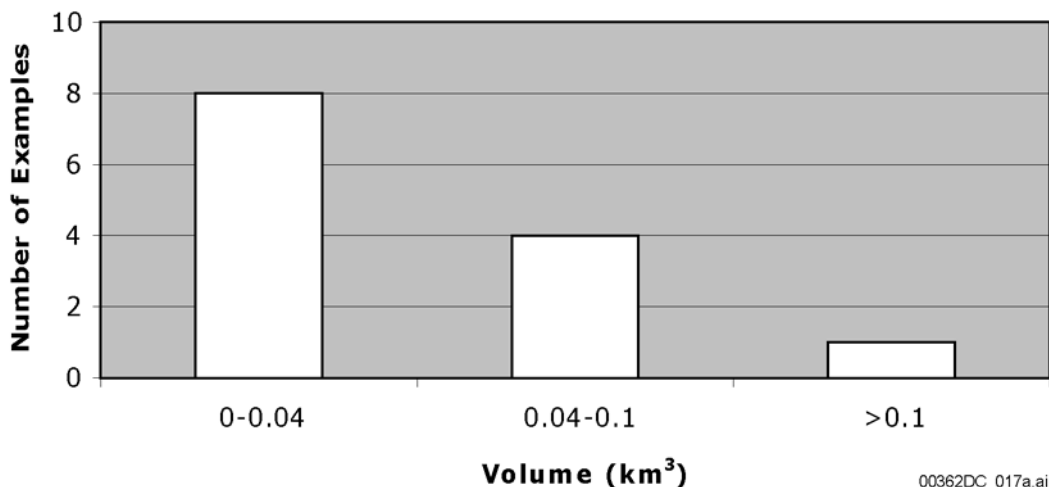
Figure 10. Changes in Cone Height During an Eruption Based on Observed Strombolian Activity

For the duration of individual explosive phases that produce a high column and disperse ash widely, we adopt the same range of parameter values used in Jarzempa (1997 [DIRS 100460], pp. 136-137). The data supporting this range are shown in Table 13, which also includes the estimated mass discharge rate for the eruptions, using an estimated magma specific heat of 1,000 J/kg-K (see, for example, the range of values in Best 1982 [DIRS 147740], p. 301) and temperature of 1,350 K. Explosive phases lasted from about half an hour to 73 days. However, we note that the longer duration events occurred at volcanoes of larger volume than is typical of the YMR in the Quaternary. For example, the final volume of Parícutin volcano after nine years of eruption is more than an order of magnitude larger in volume ( $2.1 \times 10^9 \text{ m}^3$ ; Wood 1980 [DIRS 116536], p. 390) than the Lathrop Wells volcano.

#### 6.3.3.4.2 Volume and Scale of Scoria Cones of Strombolian Eruptions

The choice of Lathrop Wells Cone as an analog for a potential disruptive volcano at the repository is based on geologic setting, its proximity to the repository, its composition and type of eruption, and its youth (~80,000 years). One persistent issue in discussions of YMR volcanism is the scale of the Lathrop Wells Cone compared with scoria cones elsewhere in the world (e.g., NRC 1999 [DIRS 151592], Table 3). Previous reports used, for comparison of scale

and eruption style, the following volcanoes: Parícutin, Mexico; Tolbachik 1 and 2, Russia; Heimaey, Iceland (also called Eldfell in Figure 10); Serra Gorda, Azores; Cerro Negro, Nicaragua; and Sunset Crater, Arizona (Table 9). In this section, we expand the data set on scoria cones beyond these seven scoria cones (Figure 11 and Table 9). In this comparison, the Lathrop Wells scoria cone is in the first category, with a volume of 0.018 km<sup>3</sup> (see Section 6.4.3), similar to the majority of examples in this data set.



Sources: Table 9

Figure 11. Scoria Cone Volumes

*Data on Scoria Cones.* Settle (1979 [DIRS 162846]) published a study of 1,089 cinder cones (scoria cones), which were broadly categorized by structural setting, cone basal diameter, and cone height. One category (“platform cone field”) includes 629 cones and is most similar to the tectonic setting for Lathrop Wells Cone and Crater Flat volcanoes (Figure 12 and Table 10). This category includes the cones from the San Francisco Peaks volcanic field, Arizona, the Parícutin region, Mexico, and the Nunivak Island field, Alaska. Cone volume is not determined, but as shown below, there is a strong connection between volume and cone basal diameter with regard to the magnitude of eruptions forming those cones. Lathrop Wells Cone (diameter ~700 m), among the largest in the Crater Flat field, is plotted on Figure 12 for comparison with Parícutin, Tolbachik, and Sunset Crater cones.

Table 9. Comparison of Lathrop Wells Cone with Scoria Cone Data Sets

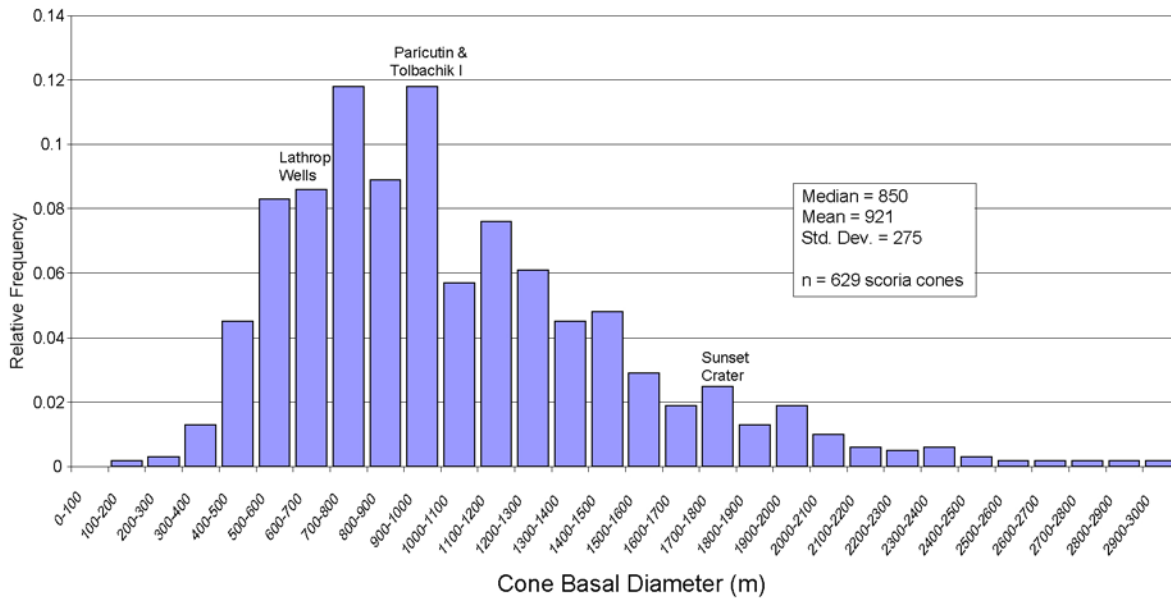
Volumes of Scoria Cones and Associated Deposits (Historic–Holocene)				
Volcano	Cone (km <sup>3</sup> )	Lavas (km <sup>3</sup> )	Fallout (km <sup>3</sup> )	Total (km <sup>3</sup> )
<b>Lathrop Wells Cone, Nevada</b>				
Lathrop Wells—Best estimate; planimeter (Section 6.4.3)	0.018	0.0292	0.039	0.0862
Lathrop Wells—Fallout: method of Pyle 1989 [DIRS 123891] (Section 6.4.3)			0.037	
Lathrop Wells (Crowe et al. 1983 [DIRS 100972], Table 1)				.057
Lathrop Wells (Perry et al. 1998 [DIRS 144335], Table 3.1)				0.14
Lathrop Wells (NRC 1999 [DIRS 151592], Table 3)	0.024	0.038	0.048	0.11

Table 9. Comparison of Lathrop Wells Cone with Scoria Cone Data Sets (Continued)

<b>Volumes of Scoria Cones and Associated Deposits (Historic–Holocene)</b>				
<b>Volcano</b>	<b>Cone (km<sup>3</sup>)</b>	<b>Lavas (km<sup>3</sup>)</b>	<b>Fallout (km<sup>3</sup>)</b>	<b>Total (km<sup>3</sup>)</b>
<b>Crater Flat Cones (Perry et al. 1998 [DIRS 144335], Table 3.1)</b>				
Makani Cone				0.006
Black Cone				0.105
Red Cone				0.105
Little Cone				0.002
Hidden Cone				0.03
Little Black Peak Cone				0.03
<b>Crater Flat Cones (NRC 1999 [DIRS 151592], Table 3)</b>				
Hidden Cone	0.019	0.009	0.038	0.066
Little Black Peak	0.006	0.007	0.012	0.025
SW Little Cone, volume corrected for 50 percent erosion	0.002	0.022	0.004	0.028
Red Cone, volume corrected for 33 percent erosion	0.005	0.089	0.005	0.099
Black Cone, volume corrected for 33 percent erosion	0.011	0.065	0.011	0.087
<b>Other Examples of Similar Age Range and Tectonic Setting</b>				
Cinder Cone, California (Heiken 1978 [DIRS 162817], Table 1)	0.038	no data	0.032	0.07
Parícutin, Mexico (Fries 1953 [DIRS 162810] p. 611)	added to ash total	0.7	1.309	2.009
Cerro Negro, Nicaragua–1971 (Rose et al. 1973 [DIRS 116087], Figure 2)	added to ash total	0	0.07	0.07
Cerro Negro, Nicaragua–1968 (Rose et al. 1973 [DIRS 116087], Figure 2)	added to ash total	0.003	0.017	0.020
<b>Estimates (NRC 1999 [DIRS 151592], Table 3)</b>				
Tolbachik 1, Russia	0.093	0.025	0.122	0.24
Tolbachik 2, Russia	0.098	0.242	0.099	0.439
Sunset Crater, Arizona	0.284	0.15	0.44	0.874
Parícutin, Mexico	0.069	0.7	0.41	1.179
Heimaey, Iceland	0.015	0.18	0.012	0.207
Serra Gorda, Azores	0.03	0.015	0.042	0.087
Cerro Negro, Nicaragua, Sum of all eruptions, 1850-1995	0.08	0.043	0.132	0.255

Sources: Listed in table

NOTE: Cone volumes of Tolbachik 1 and Tolbachik 2 are from NRC (1999 [DIRS 151592], Table 3), who cite Budnikov et al. (1983 [DIRS 162797]). Tokarev (1983 [DIRS 163860], Table 1) gives a smaller volume for Tolbachik 1 for a measurement of July 11, 1975. The present report uses the volume presented in NRC (1999).



00362DC\_027.ai

Source: Settle (1979 [DIRS 162846], Figure 2) and Table 10 (this report)

NOTE: Basal cone diameters of the Lathrop Wells (this volume), Parícutin (Hasenaka and Carmichael 1985 [DIRS 162814]), Tolbachik 1 (Tokarev 1983 [DIRS 163860], Table 1), and Sunset Crater (USGS 1966; USGS 1969) scoria cones are noted on the figure. Cones from the Nunivak, San Francisco, and Parícutin cone fields are included.

Figure 12. Basal Cone Diameters of 629 Scoria Cones

Table 10. Basal Diameters of Scoria Cones - Platform Cone Fields

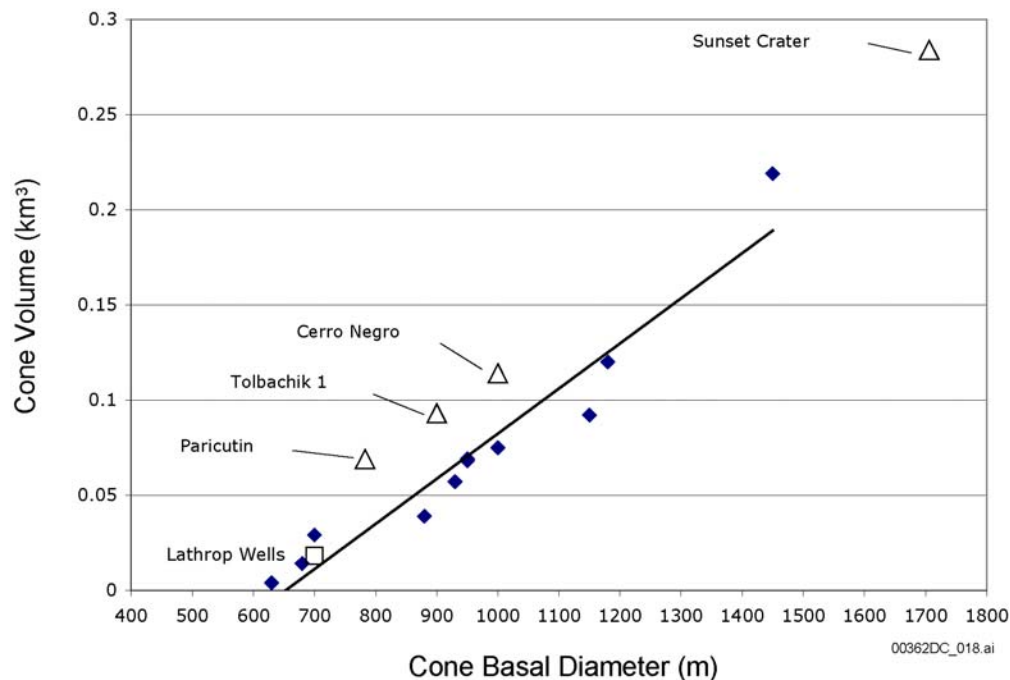
Basal Diameter (m)	Relative Frequency	Basal Diameter (m)	Relative Frequency
0-100	0	1500-1600	0.029
100-200	0.002	1600-1700	0.019
200-300	0.003	1700-1800	0.025
300-400	0.013	1800-1900	0.013
400-500	0.045	1900-2000	0.019
500-600	0.083	2000-2100	0.010
600-700	0.086	2100-2200	0.006
700-800	0.118	2200-2300	0.005
800-900	0.089	2300-2400	0.006
900-1000	0.118	2400-2500	0.003
1000-1100	0.057	2500-2600	0.002
1100-1200	0.076	2600-2700	0.002
1200-1300	0.061	2700-2800	0.002
1300-1400	0.045	2800-2900	0.002
1400-1500	0.048	2900-3000	0.002

NOTE: The data are for 629 cones from Settle (1979 [DIRS 162846], Figure 2).

Figure 13 illustrates the relation between basal cone diameter and cone volume. The data from the Trans-Mexican Volcanic Belt (Hasenaka and Carmichael 1985 [DIRS 162814], Table 18)

(Table 11) are plotted along with Parícutin, Tolbachik 1, Cerro Negro, and Sunset Crater (Table 12). The latter four cones plot above the trend on which the Lathrop Wells Cone and others reside, but still show the diameter-volume relationship.

The following observations are relevant to characterizing future volcanism in the YMR. Parícutin and Tolbachik 1 volcanoes are four to five times larger in volume than the Lathrop Wells Cone; the Tolbachik volcano in Kamchatka is associated with voluminous volcanism above a complex and rapidly subducting (~80 mm/year) oceanic plate. The Cerro Negro volcano, in Nicaragua, also in an volcanic arc setting above an actively subducting oceanic plate, has a long, complex eruptive history (22 eruptions since 1850) and has been interpreted as a nascent composite cone, rather than a scoria cone (McKnight and Williams 1997 [DIRS 162827], p. 342). Sunset Crater is sixteen times larger (volume) than Lathrop Wells and is, along with the Jorullo Volcano in Mexico, among the giants of scoria cones. Figures 11-13 place the Quaternary Lathrop Wells Cone, and the equal- or smaller-volume cones that populate the Crater Flat area, within the broader population of scoria cone sizes. The comparisons argue that the < 1-Ma YMR cones be kept in the context of their setting and relative size and that sets of smaller scoria cones are most appropriate to characterize disruptive volcanic events at Yucca Mountain.



Source: Hasenaka and Carmichael (1985 [DIRS 162814], Table 2)

NOTE: The data are for 11 cones in the Trans-Mexican Volcanic Belt (diamonds) along with the Lathrop Wells Cone (open box) and the larger Parícutin (Hasenaka and Carmichael 1985 [DIRS 162814], Tolbachik 1 (NRC 1999 [DIRS 151592], Table 3), Cerro Negro (McKnight and Williams 1997 [DIRS 162827], Figure 2), and Sunset Crater (Table 9 and USGS 1966; USGS 1969) cones. Trend line refers only to the Trans-Mexican Volcanic Belt data.

Figure 13. Scoria Cone Volume Versus Cone Basal Diameter

Table 11. Trans-Mexican Volcanic Belt Cone Field Basal Diameters and Cone Volumes

<b>Volcano</b>	<b>Cone Volume (km<sup>3</sup>)</b>	<b>Basal Diameter (m)</b>
Parícutin, Mexico	0.069	950
Volcan El Jorullo	0.219	1450
Cerro El Jabali	0.057	930
Cerro El Metate	0.039	880
Cerro La Taza	0.029	700
Hoya El Huanillo	0.068	950
Volcan La Mina	0.092	1150
El Pueblito	0.075	1000
Cerro Las Cabras	0.120	1180
Cerro Pelon	0.014	680
Santa Teresa	0.004	630

Source: Hasenaka and Carmichael (1985 [DIRS 162814], p. 112)

Table 12. Other Volcano Basal Diameters and Cone Volumes

<b>Volcano</b>	<b>Cone Volume (km<sup>3</sup>)</b>	<b>Basal Diameter (m)</b>
Sunset Crater, Arizona <sup>a</sup>	0.284	1706
Cerro Negro, Nicaragua	0.114 <sup>b</sup> ; 0.08 <sup>c</sup>	1000
Tolbachik I, Kamchatka <sup>d</sup>	0.093 <sup>c</sup>	900 <sup>d</sup>
Lathrop Wells, Nevada <sup>e</sup>	0.018	500 × 900

NOTES: <sup>a</sup>Amos et al. 1981 [DIRS 162794], p. 1085

<sup>b</sup>McKnight and Williams 1997 [DIRS 162827], p. 340

<sup>c</sup>NRC 1999 [DIRS 151592], Table 3

<sup>d</sup>Tokarev 1983 [DIRS 163860], p. 30

<sup>e</sup>This volume, Section 6.4.3

### 6.3.3.4.3 Eruption Duration and Volume

Eruption duration is difficult to estimate because, during the formation of a volcanic center, it is likely that eruptive discharge rates could have varied substantially. Wood (1980 [DIRS 116536], p. 402) provides data on the duration of scoria-cone forming eruptions, showing that they range from one day to about 15 years, with a median value of 30 days. Wood (1980 [DIRS 116536], p. 402) also states that about 93 percent of such eruptions last less than one year. Note that this duration is for the formation of the entire volcano, including lava flows, scoria cone, and fallout blanket, and may include periods of inactivity. The aa character of the Lathrop Wells lava flows implies a mass discharge rate of at least  $3 \times 10^4$  kg/s (Crowe et al. 1983 [DIRS 100972], p. 269). Using this value as a conservative minimum eruption rate, the Lathrop Wells volcano, with a total volume of about  $10^8$  m<sup>3</sup> (Crowe et al. 1983 [DIRS 100972], p. 269; mass of about  $3 \times 10^{11}$  kg calculated using an approximated magma density of 2,600 kg/m<sup>3</sup> from Table 8 in this report), would have erupted in about  $10^7$  kg/s (about 120 days) if the eruption rate was constant during that time. For comparison, the Hekla 1947 eruption reached discharge rates of about  $4.7 \times 10^7$  kg/s during highly explosive phases (Table 13). At this rate, the Lathrop Wells volcano

would have completely formed in about 1.8 hours, which is an unrealistically short time (recall that comparison with historic eruptions suggests the Lathrop Wells scoria cone could have formed in between 1 and 21 days; Section 6.3.3.4.1). For total eruption duration, that is, formation of the entire volcano, a log normal distribution with a minimum of one day, a mean of 30 days, and a maximum of 15 years is recommended. However, for implementation in TSPA, it is more relevant for the evaluation of dose to consider the duration of the more explosive phase(s) of the eruption that ejects finer-grained material into a sustained eruption column, or the violent Strombolian phase. The material within the eruption column, being subject to dispersal from winds active during the eruption and particle settling, can result in dusty, downwind atmospheric conditions that can be evaluated for inhalation pathway within TSPA. Table 13 lists durations (in log-seconds) of explosive-eruptive events for 8 historical eruptions. The data range from 3.3 log-seconds (0.55 hours: Hekla 1947) to 6.8 log-seconds, (73 days: Parícutin 1944 II and 1946). This distribution of durations for explosive-eruptive phases suggests that a range of 1 day to 75 days will capture the range of likely durations for an explosive phase of a future basaltic eruption at Yucca Mountain. A uniform probability distribution is recommended because it requires the fewest assumptions for the few available data. Note for modeling purposes that this distribution is not meant to encompass the duration for formation of the entire volcano.

Table 13 also lists calculated log power ( $P_o$ , in watts) for the volcanoes. Power is the product of mass discharge rate, heat capacity, and temperature. Mass discharge rate can be estimated by dividing volume (mass) of the erupted products by duration of eruption. Logrithm of power among these volcanoes ranges from 9 (Parícutin 1946) to 13.8 (Hekla 1947). The two Hekla volcanic eruptions are the shortest-lived and the largest volume events in Table 13. Hekla is located on the mid-Atlantic ridge and represents a sustained magma source located over a hot-spot, and is not an appropriate analog for comparison of power output with a future Yucca Mountain volcano. A range of log-power outputs for some future Yucca Mountain volcano should be captured by the remaining values of 9.0 to 12.0 and described with a uniform probability distribution. Power can be estimated for the Lathrop Wells volcano based upon the duration for formation of the entire volcano from 1 to 21 days in Figure 10. Estimated log power  $P_o$  ranges from about 11 to 12 for the Lathrop Wells Cone eruption. A longer total duration of eruption for Lathrop Wells Cone would result in a lower calculated power.

Defining 75 days as the upper duration of an explosive-eruptive phase implies a specific mass-discharge rate for the maximum volume of ash expected from a future Yucca Mountain region volcano. This volume, discussed below in Section 6.4.3.1, is  $0.08 \text{ km}^3$  and corresponds to the maximum amount of ash available for dispersal by convection and winds active during eruption. A 75-day explosive-eruptive phase equates to an average mass-discharge rate of  $3.2 \times 10^4 \text{ kg/s}$ . The mean discharge rate from Table 13 (ignoring the two Hekla eruptions) is  $2.4 \times 10^5 \text{ kg/s}$ . The values support the selection of a 75-day limit on an explosive-eruption phase, which corresponds to the longest, higher energy phase of the Parícutin 1946 eruption. Note that these discharge rates represent average rates over the durations of an explosive phase.

Total erupted volume can be obtained by multiplying eruption duration by mass discharge rate, and then dividing by magma density of  $2,600 \text{ kg/m}^3$  (a representative density for magmas for a Lathrop Wells type eruption; see Table 8). This results in a dense rock equivalent volume. The bulk volume of deposits from an eruption will be larger because of the presence of voids

(vesicles) within particles and of void space between particles. For a violent Strombolian eruption, the fallout blanket will have a density within a range specified below. If the bulk volume of a violent Strombolian eruption is needed, then one should use the bulk density (see Section 6.3.5.3) instead of the magma density.

Table 13. Explosive Eruptive Events, Duration, Power, and Estimated Mass Discharge Rates Used to Develop Probability Distributions for Eruptive Plume Dispersal Calculations

Event	Log (t) (t in s) <sup>a</sup>	Log (Po) (Po in W) <sup>a</sup>	Mass Discharge Rate (kg/s) <sup>b</sup>
Cerro Negro, 1992	4.8	12.0	$7.4 \times 10^5$
Hekla, 1970	3.9	12.8	$4.7 \times 10^6$
Tolbachik, 1975	6.1	11.7	$3.7 \times 10^5$
Parícutin, 1944 I	5.6	11.1	$9.3 \times 10^4$
Parícutin, 1944 II	6.8	11.5	$2.3 \times 10^5$
Parícutin, 1946	6.8	9.0	$7.4 \times 10^2$
Hekla, 1947	3.3	13.8	$4.7 \times 10^7$
Heimaey, 1973	6.4	9.9	$5.9 \times 10^3$

NOTES: <sup>a</sup> Jarzempa (1997 [DIRS 100460], p. 136)

<sup>b</sup> Mass discharge rates based on  $T = 1,350$  K and magma heat capacity  $c_p = 1,000$  J/kg-K (Best 1982 [DIRS 147740], p. 301). Mass discharge rate =  $Po(c_p T)^{-1}$ .

### 6.3.4 Entrainment of Radioactive Waste in Ascending Magma

Quantification of the amount of waste that could be entrained by rising magma and subsequently erupted and dispersed is difficult because of uncertainties regarding the potential interactions of the magmatic system with the repository. Some of these uncertainties are volcanological in nature, and some are related to the nature of the engineered system; the latter are beyond the scope of this report. Physical and chemical models of the interaction of magma and waste package and waste form are provided in *Igneous Intrusion Impacts on Waste Packages and Waste Forms* (BSC 2003 [DIRS 165002]).

Uncertainties are inherent in the following volcanic processes: 1) the interaction between a rising dike and perturbed stress field around repository drifts; 2) the interaction between rising, vesiculating magma and partially open drifts (e.g., would magma flow like lava for long distances down the drifts, would it pile up quickly to block the drift and, therefore, allow magma to continue rising, or would it explode down the drift); and 3) the depth to which conduits might extend (i.e., if a wide conduit is formed but extends only 200 m below the surface, then it will not have as large a disruptive effect on the repository). These issues are explored further in *Dike/Drift Interactions* (BSC 2003 [DIRS 165923]).

Xenolithic materials from country rock included in eruptive products can be used as a qualitative analog for material transport in ascending magma. Wall-rock xenoliths are incorporated into rising magma by mechanical disruption of dike walls and during conduit growth, but they do not provide a perfect analog for engineered materials that could be disrupted by magma flooding a repository drift. There are a few data available on the interaction of magma with undisturbed country rock and subsequent eruption of the lithic debris for the range of eruptive styles that can be reasonably expected at Yucca Mountain. For example, Valentine and Groves (1996 [DIRS 107052], pp. 79-84) report data on the quantity of wall rock debris erupted from various

depths during Strombolian, Hawaiian, effusive, and hydrovolcanic activity at two volcanoes. Hydrovolcanic eruptions reported by Valentine and Groves contained between 0.32 and 0.91 volume fraction of wall rock debris, with most of that originating in the uppermost ~510 m of the dike/conduit feeder systems. Strombolian, Hawaiian, and effusive eruptions ejected much lower volumes of wall rock debris, commonly resulting in total volume fractions of  $10^{-3}$  to  $10^{-5}$ . Doubik and Hill (1999 [DIRS 115338], p. 60) state that the Lathrop Wells volcano has a relatively high average lithic volume fraction of  $9 \times 10^{-3}$  for xenoliths  $> 1$  mm, based on image analysis of unspecified locations. It is possible that all the locations studied by Doubik and Hill were located in a quarry that exposes proximal cone deposits. Clarification of this issue has required analysis of more exposures at Lathrop Wells and is discussed in Section 6.4.1.2 below. Addressing this issue may be important because Doubik and Hill (1999 [DIRS 115338], p. 61) cite similarity of lithic content as a justification for using the relatively large and violent Tolbachik eruptions as analogs for the Lathrop Wells volcano (and, hence, potential eruptions at Yucca Mountain).

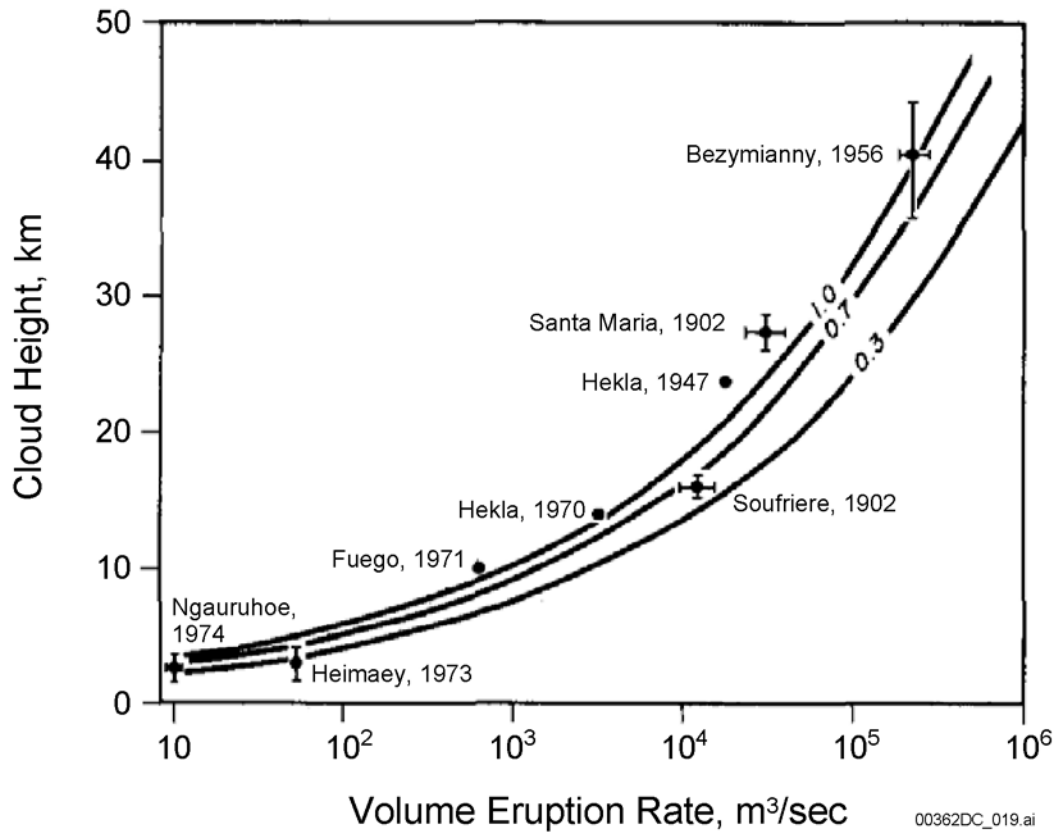
### **6.3.5 Ash Plumes and Their Deposits**

#### **6.3.5.1 Eruption Columns**

Eruption energies and volumes of tephra fall are directly linked to the nature of the eruption columns (plumes). Self and Walker (1994 [DIRS 162831], Table 1) summarized eruption column behavior for all eruption types, ranging from the least energetic (Hawaiian) to the most energetic (Plinian). Eruption columns range from small-scale bursts to large convective systems that transport large volumes of ash, volcanic gases, and entrained air. The columns all have in common a gas-thrust region (the jet of material leaving the vent, usually representing less than 10 percent of the total eruption column height), a buoyant convective-thrust region that constitutes most of the column in large Plinian eruptions and may be small in Strombolian eruptions, and the umbrella region, a momentum-driven rise and lateral spreading from which occurs most of the ash fallout. The summary, compiled for an aviation safety group, describes Hawaiian/Strombolian eruptions as frequent (5-10 per year globally) with *maximum* column heights of 7 to 10 km and durations of tens to thousands of hours.

Walker (1973 [DIRS 125609], Figure 6) did not directly address column heights, but related an “*F* value” (percentage of material finer than 1 mm and related to fragmentation energies) to a “*D*” value (area enclosed by the  $0.01 T_{\max}$  isopach, where  $T_{\max}$  is the maximum deposit thickness). Figure 14 illustrates the eruption concepts relating column height to the areal extent of ash falls.





Source: Wilson et al. (1978 [DIRS 162859]); for reference purposes only

NOTE: Plot of observed eruption cloud heights versus volume eruption rate for 8 explosive eruptions (Wilson et al. 1978 [DIRS 162859], Figure 2). The only Strombolian eruption on this plot is that of Heimaey (1973). The curves represent different values of  $F$ , which is an efficiency factor of heat usage (see Wilson et al. 1978 [DIRS 162859] for further explanation).

Figure 15. Eruption Cloud Height Versus Volume Eruption Rate

### 6.3.5.2 Bulk Particle Size and Distribution of Deposits from Strombolian and Violent Strombolian Eruptions

As described in Section 6.3.3, explosive eruptive styles of Quaternary volcanoes in the YMR include both Strombolian and violent Strombolian. Strombolian eruptions are characterized by short-duration bursts that throw relatively coarse fragments of melt out of the vent on ballistic trajectories. Most of the fragments (clasts) are deposited immediately around the vent, with only a very small fraction of finer particles rising higher and being dispersed by wind to form minor fallout sheets. Table 15 shows estimated bulk eruptive grain-size distribution parameters for the Etna Northeast Crater (Italy) eruptions of September 1971 (McGetchin et al. 1974 [DIRS 115469], Fig. 8, p. 3264). These results are probably representative of many Strombolian eruptions, being skewed toward very coarse clast sizes.

Table 14. Range of Observed Column Heights of Strombolian and Violent Strombolian Eruptions

Dates	Range of (or Highest) Observed Column Heights (m)	Tephra Volume (Cone + Fallout) (km <sup>3</sup> )	Source
<b>Fogo, Cape Verde Islands*</b>			
4/3-16/95	100-5,000	no data	Smithsonian Institution (2003 [DIRS 162848])
4/17/95	100-200	no data	
4/18/95	500-600	no data	
4/21/95	50-150	no data	
4/24/95	1,500	no data	
4/25-27/95	50	no data	
*Eruption began with lava fountaining and the ejection of large blocks. It evolved into less vigorous fountaining, then obstruction of the crater and Strombolian blasts.			
<b>Veniaminof, Alaska</b>			
6/29/94	2,290-3,000 (corrected for crater elevation)	no data	Neal et al. (1994 [DIRS 162853])
<b>Cerro Negro, Nicaragua</b>			
1867 (2.8 days)	> 1,000	0.004	Hill et al. (1998 [DIRS 151040], Tables 1, 2)
1923 (49 days)	> 300	0.017	
1947 (0.8 days)	4,000-6,500	0.008	
1950 (26 days)	> 300	0.018	
1957 (15 days)	2,000	0.0013	
1968 (42 days)	1,000-1,500	0.013	
1971 (7 days)	6,000	0.027	
1992 (0.7 days)	3,000-7,000	0.010	
1995 (4 days)	2,000-2,500	0.004	
<b>Heimaey, Iceland</b>			
1973	1,000; 5,000-10,000	0.04	Self et al. (1974 [DIRS 162845], Figure 6 and p. 542); Cas and Wright (1987 [DIRS 124939], p. 140)
<b>Tolbachik I, Russia</b>			
1975-1976	200-5,000	0.215	Budnikov et al. (1983 [DIRS 162797], p. 41); NRC (1999 [DIRS 151592], Table 3)
<b>Parícutin, Mexico</b>			
1943-1952	Mostly a few hundred meters	no data	Luhr and Simkin (1993 [DIRS 144310], p. 78)
"heavy cineritic phase" from 3/18/43 to 6/9/43	≤6,000	0.479	

NOTE: Duration days in parentheses are for tephra-fall duration.

Table 15. Estimated Bulk Clast Size Distribution Parameters for Three Violent Strombolian Eruptions (Tolbachik and Cerro Negro 1971 and 1968) and One Strombolian Eruption (Etna 1971)

	Violent Strombolian Eruptions			Strombolian Eruption
	Combined Great Tolbachik N. Breakthrough <sup>a</sup>	Cerro Negro 1971 (Overall) <sup>b</sup>	Cerro Negro 1968 (Overall) <sup>b</sup>	Bulk Etna Northeast Crater <sup>c</sup>
<b>Median (mm)</b>	0.3	0.24	0.15	95
<b>Graphic Mean (mm)</b>	0.37	0.23	0.19	110
<b>Graphic Standard Deviation (<math>\sigma_\phi</math>)</b>	2.5	1.5	1.83	3.48

Sources: <sup>a</sup> Derived from data presented in Maleyev and Vande-Kirkov (1983 [DIRS 144325], pp. 61-62)

<sup>b</sup> Rose et al. (1973 [DIRS 116087], p. 342)

<sup>c</sup> Estimated from McGetchin et al. (1974 [DIRS 115469], p. 3264, Figure 8).

Violent Strombolian eruptions, on the other hand, are characterized by vertical eruption of a high-speed jet of a gas-clast mixture. As the eruptive mixture rises in the jet, it entrains and heats air, which in turn reduces the bulk mixture density until the jet becomes buoyant and continues to rise as a plume. The plume rises to an altitude of neutral buoyancy compared to the surrounding atmosphere, in which it then spreads laterally as an anvil shape or “umbrella” cloud that is transported downwind. Clasts fall out from both the vertical eruption column and from the umbrella cloud according to their settling velocities. Such an eruption tends to produce a fallout sheet with volume comparable to the cone volume to as much as 13 times the cone volume (excluding lava flows; Crowe et al. 1983 [DIRS 100972], p. 272). Historic violent Strombolian eruptions at Parícutin (Mexico) produced a fallout sheet (cone volume ratio of about 4:1), and Sunset Crater (Arizona) produced a ratio of about 3.2:1 (Crowe et al. 1983 [DIRS 100972], p. 272). Table 15 also shows bulk eruptive clast-size distributions for three historic violent Strombolian eruptions (Tolbachik and Cerro Negro, 1971 and 1968; Maleyev and Vande-Kirkov 1983 [DIRS 144325], pp. 61-62; Rose et al. 1973 [DIRS 116087], p. 342). Mean clast diameters for these eruptions range from 0.19 to 0.37 mm, and standard deviations range from 1.5 to 2.5  $\phi$  units (defined in Section 6.1.3.4). Table 16 shows the bulk eruptive grain-size distribution for the 80,000-year-old Lathrop Wells Cone tephra sheet. Median grain size for the basal tephra is ~2.4 mm, whereas all post-hydrovolcanic tephra sizes have a median of ~1.4 mm. Within 1.0 km of the vent, the tephra sheet is dominated by coarser basal lapilli- and ash-fall and the hydrovolcanic deposits (see Sections 6.4.2 and 6.4.2.3), related to early Strombolian-type eruption followed by an explosive eruption involving the incursion of groundwater into the rising magma. The < 1-km range also encompasses occurrences of volcanic bombs and blocks. Beyond 1 km, grain sizes are more representative of the finer particles deposited from these eruptions and violent Strombolian eruptive particles, that is, ash and lapilli, which were carried upward in the eruption column by the jet of volcanic gas-clast mixture and which spread laterally as a cloud to be carried downwind and deposited. Grain-size data for this distal (1-2 km) sample population show that particles range from ~0.125 mm to ~8.0 mm; particle sizes < 0.125 mm typically account for less than 4 wt% of any sample. Comparison with tephra from the 1975 Tolbachik, Kamchatka, eruption, which contains as much as 58 wt%  $\leq$  0.1 mm (Maleyev and Vande-Kirkov 1983 [DIRS 144325], p. 61) and the 1995 Cerro Negro, Nicaragua, eruption, with ~25 wt% ash < 0.1 mm, shows the Lathrop Wells Cone tephra appears deficient in smaller sizes. Either less fragmentation of magma, shorter duration of violent eruptive phases, or greater

dispersal of airborne ash occurred during eruption. Because Lathrop Wells Cone samples are limited to within 2 km of the vent, samples could be biased to coarser grain sizes, so dispersal cannot be ruled out. In performance assessment calculations of dose, the respirable fraction between 0.01 and 0.1 mm (10 to 100  $\mu\text{m}$ ) must be accounted for in a potential eruption through the repository.

Table 16. Median Grain Sizes for the 80,000-year-Old Lathrop Wells Cone Tephra

Lathrop Wells Cone Tephra	Basal Tephra (< 800 m from Vent)	Hydrovolcanic Tephra (< 800 m from Vent)	Post-Hydrovolcanic Tephra Within 1.0 km of Vent	Post-Hydrovolcanic Tephra Beyond 1.0 km of Vent
Median (mm)	2.35	0.42	1.63	1.16
Standard Deviation ( $\sigma_\phi$ )	0.65	0.24	0.77	0.57
Number of Samples	4	6	9	10

DTN: LA0302GH831811.002

For these reasons, the mean bulk particle size distribution for modeling an energetic violent Strombolian eruption for the Yucca Mountain area is a log-triangular distribution with a minimum of 0.01 mm, mode of 0.1 mm, and a maximum of 1.0 mm, to cover 2 orders of magnitude of sizes. For comparison, Jarzempa (1997 [DIRS 100460], p. 137) gives a log-triangular distribution with a minimum of 0.1 mm, a median of 1 mm, and a maximum of 100 mm. Although this upper range accounts for the larger lapilli sizes and smaller blocks and bombs, these particles would fall ballistically on or near the cone and would not contribute much or any mass to the downwind tephra deposit. Therefore, the upper limit of 1.0 mm for the suggested distribution gives some additional conservatism to calculations by ASHPLUME (BSC 2002 [DIRS 161296]) and performance assessment.

Given a mean clast size, the standard deviation of the particle size is needed to provide ASHPLUME (BSC 2002 [DIRS 161296]) with sufficient information on the particle size distribution. Table 15 provides information on the graphic standard deviation  $\sigma_\phi$  (defined in Section 6.1.3.4). It is recommended that, for a given mean particle diameter,  $\sigma_\phi$  be sampled from a uniform distribution between  $\sigma_\phi = 1$  and  $\sigma_\phi = 3$ .

### 6.3.5.3 Clast Characteristics

The clasts produced by Strombolian and violent Strombolian eruptions can be quite different in character. Strombolian eruptions produce a much higher proportion of coarse clasts, with the mean diameter commonly being > 10 centimeters (cm) (Table 15). Common Strombolian clast types include ribbon, spindle, and cowpie bombs. Ribbon and spindle bombs take their shape as they are stretched and torn or as they spin through the air on their dominantly ballistic paths; these shapes indicate the hot, fluid state of the clasts during flight. Cowpie bombs are very hot and fluid when they hit the ground. All these clasts are hot during flight and deposition because of their large size (low surface-area-to-volume ratio minimizes heat loss) and low eruption height (they have less time to cool before hitting the ground). These large clasts may have vesicle (bubble) volume fractions up to ~70 percent. Smaller clasts, in the mm to cm range, tend to be sub-equant vesicular scoria clasts, and they can have a range of vesicularities (for example, the Cinder Cone eruption at Lassen Volcanic National Park, California, produced scoria with

vesicularities of 20 to 70 percent; Heiken and Wohletz 1985 [DIRS 106122], p. 34). Finer ash-sized clasts tend to be less vesicular, and can range from irregular to fluidal to blocky in shape.

Violent Strombolian eruptions carry clasts much higher in the air, providing more cooling time; the clasts also cool more quickly because they have a much higher degree of fragmentation. A much larger proportion of the clasts is in the mm to cm size range compared to Strombolian eruptions, and most of these clasts have irregular shapes and relatively high vesicularities.

In violent Strombolian eruptions, the long-range, downwind transport and fallout of clasts becomes an important issue for YMP performance assessment calculations. Transport and deposition of clasts depend on their settling velocity in air, which in turn depends on their bulk density (the melt density corrected for the porosity, or vesicularity, of the clasts) and shape. Calculations of clast dispersal commonly use a shape factor,  $F = (b + c)/2a$ , where  $a$ ,  $b$ , and  $c$  are the lengths of the longest, medium, and shortest axes of the clasts. Clasts produced by these types of eruptions can have a range of shapes. Jarzempa (1997 [DIRS 100460], p. 139) used a value of  $F = 0.5$  as a shape factor that is likely to be representative of common clast shapes, and in the absence of further data, we recommend this value for performance assessment calculations for YMP.

Density of erupted particles varies with particle size because larger particles tend to have a higher fraction of vesicles (bubble voids) than small particles. Detailed data are lacking, but it is recommended that the particle density be varied as follows:

- For particle diameters less than or equal to 0.01 mm, the particle density is 0.8 of the magma density (which is taken to have an average value of 2,600 kg/m<sup>3</sup> for a Lathrop Wells-type magma). This value is based on a fine-particles void fraction of 0.2 due to vesicles.
- For particle diameters greater than or equal to 10 mm, the particle density is 0.4 of the magma density. This value is based on a void fraction of 0.6 due to vesicles.
- Between 0.01 mm and 10 mm, density should decrease linearly with increasing diameter.

#### **6.3.5.4 Density of Fallout Deposits**

Bulk in situ density of fallout deposits typically ranges from 300 to 1,500 kg/m<sup>3</sup> (Sparks et al. 1997 [DIRS 144352], p. 366), but is rarely directly measured, particularly for basaltic deposits such as are most likely in the YMR. Blong (1984 [DIRS 144263], p. 208) has measured a range of fallout deposits that have a density of approximately 1,000 kg/m<sup>3</sup>. There are two reasonable ways of treating deposit density in TSPA calculations: 1) simply use 1,000 kg/m<sup>3</sup> or 2) use a sample from a normal distribution of deposit densities ranging from 300 to 1,500 kg/m<sup>3</sup> with a mean of 1,000 kg/m<sup>3</sup>.

## 6.4 PHYSICAL VOLCANOLOGY OF THE LATHROP WELLS CONE

The Lathrop Wells Cone lava flows have an eruption age of approximately  $77.3 \pm 6.0$  ka, based on seventeen  $^{40}\text{Ar}/^{39}\text{Ar}$  ages on the stratigraphically oldest lava flow. In this report, an age of ~80,000 years is used. The arguments for this conclusion are in Perry et al. (1998 [DIRS 144335]) and details of the geochronology studies are provided in Heizler et al. (1999 [DIRS 107255], Section 5.4, p. 799). The most probable interpretation for the Lathrop Wells eruptive center is that of a complex monogenetic volcanic center producing a cone, lava flows, and tephra deposit erupted within a span of a few months or years, but the center also exhibits some features that support other interpretations of age and eruptive history (Perry et al. 1998 [DIRS 144335]).

### 6.4.1 Scoria Cone

The Lathrop Wells scoria cone (Figure 16) is approximately 140 m high and oval, with its long axis oriented NNW-SSE. The cone measures 875 m by 525 m at its base and is capped by a similarly elongate, 190-m by 145-m crater that is about 20 m deep. The outer slopes of the cone range from  $28^\circ$  to  $32^\circ$  and consist of mostly loose scoria lapilli. The cone shape has been somewhat modified by erosion and is rapidly changing because of active quarrying along the south margins. The cinder cone has an approximate volume of  $0.018 \text{ km}^3$ . Quarrying is revealing the three-dimensional structure of the cone, currently exposing approximately one-quarter of the cone's interior. Figure 17 is a DEM portraying the relief of the cone and surrounding area as if illuminated from the northwest. It shows the locations of samples used for this study, most of which are discussed specifically in the following subsections.



For illustration purposes only

Figure 16. Lathrop Wells Scoria Cone and Adjacent Lava Flows (Capped by Beige, Eolian Sand) Viewed from the North



00362DC\_020a.ai

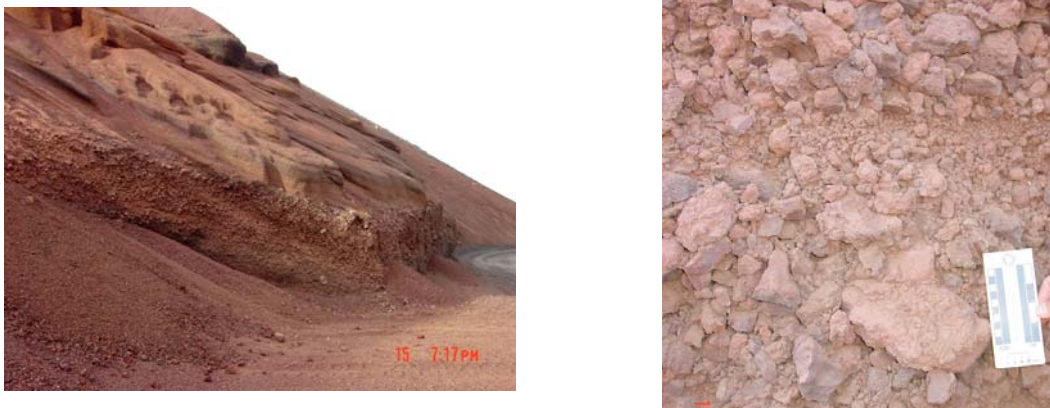
For illustration purposes only

NOTE: The Lathrop Wells Cone occupies the lower center of the map. The dots show locations of samples; the numbers correspond to the sample numbers given in this report (preceded with "DK-LW-"). Grid is NAD 1927 UTM, Zone 11 North, in meters. Contour interval is 20 feet.

Figure 17. Topographic Map and Tephra Sample Locations for Lathrop Wells Cone Area

Most cone deposits exposed in the quarry dip concentricly outward from the cone center with primary depositional slopes of 30° to 32°. Primary dips gradually decrease to ~20° near the top

of the cone. The stratigraphically lowest deposits exposed in the quarry are irregular masses of welded scoria and bombs and mostly or partly welded lapilli. Some of these agglutinate masses dip inward  $\sim 10^\circ$  toward the presumed location of the vent. The representative stratigraphic sections of the cone described below are compiled from exposures within the quarry and along bulldozer cuts from the base to the summit.



For illustration purposes only

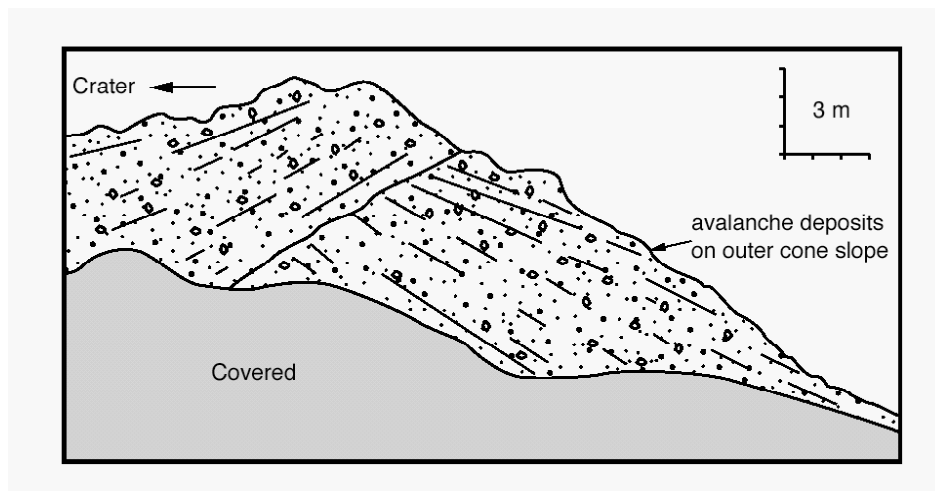
NOTE: Left photo: Exposures of cone interior showing sharp transition from nonwelded, massive or poorly bedded, lapilli- and bomb-size ballistic ejecta to overlying moderately bedded avalanche deposits of ash and lapilli (> 50 percent ash); most clasts are deposited at angles of repose as ballistic ejecta. Height of the lower coarse beds is about 2.5 m. Right photo: Close-up of ejecta (at base of left image), mostly broken scoria bombs and lapilli. The scale is 10 cm.

Figure 18. Cone Interior Showing Scoria and Close-up of Ejecta

Overlying the agglutinate unit, a basal, 2.5-m thick section (elevation  $\sim 840$  m) in the quarry, about 100 m north of the loading facility, consists of the following (Figure 18):

- The lowest 0.9 m of exposed units composed of massive, nonwelded, poorly sorted, gray to reddish-gray scoria lapilli with approximately 8 to 12 percent bombs and blocks (maximum observed was 28 cm by 18 cm).
- A 0.3- to 0.6-m thick deposit of poorly sorted lapilli, blocks, and bombs with no ash matrix. Ninety-five percent of the deposit consists of blocky, angular scoria with a few percent large (> 20 cm) cauliflower and spindle bombs.
- A 0.9-m deposit of clast-supported reversely graded lapilli and bombs, with bombs up to 0.75 m long and thin (2-3 cm) interbeds of lapilli.
- At the top, a wedge-shaped avalanche deposit (thickening down-slope from about 0.3 to > 1 m) with a slope of  $32^\circ$ , near the angle of repose. Reddish-brown lapilli and ash with 10 to 50 percent ash. This unit extends upward toward the summit. Up-slope, this deposit is cut by an irregular small channel with decreasing slope from  $\sim 30^\circ$  to near horizontal; the channel is filled with olive-gray scoria.

Uppermost deposits of the cone are visible along road-cuts near the cone summit. At this elevation (~968 m), the deposits slope into the crater at ~15° to 20°. Exposed are ~8 m of crudely bedded, vesicular, scoriaceous lapilli and coarse ash with ~5 percent bombs, and 1 to 2 m of coarser, frothy scoria lapilli. These units contain less than ~0.5 percent lithic clasts comprising angular pieces of bedded tuff and rhyolitic pumice. About 38 m below these beds (elevation ~925 m) are exposures of a sharp angular unconformity between the upper, inward-dipping lapilli beds and the underlying, outward-sloping avalanche deposits (Figure 19). These exposures were destroyed by quarry operations during Fall 2002.



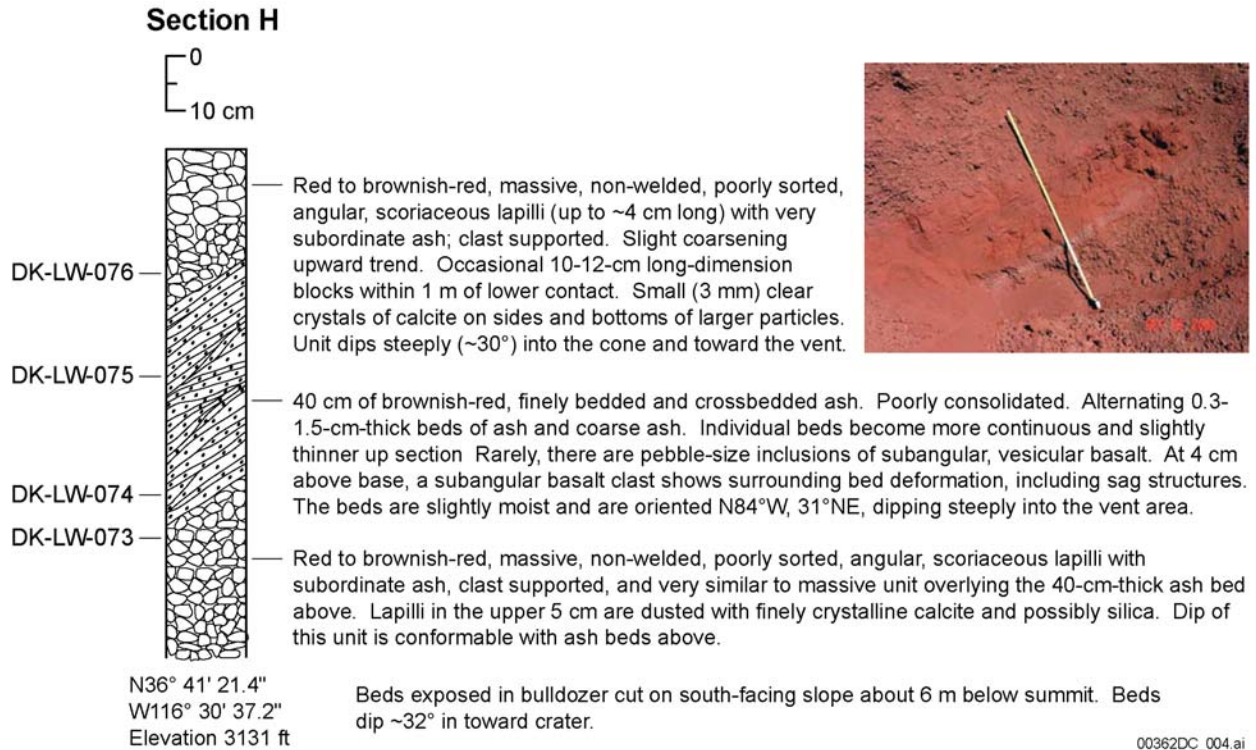
For illustration purposes only

NOTE: Elevation of the outcrop is ~925 m; top of cinder cone is ~968 m elevation.

Figure 19. Angular Unconformity Between Outward-Sloping Lapilli-Ash Avalanche Deposits and Deposits Sloping Toward the Vent

#### 6.4.1.1 Upper Hydrovolcanic Beds

About 6 m below the south summit (elevation 954 m), there is a 40-cm thick, well-sorted, finely bedded, cross-bedded ash and coarse ash deposit. Individual beds range from 3 mm to 1.5 cm thick and dip conformably 30° to 35° toward the crater. The reddish beds are sandwiched between poorly sorted beds of massive, nonwelded, angular, clast-supported, scoria lapilli. Upper and lower bed contacts are parallel to the internal bedding, and no scouring or excavation of the lower coarse bed is evident (Figure 20). Rare, rounded, clear quartz sand grains are present in a few hand specimens but are volumetrically insignificant (estimated < 0.1 vol%).



Source: Krier and Harrington (2003 [DIRS 164023], pp. 118-120)

NOTE: Inset photo is centered on the 40-cm thick, finely bedded ash; measuring tape is extended 1 m. The thin, white layer is disseminated secondary mineralization, probably carbonate.

Figure 20. Hydrovolcanic Beds Near the Top of Lathrop Wells Volcano

Grain size data for DK-LW-074 (ash and coarse ash beds 4-8 cm above the base), DK-LW-075 (20-25 cm above the base of the upper hydrovolcanic beds), and DK-LW-076 (coarse lapilli fall above the hydrovolcanic beds) are given in Table 17. This deposit appears to be the result of a brief hydrovolcanic event late in the cone-building history. Figure 21 plots grain size for these deposits; the hydrovolcanic samples stand out as much finer-grained and better sorted than the scoria fall that is more typical of the cone.

SEM analysis of the hydrovolcanic bed constituents reveals equant, rounded grains of tachylite with smooth, glassy vesicle wall remnants and less abundant sideromelane. Surface alteration of the grains is not abundant, but includes drusy silica and rare  $\mu\text{m}$ -sized, euhedral barite.

Table 17. Grain Size Data for Crater Deposits in the Lathrop Wells Cone

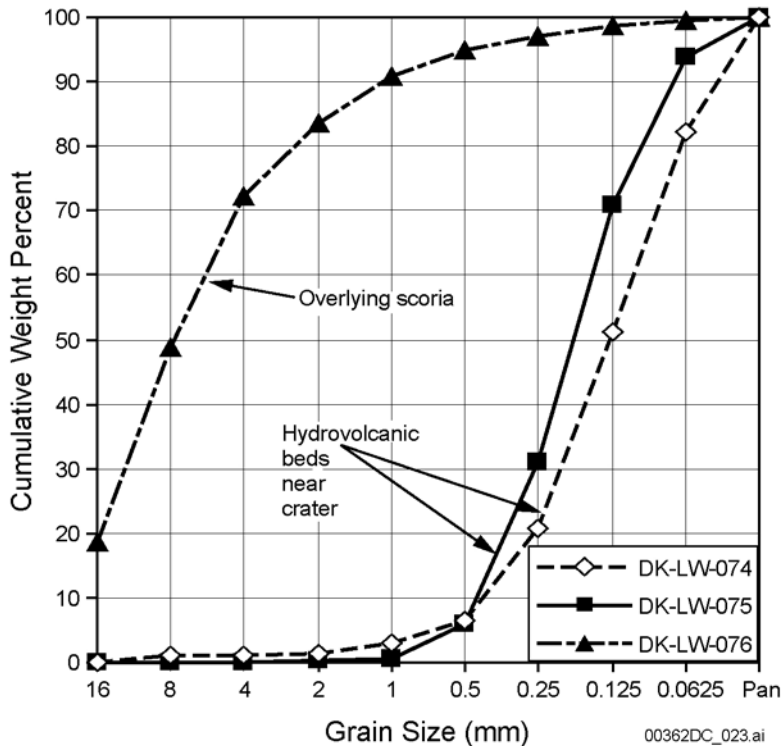
Sample Number	$Md_\phi$ (median)	$\sigma_\phi$ (sorting)	$Md$ (mm)
DK-LW-076	-2.97	1.66	7.8
DK-LW-075	2.47	1.08	0.18
DK-LW-074	2.94	1.07	0.13

DTN: LA0302GH831811.002

NOTES:  $Md_\phi$  = median grain size in  $\phi$  units (defined in Section 6.1.3.4)

$\sigma_\phi$  =  $(\phi_{84} - \phi_{16})/2$  (defined in Section 6.1.3.4)

$Md$  = median grain size in mm.



00362DC\_023.ai

DTN: LA0302GH831811.002

Figure 21. Grain Size Variations of Hydrovolcanic Beds and Overlying Lapilli Fall Near the Top of Lathrop Wells Volcano

#### 6.4.1.2 Lithic Clasts in the Lathrop Wells Cone Deposits

The best estimates for the volume and types of lithic clasts are important to repository risk assessment because the same processes that erode dike and conduit wall rock could influence the volume of waste reaching the surface (e.g., Crowe et al. 1983 [DIRS 100972], p. 269).

Larger and more interior quarried exposures provide a better opportunity to measure lithic clast abundances within the Lathrop Wells Cone than in the past (Crowe et al. 1986 [DIRS 101532]). Table 18 lists results of counts of 18 1-m<sup>2</sup> areas located at several elevations in the cone. Access

to outcrops in quarry walls and road cuts means that the elevations recorded with each measurement accurately reflect relative stratigraphic position (lower elevation: earlier cone history; higher elevations: later cone history). Measurements of lithic clasts were made in nonwelded deposits of coarse ash, lapilli, and larger material. They are not indicative of the stratigraphically lower, short pulse of hydrovolcanic activity recorded in deposits outside the cone (Section 6.4.2.3, Figure 26; Wohletz 1986 [DIRS 140956], p. 258). Counts were made with 12X and 10X hand lenses. Each visible lithic clast  $\geq 1$  mm was identified and its short and long axis measured. Lithic clast volume fractions  $F$  were determined using the following equation (Valentine and Groves 1996 [DIRS 107052], p. 80):

$$F = (\text{area fraction})^{3/2} (1.18)^3 \quad (\text{Eq. 11})$$

where areas measured are 1 m by 1 m squares on vertical exposures. Mean lithic clast abundances range from 0.29 vol% to  $< 0.002$  vol% (maximum value noted here is the mean of patches 1 through 6 measured within the same unit; maximum single measured value is 0.9 vol%). The volume data indicate that lithic clasts abundance is greatest within the measured lower stratigraphic levels in the scoria cone and decreases one to two orders of magnitude upward in younger scoria intervals. Not surprisingly, the lithic clasts production during eruption was not uniform throughout the cone construction period, and the variation suggests less vigorous conduit enlargement with time. This observation is tempered with the recognition that much of the scoria (and included lithic clasts) within volcanic cones is subject to avalanching, slumping, and redeposition during construction (McGetchin et al. 1973 [DIRS 115469], p. 3268).

Table 18. Lithic Clast Measurements in the Lathrop Wells Scoria Cone

Patch	Elevation (ft)	Volume Fraction	
17	3146	0.000140	
15	3136	0.000200	
12	3119	0.000160	
14	3106	0.000029	
13	3079	0.000083	
18	3074	0.000940	
16	3056	0.000290	
11	2940	0.000039	
7	2926	0.006700	
8	2926	0.000940	0.004985
9	2926	0.008700	Mean (7-10)
10	2924	0.003600	

Table 18. Lithic Clast Measurements in the Lathrop Wells Scoria Cone (Continued)

Patch	Elevation (ft)	Volume Fraction	
1	2886	0.009100	
2	2886	0.005800	
3	2886	0.000075	
4	2886	0.001300	0.002899
5	2886	0.001100	Mean (1-6)
6	2886	0.000018	

DTN: LA0302GH831811.003

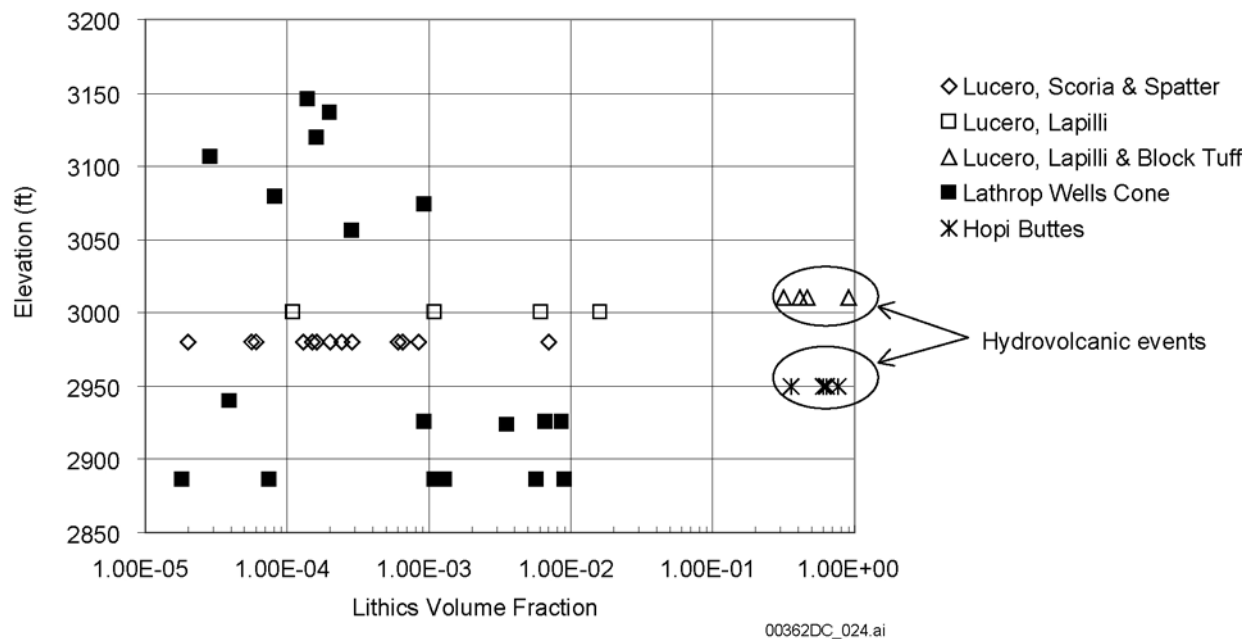
NOTE: Lithic clast measurements were done in eighteen 1-m<sup>2</sup> areas in Lathrop Wells Cone outcrops. Elevations reflect relative stratigraphic position (early to late cone activity), as explained in the text. Multiply the volume fraction by 100 to obtain a percentage.

Figure 22 is a plot of the Lathrop Wells Cone lithic volume fraction data versus elevation. The data are compared with similar data from the Lucero, New Mexico, volcanic field (Valentine and Groves 1996 [DIRS 107052], Table 1) and Hopi Buttes, Arizona (White 1991 [DIRS 124930], Figure 3), for both cone-building and hydrovolcanic deposits. The exposures at the Lucero field indicate that the so-called “lapilli and block-rich tuff” (which can contain up to 90 vol% lithic clasts) represents hydrovolcanic phases of the eruptions there and contain a mean lithic abundance of > 50 vol%. By contrast, Lucero “vesicular scoria and spatter” facies, representative of cone-building processes, average < 0.1 vol% lithic clasts. In comparison, the mean lithic clast abundance at Hopi Buttes, Arizona, perhaps an extreme example of well-exposed hydrovolcanic events, is between 50 and 60 vol%. Lathrop Wells Cone lithic clast abundances are not unusually high; even the upper hydrovolcanic beds (Section 6.4.1.1) are estimated to contain less than 0.1 vol%. Within the studied exposures, which represent a substantial vertical section through the cone, no lithic clast abundances were encountered that are indicative of significant conduit-clearing activity at the cone.

There is a common occurrence of secondary mineralization by silica and/or carbonate that coats many lapilli and larger grain surfaces that may be the cause of the elevated volume of lithic clasts obtained using computer-assisted image analysis (0.9 vol%; Doubik and Hill 1999 [DIRS 115338], p. 60; also, Section 6.3.4). Using this approach (digital images and image analysis) will result in a high estimate of lithic clasts. Results from Crowe et al. (1986 [DIRS 101532]), based on only 4 nonhydrovolcanic samples of the cone, ranged from 0.3 to 2.4 vol% in the < 0.707-mm size fraction.

#### 6.4.2 Tephra Distribution and Description

Much information about eruption processes can be gleaned from the Lathrop Wells Cone itself. However, until the cone has been totally dissected by quarrying, the most effective way of studying the sequence of eruption processes is to describe and analyze the tephra (ash-fall) deposits beyond the cone flanks. This assumes that a representative depositional record is preserved beyond the cone. The distribution of Lathrop Wells tephra and changes in grain size and pyroclast types are described here in the context of the stratigraphy as exposed in representative sections of the tephra fall deposit.



DTN: LA0302GH831811.003

NOTE: Volume fractions of lithic clasts > 1 mm were measured in the Lathrop Wells scoria cone. Lathrop Wells measurements (filled boxes) are shown in actual stratigraphic positions. Measurements from the Lucero volcanic field, New Mexico (Valentine and Groves 1996 [DIRS 107052]), and Hopi Buttes, Arizona (White 1991 [DIRS 124930]), are plotted at arbitrary elevations for comparison.

Figure 22. Volume Fractions of Lithic Clasts

### 6.4.2.1 Estimated Tephra Distribution

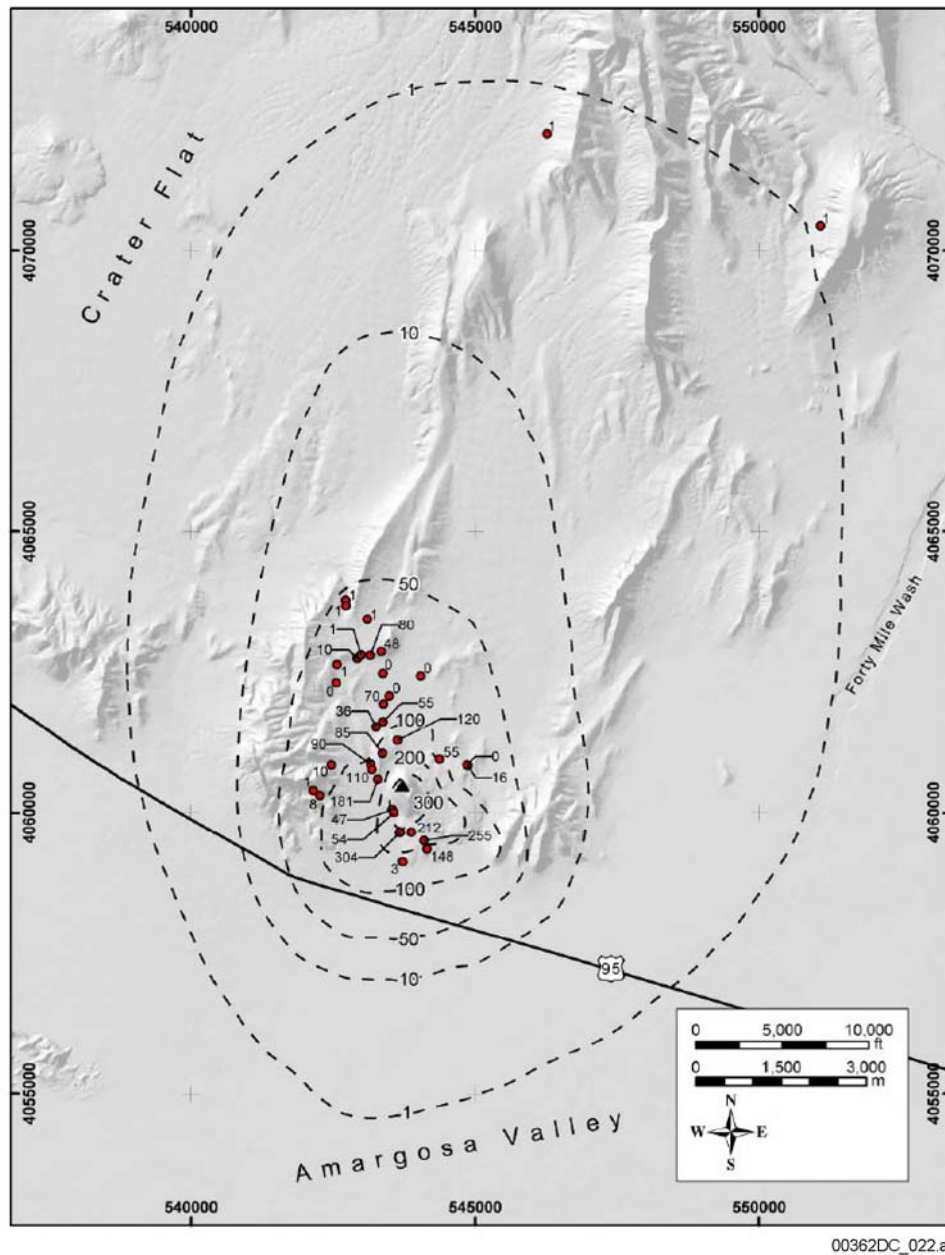
Figure 23 shows estimated isopach lines for thickness of Lathrop Wells Cone tephra using the plotted data points. The isopachs (300, 200, 100, 50, 10, and 1 cm) are drawn based on a visual fit to the data collected from both hand-dug pits and natural exposures. The tephra thicknesses in most instances represent minima because of an unknown amount of erosion of the tops of the sections of tephra. There is a relative consistency in the distribution of thicknesses that suggests that erosion was less than about 0.5 m, but this is difficult to quantify with the available data. Preservation of the tephra sheet was enhanced due to low topography and apparently rapid covering post-eruption by eolian sands, but these factors also limit the number of exposures and data points. The northern 1-cm isopach is chosen to be near the location of Solitario Canyon fault trench T8, where USGS workers exposed Lathrop Wells volcano ash concentrated within deposits in the fault plane (Perry et al. 1998 [DIRS 144335], p. 425). The amount and condition of ash particles suggest they represent ash runoff from the surrounding slopes and deposition in the fault plane when it was open during or soon after the earthquake that exposed the fault plane (Ramelli et al. 1996 [DIRS 101106] pp. 4.7-11 – 4.7-12). A second notation of scattered basaltic ash on the west side of Busted Butte (scientific notebook TWS-EES-13-LV-01-93-05 [Crowe 1996 (DIRS 164317), p. 54]) suggests that some deposition from the Lathrop Wells Cone ash-column occurred there. Without any preserved primary ash deposits to measure, a thickness of one cm of ash was used for the original thickness at this locality.

Observations of preserved tephra > 1 km west of the cone are limited to isolated, trace concentrations in detrital sediments in gullies on the hill slopes. Data on tephra thicknesses to the east and south of the cone are extremely limited and the isopachs are conjectural. There are no exposures beyond 800 m south of the cone base. The southernmost tephra location is in trench SP-7A (due south of the cone), where a 3-cm thick basaltic ash was located using a backhoe directly beneath the south toe of the lava flow (scientific notebook TWS-EES-13-LV-11-89-07 [Crowe 1992 (DIRS 162823), p. 90]). The ash lies directly upon a desert pavement. This thin ash predates the lava, but another tephra deposit (Section 6.4.2.2), exposed 500 m N-NE, is > 255 cm thick and postdates the lava. Observations in cuttings from several of Nye County, Nevada, hydrologic investigation wells (NC-EWDP-15P, NC-EWDP-2DB, NC-EWDP-3DB, NC-EWDP-9SX, and NC-EWDP-19P), located from between 2.5 km south to 6 km east of the cone, revealed no ash component within the upper 30 m of alluvial sediments there. The known tephra distribution around Lathrop Wells Cone suggests that during eruption the lofted basaltic ash column was directed predominantly northward by prevailing winds with minimal ash deposition south of the cone.

#### **6.4.2.2 Proximal Tephra Fall Near the Base of the Lathrop Wells Cone**

*Stratigraphic section at N36° 40' 54.8", W116° 30' 26," and elevation 821.7 m (2,696 feet), 650 m south of the summit of the Lathrop Wells Cone.*

Massive scoria fallout deposits at least 255 cm thick, overlying lava flows from the Lathrop Wells volcano, are exposed in a small quarry and they are used here to characterize proximal fallout (Table 19). Measured grain size variations are listed in Table 20 and plotted in Figure 24, which shows an overall median size decrease up-section. All samples are coarse grained and consist of mostly lapilli and coarse ash. The lower 130 cm has at least five reversely graded lapilli-ash fall sequences. The upper 125 cm begins with a normally graded lapilli-ash fall overlain by 2 to 3 beds of coarse and fine ash grading upward to ~0.5 m of bioturbated coarse ash mixed with eolian sand and silt. A 5-cm thick yellowish layer at 78 cm above the base contains up to 1 percent silicic pumice lithic clasts; the remainder of the sequence has few or no lithic clasts.



00362DC\_022.ai

Source: Krier and Harrington (2003 [DIRS 164023], p. 153)

NOTE: The triangle marks the volcano summit; the numbers are thicknesses, in cm, in dug pits or natural exposures.

Figure 23. Isopach Map (Estimated) of Tephra Fall from the Lathrop Wells Volcano

Table 19. Samples Used to Characterize the Proximal Scoria Fall Section

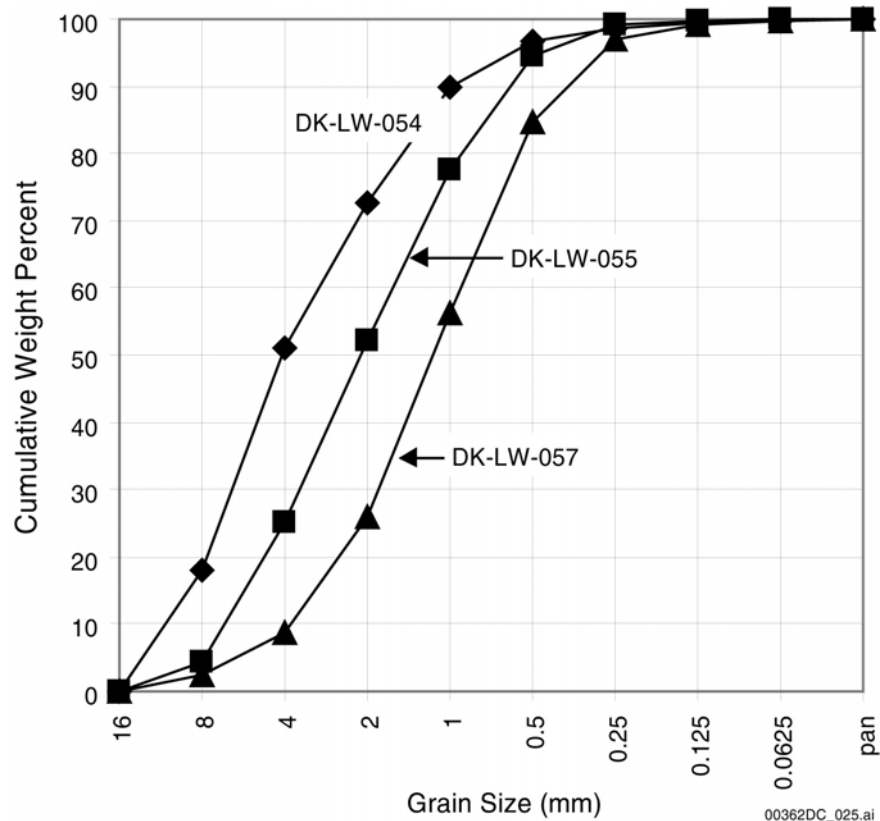
Sample	Description
DK-LW-057	Massive, brownish-gray ash and platy, vesicular lapilli fall, from an 11-cm thick bed at 180 cm above base of exposure.
DK-LW-055	Well sorted, medium to dark gray lapilli and coarse ash fall, 170 cm above base, between two continuous, thin (< 1 cm) resistant beds of calichified ash.
DK-LW-054	Well-sorted, reddish-brown lapilli and coarse ash scoria fall, 80 cm above base, and immediately above 5-cm wide yellowish color band. Largely equant, vesicular fragments. Individual fall beds 10 to 80 cm thick.

Source: Krier and Harrington (2003 [DIRS 164023], pp.57-59)

Table 20. Grain Size Variations in Scoria Fall Section Close to the Southern Base of Lathrop Wells Cone

Sample Number	$Md_{\phi}$ (median)	$\sigma_{\phi}$ (sorting)	$Md$ (mm)
DK-LW-057	-0.19	1.31	1.15
DK-LW-055	-1.11	1.43	2.2
DK-LW-054	-2.01	1.43	4

DTN: LA0302GH831811.002



DTN: LA0302GH831811.002

Figure 24. Grain Size Variations in Scoria Fall Section Close to the Southern Cone Base (“boneyard”)

*Variations in Pyroclast Types.* Table 21 lists the percent pyroclasts measured in samples from this scoria fall section. The pyroclasts are in the 0.5- to 1.0-mm size fractions, based on 300 grains, as measured using a binocular microscope.

Table 21. Percent Pyroclasts in Samples in Scoria Fall Section Close to the Southern Cone Base

Sample Number	Tachylite	Glassy Tachylite	Sideromelane	Quartz + Feldspar Sand	Tuff Clasts	Feldspar + Olivine Phenocrysts
DK-LW-057	17.6	64.3	17.6	0.0	0.0	0.3
DK-LW-055	29.0	57.0	15.0	0.0	0.0	0.0
DK-LW-054	8.0	58.6	32.6	0.3	0.3	0.0

DTN: LA0302GH831811.004

NOTE: Estimated Error = ± 0.1 percent

### 6.4.2.3 Tephra Stratigraphy Beyond the Lathrop Wells Scoria Cone

*Stratigraphic section (hydrovolcanic) at N36° 41' 42.7," W116° 30' 53.5," and elevation 863.8 m (2,834 feet), located 0.7 km NW of the summit of Lathrop Wells Cone.*

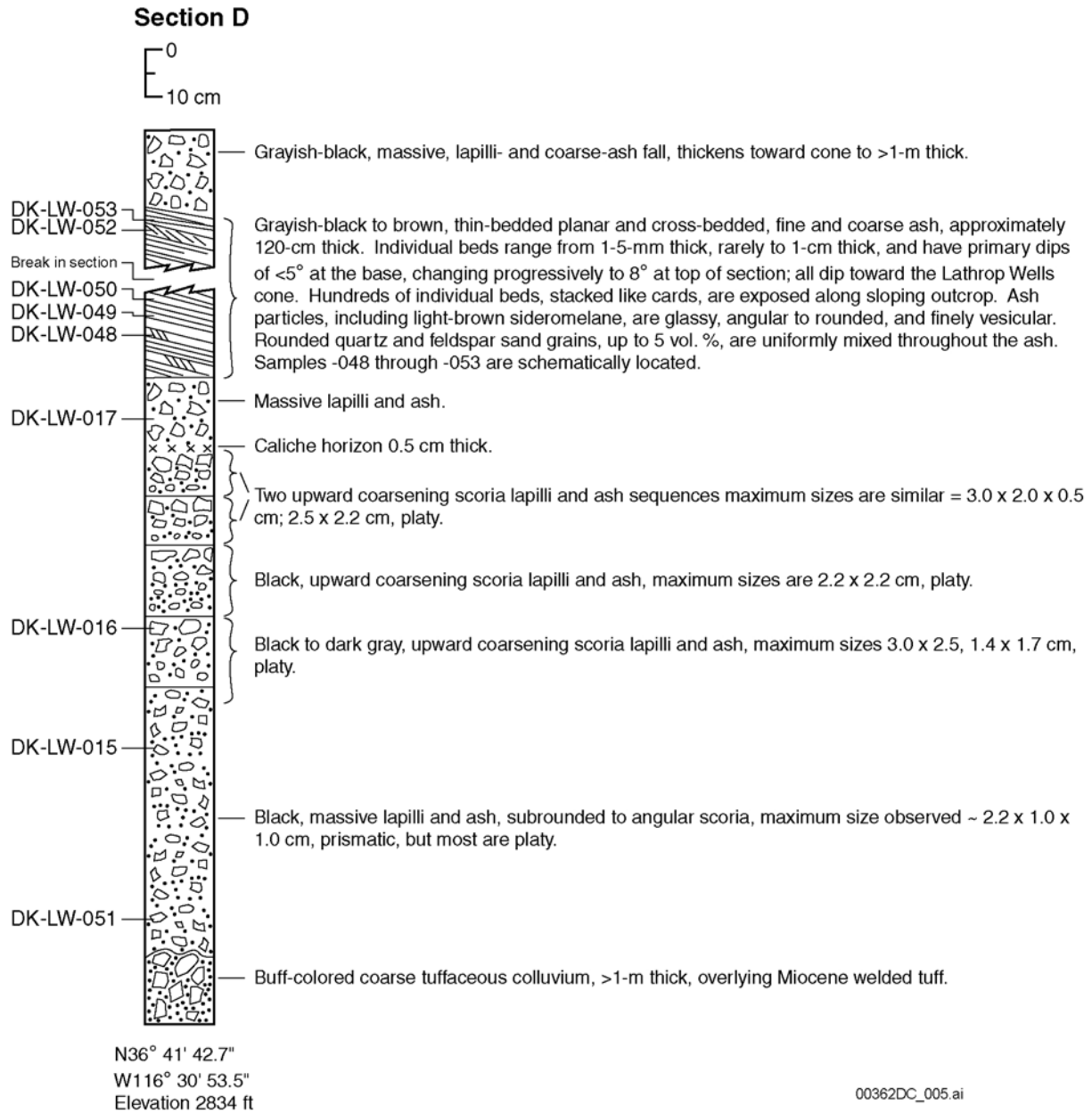
Observations were made from several pits excavated along small arroyos and by sweeping clean a portion of the outcrop along the east-facing slope of a ridge of Miocene welded tuff. A composite section comprises, from the bottom up: Miocene densely welded tuff overlain by ~1 m of coarse, angular, tuffaceous colluvium; 60 cm of massive basaltic lapilli and ash; four beds, each 10 to 15 cm thick, of reversely graded lapilli and ash; 15 cm of massive lapilli and ash; ~100 to 120 cm of slanted, thinly bedded and cross-bedded fine to coarse ash; and an overlying massive lapilli and ash bed > 1 m thick. In all, there are about 125 cm of flat-lying fallout tephra *beneath* the slanted, cross-bedded ash (Figure 25). The cross-bedded ash has consistent bedding slopes of 8 to 10° toward the cone and appears stacked like a deck of cards against the sloping hill of Miocene welded tuff (Figure 26). These ash beds have been interpreted as hydrovolcanic in origin (pyroclastic surge deposits of Vaniman and Crowe [1981 (DIRS 101620), pp. 20-21]; Wohletz [1986 (DIRS 140956), p. 258]). The hydrovolcanic beds are exposed over a distance of 58 m, along a trend radial from the vent. Figure 27 is a photograph looking up-section (toward the cinder cone) at the hydrovolcanic deposits.

Beds within the hydrovolcanic section are grayish-black (N2) to light beige, 1 to 6 mm thick, (maximum ~1.3 cm) and consist of medium- to coarse-ash-sized pyroclasts. Most are planar beds, but there are interbedded low-angle cross beds (an example has a wavelength of 36 cm and amplitude of 1 cm). Cross-beds indicate up-slope current directions away from the cone. Near the center of the hydrovolcanic section is a 44-cm long by 10-cm wide, 10-cm deep bedding plane sag caused by a block impacting wet and/or soft ash from the direction of the cone.

Within the area flanked by the cinder cone and protruding ridge of Miocene tuff, there is a transition southward, over a distance of ~400 m, from thousands of thin beds of a hydrovolcanic deposit (e.g., Figure 27) to hundreds and eventually one or two resistant ash beds sandwiched between coarse lapilli beds. Observations in trenches immediately southwest of the cone also indicate a southward thinning hydrovolcanic sequence (scientific notebook TWS-EES-13-LV-01-93-05 [Crowe 1996 (DIRS 164317)]). The field relations suggest that the

limited deposit resulted from a ground-hugging sector blast directed to the northwest. Because the unit slopes  $\sim 8^\circ$  back toward the cone and projects to beneath the cone base, the exact relations are covered with alluvium. There are currently no field data confirming a concentric tuff ring as proposed by Wohletz (1986 [DIRS 140956], p. 261). In any case, the sequence of massive and reversely graded lapilli beds *beneath* the hydrovolcanic unit indicates initial nonhydrovolcanic eruptive phases followed by a brief explosive, hydrovolcanic event.

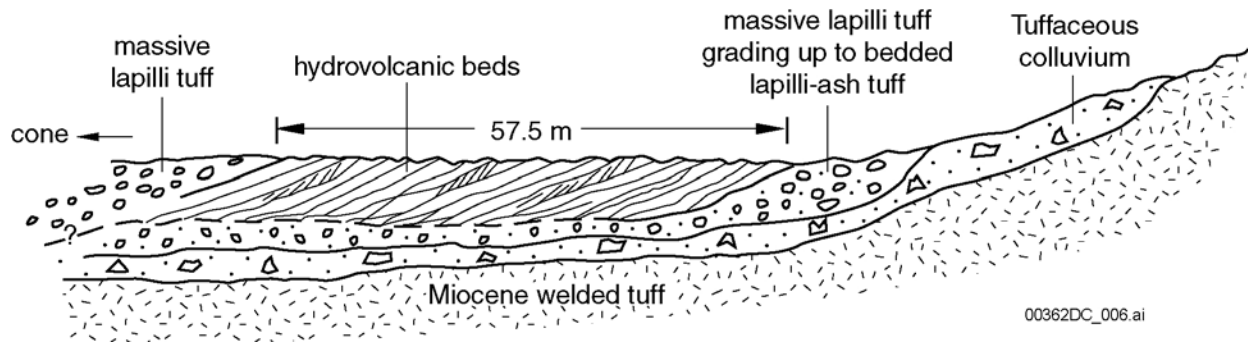
The samples used to characterize this hydrovolcanic section are described in Table 22. Measured grain size variations are given in Table 23 and plotted in Figure 28. The hydrovolcanic deposits are much finer grained than the over- or under-lying tephra fall deposits. As is the case for most dry surge deposits (little condensation of vapor before deposition), no accretionary lapilli were observed.



Source: Krier and Harrington (2003 [DIRS 164023], pp. 22, 53-54)

NOTE: Composite stratigraphic section from underlying colluvium through a scoria fall sequence, a hydrovolcanic sequence, and grading up at the top into scoria fall beds. Figure 26 shows the field relations for this section.

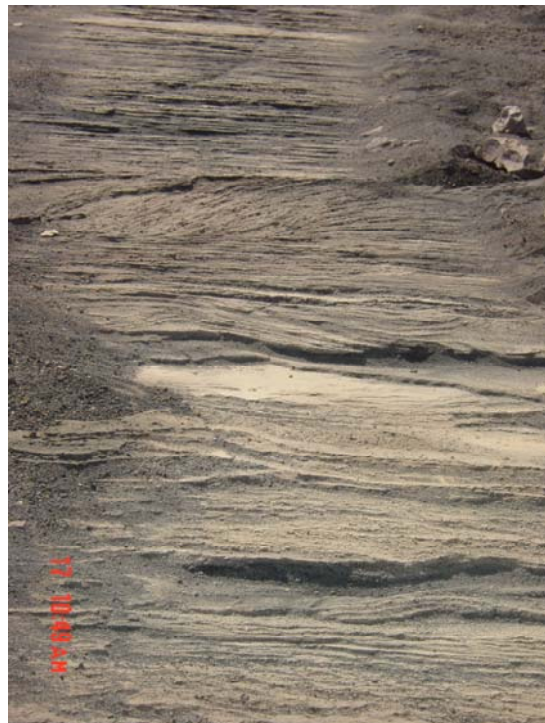
Figure 25. Tephra Fall Stratigraphy for Section D



Source: Krier and Harrington (2003 [DIRS 164023], p. 55)

NOTE: The diagram shows the tephra sequence located northwest of the Lathrop Wells Cone on an east-facing slope of Miocene welded tuff and colluvium. Overlying the colluvium is a sequence of scoria lapilli and ash fall beds, which in turn are overlain by a sequence of hydrovolcanic tuffs, which grade upward into more massive scoria lapilli fall beds. The hydrovolcanic sequence consists of mostly plane- and dune-bedded surge deposits.

Figure 26. Schematic Diagram of Hydrovolcanic Tephra Sequence



For illustration purposes only

NOTE: View is up-stratigraphic section, toward the cone (from right to left on Figure 26). Angular cobble at upper right is about 25 cm long.

Figure 27. Hydrovolcanic Deposits West and near the Base of the Lathrop Wells Cone

Table 22. Composite of Samples Used to Characterize the Hydrovolcanic Sequence and Underlying Tephra Fall Sequence (*tephra fall samples are in italics*)

Sample Number	Description
DK-LW-053	Exposed hydrovolcanic sequence. Collected from 0.8-cm-thick, light brown, ash/lapilli bed, 42.3 m above the base of the sequence.
DK-LW-052	Exposed hydrovolcanic sequence. Collected from 0.8-cm-thick, light brown, ash/lapilli bed, 42 m above the base of the sequence.
DK-LW-050	Well-bedded foreset beds of medium to coarse ash, 110 cm above the base. Pit in southern margin of exposed hydrovolcanic section.
DK-LW-049	Well-bedded ash; plane beds to small dunes, 45 cm above the base. Pit in southern margin of hydrovolcanic section.
DK-LW-048	Medium to coarse ash, 10 cm above the base. Pit in southern margin of exposed hydrovolcanic section.
<i>DK-LW-017</i>	Massive lapilli and ash fall bed.
<i>DK-LW-016</i>	Reversely graded lapilli and ash fall beds.
<i>DK-LW-015</i>	Massive lapilli and ash fall ~35-40 cm above DK-LW-051.
<i>DK-LW-051</i>	Collected 8-10 cm above colluvium and beneath the hydrovolcanic tephra sequence. Massive scoria lapilli fallout.

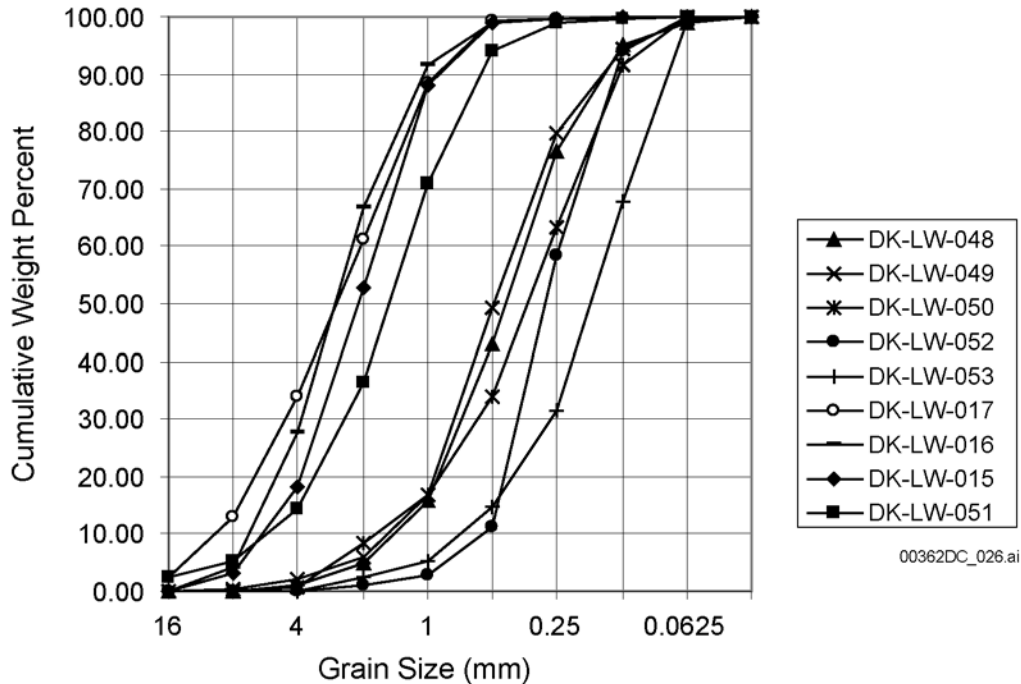
Source: Krier and Harrington (2003 [DIRS 164023], pp. 53-57)

NOTE: Samples DK-LW-015 to -017 and DK-LW-051 are fallout beds located between underlying Miocene tuff and colluvium and the overlying hydrovolcanic sequence. Samples DK-LW-052 and -053 were collected along the 42-m-long surface outcrop of the hydrovolcanic sequence.

Table 23. Grain Size Variations in Hydrovolcanic Sequence and Underlying Tephra Fall Sequence (*tephra fall samples are in italics*)

Sample Number	Md <sub>φ</sub> (median)	σ <sub>φ</sub> (sorting)	Md (mm)
DK-LW-053	2.5	1.33	0.15
DK-LW-052	1.77	0.81	0.29
DK-LW-050	1.5	1.51	0.33
DK-LW-049	1	1.42	0.5
DK-LW-048	1.1	1.34	0.42
<i>DK-LW-051</i>	-0.6	1.25	1.5
<i>DK-LW-017</i>	-1.44	1.49	2.8
<i>DK-LW-016</i>	-1.44	1.18	2.8
<i>DK-LW-015</i>	-1.11	1.14	2.2

DTN: LA0302GH831811.002



DTN: LA0302GH831811.002

NOTE: For comparison, DK-LW-051, DK-LW-015, DK-LW-016, and DK-LW-017 scoria fall beds underlying the hydrovolcanic sequence are plotted.

Figure 28. Grain Size Variations in Ash-Rich Hydrovolcanic Sequence

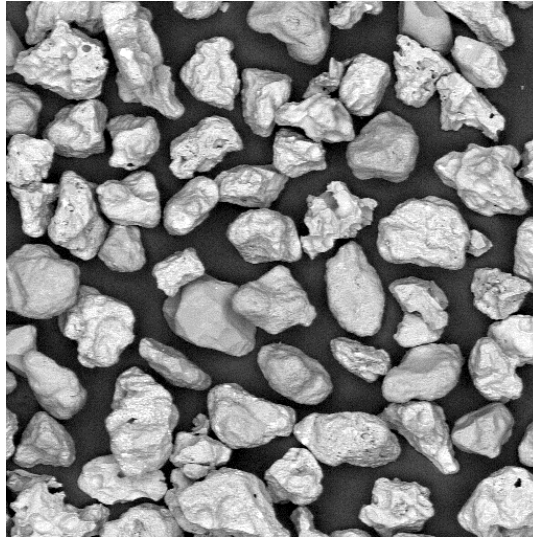
*Variations in Pyroclast Types.* Table 24 lists the percent pyroclasts measured in samples in the hydrovolcanic sequence. The pyroclasts are in the 0.5- to 1.0-mm size fractions of the samples, based on 300 grains, as measured using a binocular microscope. Figures 29 through 34 are scanning electron micrographs of different samples.

Table 24. Percent Pyroclasts in Samples in Hydrovolcanic Sequence

Sample Number	Tachylite	Glassy Tachylite	Sideromelane	Quartz & Feldspar Sand	Tuff Clasts (lithic)	Feldspar and Olivine Phenocrysts
DK-LW-048	9.3	71.6	18.6	0.3	0.0	0.0
DK-LW-049	34.6	48.0	13.6	0.6	0.0	3.0
DK-LW-050	43.6	42.0	10.6	2.6	1.0	0.0
DK-LW-052	1.6	73.0	24.3	0.0	0.3	0.6
DK-LW-053	9.6	68.6	19.3	1.3	0.3	0.6
DK-LW-051	57.0	26.0	10.3	0.0	5.3	1.2

DTN: LA0302GH831811.004

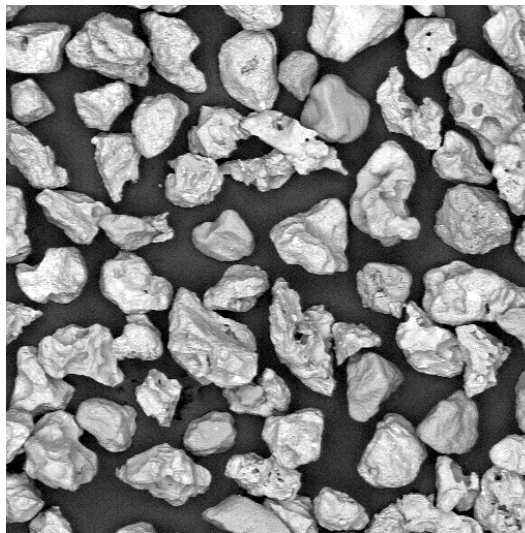
NOTE: Estimated Error = ± 0.2 percent



DTN: LA0302GH831811.004

NOTE: The sample is mostly glassy tachylite pyroclasts (vesicular, with thick vesicle walls). The more vesicular, thin-walled pyroclasts are sideromelane (basaltic glass). Most of the glassy tachylite pyroclasts have been rounded. An example of a quartz sand grain is three grains diagonally up from the lower right corner. Scale: width of image is ~1.4 mm.

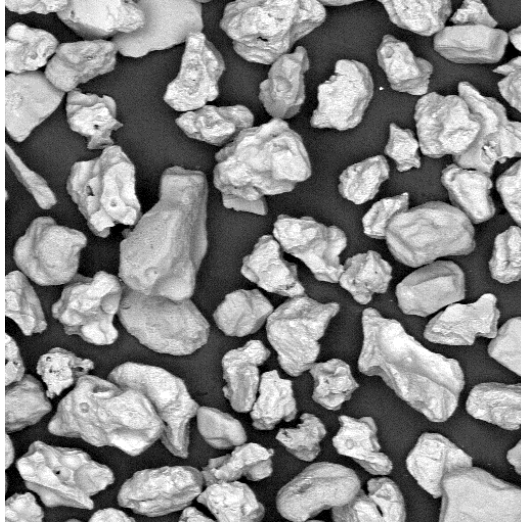
Figure 29. Scanning Electron Micrograph of the 0.125- to 0.250-mm Fraction of Sample DK-LW-048



DTN: LA0302GH831811.004

NOTE: The sample is mostly tachylite (poorly vesicular, rough grain surfaces) and glassy tachylite pyroclasts (vesicular, with thick vesicle walls). The more vesicular, thin-walled pyroclasts are sideromelane (basaltic glass). Most of the glassy tachylite pyroclasts have been rounded. Scale: width of image is ~1.4 mm.

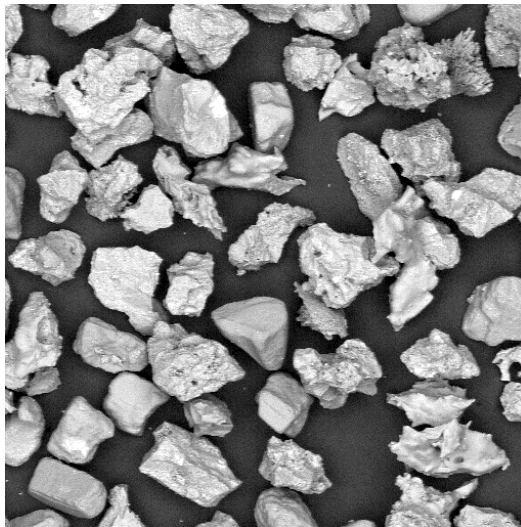
Figure 30. Scanning Electron Micrograph of the 0.125- to 0.250-mm Fraction of Sample DK-LW-049



DTN: LA0302GH831811.004

NOTE: The sample shows an increase in tachylite scoria (poorly-vesicular, rough grain surfaces). Nearly all particle types show some degree of rounding. Scale: width of image is ~1.4 mm.

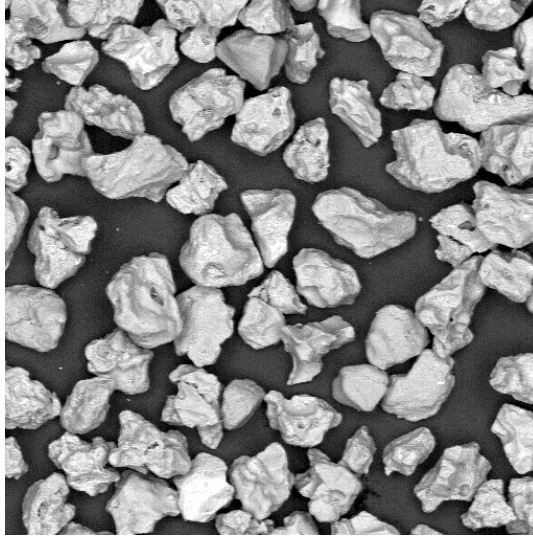
Figure 31. Scanning Electron Micrograph of the 0.125- to 0.250-mm Fraction of Sample DK-LW-050



DTN: LA0302GH831811.004

NOTE: In this sample, nearly all pyroclasts are tachylite or glassy tachylite, with little rounding. Scale: width of image is ~1.4 mm.

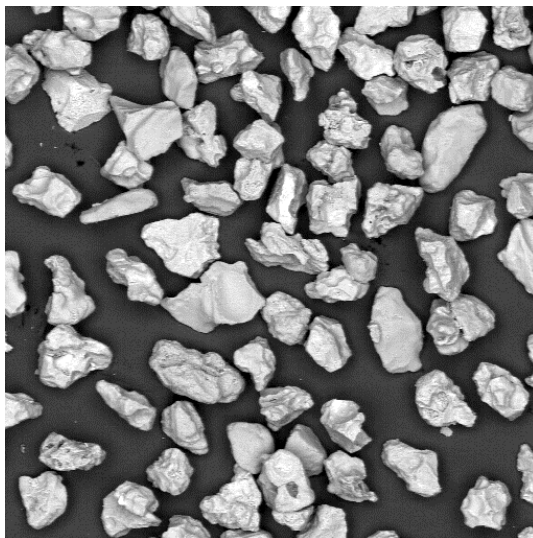
Figure 32. Scanning Electron Micrograph of the 0.125- to 0.250-mm Fraction of Sample DK-LW-051



DTN: LA0302GH831811.004

NOTE: The sample is mostly glassy tachylite pyroclasts. Nearly all particle types show some degree of rounding. Scale: width of image is ~1.4 mm.

Figure 33. Scanning Electron Micrograph of the 0.125- to 0.250-mm Fraction of Sample DK-LW-052



DTN: LA0302GH831811.004

NOTE: The sample is mostly glassy tachylite pyroclasts, with a substantial fraction of sideromelane pyroclasts. Nearly all particle types show some degree of rounding. Scale: width of image is ~1.4 mm.

Figure 34. Scanning Electron Micrograph of the 0.125- to 0.250-mm Fraction of Sample DK-LW-053

*Stratigraphic Section at N36° 41' 36.1," W116° 31' 02.4," and elevation 839.7 m (2,755 feet), located 620 m NW of the summit of the Lathrop Wells Cone.*

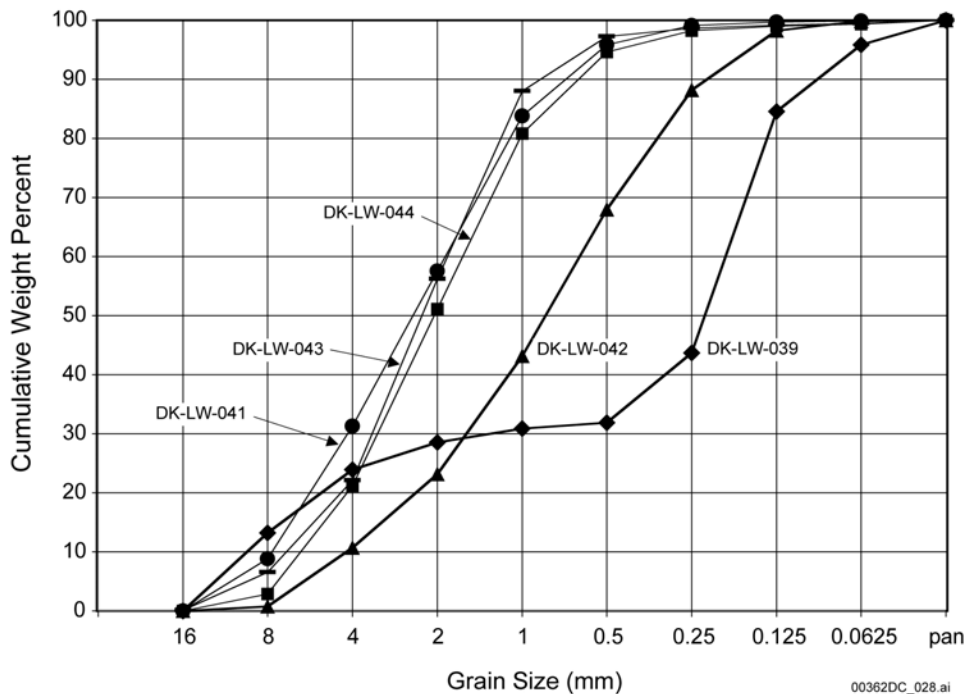
This 1.1-m-thick tephra section consists of mostly coarse ash and lapilli fall beds that were deposited directly upon older colluvium. From the base of the section, 0 to 14 cm, there are several 3- to 7-cm thick beds of reversely graded lapilli and ash (sample DK-LW-040), which

grade into 16 cm of massive lapilli fallout with maximum scoria size of 3 by 2 cm (sample DK-LW-041). From 31 to 41 cm, there are 3 resistant ash beds, each 2 to 3 cm thick (sample DK-LW-042 is a thin lapilli interbed). The 3 intercalated, resistant beds may be distal equivalents of the hydrovolcanic facies exposed NW of the cone (Section 6.4.2.3). From 41 cm to the top of the section, there is a massive lapilli and coarse ash fallout bed (samples DK-LW-044 and -043). The basal colluvium consists of angular, poorly sorted sand, pebbles, and cobbles of welded tuff with a bimodal grain-size distribution. Grain size variations for samples from this section are shown in Table 25 and Figure 35. Sample DK-LW-042 is finer grained than the fall samples (DK-LW-041, 043, 044), similar to the hydrovolcanic sequence described earlier.

Table 25. Grain Size Variations in the Colluvium and Tephra Fall Section

Sample Number	$Md_{\phi}$ (median)	$\sigma_{\phi}$ (sorting)	$Md$ (mm)
DK-LW-044	-1.05	1.29	2.1
DK-LW-043	-1.17	1.31	2.2
DK-LW-042	0.25	1.49	0.85
DK-LW-041	-1.39	1.36	2.6
DK-LW-039 (colluvium matrix)	2.13	2.91	0.23

DTN: LA0302GH831811.002



DTN: LA0302GH831811.002

Figure 35. Grain Size Variations in Colluvium and Tephra Fall Section

*Pyroclast Types.* Sample DK-LW-041 is from 22 cm above the base in massive lapilli and ash fallout; DK-LW-042 is from 38 cm above the base and between 2 thin (hydrovolcanic?),

resistant ash beds; DK-LW-044 is 60 cm above the base and representative of the 40- to 80-cm zone; and sample DK-LW-043 is from 100 cm above the base and representative of the upper 30 cm of massive fallout. Table 26 lists the percent pyroclasts measured in samples from this tephra section. The pyroclasts are in the 0.5- to 1.0-mm size fractions, based on 300 grains, as measured using a binocular microscope. No lithic clasts were identified in the grain counts.

Table 26. Percent Pyroclasts in Samples in the Colluvium and Tephra Fall Section

Sample Number	Tachylite	Glassy Tachylite	Sideromelane	Feldspar + Olivine Phenocrysts
DK-LW-043	61.6	27.3	10.6	0.3
DK-LW-044	57.0	28.0	14.6	0
DK-LW-042	34.0	51.6	14.3	0
DK-LW-041	42.3	44.0	13.6	0

DTN: LA0302GH831811.004

NOTE: Estimated Error =  $\pm 0.3$  percent

*Stratigraphic section at N36° 41' 39.2," W116° 31' 03.1," and elevation 849.8 m (2,788 feet), located 780 m NW of the summit of the Lathrop Wells Cone and on the NW side (lee side, relative to the cone) of the small ridge of Miocene welded tuff.*

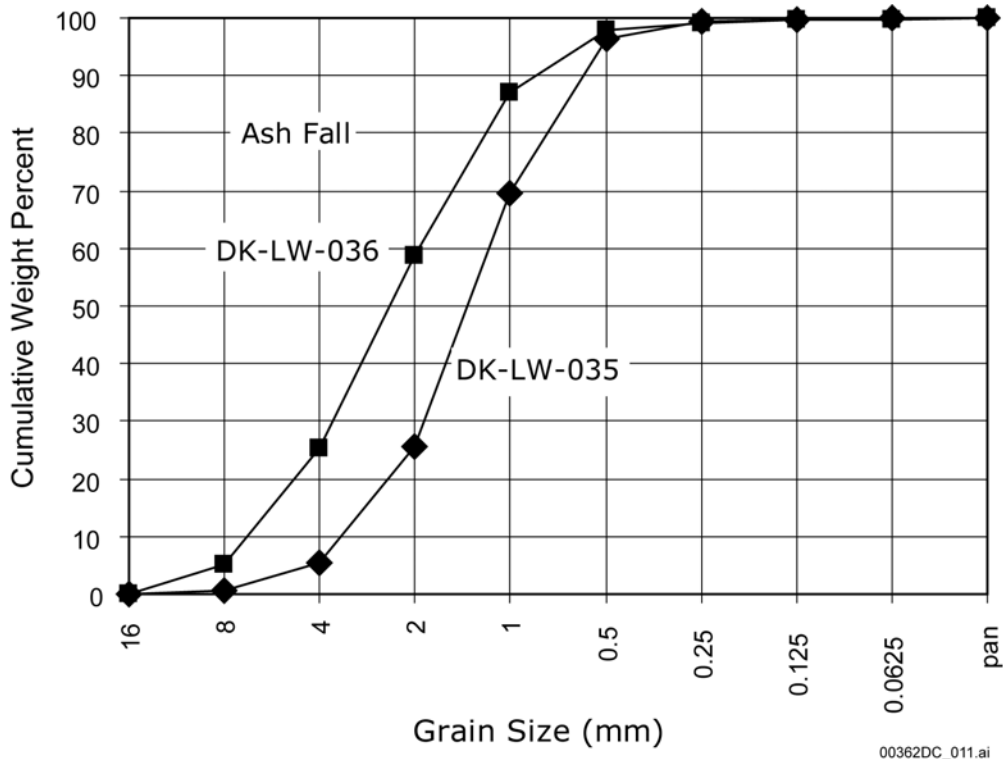
This tephra section, no base exposed, is visible in a bank of the wash. The bedding is parallel to the hill slope of  $\sim 9^\circ$ .

*Grain Size Variations.* The section consists of > 82 cm of bedded coarse ash and lapilli, reversely graded at the base and normally graded at the top, overlain by 7 cm of thinly bedded ash and lapilli that has been interpreted by Wohletz (1986 [DIRS 140956]) as hydrovolcanic in origin. The samples (Table 27 and Figure 36) are from the basal massive unit (DK-LW-035 is from 20 cm above the base of exposure; DK-LW-036 is from 70 cm above the base). Both samples appear to be tephra fall beds, on the basis of field description and grain size analyses.

Table 27. Grain Size Variations in Tephra Section Overlying Ridge of Miocene Welded Tuff

Sample Number	$Md_\phi$ (median)	$\sigma_\phi$ (sorting)	$Md$ (mm)
DK-LW-036	-1.32	1.04	2.5
DK-LW-035	-0.48	1.21	1.4

DTN: LA0302GH831811.002



DTN: LA0302GH831811.002

Figure 36. Grain Size Variations in Tephra Section Overlying Ridge of Miocene Welded Tuff

*Stratigraphic section at N36° 41' 53.0, W116° 30' 44.2," and elevation 852.2 m (2,796 feet), located 850 m NW of the summit of the Lathrop Wells Cone.*

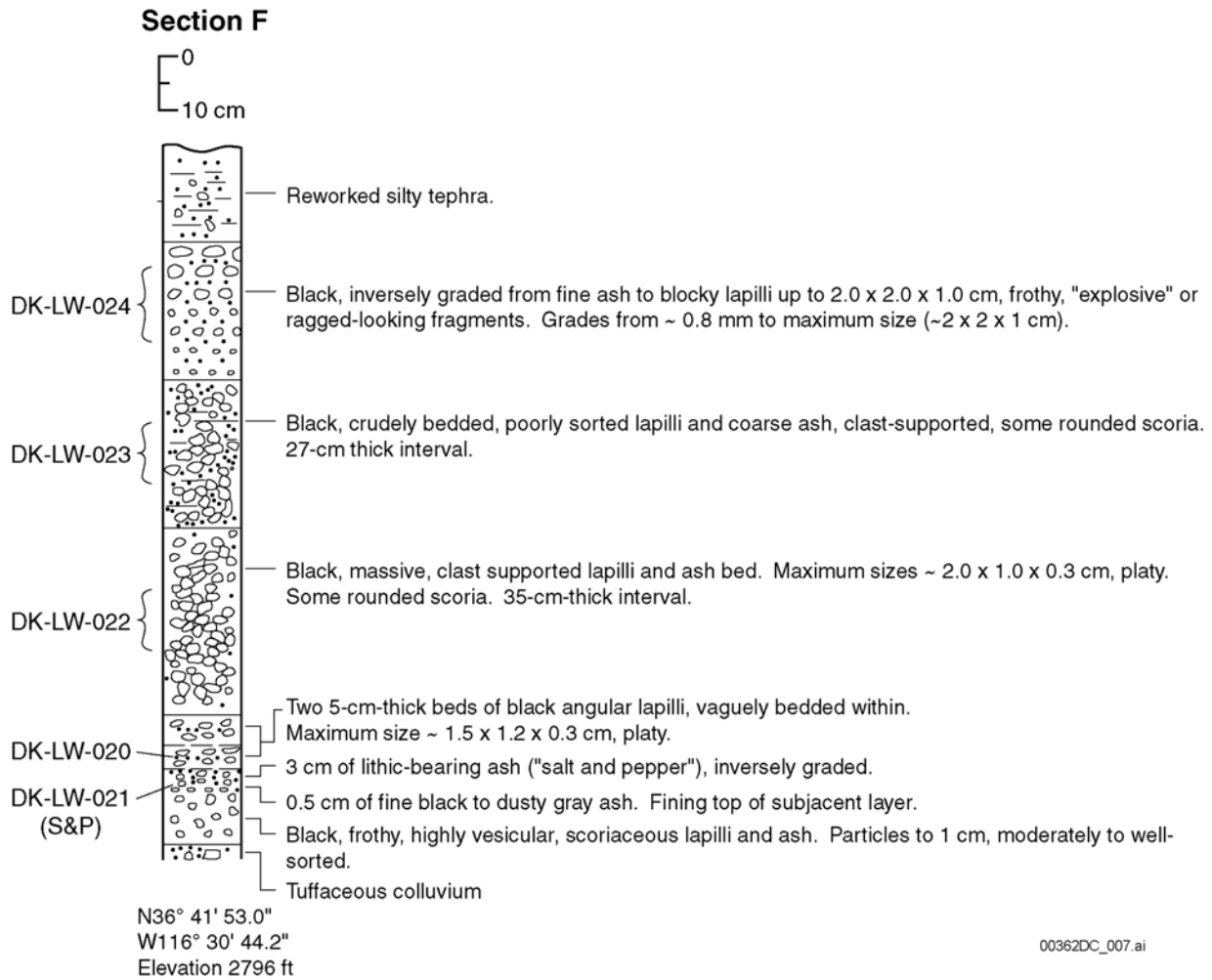
This section of tephra fall (Section F) is 1.15 m thick, overlies tuffaceous colluvium, and is, in turn, overlain by reworked silty tephra (Figure 37).

*Grain size Variations.* Samples are arranged from bottom to top of the stratigraphic section. DK-LW-021 is from a 3-cm-thick bed of lithic-bearing, highly vesicular ash and lapilli about 10 cm above the colluvium base; DK-LW-020 is from a 5-cm-thick ash-lapilli fall; DK-LW-022 is from a 35-cm thick bed of clast-supported lapilli and ash; DK-LW-023 is from poorly sorted lapilli and coarse ash; and DK-LW-024 is from a reversely graded bed of fine ash to lapilli. The measured grain size variations are shown in Table 28 and Figure 38.

Table 28. Grain Size Variations in Tephra Fall for Section F

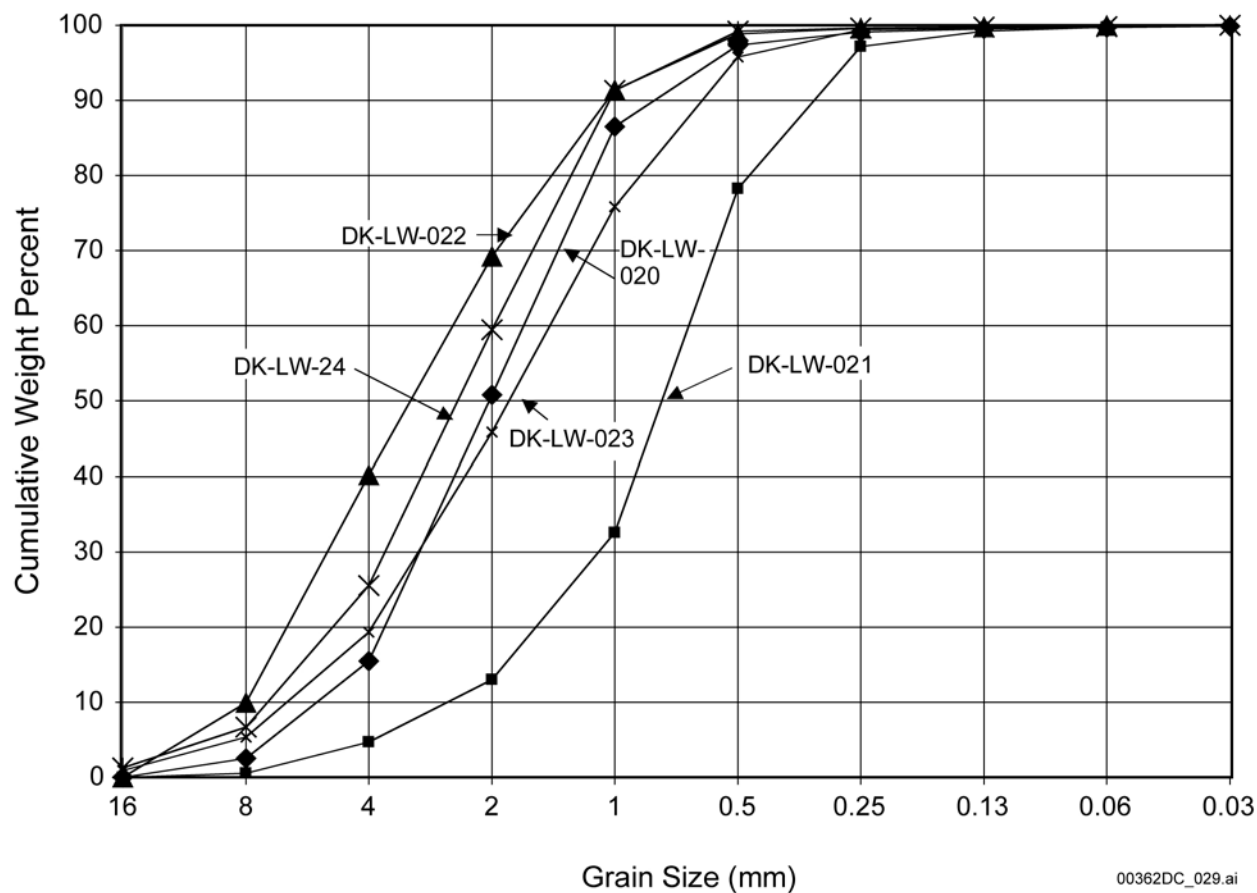
Sample Number	$Md_{\phi}$ (median)	$\sigma_{\phi}$ (sorting)	$Md$ (mm)
DK-LW-024	-1.43	1.04	2.7
DK-LW-023	-0.92	1.21	1.9
DK-LW-022	-1.68	1.13	3.2
DK-LW-020	-1.0	1.0	2.0
DK-LW-021	0.32	1.02	0.8

DTN: LA0302GH831811.002



Source: Krier and Harrington (2003 [DIRS 164023], p. 26)

Figure 37. Tephra Fall Stratigraphy for Section F



DTN: LA0302GH831811.002

Figure 38. Grain Size Variations in Tephra Fall for Section F

*Variations in Pyroclast Types.* Percent pyroclasts in the 0.5- to 1.0-mm size fractions of samples DK-LW-020 to DK-LW-024, based on 300 grains, as measured using a binocular microscope, are listed in Table 29.

Table 29. Percent Pyroclasts in Samples in Tephra Fall for Section F

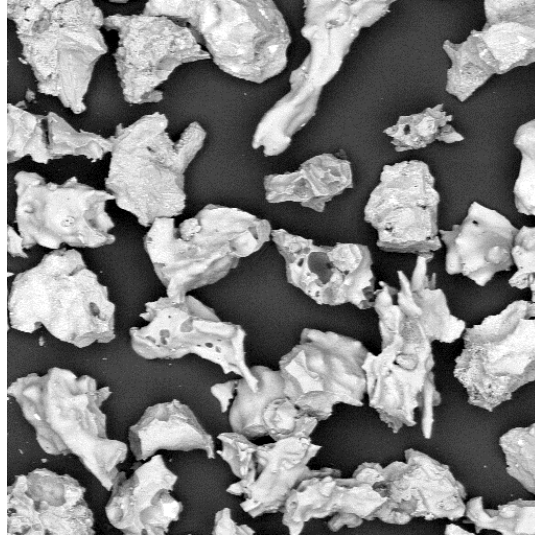
Sample Number	Tachylite	Glassy Tachylite	Sideromelane	Quartz & Feldspar Sand	Carbonate Clasts (lithic)	Tuff Clasts (lithic)	Feldspar & Olivine Phenocrysts
DK-LW-024	56.3	24.3	19.3	0.0	0.0	0.0	0.0
DK-LW-023	75.0	17.3	7.6	0.0	0.0	0.0	0.0
DK-LW-022	59.0	27.6	13.0	0.0	0.0	0.0	0.3
DK-LW-020	77.3	7.3	11.3	1.0	1.0	0.0	2.0
DK-LW-021	21.6	18.0	52.0	0.3	0.3	7.6	0.0

DTN: LA0302GH831811.004

NOTE: Estimated Error = ± 0.1 percent.

The eruption sequence for this section begins with 10 cm of frothy lapilli fall, superposed by lithic-bearing hydrovolcanic(?) ash, dominated by sideromelane pyroclasts, but changes to

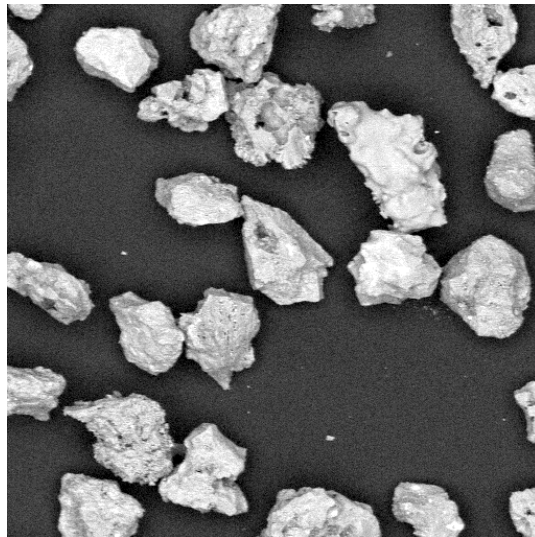
lithic-poor lapilli and ash, which is mostly tachylite and glassy tachylite. Figures 39 to 43 are illustrations of the particle populations (0.125 to 0.5 mm fraction) in SEM images.



DTN: LA0302GH831811.004

NOTE: The sample is dominated by vesicular sideromelane (basaltic glass) pyroclasts. Scale: width of image is ~1.4 mm.

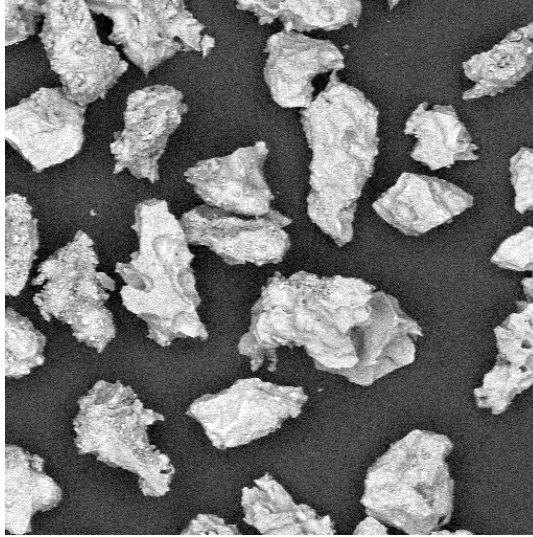
Figure 39. Scanning Electron Micrograph of the 0.125- to 0.250-mm Fraction of Sample DK-LW-021



DTN: LA0302GH831811.004

NOTE: In this sample, there is a noticeable increase (from DK-LW-021) in tachylite and glassy tachylite pyroclasts. Scale: width of image is ~1.4 mm.

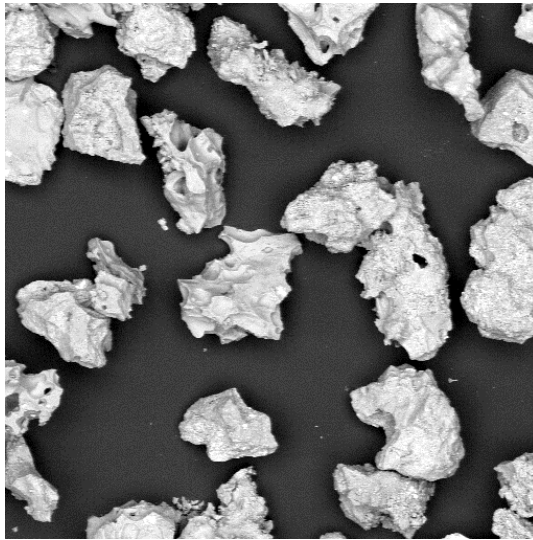
Figure 40. Scanning Electron Micrograph of the 0.125- to 0.250-mm Fraction of Sample DK-LW-020



DTN: LA0302GH831811.004

NOTE: Most pyroclasts in this sample are tachylite or glassy tachylite. Scale: width of image is ~1.4 mm.

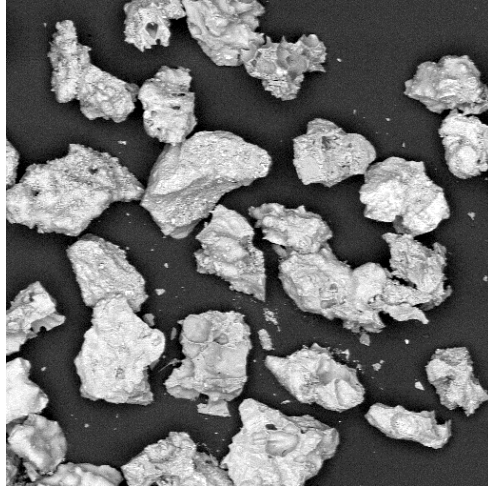
Figure 41. Scanning Electron Micrograph of the 0.125- to 0.250-mm Fraction of Sample DK-LW-022



DTN: LA0302GH831811.004

NOTE: Most pyroclasts in this sample are tachylite or glassy tachylite. Undisturbed fallout has no edge modification of pyroclasts. Scale: width of image is ~1.4 mm.

Figure 42. Scanning Electron Micrograph of the 0.125- to 0.250-mm Fraction of Sample DK-LW-023



DTN: LA0302GH831811.004

NOTE: The sample is mostly vesicular and non-vesicular or poorly vesicular tachylite pyroclasts. There are no lithic clasts. Scale: width of image is ~1.4 mm.

Figure 43. Scanning Electron Micrograph of the 0.125- to 0.250-mm Fraction of Sample DK-LW-024

*Stratigraphic section at N36° 42' 14.0", W116° 30' 14.0," and elevation 861.1 m (2,825 feet), located 1.6 km NNW of the summit of the Lathrop Wells Cone.*

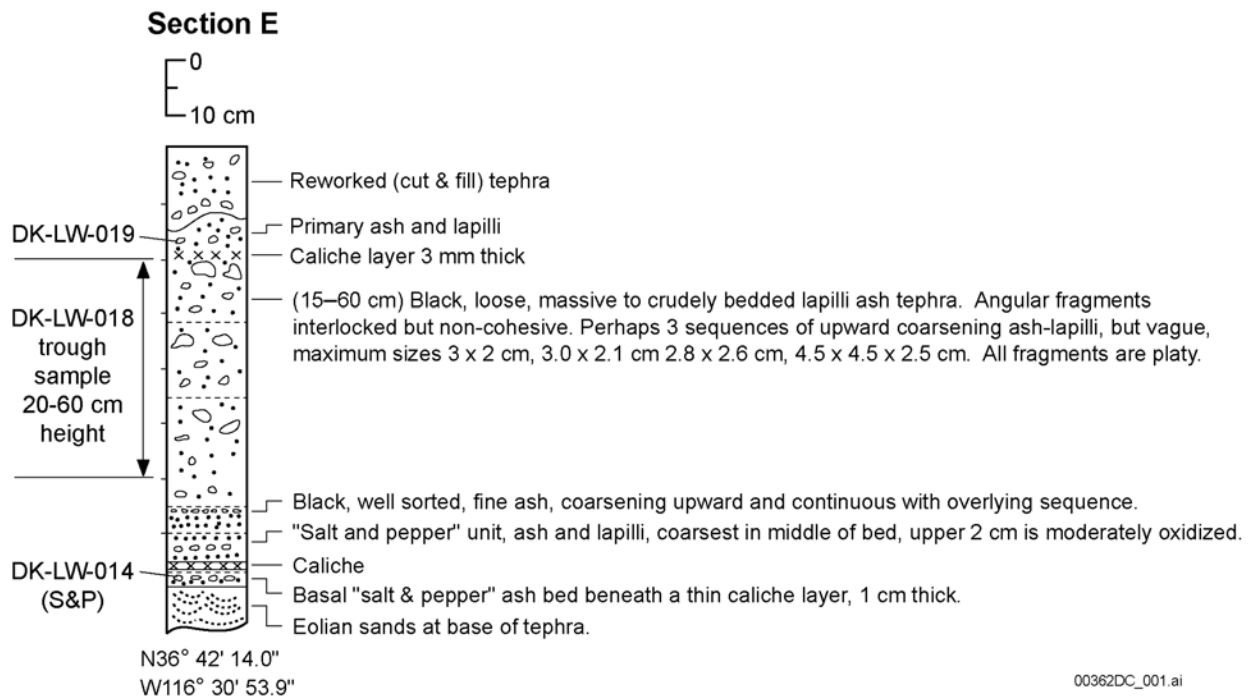
In this 70-cm-thick stratigraphic section, the tephra overlies eolian sand deposits and consists of well-bedded medium to fine-grained ash in the lower 15 cm, grading upward into massive to crudely graded lapilli and ash bed. The top of the sequence has been reworked. The basal 3 cm is bedded ash with lithic sand grains giving it a “salt and pepper” appearance.

*Grain size Variations.* Samples are arranged from bottom to the top of the stratigraphic section. DK-LW-014 is from the basal fallout unit; DK-LW-018 is of a massive lapilli fall; and DK-LW-019 is from tephra fall near the top of the stratigraphic section (Figure 44). The measured grain size variations are shown in Table 30 and Figure 45.

Table 30. Grain Size Variations in Tephra Fall for Section E

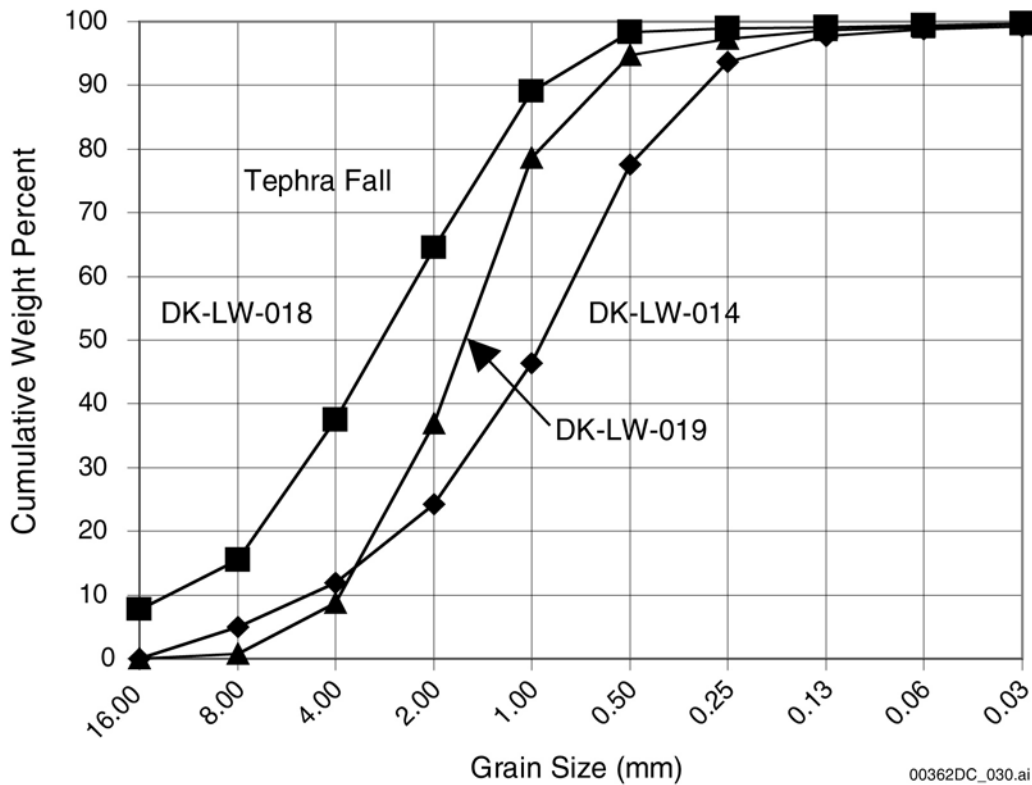
<b>Sample Number</b>	<b><math>Md_{\phi}</math> (median)</b>	<b><math>\sigma_{\phi}</math> (sorting)</b>	<b><math>Md</math> (mm)</b>
DK-LW-019	-0.85	1.05	1.8
DK-LW-018	-1.63	1.40	3.1
DK-LW-014	0.07	1.62	0.95

DTN: LA0302GH831811.002



Source: Krier and Harrington (2003 [DIRS 164023, p. 25])

Figure 44. Tephra Fall Stratigraphy for Section E



DTN: LA0302GH831811.002

Figure 45. Grain Size Variations in Tephra Fall for Section E

*Variations in Pyroclast Types.* Percent pyroclasts in the 0.5- to 1.0-mm size fractions of samples DK-LW-014, DK-LW-018, and DK-LW-019, based on 300 grains, as measured using a binocular microscope, are listed in Table 31.

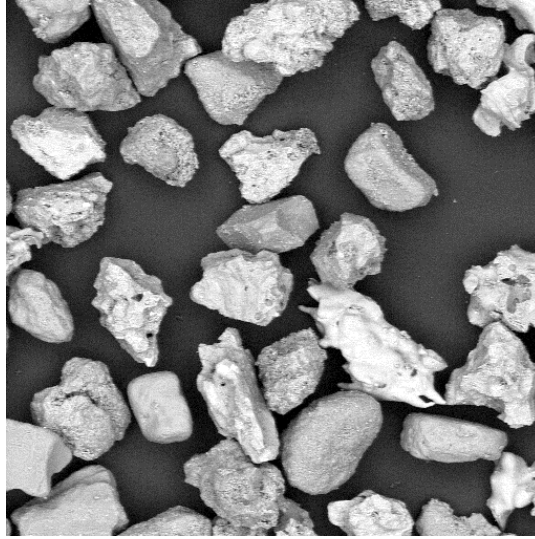
Table 31. Percent Pyroclasts in Samples in Tephra Fall for Section E

Sample Number	Tachylite	Glassy Tachylite	Sideromelane	Quartz & Feldspar Sand	Tuff Clasts (lithic)
DK-LW-019	31.6	52.0	8.0	0.0	8.3
DK-LW-018	43.6	47.3	7.0	0.6	1.3
DK-LW-014	23.6	34.0	27.6	1.3	13.3

DTN: LA0302GH831811.004

NOTE: Estimated Error =  $\pm 0.2$  percent

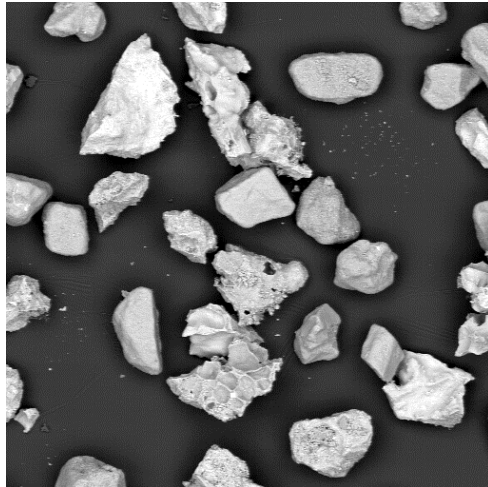
The most evident changes include the decreasing sideromelane and increasing tachylite and glassy tachylite pyroclasts up-section. Below are illustrations of the particle populations (0.125- to 0.5-mm fraction) in SEM images (Figures 46 to 48).



DTN: LA0302GH831811.004

NOTE: The smooth-skinned, droplet-like pyroclasts are sideromelane (basaltic glass). The angular, rough-surfaced grains are tachylites; those with smooth, glassy vesicle walls are glassy tachylites. The rounded, rough-surfaced grains are fine-grained tuff. Scale: width of image is ~1.4 mm.

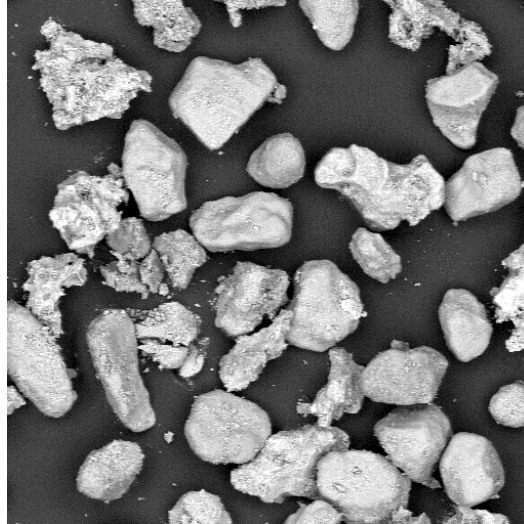
Figure 46. Scanning Electron Micrograph of the 0.125- to 0.250-mm Fraction of Sample DK-LW-014



DTN: LA0302GH831811.004

NOTE: Same description for pyroclast types as previous figure. Scale: width of image is ~1.4 mm.

Figure 47. Scanning Electron Micrograph of the 0.125- to 0.250-mm Fraction of Sample DK-LW-018



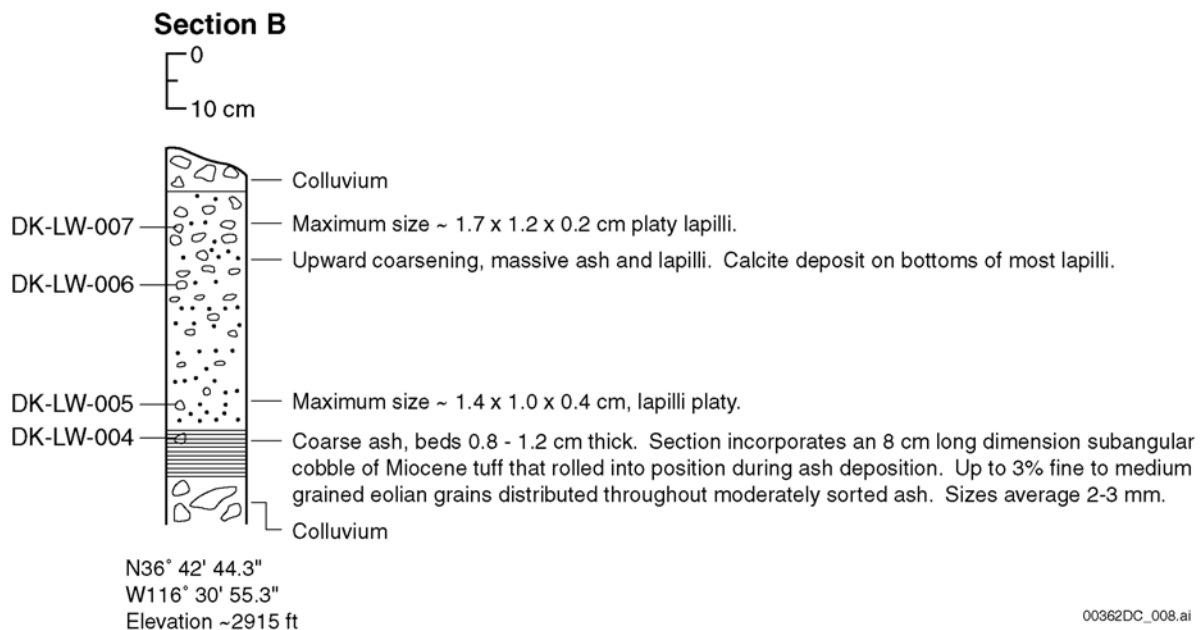
DTN: LA0302GH831811.004

NOTE: The difference between this sample and those from lower in the section is the rounding and edge modification of many of the particles, implying grain interactions. Scale: width of image is ~1.4 mm.

Figure 48. Scanning Electron Micrograph of the 0.125- to 0.250-mm Fraction of Sample DK-LW-019

*Stratigraphic Section at N36° 42' 44.3", W116° 30' 55.3," and elevation 890.0 m (2,920 feet), located 2.5 km NNW of the summit crater of the Lathrop Wells Cone.*

This section and other nearby exposures of primary or reworked tephra are located in small drainages on the south-facing slopes of the low hills ~2.5 km north of the cone (Figure 49).



Source: Krier and Harrington (2003), p. 14 [DIRS 164034]

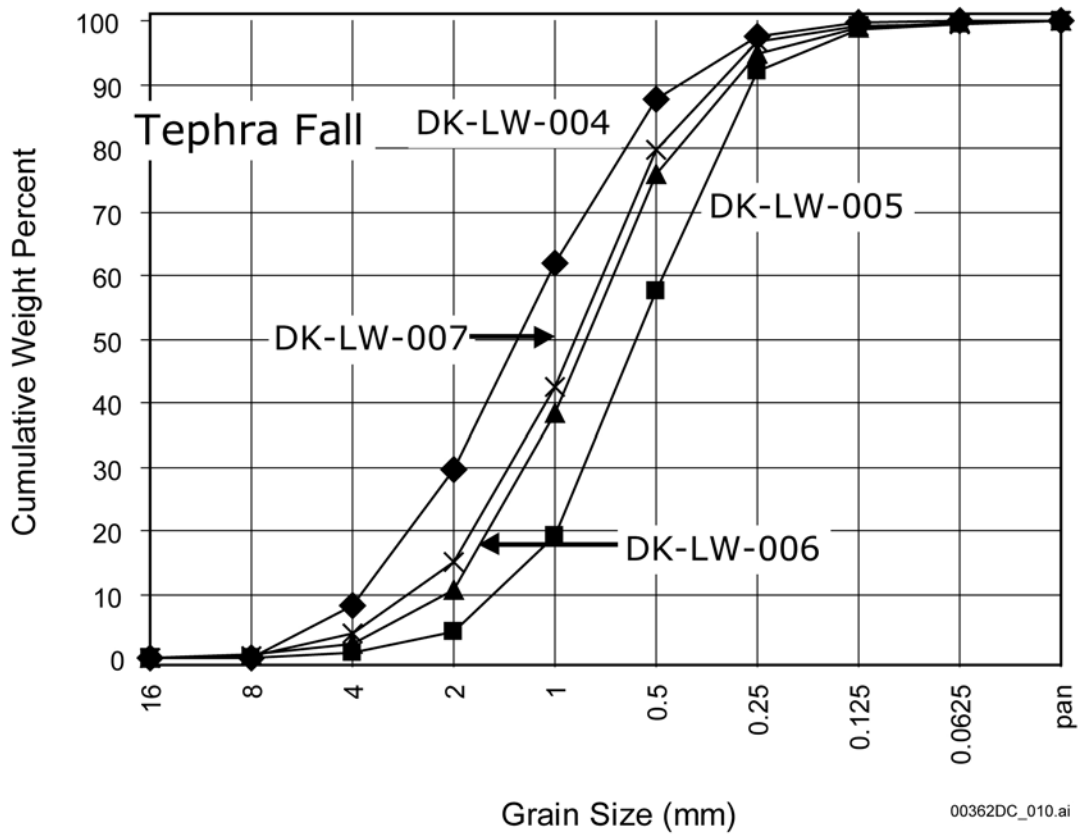
Figure 49. Tephra Fall Stratigraphy for Section B

*Grain Size Variations.* The measured grain size variations for this section are given in Table 32 and Figure 50.

Table 32. Grain Size Variations in Tephra Fall for Section B

Sample Number	$Md_{\phi}$ (median)	$\sigma_{\phi}$ (sorting)	$Md$ (mm)
DK-LW-007	0.15	1.75	0.90
DK-LW-006	0.32	1.19	0.80
DK-LW-005	0.62	1.25	0.65
DK-LW-004	-0.38	1.20	1.30

DTN: LA0302GH831811.002



DTN: LA0302GH831811.002

Figure 50. Grain Size Variations in Tephra Fall for Section B

*Pyroclast Types.* Pyroclast types, in vol% and determined with binocular examination of 300 grains in the 0.5- to 1.0-mm size fractions, are listed in Table 33.

Table 33. Percent Pyroclasts in Samples in Tephra Section B

Sample Number	Tachylite	Glassy Tachylite	Sideromelane	Feldspar + Olivine Phenocrysts	Tuff Clasts
DK-LW-007	63.3	26.6	9.6	0.3	0
DK-LW-006	75.3	15.0	8.6	0.6	0
DK-LW-005	31.3	21.6	39.0	0.6	7.3
DK-LW-004	52.3	37.6	10.0	0	0

DTN: LA0302GH831811.004

NOTE: Estimated Error = ± 0.3 percent.

*Distal ashfall.* Primary tephra deposits from the Lathrop Wells volcano have not been located beyond ~2.5 km north of the cone. Reworked basaltic ash has been identified in several trenches excavated along 3 faults at distances of 10 km (Windy Wash fault, Whitney et al. 1996 [DIRS 107313], p. 4.9-12), 12 km (Fatigue Wash fault, Coe et al. 1996 [DIRS 101527], pp. 4.8-9, 4.8-12), and 14 km (Solitario Canyon fault) north of the cone (Ramelli et al. 1996 [DIRS 101106], p. 4.7-11). The trenches were previously excavated as part of the YMP seismic hazards program.

Basaltic ash in each occurrence was found as a fissure-filling unit within fault-plane deposits and ranged from an ash component in matrix of coarse cobbles (e.g., Windy Wash fault) to a nearly pure ash deposit (trench T8, Solitario Canyon fault). The ash within the Solitario Canyon fault was correlated to Lathrop Wells volcano tephra by geochemical analysis of trace elements (Perry et al. 1998 [DIRS 144335], p. 4-26). The ash particles, along with other volcanic and carbonate clasts, fill the bottom 1 m of the narrow fissure and appear to have been transported over short distances down-slope to their present position when the fissure was open.

Another occurrence of ash is found on the west side of Busted Butte, ~11 km E-NE of Lathrop Wells Cone. Basaltic ash was noted within drainage sediments in the wash near outcrops of Paintbrush Tuff (scientific notebook TWS-EES-13-LV-01-93-05 [Crowe 1996 (DIRS 164317)]). Only trace amounts were seen under binocular microscope, and positive correlation with the Lathrop Wells eruption has not been made.

These distal occurrences of basaltic tephra, of which at least one is correlated with the Lathrop Wells eruption, are used for estimations of ash volume from the Lathrop Wells Cone eruption, discussed below.

At other locations distant from the cone, small amounts of basaltic ash are found scattered on ground surfaces, concentrated as part of coarse sand deposits in small gullies, or preserved in banks along small drainages. An example of the latter occurrence is found on south slopes of the hills ~1.6 km W-SW of the cone. None of these ashes are positively correlated with the Lathrop Wells Cone.

### 6.4.3 Lathrop Wells Volcano—Volume Estimations

Locations and thicknesses of Lathrop Wells volcano tephra were used to develop a 1:72,000 scale isopach map for the area around the cone (Figure 23). Lines representing equal tephra thicknesses (isopachs) were hand-drawn through the data to estimate distribution and

volume of the ash from the eruption. Using the two occurrences of distal ash at Solitario Canyon and Busted Butted described in Section 6.4.2.3, isopachs of 300, 200, 100, 50, 10, and 1 cm were drawn. Based on this map, the area covered by  $\geq 1$  cm of tephra is  $\sim 182$  km<sup>2</sup>. Two limitations of this estimate are 1) data are unavailable for tephra thicknesses  $< 1$  cm and 2) the area south of the cone is devoid of data, biasing the distribution largely to the north and west of the cone.

Table 34 lists values for the Lathrop Wells tephra, lava, and cone. Tephra volume estimates were made by two methods. The first used a planimeter for calculating areas between neighboring isopachs and multiplying by the mid-value between them. This method gives a tephra volume of 0.039 km<sup>3</sup>. The second method used the volume equation developed by Pyle (1989 [DIRS 123891]), further evaluated by Fierstein and Nathenson (1992 [DIRS 162804]), that accounts for the observation that most tephra thin exponentially away from the source:

$$\text{Volume} = (2T_0)/(k^2) \quad (\text{Eq. 12})$$

where

$T_0$  is the thickest tephra (extrapolated, as necessary)  
 $k$  is the slope of the line on a  $\ln T$  versus  $(\text{area})^{1/2}$  plot.

The Pyle method yields a tephra volume of 0.037 km<sup>3</sup>, but also accounts for thicknesses beyond the 1-cm isopach, whereas the planimeter method did not. Lava flow estimates were also made by planimeter; area covered by lava flows is 1.946 km<sup>2</sup>. A field-derived estimated mean thickness of 15 m was assumed for the flows to obtain lava volume of 0.0292 km<sup>3</sup>. Cone volume, 0.018 km<sup>3</sup>, was calculated using the standard cone formula and a mean radius of 700 m. No correction was made for the estimated 6 m of erosion from the top of the cone (Perry et al. 1998 [DIRS 144335]). The Lathrop Wells Cone volumes in Table 34 are the recommended estimates for use in calculations.

Table 34. Volumes of Lathrop Wells Cone, Lava, and Tephra

Lathrop Wells Cone	Cone (km <sup>3</sup> )	Lavas (km <sup>3</sup> )	Tephra (km <sup>3</sup> )	Total (km <sup>3</sup> )	Comments
Planimeter <sup>a</sup>	0.018	0.0292	0.039	0.0862	Best estimate of event volume
Method of Pyle (1989 [DIRS 123891]) for fallout <sup>b</sup>	—	—	0.037	—	
Perry et al. 1998 [DIRS 144335]	—	—	—	0.14	Assumed ash $\sim 5X$ cone volume

DTN: LA0305DK831811.002

NOTES: <sup>a</sup>Planimeter: Cone volume calculated as  $V = (1/3)\pi r^2 h$ , where  $r = 350$  m and  $h = 140$  m. Volumes of lavas and fallout tephra are from planimeter areas.

<sup>b</sup>"Method of Pyle": Fallout tephra volume calculated using Pyle (1989 [DIRS 123891]). See also Fierstein and Nathenson (1992 [DIRS 162804]).

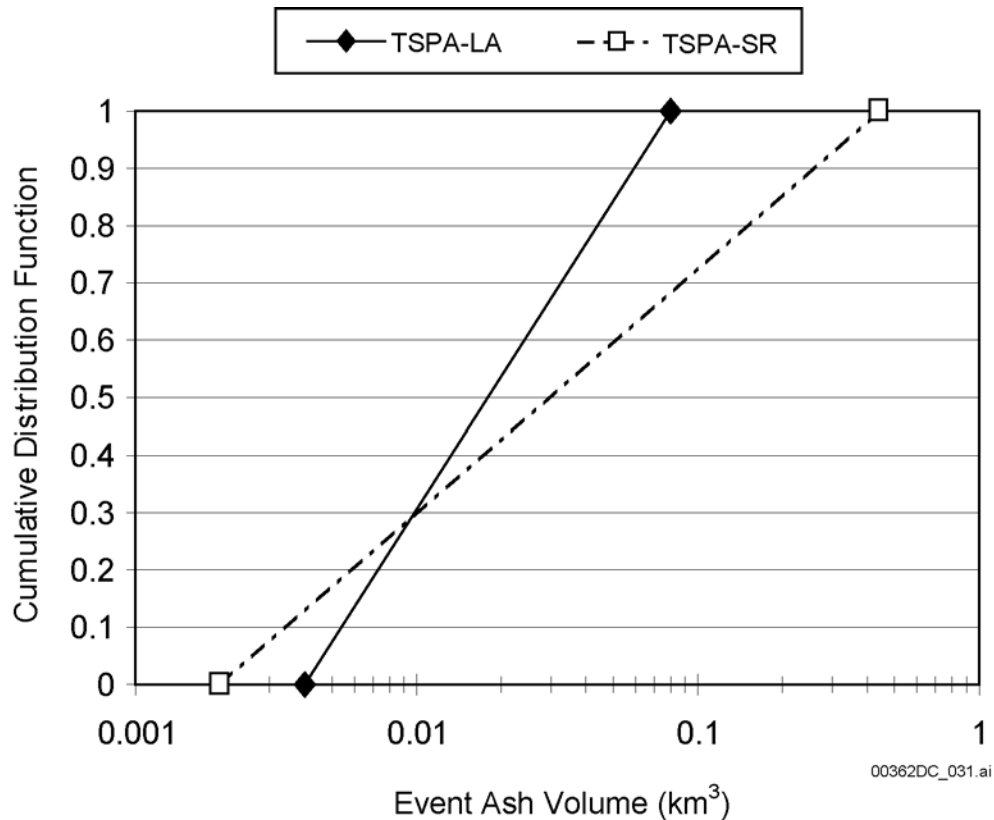
### 6.4.3.1 Recommended Ash-Volume Distribution for a Future Yucca Mountain Region Basaltic Eruption

The TSPA for the proposed Yucca Mountain repository requires a basaltic ash-volume distribution to calculate risk due to a possible disruption by a volcanic dike accompanied by an

ash eruption. We consider the amounts of tephra accompanying analog volcanic cones with a range of volumes and their ashfall/cone volume ratios. The literature on analog cones and their tephra volumes is limited, but ashfall volumes are generally about two times their cone volumes, based upon data that includes Tolbachik 1 (ratio 1.3), Tolbachik 2 (ratio 1.0), Sunset Crater (ratio 1.6-3.2), Heimaey (ratio 0.8), Serra Gorda (ratio 1.4), Cerro Negro (ratio 1.7, even based upon eruptions from 1850-1995), and Parícutin (ratio 4-5.9, which is by far the greatest) (NRC 1999 [DIRS 151592], Table 3). The average of these ratios is 1.9. At Lathrop Wells volcano, based on current data, tephra fall volume is  $\sim 0.04 \text{ km}^3$  and the cone is  $0.018 \text{ km}^3$ , for a ratio of 2.2. To account for uncertainties in this ratio, and to define a maximum potential ash volume for the YMR, it is recommended to double the expected tephra/cone ratio to four to capture the probable potential future ash eruption volumes. Therefore, doubling the Lathrop Wells tephra volume of  $0.04 \text{ km}^3$  yields the recommended maximum volume of  $\sim 0.08 \text{ km}^3$  of potential ash. This value would correspond to the volume of ash discharged from a volcano twice the size of Lathrop Wells, according to this formula. The maximum (cone + ash) volume for this future scenario is greater than any single eruptive event within the Crater Flat volcanic field, with the possible exception of aeromagnetic anomaly B (O'Leary et al. 2002 [DIRS 158468] pp. 10-11, 28, 29). Anomaly B is likely one or more volcanic centers, has an estimated volume of  $\sim 0.4 \text{ km}^3$ , and a possible age of  $\sim 3.85 \pm 05 \text{ Ma}$ , based on basalt in drill cuttings in nearby well 25-1 (Crowe et al. 1995 [DIRS 100110], p. 2-19).

Minimum potential volume should be captured in a similar ratio associated with the smallest volcanic cone in the YMR, probably NE Little Cone. The eroded mass of NE Little Cone is 15 m high with a diameter of  $\sim 230 \text{ m}$ . Accounting for 25 m of burial by younger alluvium based on ground magnetic survey data (Stamatakis et al. 1997 [DIRS 138819], p. 328), assuming a 50 percent erosion of the cone height (NRC 1999 [DIRS 151592], Section 4.2.5.3.1, Table 3), and cone radius of 230 m, the resulting volume for NE Little Cone is  $\sim 0.001 \text{ km}^3$ . Four times this volume,  $0.004 \text{ km}^3$ , is chosen as a minimum volume of tephra for a potential future eruption. The estimated NE Little Cone tephra volume of  $0.004 \text{ km}^3$  compares with Lathrop Wells Cone tephra volume of  $0.04 \text{ km}^3$ . Therefore, the recommended range of distribution of potential tephra volumes for the YMR is  $0.004$  to  $0.08 \text{ km}^3$ .

The population of young cinder cones in the YMR is small and does not constrain the probability of one particular volume relative to another volume. We conclude that the probability of any volume is equal to the probability of any other volume within the given range. Figure 51 shows the range of expected ash volumes for use in TSPA-LA and compares it to the previous range for TSPA-SR, which was  $.002$  to  $0.44 \text{ km}^3$  (CRWMS M&O 2000 [DIRS 153246], p. 33). The previous larger volume was based on the voluminous Sunset Crater, Arizona, eruption, which overestimates potential ash volumes in the YMR (Sections 6.3.3 and 6.3.5).



Source: CRWMS M&O (2000 [DIRS 153246]); this report

NOTE: This log-uniform plot of ash volume shows the range for TSPA-LA (this report) relative to the larger range for the SR.

Figure 51. Potential Volume of Erupted Ash for a Yucca Mountain Region Basaltic Volcano

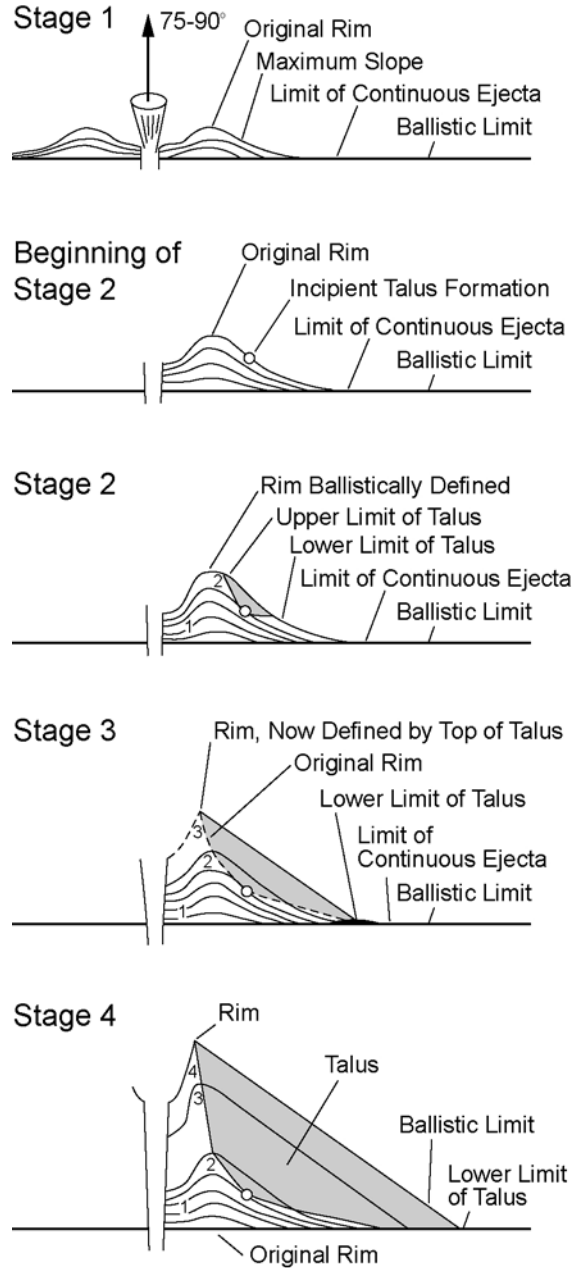
The range of ash volume selected for the TSPA-LA represents a more geologically sound estimate than that used for the TSPA-SR for the YMR based on the neighboring population of Quaternary volcanoes.

#### 6.4.4 Eruption Mechanisms and History for the Lathrop Wells Cone and Tephra Fall

Evidence for variations in the eruption phenomena that built the Lathrop Wells Cone can be found in the tephra fallout sequence. Representative fallout sections are used here to illustrate these variations. The descriptions of these beds are tied to a general model of scoria cone formation proposed by McGetchin et al. (1974 [DIRS 115469]), Figure 52, and include observations from Crowe et al. (1995 [DIRS 100110]) and Perry et al. (1998 [DIRS 144335]) as follows.

1. Within a kilometer of the vent, the earliest eruption phase deposited moderately sorted coarse ash with up to 52% vesicular sideromelane droplets (Figure 53). These are similar in shape and composition to glassy droplets produced in fire (lava) fountains. The fire fountaining could have been from a N-S-trending fissure (parallel to the long axis of the oval-shaped Lathrop Wells Cone and equivalent to stages 1 and 2 in Figure 52). The predominantly glassy droplets imply a largely unimpeded spray of

melt from a vent or fissure. Some conduit opening is implied from the 7.6% tuff lithic clasts in the ash. Closer to the vent, a greater proportion of tachylite and glassy tachylite than sideromelane is present, indicating that some quench-crystallization was occurring within the rising magma, possibly due to avalanching of scoria and ash back down the incipient crater slopes to intermittently block the vent. There are four or five repeating, upward coarsening tephra sequences in the lowest 125 cm of the observed section, with no recognized unconformities. This can be interpreted either as a continuous “pulsing” eruption manifest at the surface or the result of varying wind directions during this part of the eruption.



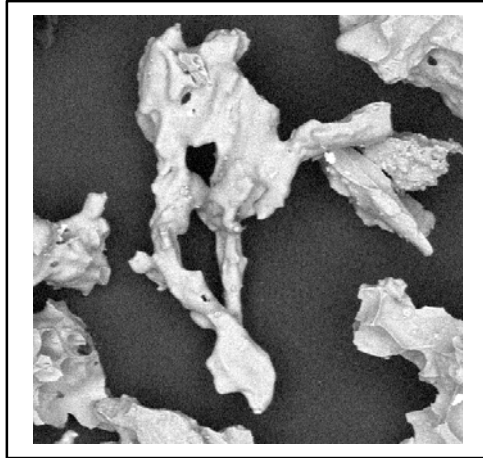
00362DC\_035.ai

Source: McGetchin et al. (1974 [DIRS 115469], p. 3268)

NOTES: In stages 1 and 2, nearly all tephra are deposited ballistically (with the exception of finer material carried away by the wind). Much of this activity could be characterized as lava fountaining. At the Lathrop Wells Cone, this sequence would include hydrovolcanic activity that formed hydrovolcanic beds outside the low-rimmed scoria ring. Early activity could have consisted of fountaining along a fissure, accounting for the N-S elongation of the cone.

In stages 3 and 4, cone growth is accompanied by Strombolian activity consisting of bursting gas bubbles in ponded lava; blockage of the vent by the slumping of unconsolidated ejecta leads to intermittent Strombolian blasts. Occasional interbeds of hydrovolcanic tephra reflect intermittent interaction with groundwater.

Figure 52. Stages of Scoria Cone Formation



For Illustration Purposes Only

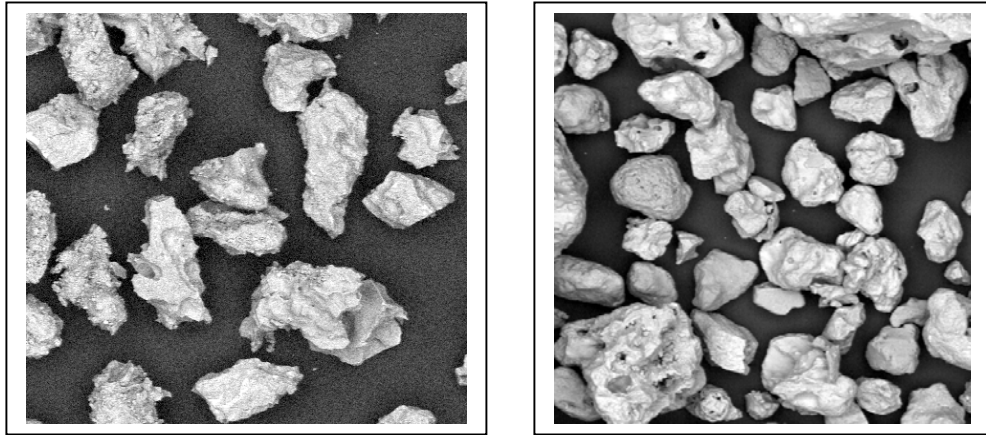
NOTE: The sample, located 850 m NW of the summit of the Lathrop Wells Cone, has mostly vesicular sideromelane (basaltic glass) pyroclasts with fluidal surface textures. Scale: width of image is ~617  $\mu\text{m}$ .

Figure 53. Pyroclasts from Fallout Sequence in the 0.125- to 0.250-mm Fraction of Sample DK-LW-021

2. The tephra sequence immediately northwest of the Lathrop Wells Cone is representative of the hydrovolcanic phase of the eruption (Vaniman and Crowe 1981 [DIRS 101620], p. 21; Wohletz 1986 [DIRS 140956]). Hydrovolcanic activity requires that rising magma come into contact with water in an aquifer(s) or a shallow water body at the ground surface (Fisher and Schmincke 1984 [DIRS 162806], pp. 231-234; Wohletz and Heiken 1992 [DIRS 105544], pp. 85-134). The resulting steam explosion finely fragments the magma and produces large amounts of kinetic energy. If the encounter occurs below the ground surface, the host rocks are highly fractured and the eruption products contain more lithic clasts. Hydrovolcanic deposits consist mostly of ash deposited in density currents (surges), leaving distinctive thin planar beds and cross-beds, which are typical of the sequence immediately northwest of Lathrop Wells Cone. The fragmentation process produces consistently finer-grained tephra (Figures 54 through 56). At Lathrop Wells Cone, median grain size for this tephra sequence ranges from 0.15 mm to 0.5 mm (an interbedded fall layer has a mean grain size of 1.5 mm). Volume fractions of lithic clasts in the fine-grained ash deposits range from 0.003 to 0.036 and consist mostly of white tuff and rounded quartz and feldspar sand grains. The presence of rounded quartz and feldspar grains and tuff xenoliths in the hydrovolcanic deposits suggest the water-magma encounter may have occurred in the shallow surficial deposits upon which the cone was built. Crowe et al. (1986 [DIRS 101532] p. 38) ascribe the dominant tuff xenolith to the Tiva Canyon Tuff, which forms most of the surface outcrops in the area and is also a major constituent of the surficial colluvium. Because of the minimum 1-m thickness of tephra fall beneath the hydrovolcanic beds, this hydrovolcanic event occurred during the early phases of the eruption.

Most basaltic hydrovolcanic pyroclasts in hydrovolcanic deposits are glassy and have low vesicularity and blocky shapes (Heiken and Wohletz 1985 [DIRS 106122]). However, in many examples, there is some rounding, perhaps by grain-to-grain

interactions in surges. Pyroclasts in hydrovolcanic surge deposits of the Lathrop Wells volcano are characterized by considerable edge modification (rounding). For comparison, Figures 54 and 55 below are images of pyroclasts from fall and surge deposits that have very similar pyroclast types. The rounding of pyroclasts is evident in the hydrovolcanic tephra (Figure 54). The rounding and edge modification of tachylitic pyroclasts is even more evident when looking at individual grains (Figure 55).

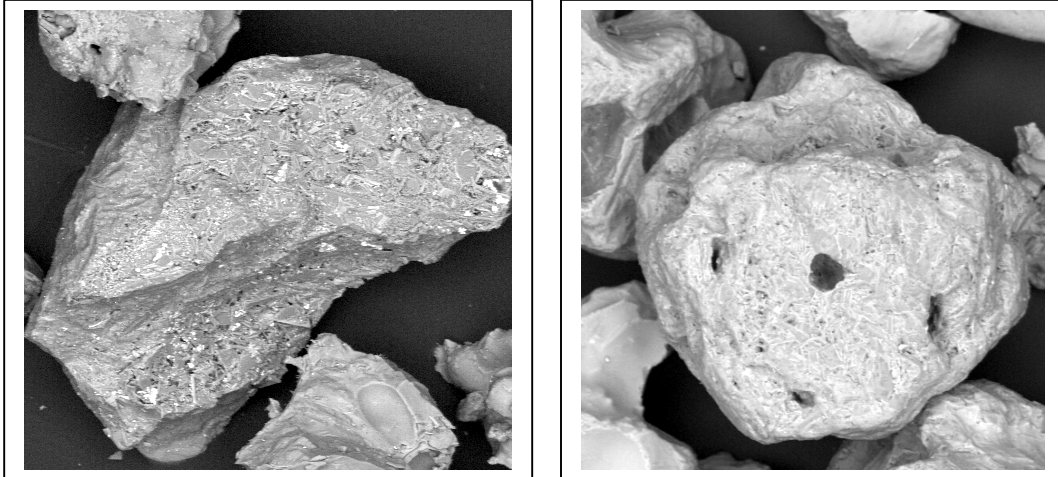


DTN: LA0302GH831811.004

NOTES: The left panel is from fall deposits 780 m NW of the Lathrop Wells Cone (Sample DK-LW-022, 0.125- to 0.250-mm fraction). Most pyroclasts are tachylite or glassy tachylite with rough grain surfaces and delicate edges. Scale: width of image is ~1.4 mm.

The right panel is from surge deposits 700 m NW of the Lathrop Wells Cone (Sample DK-LW-048, 0.125- to 0.250-mm fraction). Note the degree of rounding of all pyroclast types. Scale: width of image is ~1.4 mm.

Figure 54. Scanning Electron Micrographs Showing Differences in Fall Deposits (left) Versus Surge Deposits (right) of Hydrovolcanic Tephra

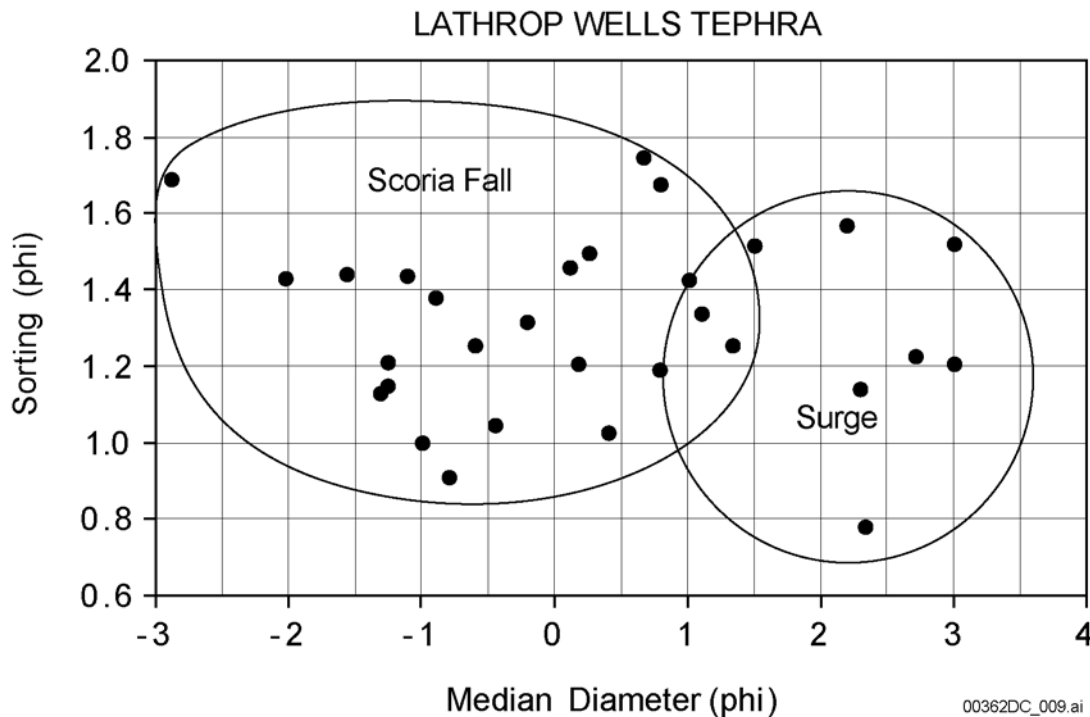


DTN: LA0302GH831811.004

NOTES: The left panel is of pyroclasts from fall deposits 780 m NW of Lathrop Wells Cone (sample DK-LW-024, 0.125- to 0.250-mm fraction). In the center is a tachylite pyroclast, with typical quench textures, angular shape, and sharp edges. The edge of the vesicle wall is visible in the lower left corner of the grain. In contrast is the small vesicular sideromelane pyroclast at the bottom of the image. Scale: width of image is ~400  $\mu\text{m}$ .

The right panel is of pyroclasts from surge deposits 700 m NW of Lathrop Wells Cone (sample DK-LW-049, 0.125- to 0.250-mm fraction). This tachylite pyroclast is very similar in composition to the grain in the image to the left. However, it has been mechanically rounded. Scale: width of image is ~300  $\mu\text{m}$ .

Figure 55. Scanning Electron Micrographs of Individual Grains Showing Differences in Fall Deposits (left) Versus Surge Deposits (right) of Individual Grains of Tephra



DTN: LA0302GH831811.002

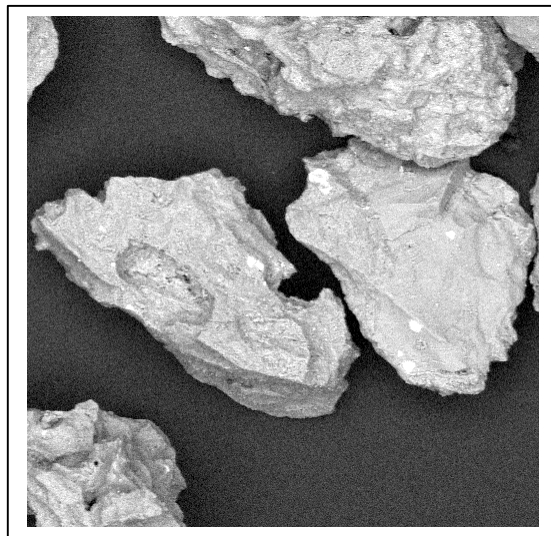
NOTE: The hydrovolcanic surge deposits are consistently finer-grained (higher phi number) than the scoria (tephra) fall deposits. Phi ( $\phi$ ) numbers are defined in Section 6.1.3.4.

Figure 56. Median Diameter Versus Sorting of Tephra Deposits Around the Lathrop Wells Cone

3. Later cone-forming activity deposited moderately sorted lapilli with 81% to 92% tachylite and glassy tachylite pyroclasts (Figures 57 and 58). These are similar to ash and lapilli formed during later stages of scoria cone construction (Figure 53, stages 3 and 4; Heiken and Wohletz 1985 [DIRS 106122], pp. 34-45). During later stages of cone formation, avalanching of scoria and ash down crater slopes blocked the vent, allowing rising magma to degas and for quench-crystal growth to occur (in contrast with the glass droplets formed during lava fountaining). Sporadic blasts carried out a mixture of scoria bombs, comminuted fragments of partly crystalline melt (quenched) and recycled scoria bombs, lapilli, and ash that slumped into the crater. Lithic clast concentrations are low in these tephra fall deposits.
4. An abrupt transition, exposed within the lower quarry wall, from coarse scoria lapilli to fine lapilli and ash, is inferred to mark an increase in eruption energy from Strombolian to violent Strombolian. The sudden abundance of lapilli and ash on the upper slopes of the cone became oversteepened and continuously avalanched downslope to be deposited as debris-flow material along with primary material raining down from an eruption column. The lapilli and ash directly overlie the coarser non-welded scoria representative of more Strombolian-like eruption (Figure 18). The large volume of lapilli and ash from this eruption phase, making up to an estimated two-thirds of the cone, is the main product of the mining operations at the cone. The

bulk of the ashfall that is mapped beyond the scoria cone is inferred to be related to this phase of the eruption.

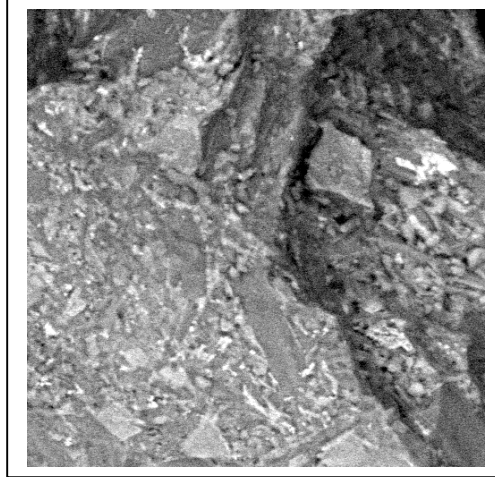
5. Quarry exposures of the cone suggest cone building continued largely unabated. An event toward the end of the eruption deposited nearly a half-meter of inward dipping, thin planar ash beds and cross beds, interpreted as hydrovolcanic in origin. Rounded quartz grains, although not numerous in the deposit, suggest this event may have occurred, once again, at shallow depth in or near the elevation of pre-volcanic surficial deposits. Shallow groundwater in alluvium or sand ramp deposits is inferred to have reached the near-surface conduit system, providing for a steam explosion. Above these fine-grained beds, coarse scoria deposits suggest the abrupt return to the less violent eruptive phase that preceded this brief hydrovolcanic event. These scoria deposits are the last observed units to be deposited on the cone.



DTN: LA0302GH831811.004

NOTE: The sample, located 850 m NW of the summit of the Lathrop Wells Cone, has angular, blocky tachylite (center) and glassy tachylite (top and bottom), which are characteristic of later stages in Strombolian eruptions. Scale: width of image is ~600  $\mu\text{m}$ .

Figure 57. Pyroclasts from Fallout Sequence in the 0.125- to 0.250-mm Fraction of Sample DK-LW-023



For Illustration Purposes Only

NOTE: Quench crystals, including laths of pyroxene and plagioclase, surrounded by dendritic growths of pyroxene and Fe-Ti oxides are visible on the tachylite pyroclast surface. Scale: width of image is ~100  $\mu\text{m}$ .

Figure 58. Detailed View of Tachylite Grain Surface

## 6.5 REDISTRIBUTION PROCESSES OF BASALTIC ASH AND WASTE PARTICLES

### 6.5.1 Characteristics of Ash Redistribution Processes

This section provides the technical basis for assessing the effect on the reasonably maximally exposed individual (RMEI) from secondary transport of contaminated ash following initial ash-fall deposition. Dilution studies were undertaken to characterize the sedimentological processes that redistribute contaminated ash from points of primary deposition to points downstream and to the location of the RMEI. This section includes data from samples collected from the Lathrop Wells Cone tephra sheet and presents a qualitative scoping analysis to assess the potential particle mixing and dilution of basaltic ash. The section also presents results of cesium-137 ( $^{137}\text{Cs}$ ) studies used to characterize landform stability and infiltration. The primary emphasis in this section is redistribution of ash in a regional context.

Particle mixing is a normal sedimentological process whereby the sediment loads of intersecting stream channels are blended such that, after some distance of transport, the combined drainage has a fairly homogeneous sediment load. This principle is applied to the transport and redistribution of basaltic ash that would be deposited along the eastern flank of Yucca Mountain following a potential volcanic eruption through the repository. The eastern flank of Yucca Mountain is highlighted because it drains water and sediment into the Fortymile Wash, which is the main channel for the transport of sediment south to Amargosa Valley and to the regulatory compliance point. To understand ash redistribution, the Lathrop Wells volcanic cone and two adjacent drainage systems are used as an analog setting. Specifically, we use information of the erosion of the tephra sheet exposed on the northwest of the cone to understand how the process of ash dilution occurs when primary ash is mixed with diluting sediments consisting of siliceous tuffs and eolian sand.

### **6.5.1.1 Ash Dilution Processes**

In small drainages developed on basaltic tephra sheets, material is moved down-slope by incorporating basaltic ash and sand mixed with water along small debris flow channels. When sufficient rainfall occurs up-slope and a small stream runs onto the tephra, ash particles are picked up and carried down-slope, leaving behind an incipient channel. The running water continues to acquire additional particles until the stream becomes overloaded with sediment; subsequently, the mixture floods over the leading edge of the sediment wedge as a debris flow and carries material down-slope away from the channel. Subsequent debris flows transport additional tephra material farther down-slope. This repeating action results in the progressive movement of material to the base of the tephra sheet and, in this scenario, to a drainage channel at the base of the slope. That drainage, situated marginally to the tephra, will also be carrying a sediment load, the majority of which is non-ash sediments. In the Yucca Mountain area, these sediments are dominantly clasts of siliceous tuff, rhyolitic ash, and quartz sand. When the two sediment types are combined in the drainage channel, mixing of the sediment particles occurs rapidly, and the more abundant sediment dilutes the ash component in the total sediment volume. The basaltic ash becomes a progressively smaller proportion of the total sediment load as the sediment is transported down the drainage.

If the area is subject to high wind velocities, eolian sand and coarse silt would be intermixed with the fluviually transported ash and other material in the channel. Additionally, eolian material carried onto the tephra sheet would result in deposition of medium to fine sand in the ash interstices and, over time, a sand component would increase in the near surface of the ash sheet. As the material is transported down-slope and along channels over time, more non-ash eolian material would be incorporated. When a channel joins larger-order channels that carry mainly nonbasaltic material, the dilution progressively increases. After some length of transport through subsequent stream intersections, the proportion of basaltic ash within the sediment becomes extremely small.

Ash dilution occurs during transport through the Yucca Mountain drainage systems, to the Amargosa Valley, and onto the Amargosa alluvial fan. Because the transport distance from the repository to the fan is approximately 25 km, significant sediment mixing and dilution of ash is expected to occur prior to transport past or deposition near the RMEI. In the Yucca Mountain repository eruption scenario, a volume of transported sediment with a highly diluted ash/waste component would have less impact on the RMEI than would primary ashfall that fell directly on, or nearby to, the RMEI. Therefore, the likely “worst-case scenario” is one in which winds direct the initial eruption column south from the repository toward the RMEI. It is the only scenario in which ash would reach the RMEI without some modicum of transportation and dilution.

### **6.5.1.2 The Ash Dilution Study at Lathrop Wells Cone**

The ash dilution study focused on the Lathrop Wells Cone tephra sheet as an analog for ash that could potentially cover the eastern flank of Yucca Mountain in some future basaltic eruption. The portion of the tephra sheet used for this study encompasses roughly 500 m<sup>2</sup> of a tuff-bedrock hillslope (~10 percent slope) to the northwest of the Lathrop Wells Cone and is approximately 100 m horizontally from top of the hillslope to the bottom (Figure 59). Small drainage channels have been excavated by debris-flows into this sheet, and two larger drainage systems transport

ash and sediment away from the hillslope. One drainage transports material around the west side of the cone and southward, ultimately into the Amargosa Valley. The other drainage heads near the top of tephra sheet exposure and transports material around the eastern side of the cone. Eventually, each of these channels joins much larger channels carrying non-ash components. Farther south in the Amargosa Valley, these parallel channels run marginal to the edge of the Fortymile Wash alluvial fan and terminate in nearly the same location in the valley. All sample locations within this setting for the ash-dilution study and cesium study (see below) are shown in Figure 60.

Sediment samples were collected from the drainage located on the western edge of the tephra sheet. In the upper part of the channel, sample spacing was 100 m. In the lower reach, below the junction with the larger, non-ash-bearing channel, sample spacing was 600 m. On the eastern side of the Lathrop Wells Cone ash sheet, sample spacing was 150 m from the very head of the ash sheet, down a debris-flow channel, and into a channel that runs marginally to the tephra sheet exposure. This channel drains northeast around the edge of the lava flows to the eastern side of the cone. Sample spacing below this point was 600 m. This channel network is joined by a much larger channel that drains areas from the north along the Stagecoach Road fault. This channel delivers large quantities of tuffaceous sand and gravel into the sampled drainage. Downstream from the juncture, the channel drains south into the Amargosa Valley along the western edge of the Fortymile Wash fan.



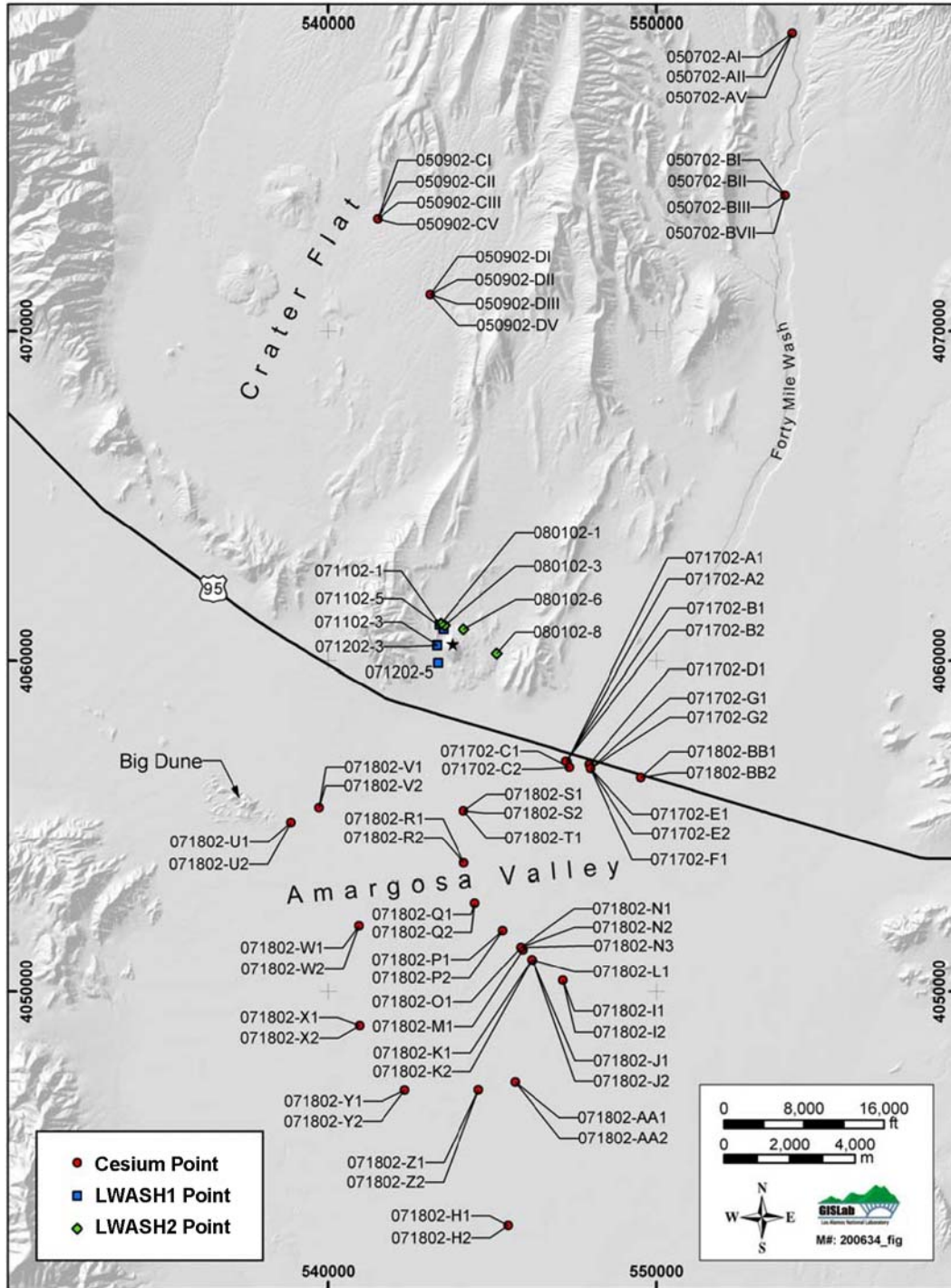
For Illustration Purposes Only

00362DC\_014.ai

For Illustration Purposes Only

NOTE: North is to the top of the photo. Associated lavas are dune-covered immediately east of the cone. The sampled drainages are west and east of the cone and lava flows. For scale, the N-S road from the highway to the cone is 1.6 km long.

Figure 59. Ortho-Photograph of the Lathrop Wells Volcanic Cone



00362DC\_015.ai

Source: Harrington (2003) [DIRS 164775]

NOTE: Lathrop Wells Cone is indicated with a star symbol. Yucca Mountain is the N-S linear mountain in the north-central part of the map.

Figure 60. Sample Locations for Ash Dilution and Cesium Studies

### **6.5.1.3 Areas of Yucca Mountain and the Fortymile Wash Drainage System**

The drainage system on the eastern flank of Yucca Mountain is a parallel system whereby individual channels have few tributaries. Lower on the flank, several stream channels, whose upper reaches follow north-south fault traces, collect the smaller drainages from Yucca Mountain and discharge into Fortymile Wash at three major input locations: Yucca Wash, Drill Hole Wash, and Lower Abandoned Wash.

Fortymile Wash is the major drainage along the east side of Yucca Mountain. This drainage system heads along the southern flanks of Rainier and Pahute Mesas approximately 30 km north of Yucca Mountain. The Fortymile Wash system collects sediment from Rainier and Pahute Mesas, the Buckboard Mesa area, Cat Canyon, and the Timber Mountain caldera. The basin supplies a continuous sediment load from these upper reaches that is greater than the contribution from the flanks of Yucca Mountain.

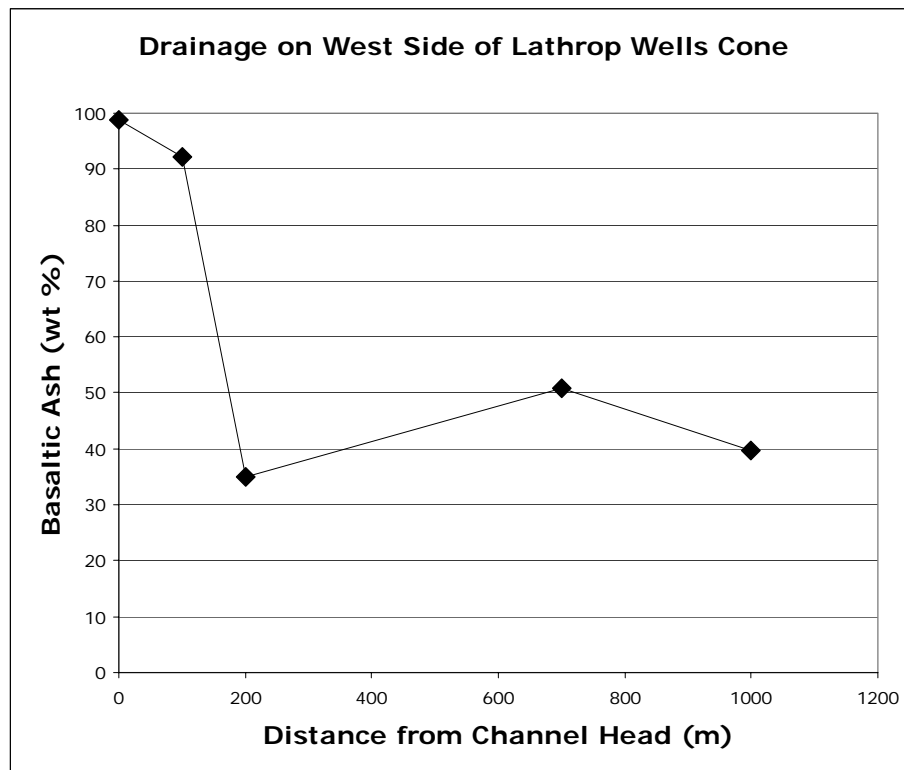
### **6.5.1.4 Results and Interpretation**

The Lathrop Wells Cone ash-dilution study results from the two drainages are shown in Table 35. Five samples covering a distance of 1,000 m were collected from the western drainage through three confluences with larger channels; the latter channels drain progressively larger areas that do not contain Lathrop Wells Cone tephra at the surface. The results plotted in Figure 61 show that after only 1,000 m of transport, significant dilution to ~40 wt% ash by addition of other tuffaceous sediments has occurred, thus reducing the ash component by nearly two-thirds over one kilometer. Dilution occurs by the addition of tuffaceous sediments from adjoining drainages and by incorporation of a large eolian sand load. Continued transport, with the addition of clasts of welded tuff and eolian grains, acts to wear down the scoria clasts to smaller particle sizes. This decreased particle size during transport shows two major trends down-channel. High on the tephra sheets, the particle size is dominated by the 2- to 4-cm granule sizes with few sand size grains present in the sample. Once beyond the tephra sheet, however, the sand sizes < 2 mm become the dominant component due to the incorporation of eolian sands blowing in from the Big Dune area and through grain-to-grain diminution of larger clast sizes. With continued transport southward into the Amargosa Valley, these two processes remain important, leading to the final nature of the deposit that reaches the compliance point.

Table 35. Ash Weight Percentages in Samples of Drainage Channels near Lathrop Wells Cone

Sample Number	Basaltic Ash (wt%)	Approximate Distance from Head of Channel (m)
Lathrop Wells Cone, West Side		
LWASH1-07/11/02-1	98.7	0
LWASH1-07/11/02-3	92.3	100
LWASH1-07/11/02-5	35.0	200
LWASH1-07/12/02-3	50.8	700
LWASH1-07/12/02-5	39.6	1,000
Lathrop Wells Cone, East Side		
LWASH2-08/1/02-1	54.9	0
LWASH2-08/1/02-3	59.4	400
LWASH2-08/1/02-6	10.1	1,200
LWASH2-08/1/02-8	0.8	2,500

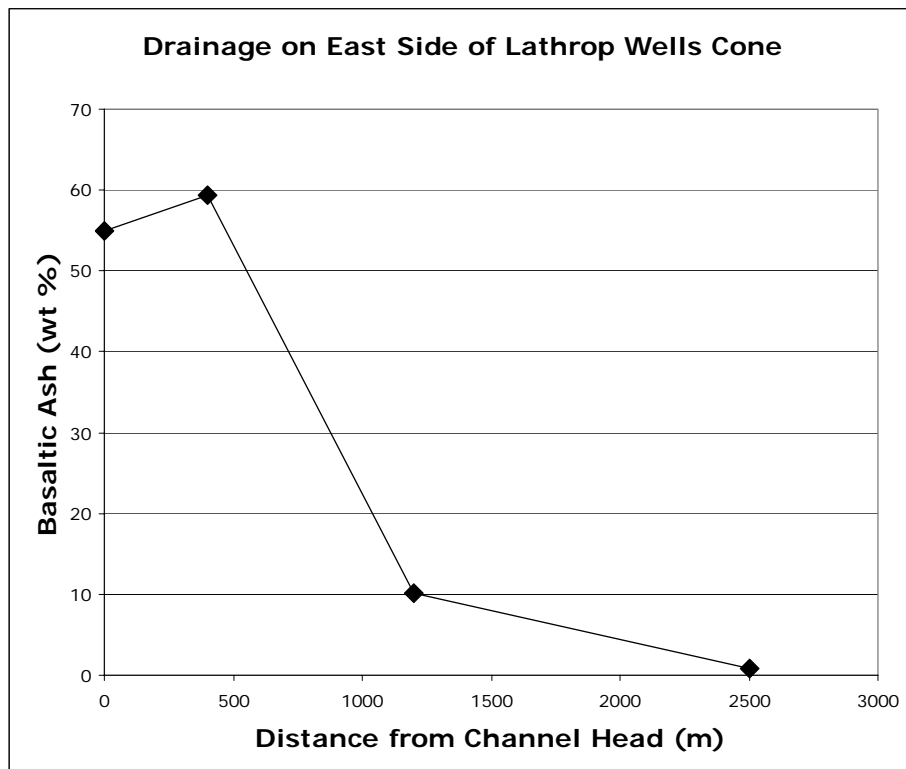
DTN: LA0308CH831811.001



DTN: LA0308CH831811.001

Figure 61. Ash Dilution Percentages in Drainage Along the West Side of Lathrop Wells Cone

The second set of drainages sampled at Lathrop Wells Cone traverse the north and east side of the scoria cone and lava flows. There are three confluences with larger streams along this sampling transect. Four samples were collected over 2,500 m (Table 35 and Figure 62). The sample from the top of the tephra sheet, at the head of a debris-flow channel, shows the effects of eolian sand deposition and yields about a 50/50 mixture of ash and sand. After transport off the tephra sheet and into a marginal channel at the base of the slope, the ash content in the sample is still about ~60 wt% (sample LWASH2-08/1/02-3) because the location is adjacent to the tephra sheet. Below the point where the channel joins the first drainage bringing tuffaceous material from the north, the ash content is reduced by dilution to 10 wt% (sample LWASH2-08/1/02-6). After an additional 1,300 m, the channel intersects another larger wash that delivers tuffaceous sediments from along the Stage Coach Road fault area (Figure 60). Down-gradient from where the sediments from the two channels merge, the basaltic ash present is barely measurable (0.8 percent ash, sample LWASH2-08/1/02-8). The near-complete reduction in volume of ash per volume of sediment occurs within a distance of < 3 km.



DTN: LA0308CH831811.001

Figure 62. Ash Dilution Percentages in Drainage Along the East Side of Lathrop Wells Cone

The dilution studies documented at Lathrop Well Cone demonstrate that significant reduction of volume of basaltic ash per volume of sediment occurs over short distances during transport due to the continuous addition of other tuffaceous material to the drainage systems. However, it is not feasible to develop a simple scaling factor for the ash-dilution rate to apply to the much larger drainage area of Fortymile Wash because of the complexities due to differences in the basin area, bedrock types, gradients, vegetation, elevation, and precipitation. For the Lathrop

Wells Cone area, however, the ratio of the drainage basin that includes the Stagecoach Road fault to the area down-gradient from the tephra sheet exposure is about 6:1, meaning that the size of drainage area that supplies non-ash sediment is six times larger than that which supplies ash from the tephra sheet. For the Fortymile Wash drainage, the basin area above the repository site is approximately 8 times larger than the area down-gradient from the repository site. If a future volcanic eruption through Yucca Mountain deposited contaminated ash within or across this basin area, rapid and aggressive mixing and dilution of basaltic ash with siliceous tuffaceous sediments will occur during the transport toward the RMEI location.

## **6.5.1.5 An Ash Redistribution Scoping Analysis**

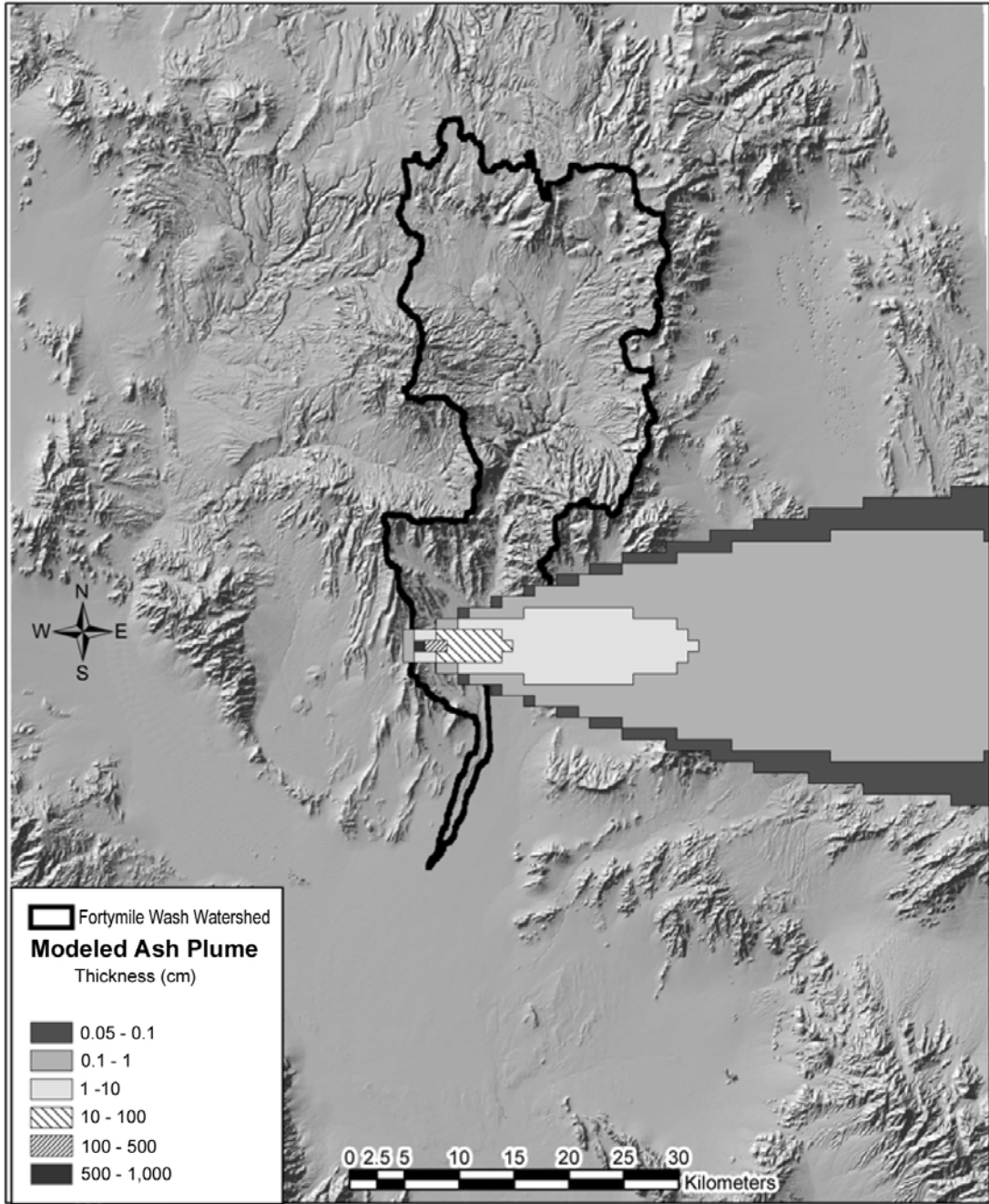
### **6.5.1.5.1 Introduction**

A qualitative scoping analysis was performed to begin evaluation of a path forward for a quantitative estimation of particle mixing that would take place between basaltic ash and background sediment within Fortymile Wash in the event of a volcanic eruption. The scoping analysis uses parameter values not specific to Yucca Mountain or Fortymile Wash and the simplest physical representation of the mixing process. The analysis uses the ARC Map GIS as a framework for performing a mass-balance-based analysis of sediment and ash yield to a point downstream of a hypothetical ashfall zone.

### **6.5.1.5.2 Method**

A set of digital spatial data layers was imported into the ARC Map GIS to perform the analysis. The spatial data layers included USGS digital elevation data for the Fortymile Wash watershed (10-m by 10-m grid cell size), ashfall thicknesses (cm) generated by the ASHPLUME v. 1.4LV (BSC 2002 [DIRS 161296]) software, and sediment yield values for the ashfall zone and for the unaffected region of the watershed. ASHPLUME v. 1.4LV (BSC 2002 [DIRS 161296]) was the version of software used in TSPA-SR; however, for TSPA-LA, a different version (2.0) will be used that is more representative of a possible eruption at Yucca Mountain. Generally, ASHPLUME v. 1.4 (BSC 2002 [DIRS 161296]) modeling results in a tephra sheet with more ash deposited closer to the vent area and thereby increases the amount of ash available for transport in this scoping study. Because the present scoping study is illustrative in nature, a comparative analysis between ASHPLUME v. 1.4LV (BSC 2002 [DIRS 161296]) and v. 2.0 is not necessary. ASHPLUME v. 2.0 is described in *Atmospheric Dispersal and Deposition of Tephra from a Potential Volcanic Eruption at Yucca Mountain, Nevada* (BSC 2003 [DIRS 161840]).

Figure 63 shows the outline of the Fortymile Wash watershed and the modeled ashfall thicknesses overlain on a hillshade representation of the DEM. The scoping analysis was performed within the approximately 800-km<sup>2</sup> watershed. Less than ten percent of this area is affected by ashfall. For this scenario, ASHPLUME v. 1.4LV (BSC 2002 [DIRS 161296]) was run using 0.04 km<sup>3</sup> ash and a 10.3 m/s wind blowing due east. The ash volume is similar to volume of tephra estimated for the Lathrop Wells Cone earlier in this report.



For Illustration Purposes Only

00362DC\_012.psd

For illustration purposes only

NOTE: Ashfall thicknesses in cm (0.05-0.1, 0.1-1.0, 1.0-10, 10-100, and 100-1,000; thickness < 0.05 cm are not plotted) from the ASHPLUME (BSC 2002 [DIRS 161296]) model are shown as gray contours over a hillshade representation of the DEM. Approximately 800 km<sup>2</sup> of the Fortymile Wash watershed is shown with a black outline. The scoping analysis applies only within the delineated Fortymile Wash watershed. Ash outside the watershed boundary does not contribute to the yield at the basin outlet (southern tip of watershed boundary).

Figure 63. Ashfall Thicknesses from the ASHPLUME v. 1.4LV Model

The scoping analysis strives to represent the sediment and ash yields that might occur during a large, historic flood. In this analysis, the ratio of ash to clean sediment at the basin outlet is proportional to the area in the watershed covered by ash and dependent on the time since the eruption. Data from Mount St. Helens and Pinatubo volcano (Umbal 1997 [DIRS 166018], p. 3) show ash/sediment yield declines exponentially with time after eruption. Yield per unit-area of ash from the ashfall zone is considered to be several orders of magnitude higher than the sediment yield per unit area from unaffected areas immediately after eruption. Here we use a background, clean sediment yield of 0.001 cm/year, based on the two highest short-term sediment yield rates from Kirchner et al. (2001 [DIRS 162820], Figure 1), and 1.0 cm/year ash-yield rate from the ashfall zone, based on measurements from the Toutle River drainage at Mount St. Helens in the first four years following the 1980 eruption (Hayes et al. 2002 [DIRS 162816], Figure 1).

The total yield of ash and sediment,  $C$ , at any point was determined as follows:

$$C = [A_{\text{ash}}(t) \cdot Y_{\text{ash}}(t)] + [A_{\text{back}}(t) \cdot Y_{\text{back}}(t)] \quad (\text{Eq. 13})$$

where

- $A_{\text{ash}}(t)$  is the area in the Fortymile Wash watershed covered by ash in year  $t$
- $Y_{\text{ash}}(t)$  is the annual sediment yield from the ashfall area in year  $t$
- $A_{\text{back}}(t)$  is the area unaffected by the ashfall
- $Y_{\text{back}}(t)$  is the background annual sediment yield.

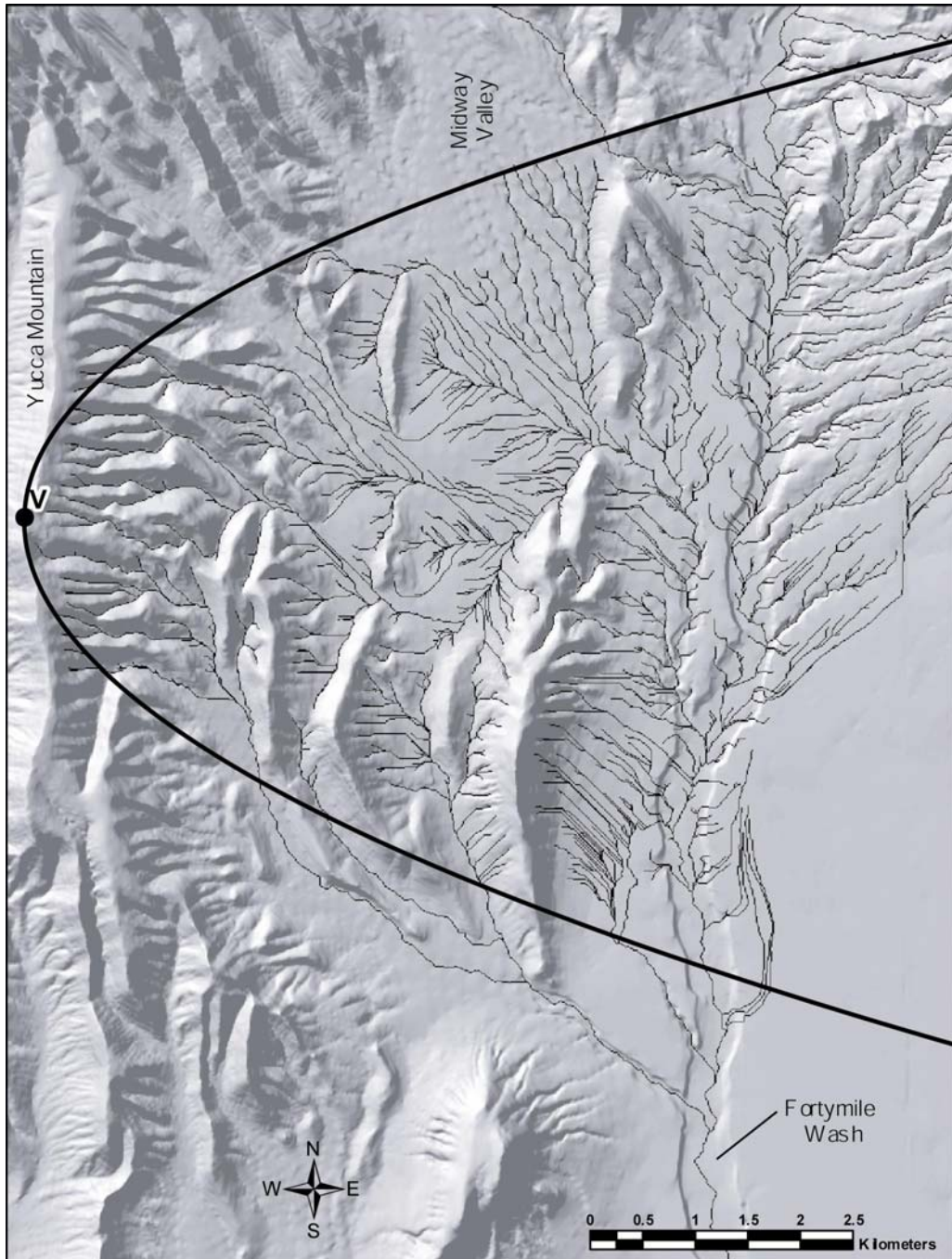
The analysis assumes instantaneous transport from *all* parts of the watershed to that point. Every grid cell contributes sediment or ash to the total yield value.

Figure 64 illustrates how output from the mixing calculation can be represented when the sediment delivery point is chosen to be in Fortymile Wash south of the major confluences. The presence of dark lines running along small stream drainages within the ashfall zone (shown as the parabolic curve) indicate that ash yield in upland streams is higher than background sediment yield in upland streams outside the ashfall zone. In this black-and-white demonstration, the dark drainage lines begin where the cumulative amount of ash delivered from the hillslopes to the stream is larger than a threshold value of 100 units. The size of the unit (e.g.,  $\text{cm}^3$ ,  $\text{m}^3$ , kg, or tons) will depend on the rate of ash erosion relative to the rate of background sediment erosion. Once better data for model parameterization are available, the actual variation in values of sediment or ash yield to each point along every stream and along the length of Fortymile Wash can be shown in, for example, a gradational scale. Calculations will show the spatially distributed impact of increased erosion and transport of ash in a color-coded manner, providing a visual and quantitative tool for evaluating ash redistribution within the entire drainage basin.

### 6.5.1.5.3 Limitations

The scoping study contains a number of issues that could be addressed to provide robust predictions with finite uncertainties. At this time, the analysis does not account for a number of processes: variable travel times from near and far sources, variations in sediment yield relating to hillslope or channel gradient, differential grain settling, sediment storage, variable nature of climate in space and time, and site-specific sediment yield data.

However, the GIS framework is ideally suited to handling better sediment and ash transport processes and descriptions, and these algorithms could be implemented to produce good estimations of ash redistribution in space and time. Various analytical approaches might consider data on site-specific erosion, sediment yield, runoff, and climate, which would establish the bounds of uncertainty. This supporting analysis will be updated as necessary.



00362DC\_013a.ai  
For illustration purposes only

NOTE: Sediment yields from each grid cell are accumulated along flow paths that were calculated by ARC Map™ from the digital elevation data. The parabolic curve encompasses the ASHPLUME v. 1.4LV (BSC 2002 [DIRS 161296]) depositional area shown in Figure 63 (note scale difference). The hypothetical vent is marked with a "V." Most of the smaller stream lines in the ashfall zone indicate high ash yield (dark gray), whereas most of the smaller drainage lines north and south of the ashfall zone have less than 1,000 units of sediment yield.

Figure 64. Sediment Yields Using ARC Map™

## 6.5.2 Cesium-137 Studies

### 6.5.2.1 Cesium-137 Study of the Fortymile Wash Alluvial Fan

Radioactive  $^{137}\text{Cs}$  was distributed worldwide as a result of atmospheric nuclear weapons tests beginning around 1950 (Ely et al. 1992 [DIRS 164076], p. 196). As cesium accumulated on ground surfaces, it was incorporated into any sediments subsequently formed by transport and deposition. Therefore,  $^{137}\text{Cs}$  can serve as a time-marker for sediments formed during the last 50 years. As such, the measurement of the concentration of  $^{137}\text{Cs}$  with depth in the soil can be used to examine erosion and deposition rates over this short time period. Uncertainty enters when relating processes and rates acting over a short time period (~50 years) to erosion/deposition over much longer time periods (> 1 ky). However, careful examination of where and how modern erosion and deposition are occurring can help elucidate what is likely to occur sometime into the not too distant future.

In earlier  $^{137}\text{Cs}$  landscape-component studies (Chappell 1999 [DIRS 163891], p. 138), the investigated sites were either along transects or on plots of about a dozen  $\text{km}^2$ . The current study examines the movement of sediment through the drainage systems for an area that encompasses several hundred square kilometers, including the Yucca Mountain site and Fortymile Wash alluvial fan (the fan alone encompasses  $100 \text{ km}^2$ ). Because of the uncertainties in applying this technique to this large area, the purpose is to note trends or similarities for sites of erosion or deposition.

$^{137}\text{Cs}$  preferentially attaches to silt- and clay-size particles in normal sedimentary profiles, but also to dune sand as, for example, in the sands of Big Dune (Amargosa Valley, Figure 60), and to sand grains in small coppice dunes that traverse surfaces of alluvial fans. The cesium analyses discussed below show some of the highest cesium values from these dune materials, which possess almost no fine-grained material.

In the study area, most alluvial surfaces contain a prominent vesicular A-horizon composed of silt with minor amounts of clay, often directly beneath a desert pavement. Because desert pavements develop over thousands of years, they are characteristic of very stable surfaces. Part of this study (the reference sample suite) was designed to verify that  $^{137}\text{Cs}$  does not infiltrate rapidly into the deeper sediments so that depth profiles among sites could be compared confidently. The remainder of the study examines the cesium quantities in the material, vertical cesium profile, and particle-size composition of the upper 6 to 10 cm of sediments to help determine erosion/deposition sites on the Fortymile Wash alluvial fan surfaces.

### 6.5.2.2 Reference Sites for Cesium-137 Study

Previous studies using  $^{137}\text{Cs}$  in North America (Wallbrink et al. 1994 [DIRS 164092], p. 95) did not find a single value that could be used as a calculated background value for every study. Thus, a scoping study was performed to determine the nature of cesium distribution around Yucca Mountain, and reference samples were used to compute the Yucca Mountain background value. Samples were collected at four locations along Fortymile Wash and within Crater Flat (Figure 60). For each sample location, alluvial surfaces were selected based on characteristics associated with their long-term stability to at least pre-Holocene time (10,000 years). These

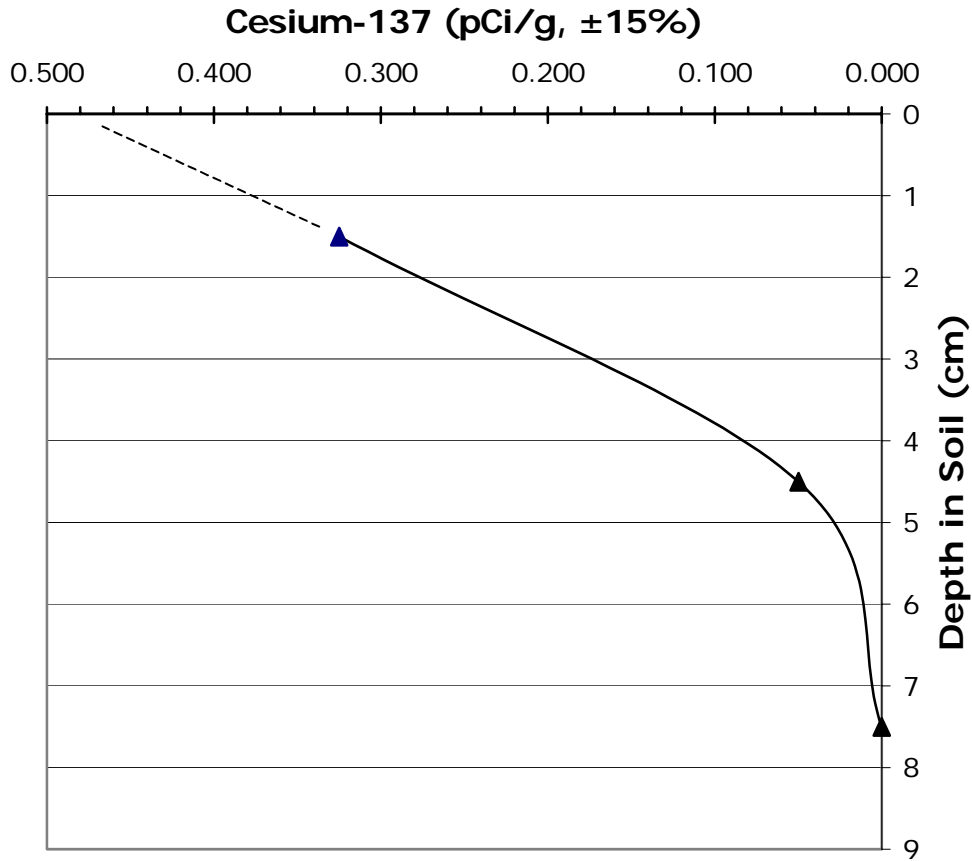
characteristics included presence of a well-developed desert pavement overlying a well-developed, 4- to 6-cm thick, vesicular A-horizon. Two sample locations, about 3 km apart, were located on a high, river-cut terrace in Fortymile Wash, and two sampling sites were located in central Crater Flat, about 2 km west of Yucca Mountain. Sample pits were hand-dug to ~0.5 to 0.75 m depth. At each location, three samples were collected from a 0-3, 3-6, and 6-9 cm depth. Commonly, a caliche layer within the alluvium was visible in the bottom of the pit but was not sampled. Carbonate in the soil at this depth indicates the age of the overlying soil as Pleistocene (10,000+ years) (Gile et al. 1981 [DIRS 144518], pp. 67-68). In addition, the lower alluvium commonly contained thin, subvertical carbonate stringers, which usually take > 1,000 years to develop in soils (Machette 1985 [DIRS 104660], pp. 5-11).

### **6.5.2.3 Results and Interpretation of Reference Samples**

The analytical results show that most of the  $^{137}\text{Cs}$  is present within the upper 3 centimeters of the A-horizon in these stable environments (Figure 65). Hence, there is little evidence in the Yucca Mountain area of any significant cesium infiltration (below 6 cm) into the deeper sediments during the last 50 years.

If cesium infiltration were a significant process over the past 50 years, these stable surfaces would exhibit the greatest depths of cesium infiltration, because nothing would have been modifying these stable surfaces post-deposition. However, the uppermost soil layer (vesicular-A), composed mostly of eolian-derived silt, should also act to retain the  $^{137}\text{Cs}$  in the near-surface.

Depth profiles for  $^{137}\text{Cs}$  show similar trends among the suite of reference samples. A typical profile has a maximum value of about 0.325 picocuries per gram (pCi/g) (range 0.251 to 0.421 pCi/g) in the upper 3 cm of soil, a lower average value of ~0.050 pCi/g in the 3- to 6-cm layer, and effectively no  $^{137}\text{Cs}$  in the 6- to 9-cm depth layer. This trend is shown schematically in Figure 65. The reference samples retain almost their entire inventory of  $^{137}\text{Cs}$  very near the surface because the  $^{137}\text{Cs}$  attaches to fine-grained material in the upper part of the soil profile soon after deposition and remains immobile. Hence, the reference profiles suggest minimal infiltration of  $^{137}\text{Cs}$  in the profile. This “typical” depth profile for the reference suite can be a useful tool for comparison with other samples, and characteristics of the Fortymile Wash alluvial fan samples can be evaluated. The typical depth profile used for comparison to the fan samples is a composite derived from the reference samples (Figure 65). The whole profile at each sample location is used in the comparison process.



DTN: LA0308CH831811.002

NOTE: Sample depth is plotted at midpoints of 3-cm intervals.

Figure 65. Cesium-137 Profile with Depth in Sediment for Composite of 15 Reference Samples

#### 6.5.2.4 Sampling of the Fortymile Wash Alluvial Fan

Sediment samples for  $^{137}\text{Cs}$  analysis were taken along three latitudinal transects across the Fortymile Wash alluvial fan (Figure 60). Additional samples were collected from south of Lathrop Wells Cone to near the toe of the fan, as well as from Big Dune and the geomorphic surface on which it sits. Sixty-six cesium samples, including 15 reference samples, were collected from 28 sample sites. Samples are representative of the Fortymile Wash channel, tributary drainage channels, overbank deposits, interstream divide areas, coppice dunes near channels, and large sand-covered tracts around Big Dune. Analytical results from these laboratory measurements are listed in Table 36 and archived with DTN: LA0308CH831811.002.

Table 36. Interpretation of 137-Cesium Profile Values for Samples from the Fortymile Wash Alluvial Fan

Sample #	Layer Depth	137-Cs (pCi/g) in Layer	Topographic Position	Interpretation of 137-Cesium Profile Values
Cs-071702-A1	0-3 cm	0.259 +/- 0.045	In old channel-overbank	About 0.5 cm removed by wind erosion
Cs-071702-A2	3-6 cm	0.054 +/- 0.016		
Cs-071702-B1	0-3 cm	0.146 +/- 0.030	Channel	Sediments well mixed before deposition
Cs-071702-B2	3-6 cm	0.125 +/- 0.023		
Cs-071702-C1	0-3 cm	0.209 +/- 0.036	Interstream divide	About 1 cm of eolian removal
Cs-071702-C2	3-6 cm	0.049 +/- 0.012		
Cs-071702-D1	0-6 cm	0.276 +/- 0.049	Flood channel-overbank	Old deposit, slightly stripped (< 0.25 cm)
Cs-071702-E1	0-3 cm	0.159 +/- 0.030	Interstream divide	About 1.5 - 2 cm of material removed
Cs-071702-E2	3-6 cm	0.049 +/- 0.015		
Cs-071702-F1	0-6 cm	0.306 +/- 0.053	Coppice dune	Wind deposition site, although temporary
Cs-071702-G1	0-3 cm	0.118 +/- 0.025	Interstream divide	Appears to have lost more than 2 cm
Cs-071702-H1	0-3 cm	0.191 +/- 0.035	Interstream divide	Appears to have lost ~2 cm
Cs-071702-H2	3-6 cm	0.006 +/- 0.013		
Cs-071802-I1	0-3 cm	0.374 +/- 0.065	Interstream divide	Stable site with no removal
Cs-071802-I2	3-6 cm	0.015 +/- 0.014	pebbly pavement	
Cs-071802-J1	0-3 cm	0.099 +/- 0.022	In active channel bottom	Mixing of sediments during transport in channel
Cs-071802-J2	3-6 cm	0.056 +/- 0.025		
Cs-071802-K1	0-3 cm	0.325 +/- 0.055	Interstream divide with gravel surface	Stable site, if material removed only 0.2 cm
Cs-071802-K2	3-6 cm	0.015 +/- 0.008		
Cs-071802-L1	0-6 cm	0.322 +/- 0.057	Coppice dune	Stable sand deposit
Cs-071802-M1	0-3 cm	0.031 +/- 0.017	Main channel	Material in channel moved fairly recently
Cs-071802-N1	0-3 cm	0.198 +/- 0.037	Flood surface with overbank deposits	Typical overbank deposits
Cs-071802-N2	3-6 cm	0.020 +/- 0.012		
Cs-071802-N3	6-9 cm	-0.012 +/- 0.013		
Cs-071802-O1	0-6 cm	0.111 +/- 0.022	Coppice dune	Sand has been moving across surface
Cs-071802-P1	0-3 cm	0.231 +/- 0.040	Interstream divide	At least 1 cm of removal by wind
Cs-071802-P2	3-6 cm	0.014 +/- 0.013		
Cs-071802-Q1	0-3 cm	0.204 +/- 0.037	Interstream divide with eolian winnowing/lag	At least 2 cm of removal by wind
Cs-071802-Q2	3-6 cm	0.001 +/- 0.012		
Cs-071802-R1	0-3 cm	0.227 +/- 0.042	Interstream divide with pebbly lag/eolian removal	At least 1 cm removal by wind
Cs-071802-R2	3-6 cm	0.010 +/- 0.012		
Cs-071802-S1	0-3 cm	0.251 +/- 0.043	Old fan with poorly developed pavement	Stable fan surface, ~0.5 cm removed
Cs-071802-S2	3-6 cm	0.034 +/- 0.010		
Cs-071802-T1	0-6 cm	0.104 +/- 0.022	Coppice dune	Active dune with sand held only temporarily
Cs-071802-U1	0-3 cm	0.073 +/- 0.018	Sand surface near Big Dune; active sand movement	Active sand movement on this surface
Cs-071802-U2	3-6 cm	0.060 +/- 0.018		
Cs-0071802-V1	0-3 cm	0.322 +/- 0.056	Interstream divide with well developed pavement	Stable surface, almost no infiltration of cesium
Cs-0071802-V2	3-6 cm	0.002 +/- 0.011		
Cs-071802-W1	0-3 cm	0.097 +/- 0.026	On active fan surface with flood deposits/overbank	Active surface with recent flood/overbank deposition
Cs-071802-W2	3-6 cm	0.038 +/- 0.014		
Cs-071802-X1	0-3 cm	0.200 +/- 0.035	Old fan surface/divide; pebble lag indicates eolian processes	About 1 - 1.5 cm of removal by eolian processes
Cs-071802-X2	3-6 cm	0.028 +/- 0.012		
Cs-071802-Y1	0-3 cm	0.088 +/- 0.020	Active fan surface, but seldom flooded	Sediment mixed
Cs-071802-Y2	3-6 cm	0.045 +/- 0.014		
Cs-071802-Z1	0-3 cm	0.240 +/- 0.043	Surface with a silt cap indicating ponding in the past	Surface has been stable except for 1 cm of removal
Cs-071802-Z2	3-6 cm	0.078 +/- 0.016		
Cs-071802-AA1	0-3 cm	0.275 +/- 0.047	Interstream divide area with pebble lag/eolian removal	Surface has 1 cm of removal
Cs-071802-AA2	3-6 cm	0.016 +/- 0.011		
Cs-071802-BB1	0-2 cm	0.255 +/- 0.045	Interstream divide with eolian activity; produced a pebble lag	Surface has eolian removal of at least 1 cm
Cs-071802-BB2	2-5 cm	0.066 +/- 0.015		

DTN: LA0308CH831811.002

### **6.5.2.5 Cesium-137 Results and Interpretation of Data**

Sample locations whose  $^{137}\text{Cs}$  profiles most resemble the reference-sample (stable surface) profiles are located on interstream divide areas between distributary channels. Interstream divide areas have the least likelihood of having been submerged during floods over the last fifty years. These profiles are similar to the reference profiles that have low  $^{137}\text{Cs}$  values (in the range of 0.02 to 0.08 pCi/g) in the 3- to 6-cm layers. However, the surface layers (1-3 cm depth) typically have values much less than the reference samples from equivalent depths, which range from 0.251 to 0.421 pCi/g. It appears, then, that many of these interstream divide areas have had part of the upper layer removed. The amount of material removed is estimated by comparing the  $^{137}\text{Cs}$  value of the upper 3-cm layer to that of the reference value and calculating the thickness of the layer that would have to be removed to obtain the lower value. Application of this estimating method across the interstream divide sample locations shows that most of the interstream divide areas have had 1 to 3 cm of material removed from their surfaces in the last 50 years. Overbank deposits on the divide areas that would suggest periodic flooding are uncommon and restricted to narrow strips along the channel banks. The overbank and channel deposit samples have similar  $^{137}\text{Cs}$  signatures; the 3- to 6-cm layers and the 6- to 9-cm layers also have nearly the same values (in the 0.100-0.200 pCi/g range), indicating that the material from each environ was mixed during transport and deposited as a homogeneous sediment. We conclude that it is unlikely the erosion of these slight topographic highs on the fan resulted from fluvial processes.

The loss of material from these otherwise stable surfaces appears to be due to eolian processes. Evidence for wind playing a predominant role in erosion of the interstream divide areas includes the lack of new or developing stream channels and the presence of modern coppice dunes near channels on interstream divides. Erosion of a divide area with little evidence of recent water movement is most easily explained by eolian removal. The presence of nearby Big Dune and other eolian deposits provides strong support for eolian erosion and transport. Eolian transport of fine-grained material from the alluvial fan surfaces is more effective than the running water that so infrequently crosses interstream divides.

The absence of many overbank deposits along the channel margins today indicates that flows sufficient to form extensive overbank flooding down Fortymile Wash and its distributary channels have not occurred in well over 50 years. Therefore, the channels currently transport most of their sediment load across the fan until it reaches the toe of the fan, where deposition occurs on the broad flats to the south or into the channel of the Amargosa River.

## **6.5.3 Discussion**

### **6.5.3.1 Ash Dispersal from the Proposed Repository**

If a future basaltic eruption through the repository did occur, the ash plume would most likely be transported in the direction of the prevailing winds, and although that could be any direction in the future, the most probable direction would be from southwest to northeast (NOAA 1995 [DIRS 154435]). The ash redistribution scenario that would result in delivery of the most basaltic ash through the Fortymile Wash system would be an ash plume that was deposited north-northeast along the axis of upper Fortymile Wash. In this scenario, tephra would be

thickest near the vent above the repository and would cover the eastern flank of Yucca Mountain, and much of the upper Fortymile Wash drainage basin.

On the upper hillslopes, scoria and ash would potentially fill the heads of these small valleys. Because this material would be largely situated on  $> 30^\circ$  slopes, precipitation on these hillslopes would flow into or over the tephra and incise into it. The drainages would not be hydraulically plugged because of the slope steepness and the loose, permeable nature of the tephra. The process of removal of the material begins immediately, as illustrated at Parícutin for loose, nonwelded ash and lapilli fallout (Luhr and Simkin 1993 [DIRS 144310], Fig. 171). On the upper slopes of Yucca Mountain, the parallel drainages would act like flumes and steadily move the tephra through as often as there were thunderstorms sufficient to move the tephra to the floors of adjacent valleys. This flow would continue to transport water and finer sediment until reaching Fortymile Wash.

### **6.5.3.2 Storms and Climate Change in the Yucca Mountain Region**

Storms at Yucca Mountain can be classed into two types of rainstorms: the local, infrequent, high-intensity storms (summer monsoonal thunderstorm) and the larger, lower-intensity regional storms, which cover very broad areas on scales larger than entire drainage basins (Coe et al. [DIRS 104691], p. 15). Typically, regional storms have longer durations with periods of heavy rains during part or most of the storms. These storms occur more commonly during winter, although they can occur at any time of the year.

It is the intense, localized thunderstorm that would be the likely initiator of movement of the scoria and ash particles from the ridgetop drainage heads into the parallel channels. Undercutting of slopes of scoria and ash could cause sloughing of masses of tephra and result in addition of disaggregated scoria and ash to the drainage systems. In most localized thunderstorms, water rapidly infiltrates into the underlying soil and does not carry its bedload long distances. At Yucca Mountain, these storms seldom feed abundant material into Fortymile Wash (Coe et al. 1997 [DIRS 104691], pp. 24-26). To get abundant material into the wash and to transport it a long distance requires the much broader, longer-period regional rainstorms.

The flood of 1969 (probably the most severe in recent times) had an estimated peak flow in Fortymile Wash of about 20,000 cubic-feet/second (Squires and Young 1984 [DIRS 102783], p. 12). During this flood, water flowed through the length of the wash, across the alluvial fan, into the Amargosa River, and ultimately into Death Valley, where a shallow lake was impounded over an area of 80 mi<sup>2</sup> (207 km<sup>2</sup>) (Hunt 1975 [DIRS 159900], p. 15). It is these long-duration regional storm systems that rain on entire drainage basins, flush the hillslopes, and move large quantities of materials into the wash. If movement of erupted ash began in the upper watershed of Fortymile Wash, mixing of materials would occur along the entire length of transport, up to 70 km.

If overall climate in the YMR were to change to wetter weather patterns, there would be several impacts on the landscape, including a major change in the dominant storm type. During wetter conditions, long-duration regional storms would become more frequent and summer monsoon storms would become more infrequent or, perhaps, disappear. Landscape vegetation would become more abundant, and in situ weathering would decrease overall particle sizes and enhance

deeper soil development. This change would result in a greater capacity to retain sediments on the hillsides and reduce the sediment load in streams, while, because of the increase in rainfall, there would be more water in the system. When the sediments were put in transport, mixing would still be an effective agent in the dilution of contaminated sediment along the journey to the Fortymile Wash alluvial fan.

## **6.6 POTENTIAL ERUPTION SCENARIO AT THE YUCCA MOUNTAIN REPOSITORY**

A future basaltic magma intrusion into the subsurface of Yucca Mountain followed by a surface eruption of scoria, lava, and ash would have relatively predictable physical volcanological and sedimentological consequences. Based on the properties of basaltic magma and the eruption and sediment transport processes discussed in Sections 6.1 through 6.5, one scenario of a surface eruption is compiled below. This scenario is proposed as a guide to a possible sequence of eruption phenomena at the surface and is not proposed as a conservative event sequence. The physical effects of a magmatic dike approaching and intruding the repository drifts filled with waste packages is discussed in *Dike/Drift Interactions* (BSC 2003 [DIRS 165923]). The calculation of the number of waste packages encountered by the magma intruding a repository is presented in *Number of Waste Packages Hit by Igneous Intrusion* (BSC 2003 [DIRS 164650]). The effects of magma and exsolved volatiles on waste package materials are described in *Igneous Intrusion Impacts on Waste Packages and Waste Forms* (BSC 2003 [DIRS 165002]). Finally, models for eruption, ashfall distribution, and redistribution of ash from the point of deposition by erosive processes are included in *Atmospheric Dispersal and Deposition of Tephra from a Potential Volcanic Eruption at Yucca Mountain, Nevada* (BSC 2003 [DIRS 161840]).

1. A north-south-trending fissure opens on the upper flanks of Yucca Mountain over a distance of tens to hundreds of meters, accompanied by the violent release of gases from the fissure over a period of a few hours. Incandescent basaltic scoria and small bombs, ballistically ejected from a rising magma front, begin to accumulate on the surface along the fissure.
2. There is a rapid buildup in the mass discharge rate of magma, producing lava fountains that eject a mixture of basalt bombs, cinders, and finer-grained droplets of basaltic glass. The bombs and cinders are deposited ballistically around the vent, constructing an elongate spatter rampart or cone along the fissure. An elongate spatter rampart and fissure would control the eventual shape of the cone, as occurred at Lathrop Wells Cone. Winds will likely push the eruption plume to the north-northeast, covering the terrain with tephra fallout having a median grain size of ~1.5 mm.
3. Early in the history of the volcano and, perhaps to a lesser extent, throughout the eruption, there may be interaction of rising magma with shallow alluvial groundwater, resulting in energetic hydrovolcanic eruptions, which leave deposits of fine-grained (median grain size = 0.4 mm) tephra, deposited mostly as pyroclastic density currents (surges). Depending on the duration or magnitude of the hydrovolcanic activity, the deposits could range from a few fine-grained surge beds interbedded with scoria fall deposits to a tuff ring with a broad crater in which the main scoria cone is later constructed. Any hydrovolcanic eruptive phases would be important in widening a

conduit below the volcano; such activity would be reflected in increased lithic clast concentrations of both surge and fall deposits. Total lithic clast volumes estimated for the entire eruption could range from  $5.4 \times 10^4 \text{ m}^3$  to  $5.2 \times 10^6 \text{ m}^3$ , based upon the minimum and maximum values observed within the Lathrop Wells Cone (Section 6.4.1.2). Assuming a conduit diameter of 50 m and a cylindrical shape, the conduit depth range would be from 94 m to 3,300 m; conduit growth would add to the disruption of a repository intersected by the eruption.

4. Early in the history of the volcano, lava flows emerge from vents in the base of the cone, flowing down-slope toward Jackass Flat.
5. The cone has evolved to the point where much of the coarse-grained ballistic material (bombs, blocks, lapilli) landing on cone slopes has reached the angle of repose of  $\sim 32^\circ$ . Loose pyroclasts avalanche down the flanks and into the crater. The vent is frequently clogged by loose debris and eruptions are sporadic blasts of tachylitic bombs, blocks, lapilli, and ash. These blasts produce columns that rarely go higher than 500 m above the crater rim. The ash is carried downwind, forming the fallout deposit, with a median grain size of 1.65 mm, within 1.5 km of the volcano, gradually decreasing to 0.8 mm beyond the 1.5-km line. Some of the fallout blankets moving lava flows.
6. There may be eruption phases, perhaps a few hours long but extending to as long as two weeks, of violent Strombolian activity, in which sporadic bursts give way to a continuous eruption with high mass discharge rate. Column height will depend on eruption duration and discharge rate during these phases.
7. The eruption lasts nearly four weeks. The final product is an elongate scoria cone with an average basal diameter of 700 m, a height of 120 m, a volume of  $\sim 0.02 \text{ km}^3$ , and a tephra fall sheet with a volume of  $\sim 0.08 \text{ km}^3$ . The area covered by tephra at least 1 cm deep is about  $234 \text{ km}^2$  (conservative estimate).
8. There is cooling of the deposit (hot pyroclasts in the cone, especially any welded spatter deposits). The dike or dikes below the cone and the lava flows may take decades to reach ambient temperatures. Volcanic gases and steam produced by heating ground water or infiltrated rainfall may oxidize the basaltic scoria deposits in zones overlying the conduit/dike system.
9. From the time of ash deposition, winds blowing from the direction of the Amargosa Valley have transported and deposited eolian fine sand that becomes trapped by the scoria and ash fragments in the near-surface of the tephra sheet. The sand infiltrates into the tephra sheet and dilution of the pure ash begins.
10. Soon after deposition, ash particles and included eolian material begin to be transported to the base of the tephra sheet by debris flow. At the base, the ash enters small channels and is transported into progressively larger channels. Mixing of ash with other sediments occurs during transport. The  $800\text{-km}^2$  drainage area of Fortymile Wash contributes large quantities of sediments to the channel system. Continued

fluvial transport and mixing results in a progressively smaller volume of basaltic ash per volume of total sediment.

## **6.7 UNCERTAINTIES (INPUT)**

### **6.7.1 Input Parameters and Uncertainty**

This subsection summarizes input data and parameters for the analyses that are detailed in this scientific analysis report (Table 37). This subsection is coordinated with Section 4. In Table 37, column 5, “epistemic” refers to an uncertainty that could be reduced by further knowledge, for example, by further sampling and analysis. In addition, the uncertainties associated with these inputs are identified and discussed in the following subsections.

#### **6.7.1.1 Forty-five Chemical Analyses of Products from the Lathrop Wells Volcano**

There is a low degree of uncertainty associated with the mean chemical composition of Lathrop Wells volcano lava. These data are used to estimate physical properties of a future magma (of similar composition) as it ascends through the crust, intercepts and interacts with the repository, and erupts onto the surface. The statistics provided in Table 6 for the major element chemical composition data reflect the natural variations expected among multiple samples of the same lava flow, as well as the variations expected for multiple samples from different lava flows from the same monogenetic volcanic event. There is a very low degree of uncertainty associated with any one major oxide determination because of the tight clustering of values (reflected in their standard error and standard deviation) among 45 rock samples and the use of modern analytical methods of chemical analysis. Additional analyses would only serve to decrease the standard deviations of any one mean.

#### **6.7.1.2 Lithic Contents of Products of the Lathrop Wells Volcano**

These data are used to characterize qualitative aspects of explosive violence of the eruption, lithologies affected by the feeder dike(s) and conduit, and approximate width of the conduit.

*Lathrop Wells Cone:* There is a moderate degree of uncertainty associated with the xenolithic volume determinations within the cone. Locations of counts were chosen in fresh quarry or road-cut outcrops and provided unprecedented views of the interior of the volcanic edifice. Xenolith lithologies present in the dark basaltic rocks represent older silicic volcanic, volcanoclastic, or carbonate rocks and, hence, their color contrasts are extreme and their dimensions readily determined. Identification of xenolith dimensions down to 0.1 cm in the field using a 12-power magnification hand lens is done with confidence under these circumstances. Outcrop selection is limited by the size and placement of the quarry excavations; however, the quarry excavation is mature and continuous from basal exposures to the top of the crater. Several shear walls are inaccessible and the quarry is located exclusively on the south side of the cone. Excavation has proceeded into an estimated one-quarter to one-third of the basal diameter of the cone. Volume fractions of lithic clasts are estimated by taking the two longest dimensions of individual lithic measurements within a square-meter patch and assuming their extension (third dimension) through an entire cubic meter. This method maximizes the volume fraction based on the counts, but obviously misses xenoliths that are not exposed. Additional xenolithic

volume determinations would likely drive volume estimates downward unless extensive xenolith-rich exposures are opened in future quarrying operations.

*Lathrop Wells Cone tephra:* There is a moderate to high degree of uncertainty associated with determination of lithics volume within tephra deposits. Grain counts using a binocular microscope concentrated on the tephra facies that have the highest concentration of xenolithic material, namely, the ~1-m-thick hydrovolcanic facies within 0.5 km northwest of the cone. Some other locations of tephra excavated by shovel have two thin (1-2 cm) lithic-bearing layers (silt-size and smaller) at the base of the tephra section, but these are volumetrically insignificant. Additional xenolith determinations at these intervals would provide a better volume estimate, but would not significantly affect the determination of total lithic volume.

### 6.7.1.3 Fifty-three Grain Size Data (Sieve Fractions) for the Lathrop Wells Volcano Tephra

There is a low degree of uncertainty associated with grain-size determinations. These data are used to create a history of eruption dynamics and to estimate the areal extent of ash distribution resulting from that eruption. These data were developed from tephra samples representing the variety of locations where the tephra blanket was found and from nearly all recognizable stratigraphic layers within most sections. Standard sieve ( $\phi$ ) sizes were used according to common practice in studies of volcanic ash deposits worldwide. Uncertainty arises from the absence of tephra outcrops or subcrops beyond about 2 km north of the cone and 1.3 km west of the cone. Tephra deposits south and east of the lava flows of Lathrop Wells Cone are either deeply buried by younger alluvium or are non-existent and could not be sampled. Based on comparison with grain-size data for cones of similar composition elsewhere, the range of grain sizes present in the measured sections should be representative of a typical low-volume and relatively short-lived cinder-cone event.

Table 37. List of Input Parameters and Uncertainty Type

Input Name	Input Description	Input Source	Value or Distribution	Type of Uncertainty
45 chemical analyses of products from Lathrop Wells volcano	Mean major-element chemical composition (and related statistics) of Lathrop Wells lava.	DTN: LA00000000099.002	Means (see Table 6 for complete statistics) SiO <sub>2</sub> -48.50% TiO <sub>2</sub> -1.93% Al <sub>2</sub> O <sub>3</sub> -16.74% Fe <sub>2</sub> O <sub>3</sub> T-11.63% [Fe <sub>2</sub> O <sub>3</sub> 1.74%] [FeO 8.90%] MnO-0.17% MgO-5.83% CaO-8.60% Na <sub>2</sub> O-3.53% K <sub>2</sub> O-1.84% P <sub>2</sub> O <sub>3</sub> -1.22%	Epistemic
Lithic contents of products of Lathrop Wells volcano	Volume of xenolithic clasts per m <sup>3</sup> exposed in quarry or road-cut exposures for 18 1-m <sup>2</sup> measurement.	DTN: LA0302GH831811.003	Volume fraction ranges from 0.000018 to 0.0091	Epistemic
53 grain size data (sieve	Description of volcanic history of Lathrop Wells	DTN: LA0302GH831811.002	Refer to DTN for range	Epistemic

fractions) for Lathrop Wells volcano tephra	volcano, including grain size distribution and sorting characteristics.			
Grain counts from tephra deposits around Lathrop Wells volcano	Description of volcanic history of Lathrop Wells volcano, including particle morphology and composition.	DTN: LA0302GH831811.004	Refer to DTN for range	Epistemic
Tephra thicknesses, Lathrop Wells volcano	Thicknesses of explosive tephra deposits at different map locations in vicinity of Lathrop Wells volcano.	DTN: LA0305DK831811.001	Tephra thicknesses at various map points range from 1 to 304 cm	Epistemic
<sup>137</sup> Cs analyses for Fortymile Wash alluvial fan	66 analytical concentrations of <sup>137</sup> Cs in samples from locations on a major YMR drainage alluvial fan.	DTN: LA0308CH831811.002	<sup>137</sup> Cs analyses range from 0.002 to 0.322 pCi/gram	Epistemic
Basaltic ash content of surficial material around Lathrop Wells Cone	9 analyses of wt% basaltic-ash particles from Lathrop Wells volcano in samples from surrounding drainages.	DTN: LA0308CH831811.001	Basaltic ash content ranges from 0.8 to 98.7 wt%	Epistemic

#### 6.7.1.4 Grain Counts from Tephra Deposits Around Lathrop Wells Volcano

There is a low degree of uncertainty associated with the determinations of particle-type percentages from samples of tephra. Expert identification of particle type is used along with an adequate number of counted grains to provide a reasonable estimate of grain types. There is a moderate degree of uncertainty associated with representativeness of the samples with respect to the entire tephra deposit because of the small sample size. The samples are largely representative of tephra layers containing a moderate to abundant proportion of xenolithic grains. Additional grain counts of samples would increase confidence in the distribution of particle types, but would not significantly alter interpretations of the eruptive history of Lathrop Wells volcano.

#### 6.7.1.5 Tephra Thicknesses for the Lathrop Wells Volcano

There is a moderate degree of uncertainty associated with the determinations of tephra section thicknesses. These data are used to estimate the volume of ash and lapilli ejected during the more violent phases of the eruption—and the evolution of eruption type—for development of the volcanic history. Most recent excavations of tephra sections were limited to using a shovel, whereas excavations during several past field seasons were often done using a motorized back-hoe. Most of the latter excavations were localized around the base of the cone and, therefore, provide constraints on the thicker accumulations of ash. The most recent excavations could not always expose the base of the tephra when the thickness of tephra was greater than about 1 m, due to its unconsolidated nature. Geologic evidence suggests that the tephra was buried and protected by eolian sands and silts soon after deposition, but some erosional stripping of the tops of sections is expected to have occurred. Therefore, the tephra thicknesses represent minimum values in nearly all cases. Additional excavations using mechanized equipment would

reduce the uncertainty associated with tephra thickness, which overall would impact the estimate of tephra volume.

#### **6.7.1.6 Cesium-137 Analyses for the Fortymile Wash Alluvial Fan**

There is a low degree of uncertainty associated with the  $^{137}\text{Cs}$  analyses of individual samples collected from locations on the alluvial fan. Analysis is performed by calibrated gamma spectroscopy in a certified analytical laboratory performing under strict QA requirements.

#### **6.7.1.7 Basaltic Ash Content of Surficial Material Around the Lathrop Wells Cone**

There is a low degree of uncertainty associated with the determination of basaltic ash content of alluvial samples from the Lathrop Wells Cone area. The techniques of sieving samples, optical binocular microscope identification, magnetic separation, and weighing hand-picked basaltic and nonbasaltic components are straightforward, if tedious. Uncertainty arises from 1) how representative the sample population is of the natural system and of the surficial processes resulting in mixing of basaltic ash with other materials and 2) the selection of enough samples to capture the natural variation expected among locations along any one wash (stream drainage). In addition, some basaltic ash particles (especially in the finer fractions) do not possess the characteristics to be recognized as ash, while other particles that may be identified as basaltic ash are not. Expertise is required and employed for correct optical identification.

## **7. CONCLUSIONS**

This scientific analysis report provides technical bases for parameter values that will be used for the TSPA-LA related to the effects of a volcanic eruption through the Yucca Mountain repository. Uncertainties in the output parameters are described in the text as appropriate and summarized in Table 38. The information and data in this report, which is direct input to the TSPA, are based largely on literature values and simple calculations as described in Section 6 and discussed in CRWMS M&O (2000 [DIRS 156980], p. 17). Other information that indirectly relates to assessment of a potential igneous disruption of the repository and post-eruption processes, such as descriptions of the Lathrop Wells Cone and redistribution of ash, is based on field studies and supporting laboratory analyses.

### **7.1 SUMMARY OF SCIENTIFIC ANALYSIS**

The Technical Product Output (Table 38) of this scientific analysis report provides distributions for parameters to be used by the YMP LA to describe the physical properties of basaltic magmas, volcanoes, eruptive processes, and volcanic products related to a volcanic eruption through the Yucca Mountain repository. Specific output parameters and uncertainties are described in the text and summarized in Section 7.2 (below). Other processes are qualitatively described that relate to the progression of eruptive processes, based on both literature-derived data from observations of volcanic eruptions worldwide and on data from Lathrop Wells Cone, Nevada. Lathrop Wells Cone is a relevant source of information because it is the youngest volcanic event (~80,000 years) near Yucca Mountain and, along with other young basaltic cinder cones and flows in the area, forms the basis for the potential disruptive volcanic event for the repository. Processes that affect the post-eruptive redistribution of volcanic ash are also described in

Section 6.5 from observations of ash transport and mixing with other tuffaceous sediments within the areas of Lathrop Wells Cone, Fortymile Wash, and Fortymile Wash alluvial fan. Therefore, processes that encompass volcanic eruption, cone construction, ash-plume dispersal and deposition, and ash redistribution are depicted in this report. Other related reports cover topics that precede or follow in time the potential eruption scenario, such as model development and results for dike propagation in the shallow crust and the effects of a magmatic dike intercepting a repository drift at atmospheric pressure (BSC 2003 [DIRS 165923]), for the number of waste packages involved in a magmatic intrusion into a repository drift filled with waste packages (BSC 2003 [DIRS 164650]), and for magmatic effects on waste packages and waste forms (BSC 2003 [DIRS 165002]). Specific results from modeling of potential ash-plume eruption, dispersal, and deposition from Strombolian and violent Strombolian eruptions of basaltic magma are described in *Atmospheric Dispersal and Deposition of Tephra from a Potential Volcanic Eruption at Yucca Mountain, Nevada* (BSC 2002 [DIRS 158966]).

The following specific parameter distributions are suggested for the eruptive processes described in this report.

- Conduit diameter-Triangular distribution, minimum diameter equal to dike width, mode diameter equal to 50 m, maximum value 150 m. Uncertainties in this parameter are related mainly to a limited amount of published data on conduit diameters for volcanoes of similar volume, composition, and eruptive mechanisms as those in the YMR. There are no restrictions on subsequent use of this range of conduit diameters.
- Dike width-Log-normal distribution, minimum of 0.5 m, mean of 1.5 m, 95th percentile value of 4.5 m. There is little uncertainty associated with this distribution because it incorporates measured basaltic dike width values in the YMR. There are no restrictions on the subsequent use of this range of dike widths.
- Number of dikes associated with formation of a new volcano-log-normal distribution with minimum of 1, mode of 3, and a 95<sup>th</sup> percentile of 6. There is little uncertainty associated with this distribution, because it incorporates observations of basaltic centers in the YMR. There are no restrictions on the subsequent use of this range of values for the number of dikes in a dike swarm.
- Dike spacing-Uniform distribution with a minimum of 100 m and maximum of 690 m. Uncertainty in this range is related to lack of dike sets in the Yucca Mountain area in which to make measurements. There are no restrictions on the use of this range of dike spacings.
- Magma chemistry-Mean Lathrop Wells composition (Table 6). Uncertainty in this composition (given as standard deviation and sample variance) is provided in Table 6 and is related to the variation in compositions directly measured on Lathrop Wells volcanic products. There are no restrictions on the subsequent use of this mean magma composition.
- Water content of magmas-Uniform distribution between 1 and 3 wt%, zero probability of 0 wt% increasing linearly to 1 wt%, zero probability of 4 wt% with linear distribution

between 3 and 4 wt%. This distribution captures all potential uncertainty in the water content of magmas as it is bounded by a value of zero at the low end and by a maximum water content (above which magmas crystallize and, therefore, could not erupt) at the high end. There are no restrictions on the subsequent use of this distribution.

- Gas composition—Derived from a suite of active volcanoes (Table 7). A measure of the uncertainty associated with the recommended gas composition is provided in Table 7 as the standard deviation; the uncertainty reflects the range of volcanic data from which the values are derived. There are no restrictions on the subsequent use of this gas composition.
- Magma temperatures, viscosities, and densities—Calculated from theoretical relations (Table 8). Liquidus temperature ranges from 1,046 to 1,169°C, viscosity ranges from 1.957 to 2.678 (log poise units), and density ranges from 2,474 to 2,663 kg/m<sup>3</sup>. Uncertainties associated with these values are expected to be small because the mathematical relationships used to calculate the values are closely tied to experimental data. There are no restrictions on the subsequent use of these values.
- Magma ascent rate below vesiculation depth—Equation 3. Uncertainties associated with this equation relate to processes and material properties not accounted for in the equation—for example, if there is a pressure driving force in addition to buoyancy between the magma and surrounding rocks or if the rheology of the magma is non-Newtonian. Subsequent use of this equation should explicitly state the sources of uncertainty and the assumptions made in the theory.
- Volatile exsolution depths—Figure 6. The depth ranges from about 9 km to zero depth for water contents between 0 and 4 wt%. Uncertainties in Figure 6 are related to the assumptions made in the theoretical approach: 1) steady and homogeneous flow and 2) lithostatic pressure within the dike or conduit. The uncertainties could be large. Subsequent use of Figure 6 should explicitly state the assumptions made in the theory and should not violate the theory.
- Fragmentation depths—Figure 7. These depths range from 0 to 900 m (approximately) for water contents between 0 and 4 wt%. Uncertainties in fragmentation depth are related to a lack of understanding of the mechanisms of fragmentation, which has been observed to occur at gas volume fractions ranging from 0.60 to 0.95. Subsequent use of these fragmentation depths should explicitly state that they are based on an assumption of fragmentation at a gas volume fraction of 0.75.
- Velocity as a function of depth—Eruption velocity  $u_{erupt}$  is estimated from Figures 8 and 9. Velocity then decreases linearly downward to  $0.1u_{erupt}$  at the fragmentation depth. Below fragmentation depth, the velocity continues to decrease linearly to  $0.01u_{erupt}$  at the depth where water exsolution begins. Uncertainty in the value of  $u_{erupt}$  is related both to the validity of assumptions made in developing the theory that produces the curves in Figures 8 and 9 (steady, homogeneous flow with lithostatic pressure in the rising magma column) and to the limitations of graphical extrapolation of the actual calculated curves. Uncertainty in the velocity versus depth functions are associated with

the simple linear nature of the recommended functions, whereas, in reality, the functions would be nonlinear due to poorly understood processes of magma ascent. Subsequent use of these velocity profiles should explicitly state the simplifications that are made to derive them.

- Eruption duration for formation of an entire volcano—For formation of an entire YMR basaltic volcano, a log-normal distribution with a minimum of one day, a mean of 30 days, and a maximum of 15 years. There are no restrictions on the subsequent use of these distributions.
- Duration of a single explosive phase constituting a violent Strombolian eruptive phase—A uniform probability ranging from 1 to 75 days. Uncertainty in this range is related to the small number of observed eruptions. The recommended maximum of 75 days encompasses the duration of the most energetic phase of Paricutin (73 days).
- Eruption volume—Uniform distribution between  $0.004 \text{ km}^3$  and  $0.08 \text{ km}^3$ . Based on the estimated volumes of Quaternary basaltic volcanoes in the YMR, this range captures most of the uncertainty associated with potential ash volume from a basaltic eruption at the repository. There are no restrictions on the subsequent use of this distribution.
- Mean particle size erupted during violent Strombolian phases—Log-triangular distribution with a minimum of 0.01 mm, a mode of 0.1 mm, and a maximum of 1.0 mm. Uncertainties associated with this parameter are due mainly to the rarity of data in the published literature that pertain to the bulk erupted particle size from violent Strombolian eruptions. The recommended distribution incorporates the range of values that have been estimated in published studies as referenced and recent work on Lathrop Wells Cone tephra sheet (this report). There are no restrictions on the subsequent use of this distribution.
- Standard deviation of particle size distribution for a given mean—Uniform distribution between  $\sigma_\phi = 1$  and  $\sigma_\phi = 3$ . Uncertainties associated with this parameter are due mainly to the rarity of data in the published literature that pertain to the bulk erupted particle size from violent Strombolian eruptions. The recommended distribution incorporates the range of values that have been estimated. There are no restrictions on the subsequent use of this distribution.
- Clast characteristics—Shape factor of 0.5. Uncertainty in this parameter is related to an absence of data in the published literature. There are no restrictions on the subsequent use of this value.
- Density of erupted particles—For particle diameters less than or equal to 0.01 mm, density is 0.8 of the magma density. For particles greater than 10 mm, density is 0.4 of the magma density. For particles between 0.01 and 10 mm, density should decrease linearly with increasing diameter. Uncertainty in this parameter is related to the wide range of vesicularities of clasts that can be erupted during a single volcanic event. There are no restrictions on subsequent use of the recommended values.

- There are two ways of treating deposit density in TSPA-LA calculations—1) Use 1,000 kg/m<sup>3</sup> or 2) a sample from a normal distribution of deposit densities ranging from 300 to 1,500 kg/m<sup>3</sup>, with a mean of 1,000 kg/m<sup>3</sup>. Uncertainties associated with this parameter are due to a lack of published data. There are no restrictions on subsequent use of the recommended values.
- Eruptive power—A uniform probability distribution (in log-power, watts) ranging from 9.0 to 12.0. The uncertainties associated with this parameter are due to a lack of published data and the inherent difficulty in derivation of power levels exhibited during volcanic eruptions. Uncertainties also arise because power, as reported in the literature, is a time-averaged value and may vary throughout the period of an eruption. There are no restrictions on subsequent use of the recommended values.

## **7.2 OUTPUT PARAMETERS AND UNCERTAINTY**

The output parameter distributions and their uncertainties, as summarized in Table 38, form the Technical Product Output for this scientific analysis report (DTN: LA0311DK831811.001).

Table 38. Technical Product Output for This Scientific Analysis Report

Parameter	Recommended Values	Uncertainties	Restrictions on Subsequent Use
Conduit diameter	Triangular distribution, minimum diameter equal to dike width, mode diameter equal to 50 m, and maximum value of 150 m.	Uncertainties in this parameter are related mainly to a limited amount of published data on conduit diameters for volcanoes of similar volume, composition, and eruptive mechanisms as those in the YMR.	There are no restrictions on subsequent use of this range of conduit diameters.
Dike width	Log-normal distribution, minimum of 0.5 m, mean of 1.5 m, and 95 <sup>th</sup> percentile value of 4.5 m.	Because this distribution incorporates measured basaltic dike width values in the YMR, there is little uncertainty associated with it.	There are no restrictions on the subsequent use of this range of dike widths.
Number of dikes associated with formation of a new volcano	Log-normal distribution with a minimum of 1, mode of 3, and 95 <sup>th</sup> percentile of 6.	Because this distribution incorporates observations of basaltic centers in the YMR, there is little uncertainty associated with it.	There are no restrictions on the subsequent use of this range of values for the number of dikes in a dike swarm.
Dike spacing	Random uniform distribution with minimum of 100 m and maximum of 690 m.	This distribution captures most potential uncertainty by exceeding the range of dike spacing in the YMR.	There are no restrictions on the use of this range of values for dike spacing.
Magma chemistry	Mean Lathrop Wells composition, Table 6.	Uncertainty in this composition (given as standard deviation and sample variance) is given directly in Table 6 of this report and is related simply to the variation in compositions directly measured on Lathrop Wells volcanic products.	There are no restrictions on the subsequent use of this mean magma composition.
Water content of magmas	Uniform distribution between 1 and 3 wt%, zero probability of 0 wt% increasing linearly to 1 wt%, zero probability of 4 wt% with linear distribution between 3 and 4 wt%.	This distribution captures all potential uncertainty in the water content of magmas, as it is bounded by a value of zero at the low end, and by a maximum water content (above which magmas crystallize and therefore could not erupt) at the high end.	There are no restrictions on the subsequent use of this distribution.
Gas composition	Table 7 of this report, which is derived from a suite of active volcanoes.	A measure of the uncertainty associated with the recommended gas composition is provided directly in Table 7 of this report as the standard deviation; the uncertainty reflects the range of volcanic data from which the values are derived.	There are no restrictions on the subsequent use of this gas composition.
Magmatic temperatures, viscosities, and densities	Calculated from theoretical relations (Table 8). For water content ranging from 4 to 0%, liquidus temperature ranges from 1,046 to 1,169°C, viscosity ranges from 1.957 to 2.678 (log poise units), density ranges from 2,474 to 2,663 kg/m <sup>3</sup> .	Uncertainties associated with these values are expected to be small because the mathematical relationships use to calculate the values are closely tied to experimental data.	There are no restrictions on the subsequent use of these values.

Table 38. Technical Product Output for This Scientific Analysis Report (Continued)

Parameter	Recommended Values	Uncertainties	Restrictions on Subsequent Use
Magma ascent rate below vesiculation depth	Equation 3: $u_f = \frac{A\eta}{4K\rho_m r} \left[ \left( 1 + \frac{64gr^3(\rho_c - \rho_m)K\rho_m}{A^2\eta^2} \right)^{1/2} - 1 \right]$	Uncertainties associated with this equation would relate to processes and material properties not accounted for in the equation. For example, if there is a pressure driving force in addition to buoyancy between the magma and surrounding rocks or if the rheology of the magma is non-Newtonian.	Subsequent use of this equation should explicitly state the sources of uncertainty and the assumptions made in the theory.
Volatile exsolution depths	Figure 6: range from about 9 km to zero depth for water contents between 0 and 0.04 weight fraction (0 and 4 wt%).	Uncertainties in Figure 6 are related to the assumptions made in the theoretical approach: steady and homogeneous flow, and lithostatic pressure within the dike or conduit. The uncertainties could be large.	Subsequent use of Figure 6 should explicitly state the assumptions made in the theory and should not violate the theory.
Fragmentation depths	Figure 7: range from 0 to 900 m (approximately) for water contents between 0 and 4 wt%.	Uncertainties in fragmentation depth are related to a lack of understanding of the mechanisms of fragmentation, which has been observed to occur at gas volume fractions ranging from 0.60 to 0.95.	Subsequent use of these fragmentation depths should explicitly state that they are based on an assumption of fragmentation at a gas volume fraction of 0.75.
Velocity as a function of depth	Eruption velocity $u_{erupt}$ is estimated from Figures 8 and 9. Velocity then decreases linearly downward to $0.1u_{erupt}$ at the fragmentation depth. Below fragmentation depth, the velocity continues to decrease linearly to $0.01u_{erupt}$ at the depth where water exsolution begins.	Uncertainty in the value of $u_{erupt}$ is related both to the validity of assumptions made in developing the theory that produces the curves in Figures 8 and 9 (steady, homogeneous flow, with lithostatic pressure in the rising magma column), and to the limitations of graphical extrapolation of the actual calculated curves. Uncertainty in the velocity versus depth functions are associated with the simple linear nature of the recommended functions, whereas in reality, the functions would be nonlinear due to poorly understood processes of magma ascent.	Subsequent use of these velocity profiles should explicitly state the simplifications that are made to derive them.
Eruption duration for formation of an entire volcano	For formation of an entire volcano, a log-normal distribution with a minimum of 1 day, a mean of 30 days, and a maximum of 15 years.	The distributions recommended for eruption duration include uncertainty associated with observations of historical scoria cone volcanoes around the world.	There are no restrictions on the subsequent use of these distributions.
Duration of a single explosive phase constituting	A uniform probability ranging from 1 day to 75 days	Uncertainty associated with this parameter is from the limited number of observed, relevant	There are no restrictions on the subsequent use of

Table 38. Technical Product Output for This Scientific Analysis Report (Continued)

Parameter	Recommended Values	Uncertainties	Restrictions on Subsequent Use
a violent Strombolian eruptive phase		explosive eruptions.	this distribution.
Eruption volume	Uniform distribution between 0.004 km <sup>3</sup> and 0.08 km <sup>3</sup> .	This distribution captures most of the potential uncertainty associated with ash volume, based upon the estimated eruption volumes of Quaternary volcanoes in the YMR.	There are no restrictions on the subsequent use of this distribution.
Mean particle size erupted during violent Strombolian phases	Log-triangular distribution with a minimum of 0.01 mm, a mode of 0.1 mm, and a maximum of 1.0 mm.	Uncertainties associated with this parameter are due mainly to the rarity of data in the published literature that pertain to the bulk erupted particle size from violent Strombolian eruptions. The recommended distribution incorporates the range of values that have been estimated.	There are no restrictions on the subsequent use of this distribution.
Standard deviation of particle size distribution for a given mean	Uniform distribution between $\sigma_\phi = 1$ and $\sigma_\phi = 3$ .	Uncertainties associated with this parameter are due mainly to the rarity of data in the published literature that pertain to the bulk erupted particle size from violent Strombolian eruptions. The recommended distribution incorporates the range of values that have been estimated.	There are no restrictions on the subsequent use of this distribution.
Clast characteristics	Shape factor of 0.5.	Uncertainty in this parameter is related to an absence of data in the published literature.	There are no restrictions on the subsequent use of this value.
Density of erupted particles	For particle diameters less than or equal to 0.01 mm, density is 0.8 of the magma density. For particles greater than 10 mm, density is 0.4 of the magma density. For particles between 0.01 and 10 mm, density should decrease linearly with increasing diameter.	Uncertainty in this parameter is related to the wide range of vesicularities of clasts that can be erupted during a single volcanic event.	There are no restrictions on subsequent use of the recommended values.
Tephra deposit density	There are two possible ways of treating deposit density in TSPA-SR calculations: (1) simply use 1,000 kg/m <sup>3</sup> or (2) a sample from a normal distribution of deposit densities ranging from 300 to 1,500 kg/m <sup>3</sup> , with a mean of 1,000 kg/m <sup>3</sup> .	Uncertainties associated with this parameter are due to a lack of published data.	There are no restrictions on subsequent use of the recommended values.
Eruptive power	A uniform probability distribution (in log-power, watts) ranging from 9.0 to 12.0	Uncertainty associated with this parameter is from the small number of observed eruptions, durations, and accompanying volume calculations.	There are no restrictions on subsequent use of the recommended values.

Output DTN: LA0311DK831811.001

## 8. INPUTS AND REFERENCES

### 8.1 DOCUMENTS CITED

The following is a list of the references cited in this document. Column 1 represents the unique six-digit numerical identifier (the Document Input Reference System [DIRS] number), which is placed in the text following the reference callout (e.g., BSC 2002 [DIRS 155950]). The purpose of these numbers is to assist the reader in locating a specific reference in the DIRS database. Within the reference list, multiple sources by the same author and date (e.g., BSC 2002) are sorted alphabetically by title.

- 103597 Altman, W.D.; Donnelly, J.P.; and Kennedy, J.E. 1988. *Peer Review for High-Level Nuclear Waste Repositories: Generic Technical Position*. NUREG-1297. Washington, D.C.: U.S. Nuclear Regulatory Commission. TIC: 200651.
- 103750 Altman, W.D.; Donnelly, J.P.; and Kennedy, J.E. 1988. *Qualification of Existing Data for High-Level Nuclear Waste Repositories: Generic Technical Position*. NUREG-1298. Washington, D.C.: U.S. Nuclear Regulatory Commission. TIC: 200652.
- 162794 Amos, R.C.; Self, S.; and Crowe, B. 1981. "Pyroclastic Activity at Sunset Crater: Evidence for a Large Magnitude, High Dispersal Strombolian Eruption." *EOS*, 62, 1085. Washington, D.C.: American Geophysical Union. TIC: 254775.
- 162795 Arrighi, S.; Principe, C.; and Rosi, M. 2001. "Violent Strombolian and Subplinian Eruptions at Vesuvius During Post-1631 Activity." *Bulletin of Volcanology*, 63, 126-150. New York, New York: Springer-Verlag. TIC: 253920.
- 122601 Baker, D.R. and Eggler, D.H. 1983. "Fractionation Paths of Atka (Aleutians) High Alumina Basalt: Constraints from Phase Relations." *Journal of Volcanology and Geothermal Research*, 18, 387-404. Amsterdam, The Netherlands: Elsevier Science. TIC: 246252.
- 147740 Best, M.G. 1982. *Igneous and Metamorphic Petrology*. New York, New York: W.H. Freeman and Company. TIC: 247662.
- 144263 Blong, R.J. 1984. *Volcanic Hazards: A Sourcebook on the Effects of Eruptions*. Sydney, Australia: Academic Press. TIC: 247016.
- 162796 Bower, S.M. and Woods, A.W. 1996. "On the Dispersal of Clasts from Volcanic Crater During Small Explosive Eruptions." *Journal of Volcanology and Geothermal Research*, 73, 1-32. Amsterdam, The Netherlands: Elsevier. TIC: 253919.
- 160130 BSC (Bechtel SAIC Company). 2001. *Characterize Eruptive Processes at Yucca Mountain, Nevada*. ANL-MGR-GS-000002 REV 00 ICN 01. Las Vegas, Nevada: Bechtel SAIC Company. ACC: MOL.20020327.0498.

- 160313 BSC 2002. *Scientific Processes Guidelines Manual*. MIS-WIS-MD-000001 REV 01. Las Vegas, Nevada: Bechtel SAIC Company. ACC: MOL.20020923.0176.
- 161296 BSC 2002. *Software Code: ASHPLUME*. 1.4LV. PC, Windows 2000/NT/98. 10022-1.4LV-02.
- 158185 BSC 2002. *Test Plan for Ash Redistribution, Lava Morphology, and Igneous Processes Studies*. SITP-02-DE-001 REV 00. Las Vegas, Nevada: Bechtel SAIC Company. ACC: MOL.20020321.0113.
- 158966 BSC 2002. *The Enhanced Plan for Features, Events, and Processes (FEPs) at Yucca Mountain*. TDR-WIS-PA-000005 REV 00. Las Vegas, Nevada: Bechtel SAIC Company. ACC: MOL.20020417.0385.
- 161840 BSC 2003. *Atmospheric Dispersal and Deposition of Tephra from a Potential Volcanic Eruption at Yucca Mountain, Nevada*. MDL-MGR-GS-000002 REV 00G. Las Vegas, Nevada: Bechtel SAIC Company. ACC: MOL.20031020.0019.
- 163769 BSC 2003. *Characterize Framework for Igneous Activity at Yucca Mountain, Nevada*. ANL-MGR-GS-000001 REV 01. Las Vegas, Nevada: Bechtel SAIC Company. URN-1106.
- 165923 BSC 2003. *Dike/Drift Interactions*. MDL-MGR-GS-000005 REV 00A. Las Vegas, Nevada: Bechtel SAIC Company. ACC: MOL.20030711.0105.
- 165002 BSC 2003. *Igneous Intrusion Impacts on Waste Packages and Waste Forms*. MDL-EBS-GS-000002 REV 00. Las Vegas, Nevada: Bechtel SAIC Company. ACC: MOL.20030711.0096.
- 164650 BSC 2003. *Number of Waste Packages Hit by Igneous Intrusion*. ANL-MGR-GS-000003 REV 00C. Las Vegas, Nevada: Bechtel SAIC Company. ACC: MOL.20030711.0099.
- 164143 BSC 2003. *Technical Work Plan -- Igneous Activity Analysis for Disruptive Events. Work Packages Numbers P4A1224DF1 / ADEM03, P4D1224DFR / ADET03, ATMT11*. TWP-WIS-MD-000007 REV 03. Las Vegas, Nevada: Bechtel SAIC Company. ACC: DOC.20030721.0003.
- 162797 Budnikov, V.A.; Markhinin, Ye.K.; and Ovsyannikov, A.A. 1983. "The Quantity, Distribution and Petrochemical Features of Pyroclastics of the Great Tolbachik Fissure Eruption." *The Great Tolbachik Fissure Eruption: Geological and Geophysical Data 1975-1976*. Fedotov, S.A. and Markhinin, Ye.K., eds. Pages 41-56. Cambridge, England: Cambridge University Press. TIC: 247236.
- 122532 Byers, C.D.; Garcia, M.O.; and Muenow, D.W. 1985. "Volatiles in Pillow Rim Glasses from Loihi and Kilauea Volcanoes, Hawaii." *Geochimica et Cosmochimica Acta*, 49, 1887-1896. New York, New York: Pergamon Press. TIC: 246241.

- 101859 Byers, F.M., Jr. and Barnes, H. 1967. *Geologic Map of the Paiute Ridge Quadrangle, Nye and Lincoln Counties, Nevada*. Map GQ-577. Washington, D.C.: U.S. Geological Survey. ACC: HQS.19880517.1104.
- 161770 Canori, G.F. and Leitner, M.M. 2003. *Project Requirements Document TER-MGR-MD-000001 REV 01*. Las Vegas, Nevada: Bechtel SAIC Company. ACC: DOC.20030404.0003.
- 124939 Cas, R.A.F. and Wright, J.V. 1987. *Volcanic Successions, Modern and Ancient*. London, United Kingdom: Allen & Unwin. TIC: 238960.
- 163891 Chappell, A. 1999. "The Limitation of Using <sup>137</sup>Cs for Estimating Soil Redistribution in Semi-arid Environments." *Geomorphology*, 29, ([1-2]), 135-152. [New York, New York]: Elsevier. TIC: 254464.
- 104691 Coe, J.A.; Glancy, P.A.; and Whitney, J.W. 1997. "Volumetric Analysis and Hydrologic Characterization of a Modern Debris Flow Near Yucca Mountain, Nevada." *Geomorphology*, 20, (1-2), 11-28. Amsterdam, The Netherlands: Elsevier. TIC: 241945.
- 101527 Coe, J.A.; Oswald, J.; Vadurro, G.; and Lundstrom, S.C. 1996. "Quaternary Faulting on the Fatigue Wash Fault." Chapter 4.8 of *Seismotectonic Framework and Characterization of Faulting at Yucca Mountain, Nevada*. Whitney, J.W., ed. Milestone 3GSH100M. Denver, Colorado: U.S. Geological Survey. TIC: 237980. ACC: MOL.19970129.0041.
- 162823 Crowe, B. 1992. *Volcanism Field Notebook #6*. Scientific Notebook TWS-EES-13-LV-11-89-07. ACC: NNA.19920918.0044.
- 164317 Crowe, B. 1996. *Volcanism Field Notebook #7*. Scientific Notebook TWS-EES-13-LV-01-93-05. URN-1096.
- 100972 Crowe, B.; Self, S.; Vaniman, D.; Amos, R.; and Perry, F. 1983. "Aspects of Potential Magmatic Disruption of a High-Level Radioactive Waste Repository in Southern Nevada." *Journal of Geology*, 91, (3), 259-276. Chicago, Illinois: University of Chicago Press. TIC: 216959.
- 101532 Crowe, B.M.; Wohletz, K.H.; Vaniman, D.T.; Gladney, E.; and Bower, N. 1986. *Status of Volcanic Hazard Studies for the Nevada Nuclear Waste Storage Investigations*. LA-9325-MS. Volume II. Los Alamos, New Mexico: Los Alamos National Laboratory. ACC: NNA.19890501.0157.
- 162823 Crowe, B. 1992. *Volcanism Field Notebook #6*. Scientific Notebook TWS-EES-13-LV-11-89-07. ACC: NNA.19920918.0044.
- 100110 Crowe, B.; Perry, F.; Geissman, J.; McFadden, L.; Wells, S.; Murrell, M.; Pothe, J.; Valentine, G.A.; Bowker, L.; and Finnegan, K. 1995. *Status of Volcanism Studies*

- for the Yucca Mountain Site Characterization Project.* LA-12908-MS. Los Alamos, New Mexico: Los Alamos National Laboratory. ACC: HQO.19951115.0017.
- 151551 CRWMS M&O (Civilian Radioactive Waste Management System Management and Operating Contractor) 2000. *Characterize Framework for Igneous Activity at Yucca Mountain, Nevada.* ANL-MGR-GS-000001 REV 00 ICN 01. Las Vegas, Nevada: CRWMS M&O. ACC: MOL.20001221.0001.
- 156980 CRWMS M&O 2000. *Data Qualification Report: Data Related to Characterization of Eruptive Processes for Use on the Yucca Mountain Project.* TDR-NBS-GS-000016 REV 0. Las Vegas, Nevada: CRWMS M&O. ACC: MOL.20000810.0002.
- 151553 CRWMS M&O 2000. *Features, Events, and Processes: Disruptive Events.* ANL-WIS-MD-000005 REV 00 ICN 1. Las Vegas, Nevada: CRWMS M&O. ACC: MOL.20001218.0007.
- 153246 CRWMS M&O 2000. *Total System Performance Assessment for the Site Recommendation.* TDR-WIS-PA-000001 REV 00 ICN 01. Las Vegas, Nevada: CRWMS M&O. ACC: MOL.20001220.0045.
- 153938 CRWMS M&O 2001. *Miscellaneous Waste-Form FEPs.* ANL-WIS-MD-000009 REV 00 ICN 01. Las Vegas, Nevada: CRWMS M&O. ACC: MOL.20010216.0006.
- 149303 Danyushevsky, L.V.; Falloon, T.J.; Sobolev, A.V.; Crawford, A.J.; Carroll, M.; and Price, R.C. 1993. "The H<sub>2</sub>O Content of Basalt Glasses from Southwest Pacific Back-Arc Basins." *Earth and Planetary Science Letters*, 117, 347-362. Amsterdam, The Netherlands: Elsevier Science B.V. TIC: 246102.
- 162798 Dasch, J.; Armstrong, R.L.; and Clabaugh, S.E. 1969. "Age of the Rim Rock Dike Swarm, Trans-Pecos Texas." *Geological Society of America Bulletin*, 80, 1819-1824. Boulder, Colorado: Geological Society of America. TIC: 254238.
- 162799 Delaney, P.T. 1982. "Rapid Intrusion of Magma Into Wet Rock: Groundwater Flow Due to Pore Pressure Increases." *Journal of Geophysical Research*, 87, (B9), 7739-7756. Washington, D.C.: American Geophysical Union. TIC: 254049.
- 145370 Delaney, P.T. and Gartner, A.E. 1997. "Physical Processes of Shallow Mafic Dike Emplacement Near the San Rafael Swell, Utah." *Geological Society of America Bulletin*, 109, (9), 1177-1192. Boulder, Colorado: Geological Society of America. TIC: 247421.
- 162800 Delaney, P. and Pollard, D. 1978. "Basaltic Subvolcanic Conduits Near Shiprock, New Mexico: Magma Flow, Heat Transport and Brecciation of Host Rocks." *Eos Transactions*, 59, (12), 1212. *Proceedings of American Geophysical Union, San Francisco, CA.* Page 1212. Washington, D.C.: American Geophysical Union. TIC: 254390.

- 162801 Delaney, P.T. and Pollard, D.D. 1981. *Deformation of Host Rocks and Flow of Magma During Growth of Minette Dikes and Breccia-Bearing Intrusions Near Ship Rock, New Mexico*. USGS Professional Paper 1202. Denver, Colorado: U.S. Geological Survey. TIC: 254050.
- 162914 Detournay, E.; Mastin, L.G.; Pearson, J.R.A.; Rubin, A.M.; and Spera, F.J. 2003. *Final Report of the Igneous Consequences Peer Review Panel*. Las Vegas, Nevada: Bechtel SAIC Company. ACC: MOL.20030325.0227.
- 162802 Dobran, F. 2001. *Volcanic Processes: Mechanisms in Material Transport*. New York, New York: Kluwer Academic/Plenum. TIC: 254051.
- 115338 Doubik, P. and Hill, B.E. 1999. "Magmatic and Hydromagmatic Conduit Development During the 1975 Tolbachik Eruption, Kamchatka, with Implications for the Hazards Assessment at Yucca Mountain, NV." *Journal of Volcanology and Geothermal Research*, 91, 43-64. Amsterdam, The Netherlands: Elsevier. TIC: 246029.
- 162803 Eichelberger, J.C.; Vogel, T.A.; Younker, L.W.; Miller, C.D.; Heiken G.H.; and Wohletz, K.H. 1988. "Structure and Stratigraphy Beneath a Young Phreatic Vent: South Inyo Crater, Long Valley Caldera, California." *Journal of Geophysical Research*, 93, (B11), 13208-13220. Washington, D.C.: American Geophysical Union. TIC: 254490.
- 164076 Ely, L.L., Webb, R.H.; Enzel, Y. 1992. "Accuracy of Post-Bomb <sup>137</sup>Cs and <sup>14</sup>C in Dating Fluvial Deposits." *Quaternary Research*, 38, 196-204. University of Washington. TIC: 254471.
- 162804 Fierstein, J. and Nathenson, M. 1992. "Another Look at the Calculation of Fallout Tephra Volumes." *Bulletin of Volcanology*, 54, 156-167. Berlin, Germany: Springer-Verlag. TIC: 254491.
- 162805 Fisher, R.V. 1961. "Proposed Classification of Volcaniclastic Sediments and Rocks." *Geological Society of America Bulletin*, 72, (9), 1409-1414. Burlington, Vermont: Geological Society of America. TIC: 254492.
- 162806 Fisher, R.V. and Schmincke, H.-U. 1984. *Pyroclastic Rocks*. Berlin, Germany: Springer-Verlag. TIC: 223562.
- 154365 Freeze, G.A.; Brodsky, N.S.; and Swift, P.N. 2001. *The Development of Information Catalogued in REV 00 of the YMP FEP Database*. TDR-WIS-MD-000003 REV 00 ICN 01. Las Vegas, Nevada: Bechtel SAIC Company. ACC: MOL.20010301.0237.
- 162810 Fries, C., Jr. 1953. "Volumes and Weights of Pyroclastic Material, Lava, and Water Erupted by Parícutin Volcano, Michoacan, Mexico." *Transactions, American Geophysical Union*, 34, 603-616. Washington, D.C.: American Geophysical Union. TIC: 253853.

- 144274 Gaetani, G.A.; Grove, T.L.; and Bryan, W.B. 1993. "The Influence of Water on the Petrogenesis of Subduction-Related Igneous Rocks." *Nature*, 365, 332-335. London, England: Macmillan Journals. TIC: 246792.
- 122542 Garcia, M.O.; Muenow, D.W.; Aggrey, K.E.; and O'Neil, J.R. 1989. "Major-Element, Volatile, and Stable Isotope Geochemistry of Hawaiian Submarine Glasses." *Journal of Geophysical Research*, 94, (B8), 10525-10538. Washington, D.C.: American Geophysical Union. TIC: 246240.
- 144518 Gile, L.H.; Hawley, J.W.; and Grossman, R.B. 1981. *Soils and Geomorphology in the Basin and Range Area of Southern New Mexico—Guidebook to the Desert Project*. Memoir 39. Socorro, New Mexico: New Mexico Bureau of Mines & Mineral Resources. TIC: 228406.
- 162813 Hallett, R.B. 1992. "Volcanic Geology of Cerro Chafo." *San Juan Basin IV: New Mexico Geological Society, 43rd Annual Field Conference, September 30-October 3, 1992*. Lucas, S.G.; Kues, B.S.; Williamson, T.E.; and Hunt, A.P., eds. Pages 19-22. Socorro, New Mexico: New Mexico Geological Society. TIC: 254042.
- 124671 Hallett, R.B. 1992. "Volcanic Geology of the Rio Puerco Necks." *San Juan Basin IV: New Mexico Geological Society, 43rd Annual Field Conference, September 30-October 3, 1992*. Lucas, S.G.; Kues, B.S.; Williamson T.E.; and Hunt, A.P.; eds. Pages 135-144. Socorro, New Mexico: New Mexico Geological Society. TIC: 239345.
- 162815 Hardee, H.C. and Larson, D.W. 1977. "The Extraction of Heat from Magmas Based on Heat Transfer Mechanisms." *Journal of Volcanology and Geothermal Research*, 2, (2), 113-144. Amsterdam, The Netherlands: Elsevier. TIC: 254497.
- 164775 Harrington, C. 2003. Ash and Soil Redistribution Studies. Scientific Notebook SN-LANL-SCI-285-V1. ACC: MOL20030411.0312.
- 162814 Hasenaka, T. and Carmichael, I.S.E. 1985. "The Cinder Cones of Michoacán-Guanajuato, Central Mexico: Their Age, Volume and Distribution, and Magma Discharge Rate." *Journal of Volcanology and Geothermal Research*, 25, 105-124. Amsterdam, The Netherlands: Elsevier. TIC: 225036.
- 162816 Hayes, S.K.; Montgomery, D.R.; and Newhall, C.G. 2002. "Fluvial Sediment Transport and Deposition Following the 1991 Eruption of Mount Pinatubo." *Geomorphology*, 45, 211-224. Amsterdam, The Netherlands: Elsevier. TIC: 254038.
- 162817 Heiken, G. 1978. "Characteristics of Tephra from Cinder Cone, Lassen Volcanic National Park, California." *Bulletin of Volcanology*, 41, 119-130. New York, New York: Springer-Verlag. TIC: 235508.
- 106122 Heiken, G.H. and Wohletz, K. 1985. *Volcanic Ash*. Berkeley, California: University of California Press. TIC: 242991.

- 107255 Heizler, M.T.; Perry, F.V.; Crowe, B.M.; Peters, L.; and Appelt, R. 1999. "The Age of Lathrop Wells Volcanic Center: An  $^{40}\text{Ar}/^{39}\text{Ar}$  Dating Investigation." *Journal of Geophysical Research*, 104, (B1), 767-804. Washington, D.C.: American Geophysical Union. TIC: 243399.
- 151040 Hill, B.E.; Connor, C.B.; Jarzempa, M.S.; La Femina, P.C.; Navarro, M.; and Strauch, W. 1998. "1995 Eruptions of Cerro Negro Volcano, Nicaragua, and Risk Assessment for Future Eruptions." *Geological Society of America Bulletin*, 110, (10), 1231-1241. Boulder, Colorado: Geological Society of America. TIC: 245102.
- 159900 Hunt, C.B. 1975. *Death Valley, Geology, Ecology, Archaeology*. Berkeley, California: University of California Press. TIC: 246234.
- 109119 Jackson, J.A., ed. 1997. *Glossary of Geology*. 4th Edition. Alexandria, Virginia: American Geological Institute. TIC: 236393.
- 100460 Jarzempa, M.S. 1997. "Stochastic Radionuclide Distributions after a Basaltic Eruption for Performance Assessments of Yucca Mountain." *Nuclear Technology*, 118, 132-141. Hinsdale, Illinois: American Nuclear Society. TIC: 237944.
- 118292 Jaupart, C. and Tait, S. 1990. "Dynamics of Eruptive Phenomena." Chapter 8 of *Modern Methods of Igneous Petrology: Understanding Magmatic Processes*. Nicholls, J. and Russell, J.K., eds. Reviews in Mineralogy Volume 24. Pages 213-238. Washington, D.C.: Mineralogical Society of America. TIC: 246394.
- 111236 Keating, G.N. and Valentine, G.A. 1998. "Proximal Stratigraphy and Syn-Eruptive Faulting in Rhyolitic Grants Ridge Tuff, New Mexico, USA." *Journal of Volcanology and Geothermal Research*, 81, 37-49. Amsterdam, The Netherlands: Elsevier. TIC: 246096.
- 162820 Kirchner, J.W.; Finkel, R.C.; Riebe, C.S.; Granger, D.E.; Clayton, J.L.; King, J.G.; and Megahan, W.F. 2001. "Mountain Erosion Over 10 yr, 10 k.y., and 10 m.y. Time Scales." *Geology*, 29, (7), 591-594. Boulder, Colorado: Geological Society of America. TIC: 254239.
- 106299 Knutson, J. and Green, T.H. 1975. "Experimental Duplication of a High-Pressure Megacryst/Cumulate Assemblage in a Near-Saturated Hawaiiite." *Contributions to Mineralogy and Petrology*, 52, 121-132. Berlin, Germany: Springer-Verlag. TIC: 225057.
- 100909 Kotra, J.P.; Lee, M.P.; Eisenberg, N.A.; and DeWispelare, A.R. 1996. *Branch Technical Position on the Use of Expert Elicitation in the High-Level Radioactive Waste Program*. NUREG-1563. Washington, D.C.: U.S. Nuclear Regulatory Commission. TIC: 226832.

- 164023 Krier, D. and Harrington, C.D. 2003. Ash Redistribution, Lava Morphology, and Igneous Processes Studies. Scientific Notebook SN-LANL-SCI-286-V1. ACC: MOL. 20030701.0109.
- 165893 Krier, D. and Harrington, C.D. 2003. Ash Redistribution, Lava Morphology, and Igneous Processes Studies. Scientific Notebook SN-LANL-SCI-286-V2. ACC: MOL.20031021.0191; MOL.20031021.0192.
- 147767 Lange, R.L. and Carmichael, I.S.E. 1990. "Thermodynamic Properties of Silicate Liquids with Emphasis on Density, Thermal Expansion, and Compressibility." Chapter 2 of *Modern Methods of Igneous Petrology: Understanding Magmatic Processes*, Nicholls, J., and Russell, J.K., editors, pp. 25-59. Reviews in Mineralogy Volume 24. Washington, D.C.: Mineralogical Society of America. TIC: 246394.
- 144310 Luhr, J.F. and Simkin, T., eds. 1993. *Parícutin, The Volcano Born in a Mexican Cornfield*. Phoenix, Arizona: Geoscience Press. TIC: 247017.
- 162821 Macdonald, G.A. 1972. *Volcanoes*. Englewood Cliffs, New Jersey: Prentice-Hall, Inc. TIC: 238023.
- 104660 Machette, M.N. 1985. "Calcic Soils of the Southwestern United States." *Soils and Quaternary Geology of the Southwestern United States*. Weide, D.L. and Faber, M.L., eds. Special Paper 203. Pages 1-21. Boulder, Colorado: Geological Society of America. TIC: 239387.
- 144419 Mader, H.M. 1998. "Conduit Flow and Fragmentation." *The Physics of Explosive Volcanic Eruptions*. Gilbert, J.S. and Sparks, R.S.J., eds. Geological Society of London Special Publication No. 145. Pages 51-71. London, United Kingdom: Blackwell Scientific Publications. TIC: 247115.
- 104663 Mahood, G.A. and Baker, D.R. 1986. "Experimental Constraints on Depths of Fractionation of Mildly Alkalic Basalts and Associated Felsic Rocks: Pantelleria, Strait of Sicily." *Contributions to Mineralogy and Petrology*, 93, 251-264. New York, New York: Springer-Verlag. TIC: 225072.
- 144325 Maleyev, Ye.F., and Vande-Kirkov, Yu.V. 1983. "Features of Pyroclastics of the Northern Breakthrough of the Great Tolbachik Fissure Eruption and the Origin of its Pale-Grey Ash." *The Great Tolbachik Fissure Eruption, Geological and Geophysical Data 1975-1976*. Fedotov, S.A., and Markhinin, Ye.K., eds. Pages 57-71. Cambridge, England: Cambridge University Press. TIC: 247236.
- 124749 Mastin, L.G. 1991. "The Roles of Magma and Groundwater in the Phreatic Eruptions at Inyo Craters, Long Valley Caldera, California." *Bulletin of Volcanology*, 53, 579-596. Heidelberg, Germany: Springer-Verlag. TIC: 239071.
- 162826 McBirney, A.R. 1959. "Factors Governing Emplacement of Volcanic Necks." *American Journal of Science*, 257, 431-448. New Haven, Connecticut: Yale University, Kline Geology Laboratory. TIC: 254240.

- 115469 McGetchin, T.R.; Settle, M.; and Chouet, B.A. 1974. "Cinder Cone Growth Modeled after Northeast Crater, Mount Etna, Sicily." *Journal of Geophysical Research*, 79, (23), 3257-3272. Washington, D.C.: American Geophysical Union. TIC: 246027.
- 162827 McKnight, S.B. and Williams, S.W. 1997. "Old Cinder Cone or Young Composite Volcano?: The Nature of Cerro Negro, Nicaragua." *Geology*, 25, 339-342. Boulder, Colorado: Geological Society of America. TIC: 254104.
- 125093 Muenow, D.W.; Graham, D.G.; Liu, N.W.K.; and Delaney, J.R. 1979. "The Abundance of Volatiles in Hawaiian Tholeiitic Submarine Basalts." *Earth and Planetary Science Letters*, 42, 71-76. Amsterdam, The Netherlands: Elsevier Science. TIC: 246833.
- 162853 Neal, C.A.; Doukas, M.P.; and McGimsey, R.G. 2003. "Volcanic Activity in Alaska: Summary of Events and Response of the Alaska Volcano Observatory 1994." Open-File Report 95-271. [Menlo Park, California]: U.S. Geological Survey. Accessed August 21, 2003. TIC: 254756  
<http://geopubs.wr.usgs.gov/open-file/of95-271/body.html>
- 162828 Newhall, C. G. and Self, S. 1982. "The Volcanic Explosivity Index (VEI): An Estimate of Explosive Magnitude for Historical Volcanism." *Journal of Geophysical Research*, 87, (C2), 1231-1238. Washington, D.C.: American Geophysical Union. TIC: 254496.
- 154435 NOAA (National Oceanic and Atmospheric Administration) 1995. *Upper Air Data: Desert Rock, Nevada, 1978-1995*. Reno, Nevada: National Oceanic and Atmospheric Administration, Western Regional Climate Center. TIC: 249335.
- 151592 NRC (U.S. Nuclear Regulatory Commission) 1999. "Issue Resolution Status Report Key Technical Issue: Igneous Activity." Rev. 2. Washington, D.C.: U.S. Nuclear Regulatory Commission. TIC: 247987. ACC: MOL.19990810.0639.
- 159538 NRC 2002. *Integrated Issue Resolution Status Report*. NUREG-1762. Washington, D.C.: U.S. Nuclear Regulatory Commission, Office of Nuclear Material Safety and Safeguards. TIC: 253064.
- 163274 NRC 2003. *Yucca Mountain Review Plan, Final Report*. NUREG-1804, Rev. 2. Washington, DC: U.S. Nuclear Regulatory Commission, Office of Nuclear Material Safety and Safeguards. TIC: 254568.
- 144330 Ochs, F.A., III, and Lange, R.A. 1999. "The Density of Hydrous Magmatic Liquids." *Science*, 283, 1314-1317. Washington, D.C.: American Association for the Advancement of Science. TIC: 246839.
- 158468 O'Leary, D.W.; Mankinen, E.A.; Blakely, R.J.; Langenheim, V.E.; and Ponce, D.A. 2002. *Aeromagnetic Expression of Buried Basaltic Volcanoes Near Yucca Mountain*,

- Nevada*. Open-File Report 02-020. Denver, Colorado: U.S. Geological Survey. ACC: MOL.20020627.0225.
- 106490 Perry, F.V. and Straub, K.T. 1996. *Geochemistry of the Lathrop Wells Volcanic Center*. LA-13113-MS. Los Alamos, New Mexico: Los Alamos National Laboratory. ACC: MOL.19961015.0079.
- 144335 Perry, F.V.; Crowe, B.M.; Valentine, G.A.; and Bowker, L.M., eds. 1998. *Volcanism Studies: Final Report for the Yucca Mountain Project*. LA-13478. Los Alamos, New Mexico: Los Alamos National Laboratory. TIC: 247225.
- 123891 Pyle, D.M. 1989. "The Thickness, Volume, and Grainsize of Tephra Fall Deposits." *Bulletin of Volcanology*, 51, (1), 1-15. Berlin, Germany: Springer-Verlag. TIC: 237451.
- 162829 Pyle, D.M. 1995. "Assessment of the Minimum Volume of Tephra Fall Deposits." *Journal of Volcanology and Geothermal Research*, 69, 379-382. Amsterdam, The Netherlands: Elsevier. TIC: 237451.
- 162830 Quarenì, F.; Ventura G.; and Mulargia, F. 2001. "Numerical Modelling of the Transition from Fissure- to Central-Type Activity on Volcanoes: A Case Study from Salina Island, Italy." *Physics of the Earth and Planetary Interiors*, 124, 213-221. Amsterdam, The Netherlands: Elsevier. TIC: 254053.
- 101106 Ramelli, A.R.; Oswald, J.A.; Vadurro, G.; Menges, C.M.; and Paces, J.B. 1996. "Quaternary Faulting on the Solitario Canyon Fault." Chapter 4.7 of *Seismotectonic Framework and Characterization of Faulting at Yucca Mountain, Nevada*. Whitney, J.W., ed. Milestone 3GSH100M, Denver, Colorado: U.S. Geological Survey. TIC: 237980. ACC: MOL.19970129.0041.
- 116087 Rose, W.I., Jr.; Bonis, S.; Stoiber, R.E.; Keller, M.; and Bickford, T. 1973. "Studies of Volcanic Ash from Two Recent Central American Eruptions." *Bulletin Volcanologique*, XXXVII-3, 338-364. New York, New York: Springer-Verlag. TIC: 246073.
- 115463 Rowland, S.K. and Walker, G.P.L. 1990. "Pahoehoe and aa in Hawaii: Volumetric Flow Rate Controls the Lava Structure." *Bulletin of Volcanology*, 52, 615-628. New York, New York: Springer-Verlag. TIC: 246030.
- 107243 Schmid, R. 1981. "Descriptive Nomenclature and Classification of Pyroclastic Deposits and Fragments: Recommendations of the IUGS Subcommittee on the Systematics of Igneous Rocks." *Geology*, 9, (1), 41-43. Boulder, Colorado: Geological Society of America. TIC: 241045.
- 162831 Self, S. and Walker, G.P.L. 1994. "Ash Clouds: Characteristics of Eruption Columns." *Volcanic Ash and Aviation Safety: Proceedings of the First International Symposium on Volcanic Ash and Aviation Safety held in Seattle, Washington in July*

1991. Casadevall, T.J., ed. Bulletin 2047. Pages 65-74. Washington, D.C.: U.S. government Printing Office. TIC: 254494.
- 1262845 Self, S.; Sparks, R.S.J.; Booth, B.; and Walker, G.P.L. 1974. "The 1973 Heimaey Strombolian Scoria Deposit, Iceland." *Geological Magazine*, 111, (6), 539-548. New York, New York: Cambridge University Press. TIC: 254495.
- 1262846 Settle, M. 1979. "The Structure and Emplacement of Cinder Cone Fields." *American Journal of Science*, 279, (10), 1089-1107. New Haven, Connecticut: Yale University, Kline Geology Laboratory. TIC: 251205.
- 126270 Shaw, H.R. 1972. "Viscosities of Magmatic Silicate Liquids: An Empirical Method of Prediction." *American Journal of Science*, 272, 870-889. New Haven, Connecticut: Yale University, Kline Geology Laboratory. TIC: 246470.
- 144351 Sisson, T.W. and Grove, T.L. 1993. "Experimental Investigations of the Role of H<sub>2</sub>O in Calc-alkaline Differentiation and Subduction Zone Magmatism." *Contributions to Mineralogy and Petrology*, 113, 143-166. New York, New York: Springer-Verlag. TIC: 246909.
- 122564 Sisson, T.W. and Grove, T.L. 1993. "Temperatures and H<sub>2</sub>O Contents of Low-MgO High-Alumina Basalts." *Contributions to Mineralogy and Petrology*, 113, 167-184. New York, New York: Springer-Verlag. TIC: 246251.
- 122549 Sisson, T.W. and Layne, G.D. 1993. "H<sub>2</sub>O in Basalt and Basaltic Andesite Glass Inclusions from Four Subduction-Related Volcanoes." *Earth and Planetary Science Letters*, 117, 619-635. Amsterdam, The Netherlands: Elsevier Science Publishers B.V. TIC: 246239.
- 162848 Smithsonian Institution. 2003. "Global Volcanism Program." <http://rathbun.si.edu/gvp/world/region06/krakatau/krakatau/var.htm>. Washington, D.C.: Smithsonian National Museum of Natural History. Accessed 2/1/2003. <http://www.volcano.si.edu/gvp/world/region18/capeverd/fogo/var.htm>
- 144352 Sparks, R.S.J.; Bursik, M.I.; Carey, S.N.; Gilbert, J.S.; Glaze, L.S.; Sigurdsson, H.; and Woods, A.W. 1997. *Volcanic Plumes*. New York, New York: John Wiley and Sons. TIC: 247134.
- 102783 Squires, R.R. and Young, R.L. 1984. *Flood Potential of Fortymile Wash and Its Principal Southwestern Tributaries, Nevada Test Site, Southern Nevada*. Water-Resources Investigations Report 83-4001. Carson City, Nevada: U.S. Geological Survey. ACC: HQS.19880517.1933.
- 138819 Stamatakos, J.A.; Connor, C.B.; and Martin, R.H. 1997. "Quaternary Basin Evolution and Basaltic Volcanism of Crater Flat, Nevada, from Detailed Ground Magnetic Surveys of the Little Cones." *Journal of Geology*, 105, 319-330. Chicago, Illinois: University of Chicago. TIC: 245108.

- 101029 Symonds, R.B.; Rose, W.I.; Bluth, G.J.S.; and Gerlach, T.M. 1994. "Volcanic-Gas Studies: Methods, Results, and Applications." Chapter 1 of *Volatiles in Magmas*. Reviews in Mineralogy Volume 30. Carroll, M.J. and Holloway, J.R., eds. Pages 1-66. Washington, D.C.: Mineralogical Society of America. TIC: 238061.
- 163860 Tokarev, P.I. 1983. "Calculation of the Magma Discharge, Growth in the Height of the Cone and Dimensions of the Feeder Channel of Crater 1 in the Great Tolbachik Fissure Eruption, July 1975." *The Great Tolbachik Fissure Eruption—Geological and Geophysical Data, 1975-1976*. Fedotov, S.A. and Markhinin, Y.K., eds. Pages 27-35. Cambridge, United Kingdom: Cambridge University Press. TIC: 247236.
- 166018 Umbal, J.V. 1997. "Five Years of Lahars at Pinatubo Volcano: Declining but Still Potentially Lethal Hazards." *Journal of the Geological Society of the Philippines*, 52, (1), 1-19. [Manila], Philippines: Geological Society of the Philippines. TIC: 255188.
- 254882 USGS 1983. Sunset Crater West, Coconino County, Arizona, 7.5-minute topographic map, Scale: 1:24,000. U.S. Geological Survey, Denver, Colorado.
- 254881 USGS 1969. Sunset Crater East, Coconino County, Arizona, 7.5-minute topographic map, Scale: 1:24,000. U.S. Geological Survey, Denver, Colorado.
- 107052 Valentine, G.A. and Groves, K.R. 1996. "Entrainment of Country Rock During Basaltic Eruptions of the Lucero Volcanic Field, New Mexico." *Journal of Geology*, 104, 71-90. Chicago, Illinois: University of Chicago Press. TIC: 246146.
- 101620 Vaniman, D. and Crowe, B. 1981. *Geology and Petrology of the Basalts of Crater Flat: Applications to Volcanic Risk Assessment for the Nevada Nuclear Waste Storage Investigations*. LA-8845-MS. Los Alamos, New Mexico: Los Alamos Scientific Laboratory. ACC: HQS.19880517.1541.
- 115585 Vergnolle, S. and Jaupart, C. 1986. "Separated Two-Phase Flow and Basaltic Eruptions." *Journal of Geophysical Research*, 91, (B12), 12842-12860. Washington, D.C.: American Geophysical Union. TIC: 239308.
- 125609 Walker, G.P.L. 1973. "Explosive Volcanic Eruptions-A New Classification Scheme." *Geologische Rundschau*, 62, 431-446. Stuttgart, Germany: Ferdinand Enke Verlag. TIC: 235930.
- 164092 Wallbrink, P.J.; Olley, J.M.; and Murray, A.S. 1994. "Measuring Soil Movement Using <sup>137</sup>Cs: Implications of Reference Site Variability." *Variability in Stream Erosion and Sediment Transport: Proceedings of a Symposium held at Canberra, Australia, December 12-16, 1994*. Olive, L.J.; Loughran, R.J.; and Kesby, J.A., eds. IAHS Publication No. 224, pp. 95-102. Wallingford, Oxfordshire, England: International Association of Hydrological Sciences. TIC: 254472.

- 124930 White, J.D.L. 1991. "Maar-Diatreme Phreatomagmatism at Hopi Buttes, Navajo Nation (Arizona), USA." *Bulletin of Volcanology*, 53, (4), 239-258. Berlin, Germany: Springer-Verlag. TIC: 239072.
- 107313 Whitney, J.W.; Simonds, F.W.; Shroba, R.R.; and Murray, M. 1996. "Quaternary Faulting on the Windy Wash Fault." Chapter 4.9 of *Seismotectonic Framework and Characterization of Faulting at Yucca Mountain, Nevada*. Whitney, J.W., ed. Milestone 3GSH100M. Denver, Colorado: U.S. Geological Survey. TIC: 237980. ACC: MOL.19970129.0041.
- 101034 Wilson, L. and Head, J.W., III. 1981. "Ascent and Eruption of Basaltic Magma on the Earth and Moon." *Journal of Geophysical Research*, 86, (B4), 2971-3001. Washington, D.C.: American Geophysical Union. TIC: 225185.
- 162859 Wilson, L.; Sparks, R.S.J.; Huang, T.C.; and Watkins, N.D. 1978. "The Control of Volcanic Column Heights by Eruption Energetics and Dynamics." *Journal of Geophysical Research*, 83, (B4), 1829-1836. Washington, D.C.: American Geophysical Union. TIC: 254493.
- 140956 Wohletz, K.H. 1986. "Explosive Magma-Water Interactions: Thermodynamics, Explosion Mechanisms, and Field Studies." *Bulletin of Volcanology*, 48, 245-264. Berlin, Germany: Springer-Verlag. TIC: 225183.
- 105544 Wohletz, K. and Heiken, G. 1992. *Volcanology and Geothermal Energy*. Berkeley, California: University of California Press. TIC: 241603.
- 110071 WoldeGabriel, G.; Keating, G.N.; and Valentine, G.A. 1999. "Effects of Shallow Basaltic Intrusion into Pyroclastic Deposits, Grants Ridge, New Mexico, USA." *Journal of Volcanology and Geothermal Research*, 92, (3), 389-411. New York, New York: Elsevier. TIC: 246037.
- 162860 Wood, C.A. 1980. "Morphometric Analysis of Cinder Cone Degradation." *Journal of Volcanology and Geothermal Research*, 8, 137-160. Amsterdam, The Netherlands: Elsevier Scientific Publishing. TIC: 225186.
- 116536 Wood, C.A. 1980. "Morphometric Evolution of Cinder Cones." *Journal of Volcanology and Geothermal Research*, 7, 387-413. Amsterdam, The Netherlands: Elsevier Scientific Publishing. TIC: 225565.
- 162861 Wylie, J.J.; Helfrich, K.R.; Dade, B.; Lister, J.R.; and Salzig, J.F. 1999. "Flow Localization in Fissure Eruptions." *Bulletin of Volcanology*, 60, 432-440. New York, New York: Springer-Verlag. TIC: 254054.
- 122589 Yoder, H.S., Jr., and Tilley, C.E. 1962. "Origin of Basalt Magmas: An Experimental Study of Natural and Synthetic Rock Systems." *Journal of Petrology*, 3, (3), 342-532. London, England: Oxford University Press. TIC: 247024.

## 8.2 CODES, STANDARDS, REGULATIONS, AND PROCEDURES

- 156605 10 CFR 63. Energy: Disposal of High-Level Radioactive Wastes in a Geologic Repository at Yucca Mountain, Nevada. Readily available.
- 163021 AP-2.22Q, Rev. 0, ICN 1. Classification Criteria and Maintenance of the Monitored Geologic Repository Q-List. Washington, D.C.: U.S. Department of Energy, Office of Civilian Radioactive Waste Management. ACC: DOC.20030422.0009.
- 161284 AP-SI.1Q, Rev 4, ICN 0. *Software Management*. Washington, D.C.: U.S. Department of Energy, Office of Civilian Radioactive Waste Management. ACC: MOL.20030113.0149.
- 166252 AP-SIII.9Q, Rev 1, ICN 2. *Scientific Analyses*. Washington, D.C.: U.S. Department of Energy, Office of Civilian Radioactive Waste Management. ACC: DOC.20031126.0001.

## 8.3 SOURCE DATA, LISTED BY DATA TRACKING NUMBER

- 147725 LA000000000099.002. Major Element, Trace Element, Isotopic, and Mineral Chemistry Data from Lathrop Wells. Submittal date: 08/02/1995.
- 164852 LA0308CH831811.001. Basaltic Ash Weight Percentages of Drainage Channel Samples near Lathrop Wells Cone. Submittal date: 08/20/2003.
- 164853 LA0308CH831811.002. Interpretation of 137-Cesium Profile Values for Samples from the Fortymile Wash Alluvial Fan. Submittal date: 08/20/2003.
- 162863 LA0302CH831811.002. Ash Redistribution, Lava Morphology, and Igneous Process Studies SITP-02-DE-001, REV 00A. Submittal date: 02/18/2003.
- 162864 LA0302GH831811.002. Grain Size of Tephra from Tephra Deposits Around the Lathrop Wells Volcano, Nevada. Submittal date: 02/19/2003.
- 162865 LA0302GH831811.003. Lithic Clasts Measured at Lathrop Wells Cone, Nevada. Submittal date: 02/25/2003.
- 162866 LA0302GH831811.004. Grain Counts-Types of Pyroclasts from Tephra Deposits Around the Lathrop Wells Volcano, Nevada. Submittal date: 02/25/2003.
- 164026 LA0305DK831811.001. Locations and Thicknesses of Tephra (Ashfall) from Lathrop Wells Cone, Nevada. Submittal date: 04/09/2003.

## 8.4 OUTPUT DATA, LISTED BY DATA TRACKING NUMBER

- LA0311DK831811.001 -Technical Product Output for ANL-MGR-GS-000002, Rev. 01

## ATTACHMENT I

### ACRONYMS

BSC	Bechtel SAIC Company. LLC
CRWMS-M&O	Civilian Radioactive Waste Management System - Management and Operating Contractor
DEM	digital elevation model
DIRS	Document Input Reference System
FEPs	features, events, and processes
GIS	Geographic Information System
LA	License Application
MDR	mass discharge rate
NRC	U.S. Nuclear Regulatory Commission
RMEI	reasonably maximally exposed individual
SEM	scanning electron microscope
TSPA	Total System Performance Assessment
TSPA-LA	Total System Performance Assessment-License Application
TSPA-SR	Total System Performance Assessment for the Site Recommendation
USGS	U.S. Geological Survey
YMP	Yucca Mountain Project
YMR	Yucca Mountain region
YMRP	Yucca Mountain Review Plan